Université catholique de Louvain
Institut de Recherche Expérimentale et Clinique
Pôle de Morphologie et Pôle de Chirurgie Expérimentale et Transplantation
Service de Chirurgie Plastique et Reconstructrice

The matrices of identity:
A subunit approach to human face and hand Vascularized Composite tissue Engineering (VCE)

Jérôme R. Duisit, DDS, MD

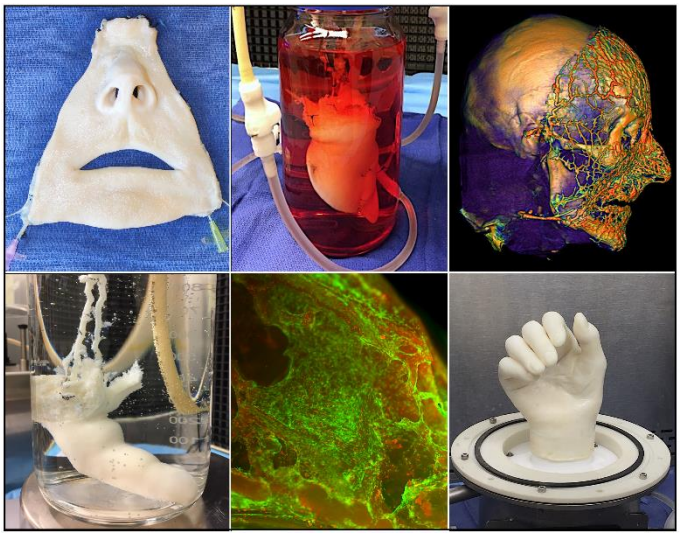

Promotor: Prof. Benoît Lengelé, MD, PhD, FRCS, KB
Co-Promotor: Prof. Pierre Gianello, MD, PhD

Thesis submitted in fulfillment of the requirements for a PhD degree
in Biomedical and Pharmaceutical Sciences
Public defence on **January 10th 2018**

A la persévérante mémoire

d'**Isabelle Dinoire**, première transplantée de la face, dont le visage a révélé au Monde l'espoir d'un nouveau chemin ;

du Dr **Gaëtan Lagneaux**, médecin des hommes puis de la vigne, dont l'œuvre nous laisse l'héritage d'un esprit passionné et bienveillant.

A **Maman** et **Papa**, qui m'ont appris d'où je viens.

A **Emma**, **Clara** et **Virginie**, les trois femmes de ma vie, qui m'apprennent où je vais.

Jury

President of the Jury:	**Prof. Vincent Grégoire** Université catholique de Louvain
Promotor:	**Prof. Benoît Lengelé** Université catholique de Louvain
Co-promotor:	**Prof. Pierre Gianello** Université catholique de Louvain
Jury members:	**Prof. Etienne Marbaix** Université catholique de Louvain
	Prof. Alain Poncelet Université catholique de Louvain
	Prof. Giuseppe Orlando Wake Forest University
Invited external jury members:	**Prof. Bernard Devauchelle** Université de Picardie Jules Verne
	Prof. Hans-Guenther Machens Technical University Munich
	Prof. Stan Monstrey Universiteit Gent

Author
Jérôme R. Duisit, DDS, MD
Service de Chirurgie Plastique et Reconstructrice
Cliniques Universitaires Saint-Luc
10, Avenue Hippocrate
B-1200 Bruxelles, Belgique
jerome.duisit@uclouvain.be

« Toute science, a dit de Maistre, commence par un mystère. Pour compléter l'idée de ce grand penseur, il faudrait dire : toute science commence et finit par un mystère, ou plutôt n'est que mystère… la notion qui nous paraît la plus claire n'est qu'une lueur entre deux abîmes… »

« All science, said de Maistre, begins with a mystery. To complete the idea of this great thinker, one would have to say: all science begins and ends with a mystery, or rather is nothing but a mystery… the notion which seems clearest to us is only a shimmer of light between two abysses… »

Jean-Marc Bourgery

« Mieux vaut vivre comme en socrate mécontent qu'en pourceau satisfait. »

Devise familiale

Remerciements

Dans un travail de Thèse, le volet concernant les remerciements est parfois pensé en premier, comme une finalité lointaine que l'on peut ainsi dès le début ancrer dans un présent, comme un gage rassurant. Car la temporalité est une dimension-clé du doctorant, dont la nature relativiste en fait un objet déroutant. Exercice finalement périlleux, pour sa lecture systématique (a contrario des 99% pages restantes) et détaillée, ajouté à la séduisante démarche de Lamartine dont le lac aurait été écrit en une nuit, les remerciements font le lit idéal d'une intense procrastination. Ma nature n'étant pas une constance facile, je ne déroge pas à cette tendance en me penchant ainsi sur ce chapitre, l'exact jour de l'impression du manuscrit. Veuillez ainsi bien me pardonner pour les oublis que je pourrai commettre, dans ce compromis entre justesse et spontanéité.

Mes premiers remerciements vont bien naturellement à l'Université catholique de Louvain et Monsieur le Recteur V. BLONDEL : je sais ce que je dois à cette noble Institution, qui m'a admis, éduqué et formé, successivement à la Médecine, la Chirurgie et enfin la Recherche. J'espère être digne de la nouvelle chance qui m'a été offerte, il y a maintenant 13 années. Je me souviendrai toujours du mail des inscriptions, reçu à l'été 2004 dans un hôtel de Kyoto, me signifiant mon admission en 2ème candidature. Cela s'accompagnait certes de l'inquiétude de l'inconnu, de tout quitter et tout risquer, pour un avenir sommes toutes incertain, mais surtout l'espoir de réaliser ses rêves. Je me souviens aussi encore très bien ce premier jour au départ de Lyon, l'arrivée à la gare de Bruxelles-Midi, portant à la main une simple mallette en guise d'apparat, avec le cœur léger et déterminé. Il y avait aussi dans l'air un sentiment de nouveauté, de conquête, à la Balzac plutôt que Daudet. De ces premières nuits en auberge de jeunesse, de ces quelques mots échangés mués immédiatement en amitié, de ce sentiment de n'avoir plus ni attache ni bien, je conserve la mémoire de jours parmi les plus heureux de ma vie. Et, aujourd'hui, je peux dire que je ne regrette rien. En Novembre 2005, j'étais alors au début de ma 3ème candidature lorsque fut réalisée la 1ère greffe de visage, côté belge, par notre Professeur d'Anatomie : événement qui, comme pour d'autres mes collègues, aura marqué à ce point d'infléchir des choix de carrière. Hasard ou nécessité, ainsi que l'exprimait Monod, j'avais déjà vécu à Lyon la 1ère greffe de main, le dénominateur commun entre ces deux événements au retentissement planétaire ayant été le Prof. J-M DUBERNARD ; plus tard, je défendais, toujours à Lyon ma thèse d'exercice en chirurgie dentaire sur les épithèses faciales avec le Prof. G. MALQUARTI, mentionnant déjà (nous sommes alors en 2004), quelques lignes sur la possibilité d'une future greffe de face, appartenant encore à la science-fiction ! Peu après a commencé à se former l'idée de fabriquer le vivant : non pas à partir du contenu, cellulaire, mais en s'orientait plutôt vers le contenant, la composante matricielle. Au hasard de l'observation des murs parsemés de lierre de la Chapelle Marie-la-Misérable. Finalement qu'est-ce qui fait la différence entre le vivant et l'inerte ? Peut-on concevoir un maillage inerte et qui, correctement conçu, sera « animé » par la suite avec le souffle cellulaire, dans une logique inversée ? C'est la question que je n'ai cessé de me poser depuis, en découvrant entre-temps que d'autres avait appelé cela « ingénierie tissulaire ». J'ai mis quelques schémas importants dans ce manuscrit, de la période préparatoire à ce projet : il appuie le fait que tout part d'une intuition, d'une idée, d'un croquis sur un coin de table- Le reste n'est que labeur et chance.

Je tiens à signifier ma gratitude la plus sincère comme la plus dévouée à mon Promoteur de Recherche, Maître de Chirurgie et d'Anatomie, le Prof. B. LENGELE, qui m'a pris sous son aile, avec une infinie bienveillance et un soutien indéfectible, comme l'aurait fait un père pour un fils. Il y a dans cette filiation une mécanique naturelle et forte, fruit de certains hasards pour une évidente nécessité. Il est difficile de concevoir pour pareille figure scientifique et humaniste, de retrouver humilité, accessibilité (certes après 21h !) et proximité. Au-delà de la transmission de son Art, il a toujours été une source d'inspiration et de motivation. Il m'aura aussi réconcilié avec mon pays, lui qui est le plus français des belges ! De la noblesse de cœur et d'esprit qu'il a toujours voulu transmettre à ses élèves, je conserve cette empreinte indélébile, du souci de perfection, de justesse et d'honetteté, tant dans les soins prodigués aux malades, que dans l'exécution de la Science. C'est un honneur et un privilège que d'espérer pouvoir, un jour, accomplir, avec mes autres collègues, certains de ses rêves que nous attendrons, guidés par son regard et portés par ses ailes. Cher Maître, veuillez recevoir dans le présent travail, tout le témoignage de ma reconnaissance et de ma plus sincère affection, en espérant me montrer digne de tout ce que vous m'avez transmis.

Toute ma reconnaissance va également à mon co-Promoteur, le Pr P. GIANELLO, à qui je dois tant. Il m'a appris, bien au-delà de la démarche inhérente à un travail de Thèse, à véritablement penser une dynamique et une stratégie de Recherche à petite et grande échelle, tant dans son questionnement scientifique que dans sa mise en réalisation pratique, en me faisant participer activement à tous ses volets. Il m'a fait confiance, laissé prendre de grandes initiatives - laissé faire mes erreurs aussi- me reprenant toujours au vol lorsque je faisais fausse route. Son soutien a été constant tout au long de ces années, avec la porte toujours ouverte de son bureau, dans un nuage bien particulier ! Je lui dois une grande partie d'un apprentissage. C'est une chance d'avoir pu côtoyer une pareille figure universitaire et humaine. On peut voir loin quand on se tient sur les épaules de géants. Qu'il veuille bien trouver ici toute ma gratitude et les marques de mon infini admiration et respect.

Au Pr G. ORLANDO, qui a aussi été un mentor inattendu, le plus américain des italiens (ou peut-être l'inverse !) qui m'a accompagné comme en recherche, avec la bienveillance d'un grand frère, et sans qui non plus ce travail n'aurait jamais abouti. Il m'a accueilli aux Etats-Unis, dans sa maison (et nourri avec les pâtes et les mots !), dans son laboratoire, avec une transparence et une confiance totale. Il m'a appris toutes les bases fondamentales scientifiques et académiques en ingénierie tissulaire, et m'a stimulé dans une démarche de productivité, à l'américaine ! je sais que de ces années de vie bruxelloises, il a laissé ici une partie de son cœur : le nôtre aussi lui sera toujours ouvert désormais, à chacun de ses passages.

Je suis honoré que la Présidence du Jury soit assurée par le Prof. V. GREGOIRE, qui a encadré ce doctorat toutes ces années, avec bienveillance et encouragements. Son exigence d'excellence a également été un moteur

important dans la productivité et le souci de qualité de ce travail. Qu'il trouve dans cette réalisation finale l'assurance de mon grand respect.

Je remercie également le Prof. A. PONCELET et le Prof. E. MARBAIX, d'avoir accepté d'être membres du jury et du comité d'accompagnement de cette Thèse, magnifiée par leurs expertises uniques. Le travail a grandement été amélioré par les remarques à chaque fois justes et pertinentes du Pr MARBAIX. Cela a été une grande joie de retrouver le Pr PONCELET au chevet du doctorat, après celui du bloc opératoire de cardiaque ! Je leur adresse ma gratitude la plus sincère.

Je suis très reconnaissant envers le Prof. B. DEVAUCHELLE, et cela triplement (en Picardie, il n'y a jamais de simple mesure !) : pour m'avoir fait l'honneur d'accepter d'être dans ce jury ; pour m'accueillir et me former en ce moment-même dans son Service comme Maître de Chirurgie ; et enfin, pour avoir été de longue date un modèle et une inspiration, illustre figure pour le jeune étudiant découvrant la reconstruction faciale d'exception.

Ein großes Dankeschön an Prof. H-G MACHENS für seine Begleitung alle seine Jahre als Mentor: Was für ein langer Weg seit unserem ersten Treffen und Ihrem Besuch im Labor! Vielen Dank für Ihr Interesse und Ihren unmittelbaren Enthusiasmus für die Arbeit, die aufgrund Ihres großen Ansehens eine große Ermutigung war, weiterzumachen. Ihre natürliche Großzügigkeit und Ihre große Sympathie haben es jedes Mal, auch auf einer persönlicheren Ebene, zu einem echten Vergnügen gemacht, Sie wieder zu treffen!

Ik dank de Prof. S. MONSTREY: beste professor, ik herinner me onze eerste ontmoeting, niet per se de meest glorieuze aan mijn zijde, tijdens deze mondelinge inhaalslag! In die tijd gaf je me nog een kans om te bewijzen dat ik de goedkeuring van mijn collega's verdiende. Ik hoop dat ik die toewijding heb gemaakt. Heel erg bedankt voor dit alles en je interesse en vriendelijkheid behouden, door me de eer te bewijzen lid te zijn van de Jury en me te verwelkomen in je Service.

Je tiens à saluer ici aussi l'apport décisif du Pr C. BEHETS, responsable du laboratoire MORF, dans la réalisation de cette Thèse, par son souci permanent de m'apporter les moyens de progresser ; pour m'avoir laissé agir et évoluer comme un chercheur à part entière, valorisé. Pour tout ce partage et ces années merci à vous Catherine ; veuillez-bien recevoir mon infinie reconnaissance et amitié.

Si cette Thèse existe aujourd'hui c'est parce que mes promoteurs ont fait le pari que cela fonctionnerait, car personne d'autre n'y croyait. Il fallait des visionnaires, des chirurgiens côtoyant les frontières de la science et de la clinique, pour oser. J'espère que ce travail honore leur confiance et les risques qu'ils ont eux-mêmes pris. De fait nous avons tout eu à créer, ou presque : les modèles, les concepts, les outils et techniques, les plateformes et les méthodologies. Il a fallu être soutenu par beaucoup d'autres personnes, sans qui également rien n'aurait été réalisé, critique en ingénierie tissulaire. Puis-je les remercier comme il se doit, maintenant.

Il faut bien être conscient que sans financement, la Recherche, même la plus pertinente et motivée, ne peut se réaliser. Je tiens à exprimer toute ma profonde gratitude envers les mécènes et donateurs. La Fondation Saint-Luc m'a permis de démarrer les deux premières années, grâce à une bourse de clinicien-chercheur -je n'aurai rien fait sans ; merci infiniment à Tessa SCHMIDBURG, et ses collaboratrices, souvent bénévoles, d'œuvrer en arrière-plan pour que tout cela soit possible. Le Fonds Dr Gaëtan LAGNEAUX, dont j'ai eu l'honneur d'être le premier récipiendaire, a permis de développer de manière critique la seconde partie du projet, avec l'exploration d'une nouvelle anatomopathologie appliquée à l'ingénierie tissulaire – Chère famille Lagneaux, merci pour votre générosité à tous égards, votre soutien et votre amitié ; j'espère avoir pu faire honneur à la mémoire du Dr Lagneaux. Je souhaite la meilleure réussite à Eugénie, qui sait où aller si elle veut faire un jour de la recherche ! J'ai également bénéficié du soutien, via le laboratoire d'un Fonds Spécial de la Recherche, pour lequel je suis encore une fois reconnaissant à l'UCL. Merci enfin à la Banque Transatlantique Belgium dont j'ai eu l'insigne honneur de recevoir le prix cette année.

La coappartenance aux deux laboratoires de Morphologie (MORF) et Chirurgie Expérimentale et Transplantation (CHEX) a été un facteur déterminant pour mener à bien ces travaux. Et dans les deux laboratoires, j'ai été accompagné de manière décisive. Il y a tout d'abord l'équipe rapprochée, avec Adeline : merci pour tout et également d'avoir enduré mes humeurs (!). La bonne réussite tient également fondamentalement à cette équipe que nous avons formé tout au long de ces années avec nos étudiants-chercheurs médecins, qui ont été, il faut le dire, exceptionnels : tant dans l'engagement que dans la qualité du travail. Merci à mes chers Riri, Fifi et Loulou, alias Hadrien A, Donovan D et Louis M. Je me félicite que chacun d'entre eux poursuivent leur chemin soit vers la chirurgie réparatrice, soit vers la recherche. Je n'oublie pas Philippe D avec qui cela a été un plaisir de travailler, même plus brièvement ! Et enfin, Christophe deT qui a également été un grand compagnon de route ! Merci à Alex G pour son apport dans les manuscrits et les techniques de préparations. Il y a eu aussi la grande contribution des mémorants de différents Instituts, dont le passage a à chaque fois été un véritable moteur pour les travaux : Simon L, Marie C, Erick M, An-CatherineH, Sarah E et Valérie K. Merci à vous et tous mes vœux de réussite. Un très grand merci à mes collègues de MORF : Christine deVdeG, pour ta grande assistance, Bernard C pour ton aide capitale et le recrutement ! Marc deB pour ton expertise histologique ; et mes collègues doctorants : Julie C, Jessica V, Virginie J, Thomas R, Sébastien L, Mickael C. Merci à toi Lisa T pour ces moments sympas, compagnonne de (cellule) bureau et boxeuse ! Et enfin bienvenue à Nicolas ! Notre plus profonde gratitude s'exprime également envers les familles des personnes ayant donné leur corps à la science – ce nous a permis une part décisive de cette avancée vers l'amélioration des soins aux malades.

CHEX fut ma base expérimentale, où j'ai passé beaucoup de nuits et de WE ! Merci pour toute l'assistance chirurgicale, amicale et alimentaire (!) de Martial V et Gwen B. Marie H a été d'une grande aide pour la microscopie électronique et la source de riches discussions ; à Daelha X, Eric L et Nizar M pour leurs aides précieuses. Excellentes suites de recherche à Tom D, à Anaïs S et Matias R! Grandes salutations à Matthieu VanS avec qui nous avons fait u bout de chemin ensemble très motivant. Merci également à Y. Nizet, F. Nizol et C. Lecuivre pour ces années de partage en CHEX. Enfin, j'en profite pour saluer Guillaume R dont les passages amicaux au labo constituent de très bons souvenirs. Merci au Prof Y. POUMAY et Mme V. De Glas pour leur temps et soutien.

Tout dans cette thèse où tout aura été épique, du début des travaux, de la rédaction des manuscrits et figures jusqu'à la finalisation de l'impression, et je tenais à remercier ici particulièrement Michelle C, Walter H et Pascale S pour leur aide précieuse et décisive (!).

Un immense merci au Dr C. BOUZIN pour notre synergie passionnante et qui ne fait que commencer ! Merci à Chantale F et Michèle deB pour la qualité de leur travail histologique.

J'ai beaucoup apprécié les échanges au cours de cette année avec le Prof. C. DESSY que je remercie pour sa disponibilité et son soutien. Ce sera un grand plaisir de continuer le travail ensemble ! Merci au Pr A. BOL pour votre sympathie et disponibilité dans la réalisation des micro-CT. Un immense merci au Pr E. COCHE pour l'apport d'imagerie, votre enthousiasme et votre disponibilité sans égale ! Merci à Claude pour son analyse d'empreintes : c'est un résultat qui a eu un grand écho ! La collaboration avec l'Ecole Polytechnique de Louvain et le Louvain Bionics furent prolifiques et ne vont que se développer, sans douter, dans les années à venir. Au Dr B. HERMAN, avec qui notre mésentente la plus cordiale ;) a pu s'épanouir et être source d'une belle productivité- merci Ben ! Merci à Léna pour tes aides dans ma thèse, tu sais que je souhaite également le meilleur ! Les travaux de TFE réalisés par Alexia, Julie et Charles ont été très précieux. La rencontre et le travail avec le Prof. T. PARDOEN, le Dr V. DESTOOP et Y-A. JANSSENS DE BISTHOVEN a été extrêmement riche Dans le décours des grands projets, il y eu le travail passionnant avec Amal A. Je dois à Marlène D et Michèle H la concrétisation de ce projet de brevet sur notre prototype, et qui sera capital dans un future proche. Merci au Dr A. PELOSO, pour l'apprentissage des techniques d'ingénierie tissulaire.

Je tiens à saluer mes maîtres de Chirurgie, qui ont forgé ma main et mon esprit. Au Prof. R.T. (Bob) WOODWARDS et à sa femme Claire: you've been there since the very beginning, and still remained close to me, as a trainee and a like a member of the family- please receive my deepest thoughts. Aux "grands frères" de chirurgie qui m'on appris toutes les bases et à avoir confiance en soi : les Drs G. CHIU et E. THOMSON, E. MAUEL, M. THOMA, F. CHATEAU, et J. NEBENDAHL. Au Prof. H. REYCHLER qui m'a beaucoup aidé dans mes choix. Au Prof. R. REDING qui m'a formé et soutenu dans mes idées de recherche. Je remercie sincèrement pour l'encadrement de ma formation de plasticien par le Prof. R. VANWIJCK et le Dr N. CALTEUX - veuillez trouver ici mon respect le plus sincère.

A l'équipe (de Rugby !) d'Amiens leur accueil et soutien dans le retour aux armes chirurgicales, pour leur compréhension et aide dans cette dernière ligne droite de rédaction : merci aux Prof. S. TESTELIN, Drs S. DAKPE, J. DAVROU et A. ALGRIN; et bien également à la fine équipe de mes co-internes Julien B, Agnès P, Nolwenn L, Eva B, Julien, Matthieu O et Pierre B (Papy) ! Une mention spéciale pour mon ami (et jeune patron !) le Dr J. BETTONI, le roi des poulets, avec qui c'est une joie de partager passions et projets d'avenir – merci pour ton accueil et ton cœur immense- je vous souhaite avec Laurine le meilleur avec l'arrivée prochaine de votre petit gars ! Je retrouverai avec grande joie l'équipe gantoise du Prof. P. BLONDEEL et mes collègues Casper S, Dries O, Bernard D, Edward deW, Bernd S et Fien D qui m'ont déjà réservé un bel accueil : de kleine franse kerel komt eraan!

Je remercie mes amis, Raja B, Tomache C et Nadia Y, Guillaume D et Eve D, Pascale C et Pierre V, Lorraine C et Olivier C, Séléna T et Bertrand H, Nadim H et Nathalie S, Mitch B, Geoffrey H, Thibaud G, Gugu K et Pierre, et aussi Charlotte deP et Chris N, Marie V et Mathieu G, Elodie H et Mickael C, Charlotte Q et Joseph Z – et sans oublier le cher Stefan A ;) eux qui m'ont trouvé nettement moins disponible ces dernières années, et restés néanmoins fidèles, j'espère qu'ils trouveront ici une explication ! Je pense également, à ces personnes chères qui se sont tues, comme disait le poète, et aux épreuves particulièrement difficiles pour certains cette année : permettez la pudeur de vous adresser ces quelques mots, qui recouvrent toute ma sympathie. A Papi et Grand-père, dont la mémoire est toujours vivante dans nos cœurs.

Au Prof G. MALQUARTI : mon cher Guillaume, mon cher parrain merci pour toute ton affection qui a été un vrai moteur. Tu as toujours été pour là pour me guider, me nourrir (!) et me soutenir. Je te dédie aussi ce travail.

Merci, ma chère Maman adorée pour ton amour et ton soutien indéfectible pendant toutes ces années. Merci Papa, toi qui m'a le premier inspiré et donné l'envie de grands desseins, toi qui a cru sans hésiter à cette nouvelle voie, je ne serai pas là sans cela. J'embrasse tendrement mes frères et sœurs Christophe, Carole et Quentin, et bien sûr Jonathan et Léa, ma belle-mère Fabienne, Bruno, Nicolas, Charles, petit Paul et mon neveu Alexandre. Merci à mes grands-parents pour leur soutien et leur foi, Mamie et Grand-Mère. A ma tante Marie-Claire et Yves. Je porte aussi la plus grand affection pour ma belle-famille: Rudy, Nadine, Nany, Mamou, Papou, Laurent et Laurawn, Jade et toi petit boy qui arrivera bientôt, Max, Tata Momo, Nineke, et bien sûr Chantale, Renaud, Audrey et Gaetan.

Ces derniers mots, ces dernières pensées, ce dernier effort d'écriture qui viennent parachever quatre années de labeur, et comme expliqué finalement bien au-delà, sont pour mon épouse Virginie et mes filles, Emma et Clara. Mais au-delà du plaisir d'avoir, enfin, le dernier mot (!), c'est de marquer tout ce qu'elles représentent : car quoi qu'il advienne du travail, des gardes, du bloc, du laboratoire, mes journées et ma vie commencent et finissent avec elles, tout comme ces messages personnels parsemés dans ce manuscrit ; une apanadiplose familiale qui s'est formée, pendant cet effort de thèse (bien productif !), par notre mariage, les naissances de Clara et d'Emma. Virginie, même si je peine souvent à l'admettre, je te dois tout ce que je suis, ce que j'ai fait de mieux dans cette presque moitié (soyons optimistes !) d'existence ; tu as été un soutien indéfectible pour tout : bien évidemment dans les aspects les plus matériels et organisationnels du quotidien, qu'il a souvent fallu adapter prenant énormément de charges en plus de ton travail exceptionnel de pédodontiste, mais surtout un guide dans la Raison, que de tels choix de vie peuvent facilement faire perdre. Je t'aime. A mes filles, mes omégas, mon grailloux, ma nénette, j'ai cherché longtemps un sens à cette existence : je réalise maintenant que j'aurai passé tout ce temps à vous chercher et vous attendre. Et maintenant vous êtes ce qu'il y a de plus heureux et de plus merveilleux dans celle-ci. Votre Papa qui vous aime infiniment… Et quand votre âge sera de raison, que dans la lecture de ces pages vous trouverez un peu de passion, puissiez-vous apprécier le travail de votre Papa et, je l'espère, en éprouver fierté et inspiration ; et me pardonner aussi, un peu, pour ce qui retient, parfois, mon temps, loin de vous.

Bruxelles, le 25 Décembre 2017.

« Un chercheur est celui qui risque sa vérité et qui se casse la figure. »

Michel Serres

Table of contents

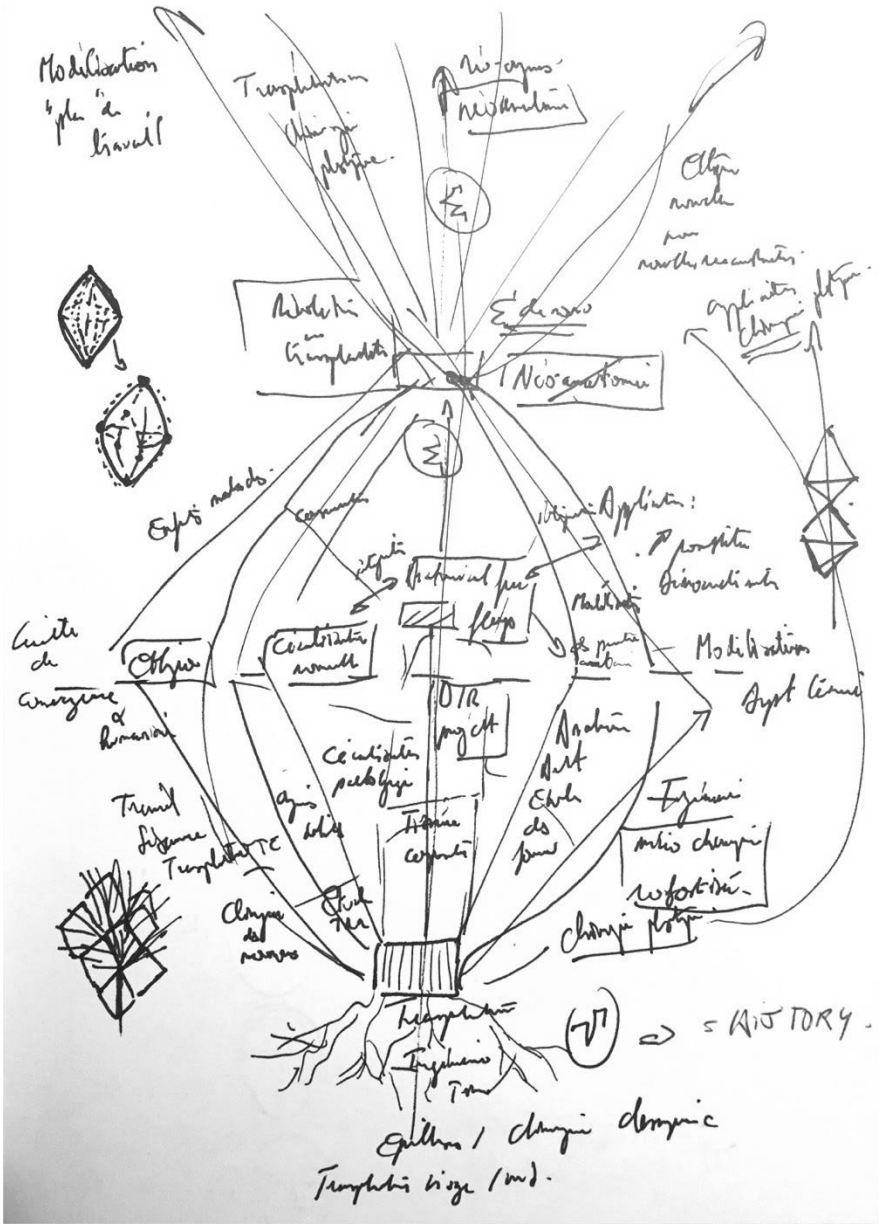

Author's notes (Barcelona, 1.9.2012)

List of principal abbreviations

AA: Angular Artery
ADM: Adipose Differentiating Medium
Agi-D: Agitation decellularization
ASC: Adipose-derived Stem Cells
BCA: Bicinchoninic Acid assay
BSA: Bovine Serum Albumin
CA: Columellar Artery
CAA: Caudal Auricular Artery
CAV: Caudal Auricular Vein
CCA: Common Carotid Artery
CM: Culture Medium
CSST: Cell-On-Scaffold-Seeding Technology
CT: Computed Tomography
CXCL: (C-X-C motif) Ligand
DAPI: 4'-6-diamidino-2-phenyl-indole
DIW: deionized water
DMAB: p-dimethylaminobenzaldehyde
DAB: 3,3'-diaminobenzidine
DFA: Distal Facial Artery
DMEM: Dulbecco's Modified Eagle Medium
ECA: External Carotid Artery
ECM: Extracellular Matrix
EJV: External Jugular Vein
EC: External Compartment
FACS: Fluorescent-Activated Cell Sorter
FA: Facial Artery
FAT: Face Allotransplantation
FB: Frontal Branch of superficial temporal artery
FBS: Fetal Bovine Serum
FF-ECM: Full Face scaffold
FF-G: Full Face Graft
GA: General Anesthesia
GAGs: Sulphated Glycosaminoglycans.
GIF: Graphics Interchange Format
GFP: Green Fluorescent Protein
GM-CSF: Granulocyte Macrophage Colony-Stimulating Factor
hASC: human Adipose-derived Stem Cells
HE-ECM: Human Ear scaffold
H&E: Hematoxylin and Eosin
IAA: Inferior Alar Artery
IC: Internal Compartment
IF: Immunofluorescence
IFN: Interferon
IG: Immunoglobulin
IHC: Immunohistochemistry
IJV: Internal Jugular Vein
IL: Interleukine
IS: Immunosuppression
ITA: Inferior Trochlear Artery
LNA: Lateral Nasal Artery
MAP: Mean Arterial Pressure
MB: Methylene Blue
MGH: Massachusetts General Hospital (miniature swine)
MIF: Macrophage migration Inhibitory Factor
MSC: Mesenchymal Stem Cells
MT: Masson's trichrome

MTT: (3-(4,5-Dimethylthiazol-2-yl)-2,5-Diphenyltetrazolium Bromide) tetrazolium reduction assay
PAA: Posterior Auricular Artery
PB: Parietal Branch of superficial temporal artery
PBMC: Peripheral Blood Mononucleated Cells
pBM-MSC: Porcine Bone Marrow Mesenchymal Stem Cells
PBS: Phosphate Buffer Saline
PCA: Peracetic Acid
PDR: Perfusion Decellularization/ Recellularization
PeaECM: Porcine ear acellular scaffold
Perf-D: Perfusion Decellularization
PG: Proteoglycans
PM: Proliferating Medium
POD: Postoperative Day
P/S: Penicillin/Streptomycin
RAA: Rostral Auricular Artery
RAF: Hemifacial rat grafts
RAF-ECM: Rat hemiface scaffold
rASC: Rat Adipose-derived Stem Cells
RAV: Rostral Auricular Vein
RM: Regenerative Medicine
RT: Room Temperature
SA: Septal Artery
SDF1: Stromal cell-Derived Factor 1
SDS: Sodium Dodecyl Sulfate
SEM: Scanning Electron Microscopy
SF-ECM: Segmental lower face scaffold
SF-G: Segmental lower face graft
SLA: Swine Leucocyte Antigen / Superior Labial Artery
STA: Superficial Temporal Artery
SOT: Solid Organ Transplantation
SVF: Stromal Vascular Fraction
TE: Tissue Engineering
TGF: Transforming Growth Factor
TNF: Tumor Necrosis Factor
TX100: Triton X-100
VC: Vascular compartment
VCA: Vascularized Composite tissue Allotransplantation
VCE: Vascularized Composite Tissue Engineering
VCT: Vascularized Composite Tissue
VEGF: Vascular Endothelial Growth Factor

Some useful definitions

- Vascularized Composite tissue Allotransplantation (VCA): stands for the transplantation of various complex (composite) tissues, including skin, subcutaneous fat, muscles, nerves, bones, and tendons, harvested from a donor and revascularized/reinnervated by microsurgical techniques.

- Allotransplantation: performed between genetically non-identical donor/recipient of the same species (another human).

- Isotransplantation: performed between genetically identical persons (i.e. twins).

- Xenotransplantation: performed by crossing species barrier (i.e. pig to human).

“Le véritable voyage de découverte ne consiste pas à chercher de nouveaux paysages, mais à avoir de nouveaux yeux.”

Marcel Proust

Summary

In the **first part** of this work we review, as a general introduction, the current surgical techniques and limitations of face vascularized composite tissue allotransplantation (VCA). The application of the latest organ tissue engineering (TE) techniques to face transplants is proposed as a potential breakthrough, in order to move forward the new frontiers of the field. Our original approach, called Vascularized Composite tissue Engineering (VCE), is based on a research plan in which the face is divided in two types of elementary morphological subunits. In the non-motor subunits, like the ear and the nose, the form is dominant and usually related to an intact cartilaginous framework. In the motor subunits, like the lips and the eyelids, the dominant functional tissue is the muscle. The first aim of this thesis was to subdivide the well-known face allografts in their elementary subunits and to set-up a reliable model of non-motor subunit in the large animal. The second step of our work was then to apply the same concepts of TE to various non-motor, motor and compound face and hand grafts from human cadaveric origin.

The **second part** of this work deals with the experimental studies.

The **first section** is dedicated to the study of the surgical models. In **chapter 1**, the human nose and lip graft variants are described as divisions of the original type I face transplant. Vascular refinements of the human ear transplant are then reported in **chapter 2**. Finally, a porcine ear model is cautiously studied in **chapter 3**, aiming to be used as the first model of face TE applications.

The **sections 2, 3 and 4** are dealing with experimental tissue engineering studies.

In **section 2** the topic is focused on TE applications to non-motor, cartilage-based, subunits: the porcine ear grafts (**chapter 4**) are successfully treated and demonstrate, after decellularization, a preserved extracellular matrix, a patent vascular tree, a complete allocompatibility with a semi-identical pig recipient; a partial recellularization is finally obtained in a bioreactor. These observations allowed a direct transposition of this model to a more advanced study using

cadaveric human ear grafts, as exposed in **chapter 5**; the positive outcomes demonstrate the possible use of grafts harvested from body donation cadavers for VCE experiments. However, the need to treat adipose tissue in a different way from porcine auricle was pointed out.

In **section 3,** we then moved to the association of non-motor subunits with motor subunits which remained to investigate. A preliminary study in the rat face graft model (**chapter 6**) allowed us to confirm its relevance for low-scale preclinical VCE benchwork. Then the ultimate goal of human face bioengineering (**chapter 7**) was investigated at a larger scale on partial and full-face allografts.

Section 4 is an application of both VCE and subunit approaches to human upper extremity, the finger graft subunit being extended to whole hand engineering (**chapter 8**). Actually, this graft was chosen as the simplest one to study a skeletal-based vascularized composite tissue. Therefore, the study explored more specifically the bone structure aspects, with an additional attention to the perfusion of these small volume subunits, easier to study than facial units, and to the use of specific bioreactors. This ongoing work will support the use of our original bioreactor, which was designed to isolate the external tegmental compartment from the deep tissues and to treat it separately during skin regeneration.

In the **last part**, we summarize the key lessons learnt from our experiments, defining and experiencing an original VCE approach. We then also discuss the major issues ahead, and the possibility to raise, in a next future, clinical applications based on our laboratory investigations.

« Un chirurgien, c'est un homme dont la pensée a dompté le geste. »

Philippe Dartevelle

Part I- Introduction: facial reconstructive techniques and bioengineering

1. State-of-the-art in facial reconstructive techniques

The face of need. Disfigurement can result from various origins: cancer, trauma, infection, resection of vascular malformations, burns or congenital deformities. In case of severe disfigurement, this condition is often associated with a poor quality of life and additional co-morbidities. Aiming to improve the patient's fate, missing facial tissues need to be replaced. In modern reconstructive surgery, three main options allow to reach this goal: alloplastic prosthesis, autologous tissue reconstruction, and allotransplantation [1, 2].

1.1 Facial prosthetics

The use of facial prostheses carved in wood or ivory is known since Antiquity. The true rise of maxillofacial prosthetics however occurred during the Renaissance period, under the impulsion of Petronius (1565) and of the famous French surgeon Ambroise Paré (XVIth century), who reported the use of several removable facial prostheses, especially for the rehabilitation of nose defects (**Figure 1**). Despite some progresses, mainly provided by Pierre Fauchard during the XVIIIth century and Claude Martin at the end of the XIXth century, the next critical evolution took place in the early XXth century, when many technical improvements were achieved, aiming to restore the facial appearance of soldiers suffering from severe gunshot injuries.

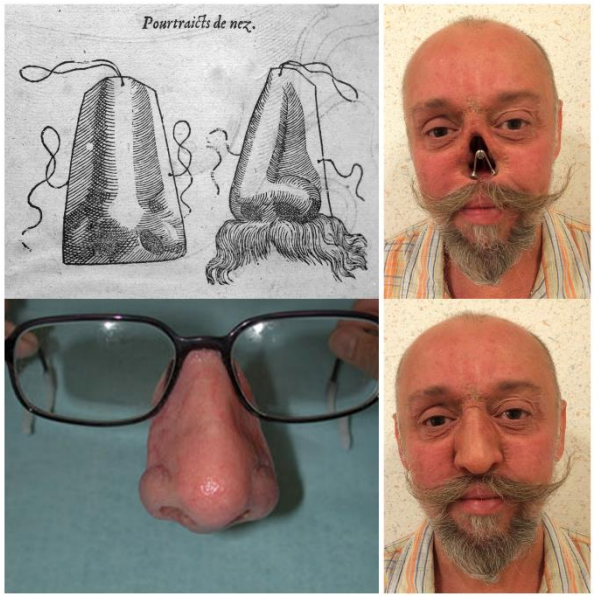

***Figure 1**: Nasal prosthesis fixed by threads as described by A. Paré in 1564 (upper left), then fixed on glasses till the XXth century (lower left, credits Société francophone de rehabilitation et prothèse maxillo-faciale); actual bone-anchored implants for stable episthesis after nose amputation (right).*

The ballistic trauma caused to the head and neck area were numerous and unmet at the time; they drove an important development of the field, with a dramatic evolution of techniques and materials used, highlighted by the work of Pont (1913), Ruppe (1917), Bubulian (1939) and Clark (1941). Rigid metallic prosthesis was progressively replaced by more pliable devices made of latex, resins and then silicone (Barnhart, 1960).

The last evolution came with the bone-anchored implants, as an outcome of the researches led by Albrektsson and Branemark about osseointegration [3], which resulted in a more stable, reliable and versatile fixation of the facial prosthesis on the underlying skeleton (**Figure 1**).

Modern facial prostheses provide excellent cosmetic results, with a true restoration of the exact missing morphology, but associated with two major issues: first, they are static, being inefficient to restore a motricity in the facial defect; second, the prostheses are removable artificial foreign bodies, which are never

psychologically accepted as a part of the body. Consequently, patients usually remain reluctant to accept them as reliable and definitive reconstruction, in the same manner as limb prostheses.

1.2 Autologous tissue reconstruction

In parallel to the development of facial prostheses, essentially driven by dentists, groups of surgeons started to work on the use of the patient's own tissues to repair the damaged body areas. This autologous tissue approach pioneered by Sir Harold Gillies, a famous plastic surgeon of the Great War, was correlated to better expectations in terms of functional recovery, durability and patient's acceptance.

Conventional approaches in plastic surgery by autologous tissue reconstruction actually consist in a transposition of the patient's own tissues in the defect to be reconstructed. According to the Gillies's principle "replace like with like", the tissue transfer is selected to match perfectly the missing tissue(s) of the defect and consists in tissue grafts or flaps, defined as following:

- A graft is a tissue that is detached from its original location and own blood supply and placed in a new area with a new blood supply. It can address both vascularized or non-vascularized tissues. For example, a skin graft, which is commonly used in burns reconstruction, depending on its thickness, consists in epidermis and varying amounts of dermis. The graft is revascularized by the newly formed blood vessels arising from the surrounding tissues of its new implantation site. Additionally, the term "graft" also regards more complex vascularized tissue transfer as in solid organ transplantation (SOT).
- A flap consists in any tissue that is retaining all or part of its original blood supply after the tissue has been harvested and then moved into the recipient defect location. Local flaps can be randomly vascularized by the neighboring dermal plexus. In loco-regional flaps (**Figure 2**), the flap blood supply originates from a proper vascular pedicle, including both an arterial inflow and a venous

outflow. The flap then rotates locally on this pedicle to reach and fill the defect to be restored. Furthermore, the flap can also be used at large distance of the tissue loss, by performing a microvascular transfer of its pedicle on recipient blood vessels, selected close to the defect area. The outset of free flaps in plastic surgery occurred as the result of the application of A. Carrel's principles about macrovascular sutures, [4] to smaller vessels of a reduced diameter of 1-3 mm. The first described microsurgical procedure was reported by Seidenberg [5], on a jejunal flap.

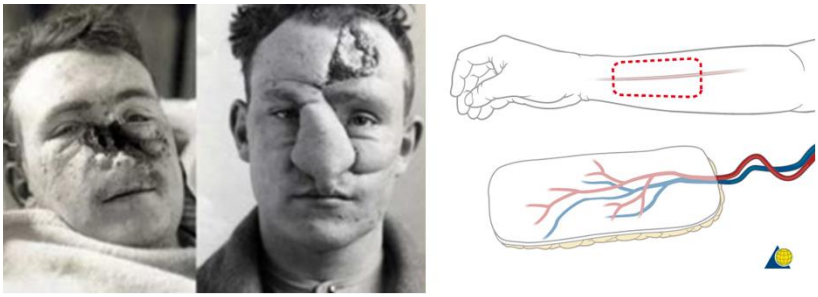

***Figure 2**: Forehead flap for nose reconstruction in WWI patient (left). Skin free flap (radial forearm) with arterial and venous pedicle (right, source: AO Surgery).*

Thereafter, many types of flaps have been described and classified, including skin flaps [6], pioneered by Ian Taylor, muscular [7] and musculo-cutaneous flaps, or bone and osteocutaneous flaps. Nowadays, the vast majority of autologous soft tissue reconstructions are performed with selective perforator flaps, selectively harvested on perforating blood vessels supplying fat and skin, in an attempt to reduce the donor site morbidity.

Advantages and limitations. Pedicled or free autologous flaps remain of major importance in modern reconstructive surgery. However, their always result in various degrees of donor sites morbidities, and sometimes fail to provide valuable options to address highly complex situations like those met in severe disfigurement (**Figure 3**), or when a single anatomical subunit of the face is missing, like a nose, a cheek, or one upper or lower lip; conventional autologous tissue reconstruction techniques allow most of the time to reach at least an acceptable cosmetic and functional restoration of the damaged face. But when two or more adjacent facial

anatomical subunits have been lost or involved, like in a tumor process, autologous tissue transfer are unable to deliver optimal results in a single stage procedure.

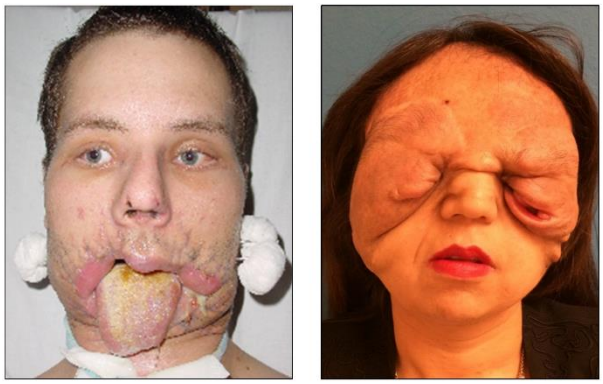

***Figure 3**: Severe disfigurements escaping the restorative potential of conventional reconstructive techniques.*

For these patients, the first face allotransplantation (FAT) [8,9] represented a true breakthrough, with unmet cosmetic and functional results.

1.3 Face vascularized composite tissue allotransplantation (VCA)

In 2005, the first face transplantation, a partial naso-bilabial graft, was performed on Isabelle Dinoire [8,9] who received a custom-made lower face allograft including the distal nose, both lips, the chin and medial cheek areas (**Figure 4**).

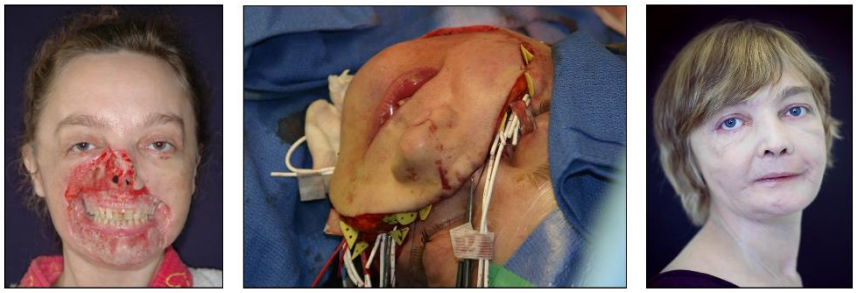

***Figure 4**: First face transplant. The patient exhibited a lower face segmental nose-lips chin defect (left); her face allograft was designed to match exactly the missing tissues (middle), and delivered an unpreceded cosmetic and functional restoration of the damaged face (right, from Devauchelle et al [9,10]).*

The main indication was supported by a functional bilabial defect, nearly impossible to restore by any other conventional technique in this critical region of the face [11]. FAT took its roots from the first successful unilateral hand VCA, performed in 1998 [12], but also from the major progresses achieved in the field of immunosuppression (IS) in SOT. But on contrary to hand VCA, for which the surgical techniques were inherited for a long time ago, from a large retrospective experienced based on autologous replantations, for the face, the anatomo-surgical techniques and the strategic concepts themselves had to be developed and created *de novo* [10]. This basic research brought many radically new progresses in treating severe disfigurement, improving dramatically the quality of life of transplanted patients. The evolution of face VCA in the following decade (2005-2015) was then essentially surgical, aiming to increase the surface and volume of transplanted tissues from partial to full face grafts [13], then to include a more or less extensive donor bone infrastructure in the recipient's face. However, the clinical development of FAT still remained limited in terms of number of treated patients. Actually, and despite the surgical refinement, only 39 cases indeed have been described worldwide so far [14]. This limitation relies on three main causes:

1- The need for an immunosuppressive treatment and its related complications, especially for a non-vital organ, are narrowing the really legitimate indications of FAT. Furthermore, these risks and side effects raise severe contraindications of FAT for large defects resulting from cancer removal or for defects involving a single facial unit. Actually, the first case of scalp/ear VCA [15] for a melanoma resulted in rapid patient's death: IS increases dramatically cancer recurrence and mortality. For similar reasons, FAT raises a lot of medical and ethical concerns in pediatric patients. At the present time children are still not eligible for face VCA [14], although an inaugural case of bilateral hand VCA has been reported in a pediatric patient [16]. In burns, experience has shown difficult outcomes due to immunization secondary to multiple transfusions and skin grafting procedures, but also to the chronic multibacterial colonization of the recipient's patient. Blindness remain a relative contraindication for cognitive functional rehabilitation process, which needs a vision input to the brain.

2- The limited graft survival [17-19]. Ten years after transplantation, indeed, Isabelle Dinoire presented an antibody-mediated rejection of her graft, with obvious signs of histological vasculopathy, resistant to rescuing any protocol, which resulted in a dramatic partial graft loss, involving the lower lip and the right cheek [18]. (**Figure 5**).

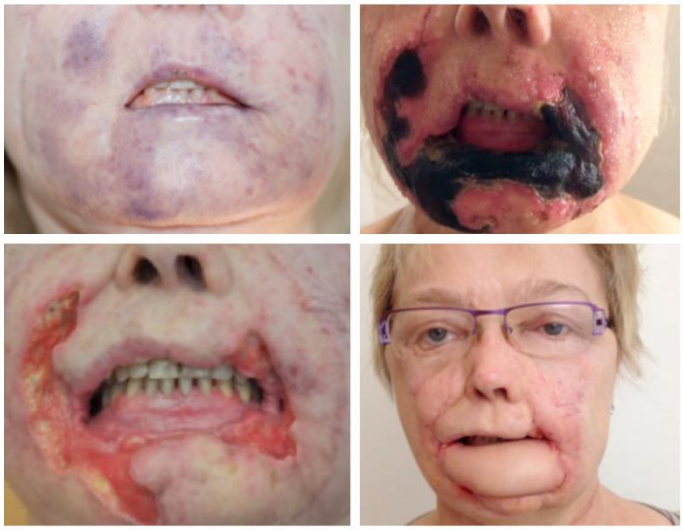

***Figure 5**: Humoral chronic rejection of the first face graft. On the lips and cheeks first signs appear as cyanotic patchy skin areas (upper left), which are followed by full-thickness necrosis (upper right) and complete loss of the lower lip and partial right cheek (lower left), which required a conventional reconstruction with an autologous forearm free flap (lower right; from Morelon et al. [18]).*

This natural evolution of the first face transplant follows the overall lifespan of any composite tissue allograft should be estimated to about a decade. The loss, even partial, of a face graft is a painful event for patients and surgical teams; it also motivates dramatically the need for further research, aiming to overcome the failures and side effects of IS or to develop new strategies to bypass this.

3- Lack of adequate donors: the limited number of donors affects VCA in the same way as for SOT. But in addition to conventional compatibility ABO match criteria, the donor face has to fulfill a morphological similitude, including several factors as perfect skin color and texture match (ethnicity), same gender and similar range of age.

Finally, despite numerous ingenious strategies developed in the field of tolerance-induction [20,21], the holy grail of IS-free transplantation has not been reached yet, even in SOT.

Consequently, even dealing with the most recent and promising approaches in severe disfigurement, we currently fail to reach the ideal reconstructive objectives:

- Achieve a one-stage optimal restoration of the recipient's morphology, identity and function.
- Avoid mutilations inflicted to the recipient, like IS treatment in allotransplantation or donor site morbidity in autologous reconstruction.
- Avoid significant mutilation of the donor in case of VCA procurement.

As a first and exclusive rule, the defect restoration of the recipient should be limited to the original missing tissues, because any healthy tissue discarded from the face to increase the surface of the graft will be definitely lost and thus critically lacking for a patient, in the case of chronic rejection and with partial or whole graft failure.

As a matter of fact, and in order to move forward in the field, it was needed to search for alternative strategies to apply the Gillies "Replace like with like" principle, to a new original pathway of IS-free, secondary morbidity-free and custom-made reconstruction. To reach this goal, Tissue Engineering and Regenerative Medicine raise new hopes.

2. Tissue engineering of tissues and organs

Creating on demand and custom-made body parts is the ultimate target of reconstructive surgery.

2.1. Definition and principles

Regenerative Medicine (RM) is the field in health sciences that aims to replace or regenerate human cells, tissues, or organs in order to restore or establish normal functions. The process of regenerating body parts can occur *in vivo* or *ex vivo* and may require cells, natural or artificial scaffolding materials, growth factors, gene manipulation, or combinations of all the above-mentioned elements [22]. RM is often related to the strict ability of tissues and organs to regenerate, like the liver in the human body or like limb in some lower animal species, which can spontaneously regrow after proximal or distal amputation (**Figure 6**).

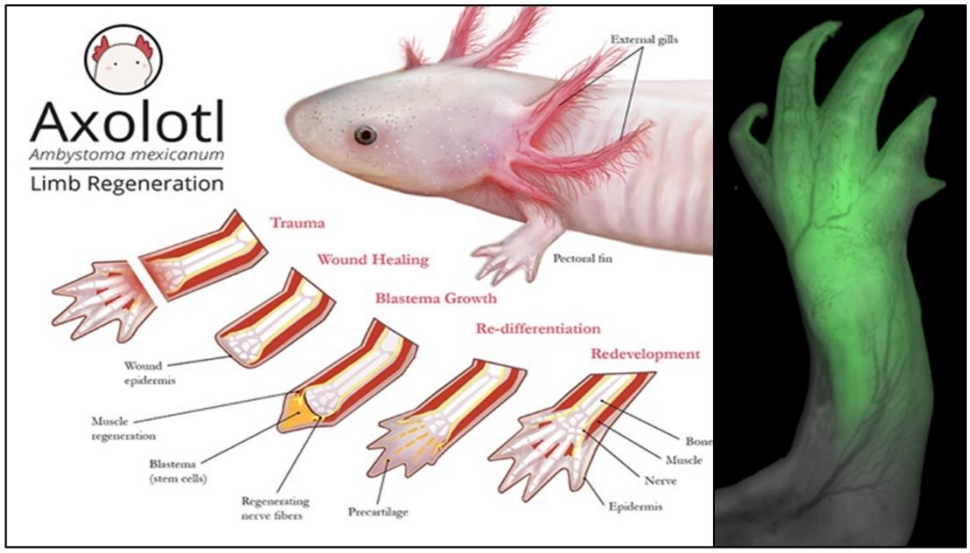

Figure 6: *Axolotl limb regeneration phenomenon (left, credits Julia Moore) and associated cellular migration (right, from McCusker et al* [23]).

This ability results from an evolutionary balance between healing repair and regeneration. The more the species is complex, the less it will allow regeneration (**Figure 7**), like in humans. By consequence, to replace body parts, we must fabricate them, through an approach called Tissue Engineering (TE).

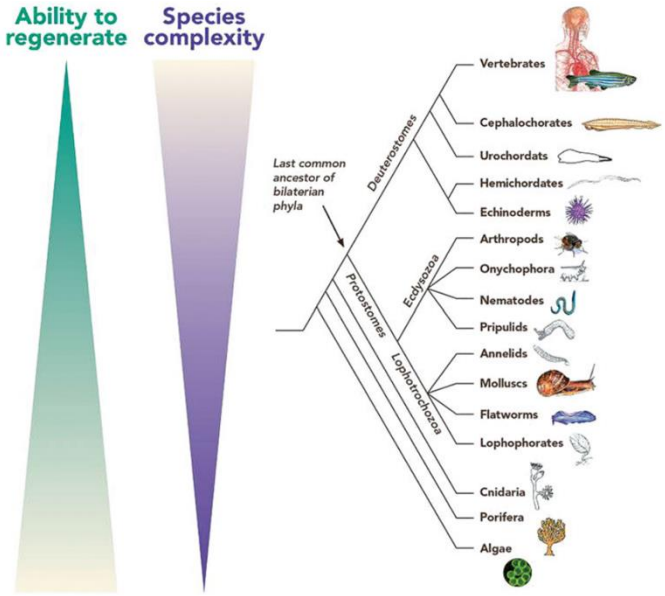

***Figure 7**: Complexity and regeneration abilities in species, from Orlando et al.* [24]

In this field of RM, TE is the more specific strategy to create *de novo* and *ex vivo* artificial and functional tissues or organs. TE was first described by Langer and Vacanti [25] in 1993, and defined as "*an interdisciplinary field that applies the principles of engineering and life sciences toward the development of biological substitutes that restore, maintain, or improve [Biological tissue] function or a whole organ*". In TE techniques, a biomaterial often called "matrix" or "scaffold" acts as a support to seed cells that will grow a new tissue or organ (**Figure 8**). The ability for cells to build on their own an entire and complex matrix is often limited, even for pluripotent stem cells, contrary to a popular thinking. That is why TE research strategies are built on two different types of approaches:

- Cells alone, like for example in bone tissue engineering [26].
- Matrix and cells, in which a scaffold is fabricated or extracted to be combined with cells [27].

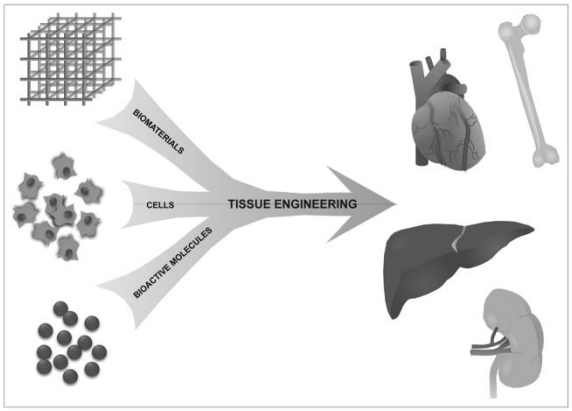

***Figure 8**: The organ-level tissue engineering paradigm, from Rustad et al.*[27]

Actually, two types of scaffolds can be used:

- **Synthetic**: often produced by polymers [28], they are obtained by 3D-printing, electro-spinning, or other synthesis techniques [29,30], to serve as an artificial biological cell support.
- **Natural**: **the extracellular matrix (ECM)** is extracted from the tissues of interest, using a technique called "decellularization". The so obtained ECM scaffold is an ideal biomaterial, bringing altogether in their natural and structural relationships, a wide diversity of biological structures, that cannot be (re-)produced at the present time by synthesis technologies, in a close respect of the Nature's genius.

2.2 Current tissue engineering approaches to the face: state of the art and limitations

The emblematic inaugural attempts to achieve human body parts engineering were originally dedicated to the ear, studied in a murine model and known as "the Vacanti mouse" (**Figure 9, left**). But the current clinical applicability of this seducing concept remained devoid of any potential clinical applications for decades because of:

***Figure 9**: Example of previous attempts in ear engineering: the "Vacanti mouse" (left, credits J. Vacanti); bioprinted synthetic ear cartilage model (middle, credits A. Seifalian); ear cartilage implant combined with conventional radial forearm free flap (credits Guo Shuzhong et al).*

- The created cartilaginous framework implanted on the back of the mouse had **no own transplantable vasculature and pedicle**. Of course, the cartilage construct can thereafter be implanted under a selected site of the recipient, in order to become revascularized by the pedicle of conventional autologous tissue flap. But this strategy, like in flap prefabrication, has been demonstrated by clinical experience to lead to very poor cosmetic outcomes. Furthermore, this additional surgical procedure represents a step back to conventional techniques, with all the drawbacks of their limitations and morbidities.
- The synthetic scaffolds basically lack the multi-tissue dimension and the 3D-complexity of a native composite tissue.
- The implanted tissues are still recognized by the recipient organism as **foreign bodies**, which are rejected or at least resorbed.

Thus, currently the best clinical results of engineering techniques in face reconstruction are those using bioengineered cartilage, as a single and non-vascularized construct layer, but still requiring to be associated with the use of coverage flaps, acting as mandatory vascular carriers [31] (**Figure 10**).

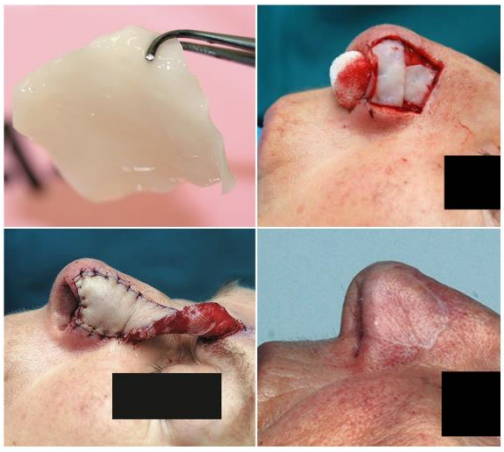

***Figure 10**: Engineered cartilage for nasal ala reconstruction, from Fulco et al.* [31]

2.3 The Extracellular Matrix

The extracellular matrix (ECM) is an assembly of complex molecules, supporting the cells, providing the 3D-specific architecture of the connective tissue. Actually, the true nature of any tissue is depending on its ECM, not only as a simple cell-supporting role, but a major component on its own with various functional properties. Its current definition, meaning literally "what is outside of cells", remains thus purely descriptive and poorly relevant of its multiple functions. The alternative terms of "matrix" or "scaffold" are also commonly used. Therefore, like in civil engineering, ECM acts as a building scaffold, like a building which is populated by living cells.

The ECM however endorses numerous functions: 1) A structural role, by maintaining the tissue architecture, supporting the cells and providing homeostasis. 2) A physical role, by its fibrillar and biochemical composition. 3) A signaling role, acting on cell differentiation, proliferation and adhesion, by the means of numerous small proteins like cytokines and growth factors, attracted to the connective fibers ; this role is fundamental in tissue engineering [32]. Among all tissues, bone ECM is the only tissue strong enough, due to mineralization, to resist naturally to the proteolytic effect of enzymes released at time of cell necrosis.

ECM composition. Basically, ECM molecules consist of three types of components:
1- Fibers, like collagen which is the most abundant macromolecule in connective tissues, or elastin which role is fundamental for mechanical properties.
2- Glycoproteins, like laminin, polysaccharides, including proteoglycans (PGs) and glycosaminoglycans (GAGs). GAGs, also called mucopolysaccharides, are highly polar and attract water, forming a hydrated gel. They represent the major part of the ECM volume and allow resistance to compression stresses; the aqueous micro-environment they create around cells allows diffusion of nutrients, hormones and other molecules from the medium to the cells or from them [33].
3- Growth factors and cytokines, molecules which play a prominent role in cellular differentiation, proliferation and adhesion, through the activation of tyrosine-kinase receptors, inflammation and *in vivo* remodeling.

2.4 Decellularization of living tissues

2.4.1. General principles

The decellularization technique consists in stripping off cells from a donor tissue or organ, in order to remove the immunogenicity from the native tissue (**Figure 11**). It is obtained by cell lysis and/or detachment. Thereafter, an important rinsing is proceeded, to eliminate cell debris and the remaining decellularizing agents. Theoretically, this process leaves an intact, acellular, tridimensional and biocompatible ECM which still contains its associated molecules, including growth factors. Thereafter, the ECM can be seeded and thus repopulated with new cells (recellularized), arising from the recipient.
The objective of this recellularization step is then to regenerate an allogeneic or xenogeneic tissue with the patient's own cells. However, the matrix is usually altered by such an aggressive treatment: **the choice in decellularizing solutions and protocols is then always the result of a compromise, in the balance between the efficiency of cell removal and the ECM preservation.**

***Figure 11**: The decellularization/recellularization principle. Native tissue with cells (red), growth factors (green) and extracellular matrix fibers (brown), left; decellularized aspect after cell removal (middle); recellularized tissue with new cells (blue), right. From "Regenerative Medicine Applications in Organ Transplantation" book, G. Orlando editor.*

Brent Bijonowski et al. [34] stated that the decellularization efficiency depends on the type of cells in the tissue, as well as the ECM composition and structure. Depending on the matrix density and thickness, on the perfusion solution (detergent versus non-detergent) and the modality (continuous or intermittent) of perfusion, the outcomes of the process will change significantly. Consequently, it is often required to mix several techniques in order to improve the process efficiency. The first decellularized tissues were quite simple, like bone and skin. Then the technique was extended to other monotissular anatomical frameworks like heart valves [35], in allo- or xeno-approaches. Finally, it was thereafter applied to more complex organs in a new perfusion approach, further described in this manuscript.

Decellularization methodologies. Many possible techniques and agents have been reported. Three main methods are described [36] : physical (i.e. freezing/thawing, hypo-/hypertonic solutions), chemical (i.e. detergent, acid/base, alcohol) and enzymatic (i.e. nuclease, trypsin, collagenase, lipase). The different techniques are listed and compared in the table below (**Figure 12**).

Method	Mode of action	Effects on ECM
Physical		
Snap freezing	Intracellular ice crystals disrupt cell membrane	ECM can be disrupted or fractured during rapid freezing
Mechanical force	Pressure can burst cells and tissue removal eliminates cells	Mechanical force can cause damage to ECM
Mechanical agitation	Can cause cell lysis, but more commonly used to facilitate chemical exposure and cellular material removal	Aggressive agitation or sonication can disrupt ECM as the cellular material is removed
Chemical		
Alkaline; acid	Solubilizes cytoplasmic components of cells; disrupts nucleic acids	Removes GAGs
Non-ionic detergents		
Triton X-100	Disrupts lipid–lipid and lipid–protein interactions, while leaving protein–protein interactions intact	Mixed results; efficiency dependent on tissue, removes GAGs
Ionic detergents		
Sodium dodecyl sulfate (SDS)	Solubilize cytoplasmic and nuclear cellular membranes; tend to denature proteins	Removes nuclear remnants and cytoplasmic proteins; tends to disrupt native tissue structure, remove GAGs and damage collagen
Sodium deoxycholate		More disruptive to tissue structure than SDS
Triton X-200		Yielded efficient cell removal when used with zwitterionic detergents
Zwitterionic detergents		
CHAPS	Exhibit properties of non-ionic and ionic detergents	Efficient cell removal with ECM disruption similar to that of Triton X-100
Sulfobetaine-10 and -16 (SB-10, SB-16)		Yielded cell removal and mild ECM disruption with Triton X-200
Tri(*n*-butyl)phosphate	Organic solvent that disrupts protein–protein interactions	Variable cell removal; loss of collagen content, although effect on mechanical properties was minimal
Hypotonic and hypertonic solutions	Cell lysis by osmotic shock	Efficient for cell lysis, but does not effectively remove the cellular remnants
EDTA, EGTA	Chelating agents that bind divalent metallic ions, thereby disrupting cell adhesion to ECM	No isolated exposure, typically used with enzymatic methods (e.g., trypsin)
Enzymatic		
Trypsin	Cleaves peptide bonds on the C-side of Arg and Lys	Prolonged exposure can disrupt ECM structure, removes laminin, fibronectin, elastin, and GAGs
Endonucleases	Catalyze the hydrolysis of the interior bonds of ribonucleotide and deoxyribonucleotide chains	Difficult to remove from the tissue and could invoke an immune response
Exonucleases	Catalyze the hydrolysis of the terminal bonds of ribonucleotide and deoxyribonucleotide chains	

***Figure 12**: Main decellularizing agents and properties, from Gilbert et al.* [36]

Each decellularization technique has its own advantages and drawbacks, with a different effect on different tissue types. For example, Sodium Dodecyl Sulfate (SDS), the most commonly used ionic detergent, will be very efficient to treat several tissue types, resulting in a significant depletion of cytokines in the decellularized ECM. Moreover, SDS exhibits a high toxicity and needs to be fully removed with caution from the ECM, in order to avoid a long-term cell exposure to the toxic remnants in the constructs, leading cells to follow a potential oncogenic fate.

ECM analysis criteria. The maintenance of the ECM integrity is achieved through its structural proteins preservation, both in quantity and spatial distribution. The optimal decellularization protocol results from the balance between removing cells and preserving the ECM: not reaching the first objective could impair the immunological stability of the scaffold and lead to an immune reaction and its destruction; on the other hand, achieving a complete cellular depletion at the price of a significant ECM alteration could restrain new cells to correctly repopulate the scaffold and, by the way, also impair their capacity to restore functional tissues.
The quality of produced ECM is commonly assessed with the following qualitative and quantitative analysis criteria:

1- Cell removal

- Hematoxylin and eosin (H&E) and 4'-6-diamidino-2-phenyl-indole (DAPI) stainings.
- DNA quantification (<50 ng/mg dry weight tissue*)*. DNA length: less than 200 pairs of bases.

2- ECM preservation

- Structure: conventional and special histology; mechanical testings.
- Composition: ECM structural proteins (collagen, GAGs, elastin) and cytokines quantification.

3- Cell compatibility (*in vitro*): static disc cell seeding. The objective of these testings is to assess, *in vitro*, the absence of ECM toxicity for cells: in a short term (viability, proliferation), and in the long term (differentiation, phenotype modification i.e. oncogenicity). These experiments however may not be considered a true recellularization step, as the cells, despite some migration, will need an active multidirectional seeding from the depth to fully migrate in the ECM. This deep seeding is especially mandatory for a dense ECM, with a high collagen content, like in dermis.

4- Ability to be recellularized. This advanced experimental step corresponds to a true repopulation of the scaffold with new cells. The process and the use of a bioreactor to achieve it will be further developed in the next chapter.

5- Biocompatibility *(in vivo)*: it is assessed by scaffold implantation into a living recipient. This ultimate experimental procedure acts as a comprehensive step to validate scaffold integration as a biomaterial, as well as its allogenicity.

2.4.2. Perfusion-decellularization/recellularization technique

The conventional decellularization techniques, as explained above for simple tissues, use stirring baths of solutions, changed regularly. The drawback of this technique is the limited tissue penetration of the decellularizing agents, narrowing the applications to simple, small and thin tissues. In order to overcome this limitation, the whole-organ perfusion-decellularization/recellularization (PDR) technique was developed: Harald Ott and Doris Taylor first described PDR on model designed for rat whole heart bioengineering [37] (**Figure 13**). In this application, the decellularizing agents are directly perfused through the arterial pedicle, with a peristaltic pump, allowing to **generate a complex ECM** with an **accessible vascular tree** (**Figure 14**). Access to the vascular tree will indeed ensure a proper distribution of decellularizing solutions, an entrance for vascular seeding at the time of recellularization, and finally sustain the regenerated graft after *in vivo* vascular implantation.
Since then, the technology has been extended to many visceral organs, like kidney [38-40], liver [41], lung [42], intestine [43] and pancreas [44].

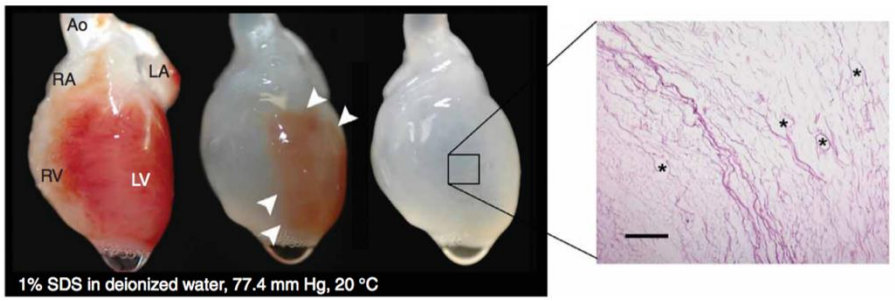

***Figure 13**: Rat heart perfusion-decellularization, from Ott et al.* [37]

The true recellularization process of a complex tissue or organ is, at the opposite of the passive seeding bi-dimensional experiment, a complex active and tri-dimensional procedure aiming at adequate cell engraftment within the scaffold. It is achieved by the mean of bioreactors.

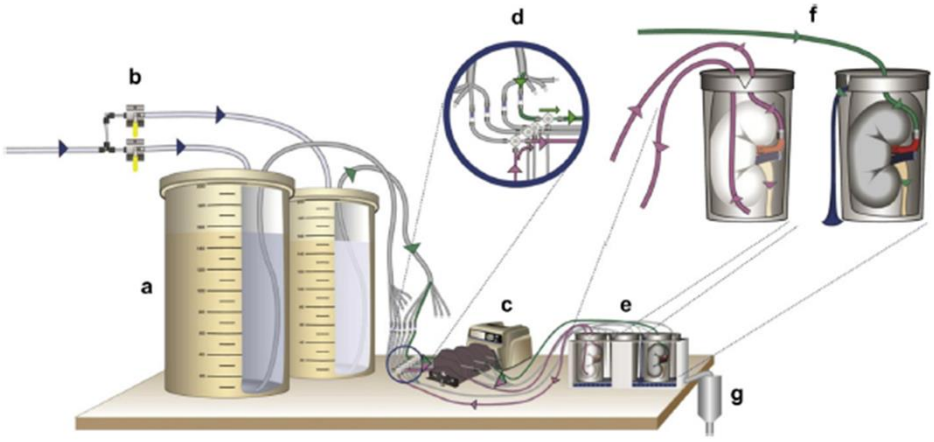

***Figure 14**: Schematic drawing of a perfusion-decellularization platform. From Sullivan et al.* [45]

A **bioreactor** is defined as biomedical device for biological culture, reproducing specific and active micro-environmental conditions to influence cellular engraftment, proliferation and eventually differentiation in the previously obtained ECM. In the experimental set up of a perfusion-bioreactor, the device should allow to reproduce the optimal culture conditions and to orientate properly the 3D-distribution of seeding cells depending on its pathway, on variations of

perfusion pressure, on the culture duration, and on the type of infused cells. The bioreactor can be used for purely *in vitro* applications, like for example mimicking a true 3D biological environment in order to study cancer cells spreading and behavior, as an alternative to *in vivo* animal experiments. But it can also be the mandatory *in vitro* step to prepare a recellularized scaffold for it secondary *in vivo* replantation.

Actually, two main types of bioreactors exist [34]:

- Non-perfused bioreactors ensure the dynamic seeding of a tissue without the use of its intrinsic vasculature. Nevertheless, they recreate specific culture conditions, using specific means to induce an appropriate cell differentiation and /or engraftment. As examples, we can cite: cartilage bioreactor with medium flow to enhance chondrocytes engraftment [46]; muscle bioreactor, including mechanical and/or electrical stimulation, in order to enhance muscular differentiation and proper fibers orientation [47].
- Perfused bioreactors, also called perfusion-bioreactor, in which the vascular (arterial) pedicle is connected to a sterile tubing, like for decellularization, and the vasculature perfused with culture medium and possibly used to seed cells (**Figure 15**).

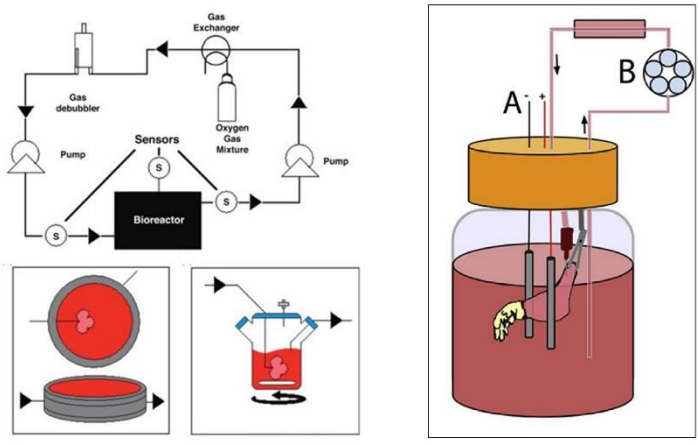

***Figure 15**: General perfusion-bioreactor layout and design (left, from Bijonowski et al [34]); limb bioreactor with electrical stimulation and specific of muscles (right, from Jank et al [48]).*

In the bioreactor, several cell-seeding pathways have to be considered according to the ECM tissue to be regenerated and its layer location. We then distinguish:

- Topical seeding: cells are deposited on the scaffold's surface, like in the static disc-seeding strategies. As the cell migration is limited, this method is mostly suitable for epithelial regeneration, like for example the restoration of a skin surface or a mucosal lining.
- Vascular seeding: this way allows the infusion of cells along the vascular tree, either to repopulate a deep parenchyma or to seed the vascular tree itself. This is also the one used to perfuse culture medium, mandatory to preserve the viability of a large and complex engineered construct.
- Needle-injection seeding: specific clusters of cells are injected in targeted scaffold areas, through repeated needle injections.
- Local cell migration seeding: cells migrate from the recipient's surrounding tissues and invade progressively the ECM. This may occur after *in vivo* implantation of the scaffold, the recipient's body then becoming its own bioreactor. Of course, this phenomenon requires a section contact between the recipient and the scaffold, as seen for composite tissues and not for organs.

2.5 Application to vascularized composite grafts: face and hand

The strategy in PDR is to change the current allotransplantation paradigm, with the introduction of an *in vitro* step between organ or tissue procurement and implantation (**Figure 16**). This additional step is aiming to regenerate the organ with the patient's own cells, and to achieve IS-free transplantation. Basically at the complete opposite of the concepts underlying other approaches like tolerance induction [20,49-52], the ultimate PDR strategy is targeted on the new paradigm that the graft must be modified to become compatible with the recipient, but the patient does not become tolerant to his graft. We hypothesized that PDR technology could be applied to a human face or hand graft, considered as an organ with its own vascular pedicle, and then address at the same time the two main

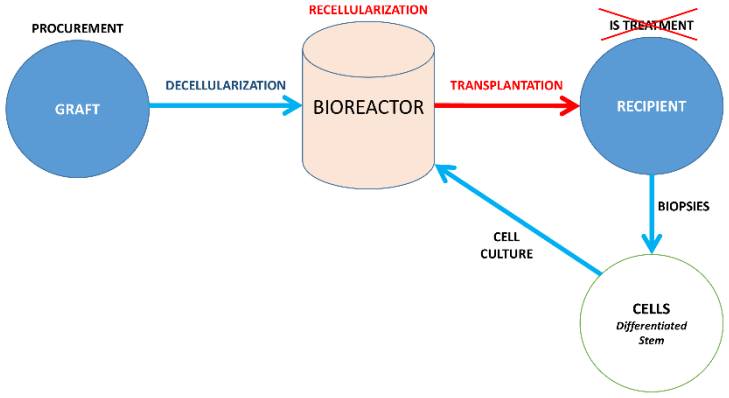

***Figure 16**: General scheme of tissue engineering steps: a change in transplantation paradigm by adding an in vitro step between the donor and the recipient.*

issues of VCA: the lack of donors and the need for lifelong IS; another goal was to push forward the frontiers of tissue engineering, trying to create more complex scaffolds, including a wide variety of structural supporting or functional tissues, with an accessible vascular tree. We called this new approach, branching from the VCA pathway, **Vascularized Composite tissue Engineering (VCE)**.

2.5.1. Considerations and challenges in face engineering

A face graft is a very particular transplant. When compared with a solid organ transplant, indeed the main differences are:

- **A complex pedicle**. The vascular pedicle consists of several main arterial stems (facial and superficial arteries on both sides), with their venous counterparts. Furthermore, the sensory (V_1, V_2 and V_3) and motor (VII) nerves in the pedicle and this anatomical disposition are a unique feature compared to organs. As demonstrated by the clinical experience, the inclusion of sensory and motor nerves in the transplant and their anastomosis with the corresponding branches of the recipient patient are critical for the functional success of the transplantations and for the reintegration of the face graft in the recipient's cortical body scheme, through brain plasticity [9].

- **Perfusion**. The facial framework is very different from a solid organ like a kidney, designed to be highly perfused. Compared to a similar parenchymal volume, indeed the facial pedicle is smaller than the renal one, and the relative vascular density is much lower in composite tissues. The skin perfusion physiology and regulation, being more peripheral than organs, are also very sensitive to environment. The renal blood flow receives about 20-25% of cardiac output, corresponding to 1 L/min/150g in a 70-kg adult male. The skin blood flow is 70 ml/min/100g.

- **A discontinuity of the parenchyma and the absence of a true capsule**. Elevated from the surrounding soft and hard tissues, a face graft exhibits a large surface of section, which needs a specific control and management, in a permanent "split organ" strategy, like in liver surgery. Contrary to organs, with a complete capsule and unique well-defined pedicle, the face allograft is a versatile tissue transfer, tailored on demand, harvested on variable vascular and nervous pedicles and showing along its deep aspect a more or less extensive discontinuous surface supposed to adhere and to create new vascular connections with the recipient's bed. The outcomes of several VCAs however seem to show that, despite this larger surface of contact, naturally prone to promote the delay of the graft on the recipient site, the transfer remains critically dependent on its original vascular pedicle.

- **The high tissue heterogeneity of the face as a composite tissue graft, and its extraordinary complexity**. The face, indeed, contains many tissue types, such as skin, fat, muscle, cartilage, bone, vessels and nerves (**Figure 17**). Among the face, all these tissues are organized as serial layers, each layer bearing specific lining, supporting or motor functions to be restored. Considering this aspect, face is really close to an organ like the heart, for which function restoration is closely related to the successful preservation of structural and mechanical properties.

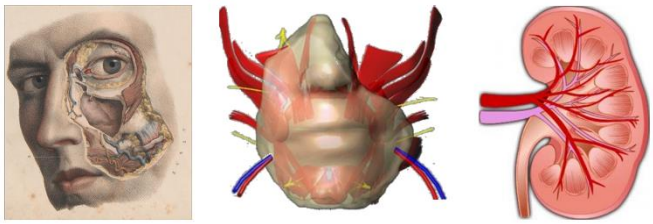

***Figure 17**: Comparison between a face allograft and a kidney transplant: harvested from the highly complex anatomical framework of the face (left, from Bourgery's anatomical book), the facial VCA is tailored on demand to match the defect to be restored. It includes several tissues for lining, support and motor function, supplied by a complex open network of small blood vessels and nerves (middle, credit B. Devauchelle); the kidney on the contrary has a single large pedicle, supplying generously a uniform parenchyma enclosed in a continuous capsule (right).*

- **Face, like hands, is always visible.** Therefore, the optimal morphological integration of the graft into the host is part of the transplantation success. Donor skin and hair match with recipient's surrounding tissues is critical indeed for the cosmetic outcomes of the operation. Consequently, the need to restore a perfect static and dynamic harmony between the donor tissues of the graft and the surrounding tissues of the recipient's defect results in adding morphological extra-criteria for donor selection (same gender, same range of age, same skin color and texture, similar face contour if bone reconstruction is required). Regarding these last requirements, the identity-bearing nature of the face explains the narrowing of the potential donor list, knowing as well that, on contrary to some SOT, there is no place for living donor donation.

- **The lack of xenotransplantation strategies**. Xenografts are very possible options for isolated tissues like dermis or bone, or solid organs. Due to the fact that human composite body parts like nose, ear, lip, breast, thorax, genitalia, finger or hand exhibit a strong morphology at this scale which is species-specific, then xenotransplantation is never an option for these anatomical subunits.

- **VCA are non-vital organs**. Therefore, even with a highly impaired quality of life, the cost-benefit balance of face transplantation had to be considered in respect with the side effects and life-threatening risks of IS. Consequently, the absolute need of IS in VCA results in a very important restriction of indications, narrowing the selection criteria to large facial defects, with functional or

palpebral impairment, from non-cancer origin, in healthy patients, neither elderly nor pediatric.

The main challenges of VCE compared to SOT tissue engineering are:

- The **absence of tissue selectivity with perfusion**, thus requiring to find very **versatile decellularization perfusion protocols**, to treat all very different tissues at once.
- The **complexity of recellularization,** due to the multiple cell types to be seeded and the very various tissue functions to be restored, both *in vitro* and/or *in vivo*.

2.5.2. State-of-the-art in composite tissues decellularization/ recellularization

The list below is summarizing the most relevant publications about PDR applied to composite tissues, found in a review of the current literature. In this enumeration, the distinction has been made between:

- The type of tissues involved: is the tissue unique or associated? And, if composite, in which association with contiguous tissue layers? Due to the very important spectrum of possible tissue associations, indeed the two main questions to address in composite tissue engineering are **"what do we have to decellularize?"** and **"how do we perform thereafter the planning of multi-tissue analysis?"**. The type amount and the various type of tissues involved in the process have indeed a direct impact on both the decellularization treatment and, later on, on the recellularization/transplantation strategies according to the functions to restore. By convention, the layer classification is always achieved from skin to deepest aspect in a skin-related graft.
- The type of decellularization/recellularization pathway: through a pedicle for vascularized (V) tissues, or with through simple impregnation/immersion methods for non-vascularized (NV) tissues.

Elementary tissue (mono-tissular)

- **Skin**: (V) [53]***** – (NV) [54].
- **Mucosa:** (V) No – (NV) No.
- **Adipose tissue:** (V) No – (NV) [55,56].
- **Elastic cartilage:** (V) No (*avascular, only associated to other tissues in flaps*) – (NV) [57].
- **Cutaneous muscle:** (V) No – (NV) No.
- **Fascia:** (V) No – (NV) [58].
- **Skeletal Muscle**: (V) No – (NV) [59,60].
- **Bone:** (V) No – (NV) [61].
- **Lymph node:** (V) No – (NV) [62].
- **Nerve:** (V) No – (NV) [63].
- **Mammary gland** (*breast*): (V) No – (NV) [64].

Simple/intermediate composite tissue

- **Skin-elastic cartilage (***ear, nose***)**: (V) No – (NV) No.
- **Skin-skeletal muscle (***musculocutaneous - any CT flap with skin paddle*): (V) No – (NV) No.
- **Skin-cutaneous muscl**e *(lips, eyelids, hypothenar flap, scrotum flap (human) – various locations (animal model)):* (V) No – (NV) No.
- **Skin-mucosa-cutaneous muscle** (*eyelids/lips*): (V) No – (NV) [65].
- **Skin-bone-tendon-joint** (*long digit/toe*): (V) No – (NV) No.
- **Skin-bone-tendon-joint-skeletal muscle** (*thumb*): (V) No – (NV) No.
- **Skin-bone-joint-skeletal muscle**: (V) No – (NV) No.
- **Skin-spongious tissue** (*penis*): (V) No – (NV) [66].
- **Skin-mammary gland** (*breast flap*): (V) No – (NV) No.
- **Specialized mucosa-skeletal muscle** (*Tongue*): (V) No – (NV) [67]*****.
- **Specialized mucosa-cartilage** (*Trachea*): (V) No – (NV) [68]*****.
- **Specialized mucosa-cartilage-muscle** (*Larynx*): (V) [69] – (NV) No
- **Endometrium-muscle** (*Uterus*): (V) [70] – (NV) no

Complex composite tissue

- **Segmental and total face, with or without bone**: (V) No – (NV) No.
- **Segmental limbs** (*hand/foot/forearm/leg*): (V) [48]***** – (NV) No.
- **Abdominal wall**: (V) No – (NV) No.
- **Thoracic wall:** (V) No – (NV) No.

***** published during current PhD

The above summarized review brings us to the obvious conclusion that, at the time of our PhD work to begin, the field of composite tissue engineering was nearly unexplored for the complex vascularized grafts. This important lack in the literature indicated that a whole scientific evidence had to be created. Interestingly, some pertinent articles were published, emphasizing that VCE becomes an emerging and fast-growing field.

2.5.3 The subunit approach

Due to the very different types of tissues involved in the face, a simplified approach had to be designed, aiming to study separately the main elementary tissue associations encountered in the complex facial framework. *De facto*, several morphological subunits were simultaneously identified as separate and specific experimental models, dividing the whole face into simpler, targeted tissue-associated grafts, and without any other equivalent in the body.

According to this basic principle, we thus distinguished and classified the following experimental morphological subunits of the face as follows (**Figure 18**):

- **Non-motor** subunits have mostly a structural function and their key tissue is elastic cartilage. They are found in nose and ear subunits.
- **Motor** subunits contain an orbicular muscle, as dominant functional tissue. Subunits of this group are represented by the lower and upper lips, and

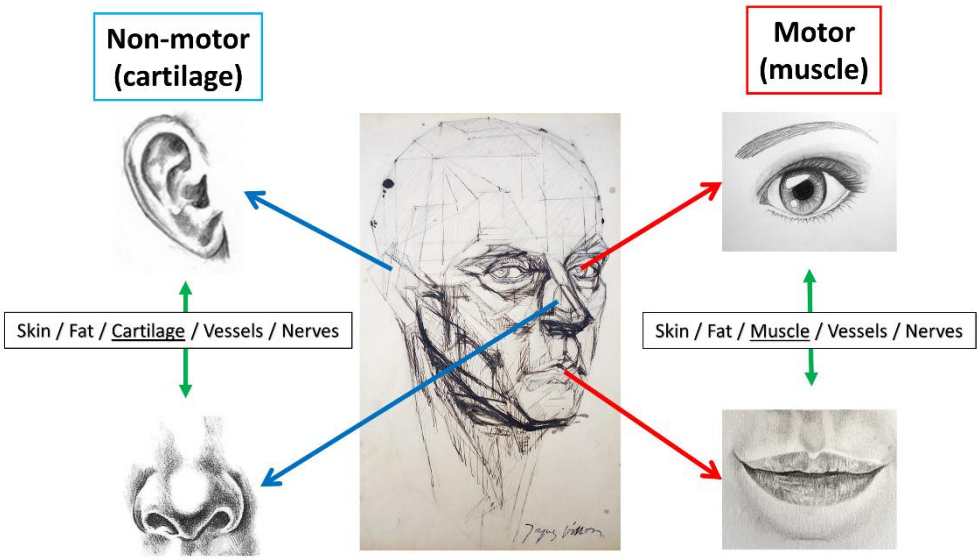

***Figure 18**: Rationalized classification of morphological face subunits models for tissue engineering, with non-motor (left) and motor (right) groups.*
(Central picture, Jacques Villon, Self-portrait, 1942)

similarly by the lower and upper eyelids, which have both a cardinal closing function on oral or palpebral clefts.

In terms of tissue engineering, the main advantages of the simplified subunit approach are the following:

- Subunit models within each group are considered similar, because of their similar tissue association. The protocol developed for the one can thus be directly applied to the other.
- Subunits are smaller than segmental or full grafts, thus easier to process.
- Findings collected from different subunits from the two different groups can unlock not only the whole soft face engineering, but also similar developments made on other important parts of the body.

The other important consideration in favor of the subunit approach is its **justification as a pre-clinical model**: the complete loss of an entire facial morphological subunit, like for example a single lip, is indeed very hard to

reconstruct by conventional techniques which usually fail to reach both aesthetic and functional results. However, this clinical situation remains at the present time considered a contra-indication to current VCA approach.

There is a direct reciprocity of both models: the existence of engineering applications to experimental subunit models will justify their surgical and anatomical study. On the other side, existing engineered subunit models will trigger new clinical applications (**Figure 19**).

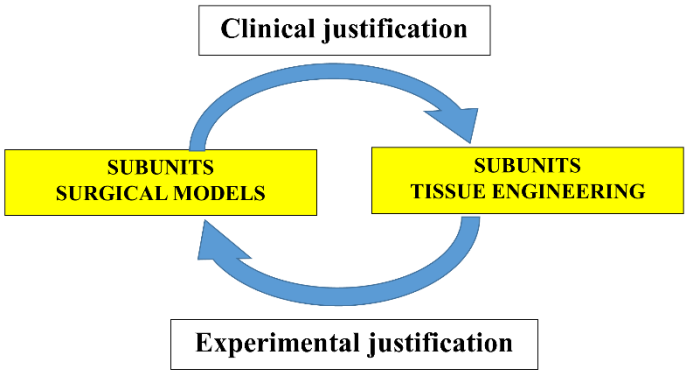

Figure 19: *Reciprocal justification of the subunit approach in face tissue engineering.*

3. Work hypotheses

All the experiments reported in the present thesis were based on the following concepts and work hypotheses:

Solid organ engineering technology can be applied to vascularized composite tissues

- Face is therefore an excellent model: because it contains a very representative and wide range of tissues of the body; because there is an urgent medical need to develop new strategies treating severe disfigurement, consequently pushing forward a lot of future clinical applications in tissue engineering.

- As a matter of fact, a versatile perfusion-decellularization protocol has to be found for composite tissues.

Subunit approach

- The face has to be divided in subunits for specific tissue associations exploration. The study of one subunit from each group will allow whole-face engineering and will also largely cover, by analogy, the needs of composite tissue engineering for the rest of the body.
- The experimental development of subunit models for TE and transplantation have also a potentially very important clinical background, reinforcing their justification.

Need and justification of new anatomical research in body parts segmentation and subunits models

- The segmental trigemino-vascular classification of face grafts was made to match clinical situations and according to embryonic and functional considerations [10]. Furthermore, lower face type I (nose-lip-chin), mid-face type II (upper lip-nose-cheek) and upper face type III (eyelids, forehead, ears) face allografts were designed to fulfill the condition that face transplantation seemed to be clinically justified if at least two neighboring subunits were lost, or at least one orbicular function was missing. In terms of tissue engineering, this concept has to be revisited.
- The subunit classification is an advanced subdivision of the previous classification, in which every segmental graft can be divided in elementary morphological or functional subunits. The ear [71] and eyelids [72] grafts are already conceptually described; the nose and lips grafts, however, have to be studied.

Challenges for decellularization and recellularization

- Regarding decellularization, a non-selective vascular access is proposed to

treat different tissues at once. Based on tissue and organ engineering review, detergent-based protocol seems to be the more efficient to decellularize face grafts.

- Regarding recellularization, several different tissues and functions to restore have to be addressed. A selective seeding for different tissues will thus be difficult to achieve. Consequently, we will have to rely on the ability of ECM to induce specific stem cells differentiation, at the different locations inside the composite grafts.

Animal and human model choices

- Graft size and weight is fundamental: we should thus start our approach to face TE on the large animal model. The pig is selected because of its preclinical relevance, with thereafter fast potential applications to human cadaveric models.
- The small rat model is not relevant for decellularization, but will be very useful to explore recellularization, because of smaller volume and lower number of cells to seed.

References

1. Wu S, Xu H, Ravindra K, Ildstad ST. Composite tissue allotransplantation: past, present and future-the history and expanding applications of CTA as a new frontier in transplantation. Transplant Proc. 2009;41:463-465.
2. Ethunandan M, Downie I, Flood T. Implant-retained nasal prosthesis for reconstruction of large rhinectomy defects: the Salisbury experience. Int J Oral Maxillofac Surg. 2010;39:343-349.
3. Albrektsson T, Branemark PI, Hansson HA, Lindstrom J. Osseointegrated titanium implants. Requirements for ensuring a long-lasting, direct bone-to-implant anchorage in man. Acta Orthop Scand. 1981;52:155-170.
4. Sade RM. Transplantation at 100 years: Alexis Carrel, pioneer surgeon. Ann Thorac Surg. 2005;80:2415-2418.
5. Chim H, Salgado CJ, Seselgyte R, Wei FC, Mardini S. Principles of head and neck reconstruction: an algorithm to guide flap selection. Semin Plast Surg. 2010;24:148-154.
6. Blondeel PN, Van Landuyt KH, Monstrey SJ et al. The "Gent" consensus on perforator flap terminology: preliminary definitions. Plast Reconstr Surg. 2003;112:1378-1383.
7. Noszczyk BH. The origins of the concept of muscle flaps. Br J Plast Surg. 1996;49:107-110.
8. Devauchelle B, Badet L, Lengelé B et al. First human face allograft: early report. Lancet. 2006;368:203-209.
9. Dubernard JM, Lengelé B, Morelon E et al. Outcomes 18 months after the first human partial face transplantation. N Engl J Med. 2007;357:2451-2460.
10. Lengelé BG. Current concepts and future challenges in facial transplantation. Clin Plast Surg. 2009;36:507-521.
11. Lengelé BG, Testelin S, Bayet B, Devauchelle B. Total lower lip functional reconstruction with a prefabricated gracilis muscle free flap. Int J Oral Maxillofac Surg. 2004;33:396-401.
12. Dubernard JM, Owen E, Herzberg G et al. Human hand allograft: report on first 6 months. Lancet. 1999;353:1315-1320.
13. Khalifian S, Brazio PS, Mohan R et al. Facial transplantation: the first 9 years. Lancet. 2014;384:2153-2163.
14. Devauchelle BL, Testelin SR, Davrou J et al. Face graft? Extrapolation of facial allotransplantation to children. J Craniomaxillofac Surg. 2016;44:925-933.
15. Jiang HQ, Wang Y, Hu XB, Li YS, Li JS. Composite tissue allograft transplantation of cephalocervical skin flap and two ears. Plast Reconstr Surg. 2005;115:31e-35e.
16. Galvez JA, Gralewski K, McAndrew C, Rehman MA, Chang B, Levin LS. Assessment and Planning for a Pediatric Bilateral Hand Transplant Using 3-Dimensional Modeling: Case Report. J Hand Surg Am. 2016;41:341-343.

17. Swearingen B, Ravindra K, Xu H, Wu S, Breidenbach WC, Ildstad ST. Science of composite tissue allotransplantation. Transplantation. 2008;86:627-635.

18. Morelon E, Petruzzo P, Kanitakis J et al. Face transplantation: partial graft loss of the first case ten years later. Am J Transplant. 2017;17:1935-1940.

19. Petruzzo P, Testelin S, Kanitakis J et al. First human face transplantation: 5 years outcomes. Transplantation. 2012;93:236-240.

20. Siemionow M, Klimczak A. Chimerism-based experimental models for tolerance induction in vascularized composite allografts: Cleveland clinic

21. Gajanayake T, Olariu R, Leclere FM et al. A single localized dose of enzyme-responsive hydrogel improves long-term survival of a vascularized composite allograft. Sci Transl Med. 2014;6:249ra110.

22. Orlando G, Wood KJ, Stratta RJ, Yoo JJ, Atala A, Soker S. Regenerative medicine and organ transplantation: past, present, and future. Transplantation. 2011;91:1310-1317.

23. McCusker CD, Gardiner DM. Positional information is reprogrammed in blastema cells of the regenerating limb of the axolotl (Ambystoma mexicanum). PLoS One. 2013;8:e77064.

24. Orlando G, Soker S, Stratta RJ. Organ bioengineering and regeneration as the new Holy Grail for organ transplantation. Ann Surg. 2013;258:221-232.

25. Langer R, Vacanti JP. Tissue engineering. Science. 1993;260:920-926.

26. Schubert T, Xhema D, Veriter S et al. The enhanced performance of bone allografts using osteogenic-differentiated adipose-derived mesenchymal stem cells. Biomaterials. 2011;32:8880-8891.

27. Rustad KC, Sorkin M, Levi B, Longaker MT, Gurtner GC. Strategies for organ level tissue engineering. Organogenesis. 2010;6:151-157.

28. Kludt NA, Vu H. Auricular reconstruction with prolonged tissue expansion and porous polyethylene implants. Ann Plast Surg. 2014;72 Suppl 1:S14-S17.

29. Kang HW, Lee SJ, Ko IK, Kengla C, Yoo JJ, Atala A. A 3D bioprinting system to produce human-scale tissue constructs with structural integrity. Nat Biotechnol. 2016;34:312-319.

30. Murphy SV, Atala A. 3D bioprinting of tissues and organs. Nat Biotechnol. 2014;32:773-785.

31. Fulco I, Miot S, Haug MD et al. Engineered autologous cartilage tissue for nasal reconstruction after tumour resection: an observational first-in-human trial. Lancet. 2014;384:337-346.

32. Hynes RO. The extracellular matrix: not just pretty fibrils. Science. 2009;326:1216-1219.

33. Schaefer L. Proteoglycans, key regulators of cell-matrix dynamics. Matrix Biol. 2014;35:1-2.

34. Bijonowski BM, Miller WM, Wertheim JA. Bioreactor design for perfusion-based, highly-vascularized organ regeneration. Curr Opin Chem Eng. 2013;2:32-40.

35. Zimmermann WH, Melnychenko I, Wasmeier G et al. Engineered heart tissue grafts improve systolic and diastolic function in infarcted rat hearts. Nat Med. 2006;12:452-458.

36. Gilbert TW, Sellaro TL, Badylak SF. Decellularization of tissues and organs. Biomaterials. 2006;27:3675-3683.

37. Ott HC, Matthiesen TS, Goh SK et al. Perfusion-decellularized matrix: using nature's platform to engineer a bioartificial heart. Nat Med. 2008;14:213-221.

38. Orlando G, Booth C, Wang Z et al. Discarded human kidneys as a source of ECM scaffold for kidney regeneration technologies. Biomaterials. 2013;34:5915-5925.

39. Orlando G, Farney AC, Iskandar SS et al. Production and implantation of renal extracellular matrix scaffolds from porcine kidneys as a platform for renal bioengineering investigations. Ann Surg. 2012;256:363-370.

40. Peloso A, Petrosyan A, Da SS et al. Renal Extracellular Matrix Scaffolds From Discarded Kidneys Maintain Glomerular Morphometry and Vascular Resilience and Retains Critical Growth Factors. Transplantation. 2015;99:1807-1816.

41. Uygun BE, Price G, Saedi N et al. Decellularization and recellularization of whole livers. J Vis Exp. 2011;

42. Ott HC, Clippinger B, Conrad C et al. Regeneration and orthotopic transplantation of a bioartificial lung. Nat Med. 2010;16:927-933.

43. Totonelli G, Maghsoudlou P, Garriboli M et al. A rat decellularized small bowel scaffold that preserves villus-crypt architecture for intestinal regeneration. Biomaterials. 2012;33:3401-3410.

44. Peloso A, Urbani L, Cravedi P et al. The Human Pancreas as a Source of Protolerogenic Extracellular Matrix Scaffold for a New-generation Bioartificial Endocrine Pancreas. Ann Surg. 2016;264:169-179.

45. Sullivan DC, Mirmalek-Sani SH, Deegan DB et al. Decellularization methods of porcine kidneys for whole organ engineering using a high-throughput system. Biomaterials. 2012;33:7756-7764.

46. Wendt D, Stroebel S, Jakob M, John GT, Martin I. Uniform tissues engineered by seeding and culturing cells in 3D scaffolds under perfusion at defined oxygen tensions. Biorheology. 2006;43:481-488.

47. Somers SM, Spector AA, DiGirolamo DJ, Grayson WL. Biophysical Stimulation for Engineering Functional Skeletal Muscle. Tissue Eng Part B Rev. 2017;23:362-372.

48. Jank BJ, Xiong L, Moser PT et al. Engineered composite tissue as a bioartificial limb graft. Biomaterials. 2015;61:246-256.

49. Fryer M, Grahammer J, Khalifian S et al. Exploring cell-based tolerance strategies for hand and face transplantation. Expert rev clin immunol. 2015;11:1189-1204.

50. Horner BM, Randolph MA, Duran-Struuck R et al. Induction of tolerance to an allogeneic skin flap transplant in a preclinical large animal model. Transplant Proc. 2009;41:539-541.

51. Lee WP, Rubin JP, Bourget JL et al. Tolerance to limb tissue allografts between swine matched for major histocompatibility complex antigens. Plast Reconstr Surg. 2001;107:1482-1490.

52. Sachs DH. Mixed chimerism as an approach to transplantation tolerance. Clin Immunol. 2000;95:S63-S68.

53. Jank BJ, Goverman J, Guyette JP et al. Creation of a Bioengineered Skin Flap Scaffold with a Perfusable Vascular Pedicle. Tissue Eng Part A. 2017;23:696-707.

54. Bannasch H, Stark GB, Knam F, Horch RE, Fohn M. Decellularized dermis in combination with cultivated keratinocytes in a short- and long-term animal experimental investigation. J Eur Acad Dermatol Venereol. 2008;22:41-49.

55. Choi YC, Choi JS, Kim BS, Kim JD, Yoon HI, Cho YW. Decellularized extracellular matrix derived from porcine adipose tissue as a xenogeneic biomaterial for tissue engineering. Tissue Eng Part C,Methods. 2012;18:866-876.

56. Flynn LE. The use of decellularized adipose tissue to provide an inductive microenvironment for the adipogenic differentiation of human adipose-derived stem cells. Biomaterials. 2010;31:4715-4724.

57. Schwarz S, Koerber L, Elsaesser AF et al. Decellularized cartilage matrix as a novel biomatrix for cartilage tissue-engineering applications. Tissue Eng Part A. 2012;18:2195-2209.

58. Johnson J, Wang LN, Chang DW, Zhang QX. Abstract 151: Decellularized musculofascial matrix for soft tissue repair and regeneration. Plast Reconstr Surg. 2013;131:

59. Fishman JM, Lowdell MW, Urbani L et al. Immunomodulatory effect of a decellularized skeletal muscle scaffold in a discordant xenotransplantation model. Proc Natl Acad Sci U S A. 2013;110:14360-14365.

60. Gillies AR, Smith LR, Lieber RL, Varghese S. Method for decellularizing skeletal muscle without detergents or proteolytic enzymes. Tissue Eng Part C,Methods. 2011;17:383-389.

61. Lee DJ, Diachina S, Lee YT et al. Decellularized bone matrix grafts for calvaria regeneration. J Tissue Eng. 2016;7:2041731416680306.

62. Cuzzone DA, Albano NJ, Aschen SZ, Ghanta S, Mehrara BJ. Decellularized Lymph Nodes as Scaffolds for Tissue Engineered Lymph Nodes. Lymphat Res Biol. 2015;13:186-194.

63. Karabekmez FE, Duymaz A, Moran SL. Early clinical outcomes with the use of decellularized nerve allograft for repair of sensory defects within the hand. Hand (N Y). 2009;4:245-249.

64. Maxwell GP, Gabriel A. Bioengineered Breast: Concept, Technique, and Preliminary Results. Plast Reconstr Surg. 2016;137:415-421.

65. Khan H, Szarko M, Butler P. Decellularization of Human Lip. J Tissue Sci Eng. 2015;6:1000149.

66. Patel MN, Atala A. Tissue engineering of the penis. ScientificWorldJournal.2011;11:2567-2578.

67. Zhao L, Huang L, Yu S, Zheng J, Wang H, Zhang Y. Decellularized tongue tissue as an in vitro model for studying tongue cancer and tongue regeneration. Acta Biomater. 2017;58:122-135.

68. Macchiarini P, Jungebluth P, Go T et al. Clinical transplantation of a tissue-engineered airway. Lancet. 2008;372:2023-2030.

69. Ma R, Li M, Luo J et al. Structural integrity, ECM components and immunogenicity of decellularized laryngeal scaffold with preserved cartilage. Biomaterials. 2013;34:1790-1798.

70. Miyazaki K, Maruyama T. Partial regeneration and reconstruction of the rat uterus through recellularization of a decellularized uterine matrix. Biomaterials. 2014;35:8791-8800.

71. Ulusal BG, Ulusal AE, Lin JY et al. Anatomical and technical aspects of harvesting the auricle as a neurovascular facial subunit transplant in humans. Plast Reconstr Surg. 2007;120:1540-1545.

72. Vasilic D, Barker JH, Blagg R, Whitaker I, Kon M, Gossman MD. Facial transplantation: an anatomic and surgical analysis of the periorbital functional unit. Plast Reconstr Surg. 2010;125:125-134.

“La transplantation faciale « totale » n’est pas un objectif en soi”

Devauchelle B, Testelin S, Dakpe S, Lengelé B, Dubernard JM

La greffe faciale, archétype de l’innovation chirurgicale ? Ann Chir Plast Esthet 2010;55:452-60.

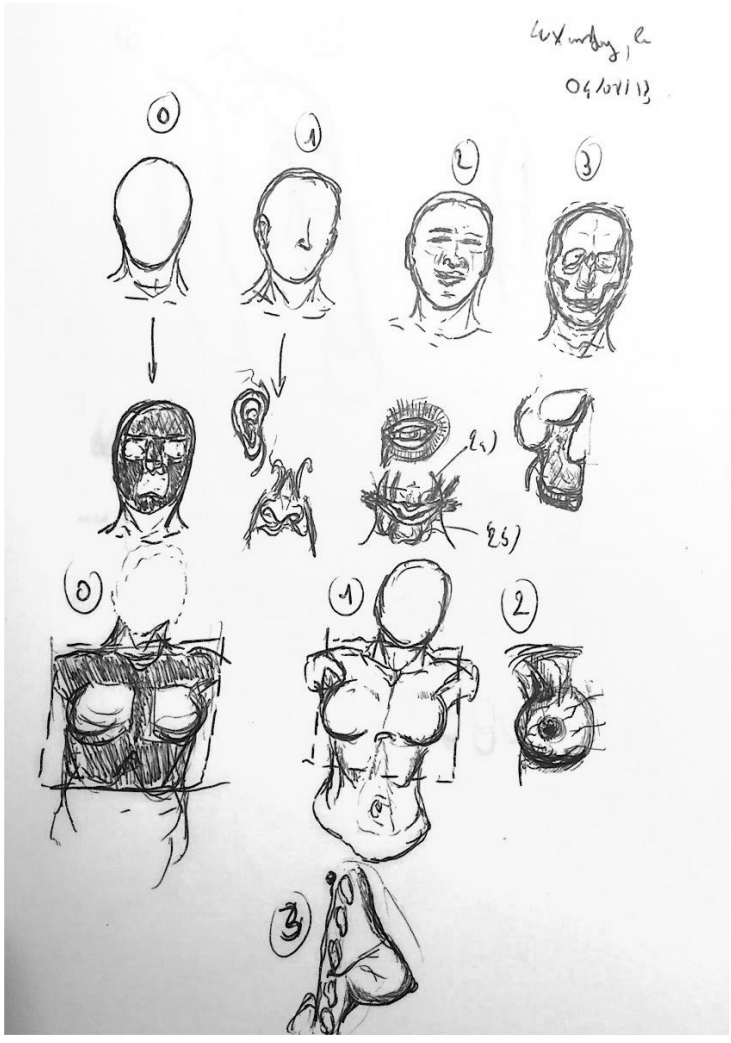

Author's notes (Luxemburg, 4.8.2013)

Part II- Experimental studies

Section 1- Face subunits anatomical and surgical studies

Summary

In this part, essentially driven by surgical techniques and anatomical findings, we describe several experimental models for facial subunit grafts. The surgical division of the emblematic human lower face allograft into nose and lip graft variants is treated in **Chapter 1**. In order to refine the original ear graft technique, we describe in **Chapter 2** a simplified harvesting method based on a single-artery pedicle approach. In **Chapter 3**, we study the anatomy and report the surgical technique for a porcine ear vascularized composite tissue, in a large animal model, targeted as a first engineering application of a non-motor facial subunit, further developed in the second section.

Chapter 1: Human nose and lip transplant models

***Nose and lips graft variants: a subunit anatomical study*.**

Plast Reconstr Surg. 2017 Nov 11;

doi: 10.1097/PRS.0000000000004116. [Epub ahead of print].

Duisit J

Maistriaux L

Gerdom A

Vergauwen M

Gianello P

Behets C

Lengelé B

ABSTRACT

Background. In the field of Vascularized Composite tissue Allotransplantation (VCA), the surgical design of facial subunit grafts is an evolving concept. The purpose of the present paper is to study the possibilities to divide the historical "nose and lips face transplant" into several morphological and functional subunit grafts, depending on their respective supply.

Methods. Our study was conducted in 20 adult cadavers. The facial artery and its branches were dissected bilaterally in 16 fresh and 4 embalmed heads. Nasolabial perfusion was assessed by selective injection of methylene blue and eosin (n=2) or indian ink (n=2) in superior labial artery (SLA) and distal facial artery (DFA). Dynamic perfusion through the DFA was illustrated by fluoroscopy (n=3). Three nose-upper lip grafts were harvested and injected with barium sulfate for micro-Angio CT analysis. Finally, three isolated nasal and bilabial grafts were procured and their vascular patency assessed by fluoroscopy.

Results. DFA can perfuse the entire nose, septum and upper lip, without any contribution of SLA. A dense anastomotic network indeed exists between the respective distal rami of both vessels. Furthermore, the exclusion of SLA from the harvested nasal subunit allowed safe bilabial subunit procurement, from the same specimen.

Conclusions. Our results demonstrate the feasibility of harvesting nasal and labial subunits, in an isolated or a combined manner. These results can find applications in subunit autologous replantation, allotransplantation, allogenic face partial retransplantation, and in the emerging field of vascularized composite tissue engineering.

1. Introduction

Since the first facial allotransplantation (FAT) in 2005, there has been an incremental surgical challenge to perform partial [1,2], subtotal [3] and then finally full face transplants [4]. This path was followed as a result of the progressive fusion of the initial segmental approach of face transplantation [5]. However, disfigurement may affect only one facial subunit. Although limited to a single missing subunit, the reconstructive challenge is still huge, especially for those involving facial muscles. Thus, there is a clinical need for the conception of an additional functional and morphological subunit allotransplantation approach [6,7]. This has previously been described for auricular [8,9] and palpebral subunits [10], and briefly for the nose [11], but not explored yet for adjacent labial and nasal subunits, even though both share their supply on the same dominant pedicle and have already been combined in the first segmental type I face allotransplant [5]. Complete nasal reconstruction remains a very demanding procedure, relying on outstanding skills and multiple steps to obtain satisfying results [12]. Likewise, large reconstruction of the oral sphincter is also highly challenging [13], even for a single lip [14], because of its motor function. Thus, approached as a single subunit, nose and lips allotransplantation could be justified. Such grafts, however, are believed to rely on the arterial anastomoses between the base of the nose and the upper lip. These are provided by the superior labial artery (SLA). Consequently, as the SLA provides significant blood supply to the septum, columella and tip via septal and columellar branches [15,16], it seems prudent to include this vessel in an isolated nasal graft [11]. However, due to the SLA course close to the vermillion, and thus far from the nose, its incorporation to the nasal graft would lead either to a tedious dissection, or to a lot of additional bulky tissue to the nasal graft. Furthermore, this inclusive strategy should preclude the simultaneous procurement of a separated upper lip graft. We therefore hypothesized that the facial artery (FA) could perfuse the entire nose subunit without the SLA inclusion, based on another perinasal anastomotic network. The objective of the present study was thus to assess the different surgical strategies in nasal and labial subunit transplantation, depending on the respective contribution of SLA and distal-to-SLA facial artery

branches (DFA) in the nasal and septal perfusion. This allowed us to describe several nose and lips subunit grafts variants, with potential related indications in the current VCA field but also for other types of applications, like Vascularized Composite tissue Engineering (VCE).

2. Methods

All experiments were conducted on human cadavers, acquired from body donation at the department of Anatomy, and with respect of the ethical rules drawn by the Université catholique de Louvain for applied medical research.

Specimens: We studied faces from 20 caucasian cadaveric heads (mean age 65-94 years, equal male/female ratio: 16 fresh (including 4 latex-injected) and 4 embalmed specimens. Fresh heads were all perfused with normal saline in the common carotid artery (CCA), until venous return was clear. Red latex (Latex and latex color, Mida, Brussels, Belgium) injection was performed bilaterally in both CCAs.

Arterial morphometric study: The FA was exposed in 25 hemi-faces (bilateral n=24, unilateral n=1), at the level of the mandibular border, then followed along the nasolabial fold (NLF), and finally traced up to the medial canthus. The following were defined for analysis **(Figure 1)**: the proximal FA (PFA) at the level of the mandibular edge; the origin of the inferior labial artery (ILA); the origin of the superior labial artery (SLA); the distal FA (DFA), starting immediately distal to the SLA; the origin of the inferior alar artery (IAA); the origin of the lateral nasal artery (LNA); the angular artery (AA), arising immediately distal to the LNA origin; the dorsal nasal artery (DNA), originating from the infratrochlear artery (ITA), at its junction with the AA. For the SLA, branches were defined as columellar (CA) and septal (SA) arteries. Subsequently, the FA main axis was divided into five segments: I, from PFA to ILA; II, from ILA to SLA; III, from DFA to IAA; IV, from IAA to LNA; V, from LNA to DNA. Segment lengths were recorded. FA branching patterns were then studied, following classification established by Lohn et al [17].

All arterial calibers were measured with a dental crown caliper and expressed in mm.

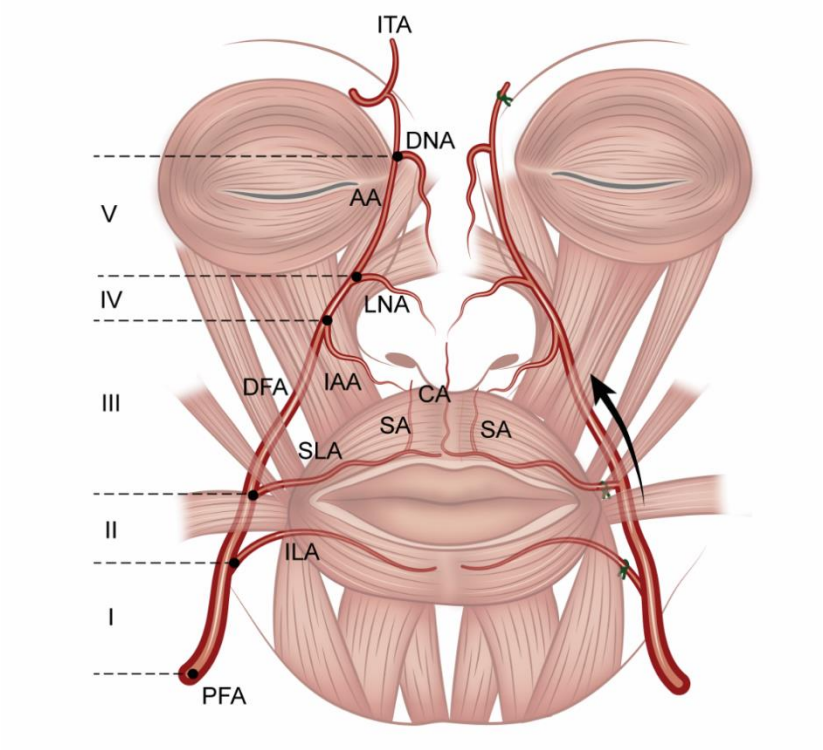

Figure 1: *Facial artery (FA) landmarks for morphometric study. On the left hemi-face are indicated the FA labelling landmarks: inferior labial artery (ILA), superior labial artery (SLA), inferior alar artery (IAA), lateral nasal artery (LNA), angular artery (AA) and dorsal nasal artery (DNA), originating from the inferior trochlear artery (ITA). Additional landmarks: proximal facial artery (PFA) and distal facial artery (DFA). SLA branches are denominated as septal arteries (SA) and columellar artery (CA). Segments are defined as following: I, PFA to ILA; II, ILA to SLA; III, SLA to IAA; IV, IAA to LNA; V, AA to DNA. On the right hemiface, the arrow shows the injection pathway followed to perfuse selectively the DFA after ILA, SLA and ITA ligation.*

Selective arterial injection study: A bilateral incision was performed along the NLF at the level of the labial commissures, aiming to identify the PFA bifurcation into SLA and DFA. To avoid back perfusion, when one artery was cannulated, the other was ligated (**Figure 1**). In the first head, the DFA was perfused unilaterally

on the right side, with a solution of methylene blue, after a 1:10 dilution in normal saline; in the same fashion, the right SLA was injected with scarlet eosin solution, at a concentration of 1g/L in normal saline. In the second head, and in order to study mucosal perfusion of nasal septum and upper lip, 15 ml of a 10% black indian ink (Fount India, Pelikan, Schindellegi, Switzerland) solution were injected bilaterally into DFA (n=2). Finally, dynamic perfusion study was achieved with fluoroscopy in three heads, with Iodixanol (Visipaque® 320mg/100ml, GE Healthcare, IL, USA) manually injected unilaterally in the DFA, after bilateral SLA ligation; dynamic fluoroscopy was acquired with a Powermobil C-Arm (Siemens, Munich, Germany).

Nose-upper lip graft study

Graft elevation: Three nose-upper lip grafts were harvested. An incision was made at the level of the mandibular body to identify the FA and facial vein (FV), then prolonged 1 cm lateral to the oral commissure and extended to the nose, following the NLF. FA and FV were fully exposed, after depressor and levator muscle division, when necessary. ILA and SLA were identified and ligated. Incision was then performed on the glabella, and extended laterally to identify the angular pedicle, which was ligated at the level of the infratrochlear vessels' origin. Thereafter, incision was prolonged inferiorly, 1 cm lateral to the nasal border, down to the periosteum, followed by a subperiosteal elevation. Infraorbital foramen was identified and the infraorbital nerve (ION) harvested within the graft. Dissection was extended medially to the piriform aperture whilst protecting the pedicle, and nasal mucosa was dissected to the nasal turbinates. Intra-orally, the mucosa was incised, down to the anterior nasal spine. A tissue elevator was then inserted in the submucosal plane in a Lefort I fashion. To free the nasal bones, lateral osteotomies were carried out. To harvest the whole nasal septum, two sagittal osteotomies were performed. After septal cartilage and nasal mucosa division, the graft was completely elevated on its vascular and nervous pedicles, including on both sides the DFA extended downwards to the PFA, the FV and the ION (**Figure 2**).

Figure 2: *Nose-upper lip graft model. (Left) Anterior view of the harvested nose-upper lip graft, with the distal facial artery (DFA), the facial vein (FV) and the infra-orbital nerve (V_2) pedicles. (Right) Lateral view of the same graft, with visible harvested extended nasal septum (NS).*

Micro-Angio CT: Grafts were injected in the arterial pedicle with 15 ml of contrast solution, obtained by a mixture in a water bath of 100 ml of saline with 3 g of gelatin powder (Merck, Darmstadt, Germany) and 40 g of barium sulfate (Micropaque colon, Guerbet, Roissy, France), heated at 40 ° C. Injected specimens were preserved at 4°C overnight. Acquisition was performed using a helical CT scanner (NanoSPECT/ CT, Bioscan Inc., Washington D.C., USA) and the CT projections were reconstructed with a voxel size of 0.221 × 0.221 × 0.221 mm^3. 3D analysis was performed with Osirix© open-source software (Pixmeo, Bernex, Switzerland) [18].

Nasal and bilabial subunit grafts procurement: In order to validate the results regarding the possible surgical division of the nose-lip anastomoses and to complete the whole set of subunit variants in the studied area, we harvested isolated nose and lip subunits from three fresh heads. For each subunit, skin incision followed aesthetic lines. Bilaterally, PFA, SLA, DFA and ITA were exposed; DFA for the nasal subunit and PFA for the bilabial subunit were respectively used as pedicles. After limited upper lip skin undermining, SLA branches were ligated at the level of the nasolabial junction, prior to full graft elevation. Additional

hemostasis was performed using ligating clips. In order to assess the preservation of a complete and homogeneous perfusion of both subunits, fluoroscopy of each isolated graft type was accomplished.

Statistical analysis: Quantitative results were expressed as mean ± SD. All statistical analyses were achieved using GraphPad Prism version 7.00 for Windows (GraphPad Software, La Jolla California USA). A paired Student t-test was used to compare the left and right sides. In absence of difference between both sides, values were averaged on a per-subject level. A significant p-value was set at $p<0.05$.

3. Results

FA pattern and morphometrics

FA axis configuration was found as type I (Figure 3) in 72% of hemifaces (18/25), with complete pedicle including DNA; type II was found in 28% of hemifaces (7/25), FA ending with LNA. Type I was bilateral in 58.3% heads (7/12), and in 8.3% (1/12) for type II. Type I/II mismatch was observed in 33.3% heads (4/12); in only one case, a bilateral I/I configuration was recorded. SLA was present bilaterally in all specimens, with an easy identification of columellar and septal arteries to the nose, originating directly from the SLA. Consistently, we found a single columellar artery, achieving anastomoses with both LNAs at the tip of the nose, as well as with SA branches and with the IAA. The columellar artery was also seen directly giving off a septal artery (**Figure 3**). Interestingly, a duplicated SLA was observed in three specimens.

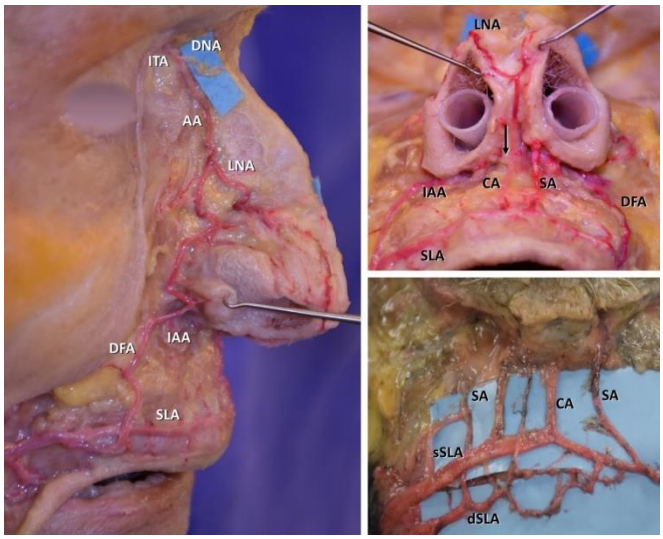

Figure 3: *FA and SLA branching pattern. (Left) type I FA configuration in a latex-injected specimen. (Upper right) Naso-labial anastomosis, between SA and IAA, CA and LNA; the arrow indicates direct SA branching from CA. (Lower right) duplicated SLA: superficial (sSLA) and deep (dSLA).*

FA pedicle segment lengths and the caliber of its branches are summarized in **Table 1;** there was no difference between left and right sides.

	Segment lengths					Branches calibers							
	I	II	III	IV	V	PFA	ILA	SLA	DFA	IAA	LNA	DNA	AA
N	9	15	22	21	13	17	15	17	17	17	17	7	10
Mean	38.3	17.3	36.5	21.5	29	2.50	1.32	1.31	1.33	0.93	1.10	0.68	0.76
SD	13.1	8.3	11.4	11	8.3	0.48	0.44	0.48	0.43	0.19	0.2	0.16	0.27
Range	22-60	3-30	22-62	8-38	18-43	1.6-3.4	0.7-2.4	0.7-2.4	0.75-2.4	0.6-1.3	0.9-1.7	0.6-1	0.5-1.2

Table 1: *FA morphometrics: FA segments lengths I to V (as described in figure 1), and FA branches calibers. (N) number, (M) mean, (SD) standard deviation and range. Proximal facial artery (PFA), inferior labial artery (ILA), superior labial artery (SLA), distal facial artery (DFA), inferior alar artery (IAA), lateral nasal artery (LNA), distal nasal artery (DNA), angular artery (AA). All results are expressed in mm.*

Selective arterial injection study

Selective perfusion of the DFA was able to stain the entire graft teguments, largely including the nasal pyramid and the superior lip, with lateral extensions to cheeks, as assessed by methylene blue injection, and revealing an extended dynamic angiosome. Secondary perfusion with eosin in SLA confirmed dual coverage of both arteries in the upper lip and septum, clearly demonstrating a dynamic reciprocity of neighboring vascular angiosomes at this location **(Figure 4)**.

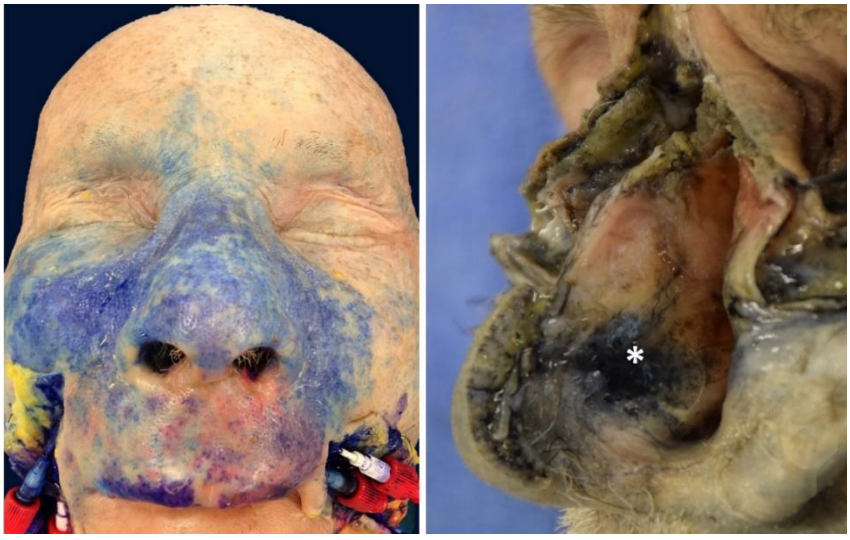

***Figure 4**: Arterial selective perfusion and angiosomes. (Left) Methylene blue injection in DFA combined to scarlet eosin injection in SLA. (Right) Lateral view the nasal septum and mucosa after black indian ink injection, with evidence of Kiesselbach's plexus (*) staining.*

Regarding septal and labial mucosae, both were positively stained by Indian ink after DFA injection. In the septum, Kiesselbach's plexus was clearly observed **(Figure 4)**, indicating that septal reperfusion can be achieved without SLA injection. Finally, dynamic observation, achieved by fluoroscopy, demonstrated retrograde contralateral pedicle filling and SLA flow after unilateral DFA injection,

even after sagittal split section of the nose (**Figure 5**; **see corresponding Video, Supplemental Digital Content 1, which shows contrast diffusion after left DFA perfusion, highlighting perialar anastomotic network and contralateral SLA perfusion)**. The anastomotic site, allowing flow redistribution, was clearly observed in the perialar area, confirming static data collected from dissection.

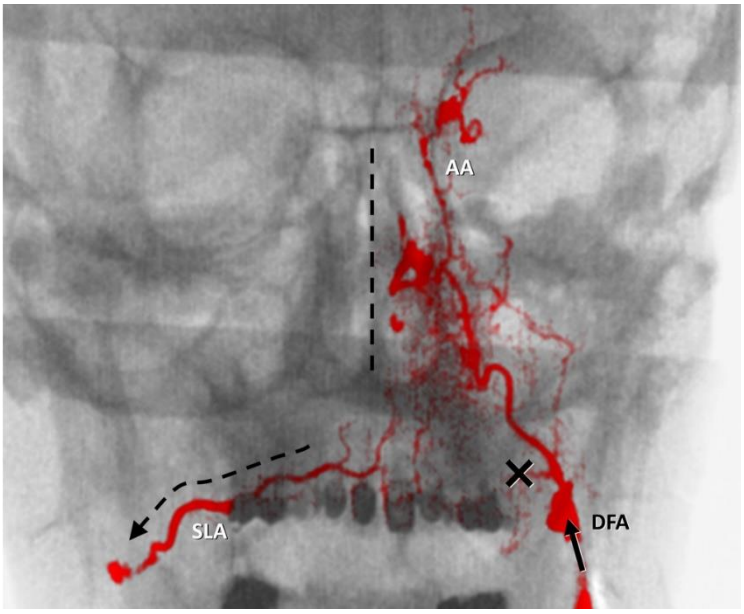

Figure 5: *Fluoroscopy. Early contrast perfusion, after selective left DFA contrast (arrow) injection and left SLA (X) ligation in a split-nose (dotted line) specimen. The flow direction in the contralateral SLA (dotted arrow) is observed.*

Micro-AngioCT (Figure 6)

All vascular trees from the three injected grafts were opacified. In all specimens, we observed dense anastomotic networks between the distal FA branches and the SLA branches, located in the perialar and columellar areas. Thus, the selective DFA injection ensured a specific flow in these networks, allowing perfusion of the whole nose, including the septum. Moreover, SLA divided into superficial and deep

arcades within the upper lip. The superficial arcade gave off the columellar and septal arteries while from the deep arcade, originated many branches to the base of the nose, connected posteriorly to the distal endings of the ethmoidal and sphenopalatine arteries.

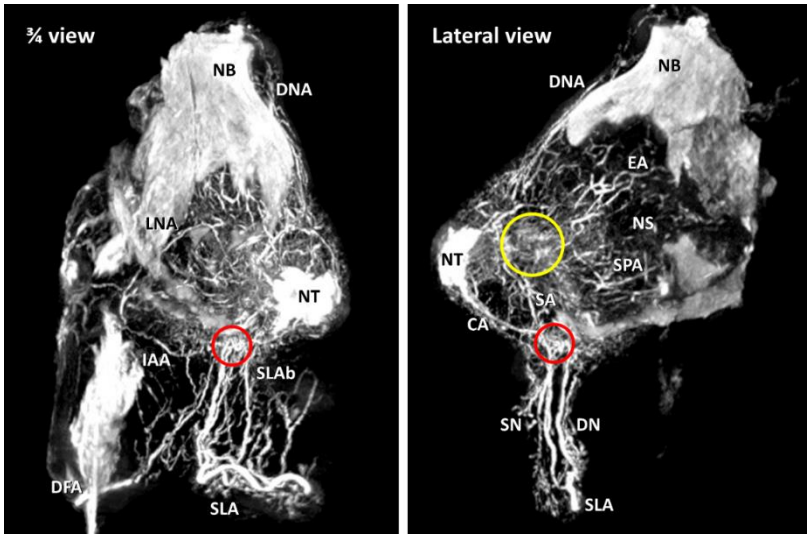

***Figure 6**: Micro-AngioCT 3D reconstruction of a nose-upper lip graft. (Left) 3/4 view of the specimen, with a dense anastomotic network (red circle) at the columellar base and the perialar area, between the inferior IAA and SLA branches (SLAb). (Right) Lateral view of a sagittal median section with highly perfused Kiesselbach's plexus (yellow circle) in the nasal septum (NS), and clear division of the SLA branches into superficial (SN) and deep (DN) networks. (NB) Nasal bones; (NT) calcified nasal tip; (CA) columellar artery; (EA) ethmoidal artery; (SPA) sphenopalatine artery.*

Surgery and fluoroscopy of nasal and labial isolated or compound grafts

Fluoroscopy demonstrated a homogenous vascular patency in both nasal and bilabial subunits, after columellar and septal arteries divisions were made to separate each subunit **(Figure 7)**.

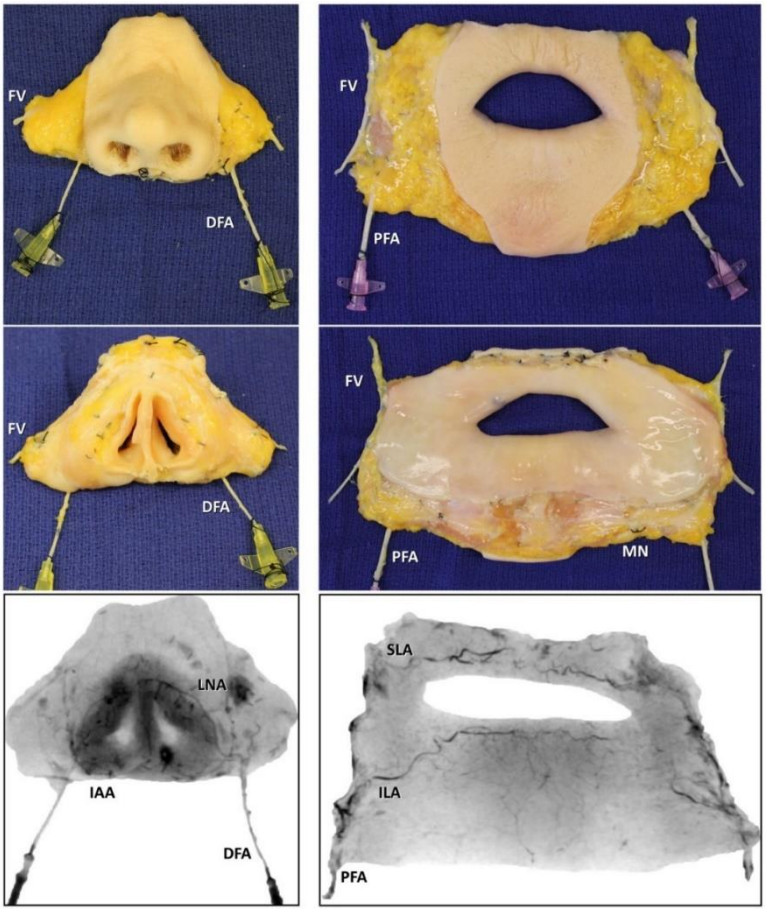

Figure 7: *Isolated nasal and bilabial subunits procurement and angiogram. Nasal subunit (Left panel) and bilabial subunit (right panel). Transplants anterior (up) and posterior (middle) views with their pedicles, with corresponding angiogram (low). (MN) mental nerve.*

We were then able to design the various possible surgical divisions of a segmental nasobilabial type I graft into pure isolated subunits, namely the nasal subunits and the upper or lower monolabial subunits, or into compound naso-monolabial and bilabial subunits, all with their corresponding arterial, venous and nervous pedicles **(Figure 8)**.

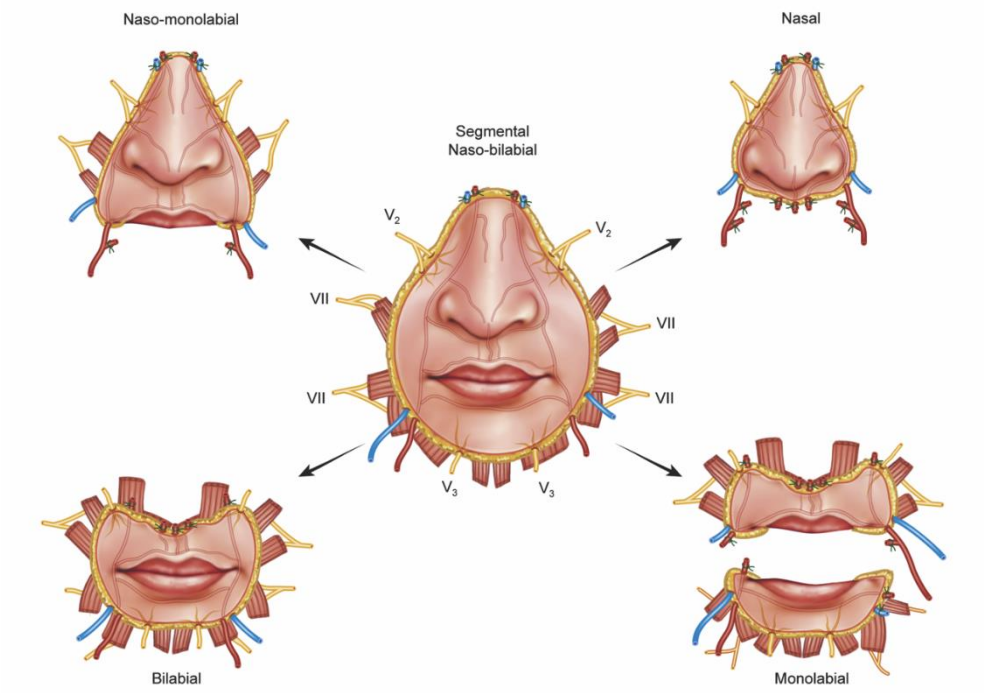

Figure 8: *Nose and lip subunits grafts variants. Schematic surgical division approach to type I segmental naso-bilabial graft: compound naso-monolabial and bilabial subunit grafts, and isolated nose, upper and lower monolabial subunit grafts. (VII) facial nerve; (V2) infra-orbital nerve; (V3) mental nerve.*

4. Discussion

We have brought here the vascular proof that the division of a segmental type I naso-bilabial facial allotransplant into its associated specialized subunits is possible, by transforming the FA axis and its branches into independent and reliable pedicles [7,19]. Division of the nose and upper lip relies on the surgical management of the SLA axis, whose preservation is technically demanding, because the artery runs close to the upper lip free margin and the high anatomical complexity of the SLA branches to the septum, as reported by our study and others [15,20,21]. SLA exclusion has the secondary advantage to leave this arterial axis available for an upper lip pedicle, or biliabial simultaneous procurement in a same

donor (**Figure 8**). The dynamic vascular independence of both nose and lip regions, as demonstrated in our study, has thus an important strategical impact on the development of a subunit approach to facial VCA. Indeed, multiple subunit procurements will allow to treat a wider range of recipients. Of course, the clinical applications will only be unlocked when an acceptable immunosuppressive management will be available. Separating a face transplant donor into its specialized subunits -namely lips, eyelids, nose, ear, and scalp, is a valuable option in the current situation of donor shortage.

The dense anastomotic networks in the perialar and columellar areas allowed graft procurement on the sole facial artery pedicle without the SLA. Our findings demonstrated that entire septum perfusion can be supported with the sole distak FA branches to the external nose, with the exclusion of septal arteries from the SLA and from other external and internal carotid artery branches to the septum. In the case of isolated nose or lip subunit procurement from a single donor, the vascular pedicle strategy should not be an issue, given the possibility of extending the pedicle dissection to the most proximal segment of the facial vessels. Angular and supratrochlear vessels could possibly be used as an alternative, as both graft pedicle and recipient vessels, as indicated by the clinical cases of successful replantation in this area [22-25]. However, in our findings and as confirmed by other teams [17,26,27], we found that the distal FA can be missing in about 30% cases. Even if transcollumellar incisions are confirmed safe for preserving nasal tip perfusion in clinical situations [16], this statement should be studied in the isolated nose graft, making previous open rhinoplasty a risk for graft survival.

Concerning the inferior monolabial and bilabial subunits, the ILA variability and its small caliber, as demonstrated by other authors [21,28,29], is a risk for unilateral pedicle procurement considering the broad variations of the facial artery anatomy in the perioral region [20,30,31]. In this situation, a bilateral pedicle procurement is advocated, aiming to perform anastomoses at the level of lower border of the mandible, or with the ECA collaterals. In the case of a bilabial graft, the pedicle is then extended to the SLA, using the DFA or, better, the PFA as pedicle and

recipient vessels. The main concern for labial-based subunits is the venous drainage, as observed in replantation cases [29,32-34]; clinical [35] and experimental [36] findings have shown however that survival could be obtained without venous anastomosis. Regarding the nervous pedicle, which is mandatory for this subunit type, mental and infraorbital nerves will provide a sensate graft; the facial nerve branches will be added to offer motor recovery, but direct neurotization must also be targeted. In the case of simultaneous harvesting of subunits from a single donor, the vascular morphometric characteristics and branching pattern variations become of tremendous interest when considering a procurement strategy and further replantation. The surgical planning is then highly dependent on the optimization of selective vascular divisions and should be associated with accurate pre-operative imaging.

Central face subunit clinical indications: In the current VCA spectrum, defects requiring a subunit allotransplantation should involve at least two adjacent aesthetic subunits. Alternatively, the defect should include a critical function supported by an orbicularis muscle. In the studied anatomical region, this situation is found in the monolabial, bilabial, naso-monolabial, and type I segmental naso-bilabial grafts. In the upper face area, this condition regards the eyelids. Despite its unique morphological nature and difficulty to reconstruct [3,25], an isolated nose allotransplantation is still hardly justified. However, an indication can be found in retransplantation strategies applied to partial or full face transplants involving the nose, because of the limited lifespan of these grafts and distal necrosis due to chronic rejection, as reported by recent studies [37]. However, this indication should be considered very carefully to avoid jeopardizing both IS treatment and morphological matching, resulting in an additional patchy or chimeric aspect of the face. Concerning partial transplant failure, revision using autologous conventional plasties thus remains the first option. Nevertheless, if the patient is already immunosuppressed, for example in the case of a Wegener's disease total nose defect, this VCA type could be considered. In all cases, the segmental division of the face should be revised, as a combination of its specialized and non-

specialized subunits, in order to better define the surgical objectives of form and function restoration in this area.

The subunit strategy in the era of tissue engineering: Going beyond the sole aspect of VCA harvesting strategy, the facial subunit approach is a critical step towards the experimental inset of human face bioengineering. In a concomitant study [38] indeed, we have initiated the application to the face of the perfusion-decellularization/recellularization technique, aiming to obtain specific scaffolds from different facial subunits, thereafter repopulated by new cells. The ultimate aim of these Vascularized Composite tissue Engineered (VCE) grafts is to overcome the immunologically limited lifespan of VCA grafts, as discussed above. Among these elementary VCE grafts, the nose subunit is the ideal model for the experimental development of a static "skin/cartilage" morphological subunit; the lip being conversely the providential model for the bioengineering of a dynamic "skin/muscle" motor subunit, as we demonstrated recently [39].

5. Conclusion

Our results demonstrated that the entire nose including the nasal septum can be perfused without harvesting the SLA, as its septal supply is ensured by a rich anastomotic network between the distal FA branches to the nasal tip and SLA branches to the septum. This allows separation of the nose from the upper labial subunit, for subsequent transplantation. This dynamic conception of the vascular independence of facial allograft variants may lead us first to broaden and to diversify our strategies in the emerging field of functional or morphological subunits transplantation. In the immediate future, our findings can also have a clinical interest for autologous replantation and allogenic retransplantation cases. On the long run, they provide reliable models in regenerative medicine strategies for the VCE of the face and its subunits.

« Un chirurgien, c'est un homme dont la pensée a dompté le geste. »

Philippe Dartevelle

Chapter 2: Human ear transplant model

Single-artery human ear graft procurement: a simplified approach.

Plastic and Reconstr Surgery 2017- In press

Duisit J
Amiel H
Debluts D
Maistriaux L
Gerdom A
Bol A
Gianello P
Behets C
Lengelé B

ABSTRACT

Background. In the field of experimental facial vascularized composite tissue allotransplantation (VCA), a human auricular subunit model, pedicled on both superficial temporal (STA) and posterior auricular (PAA) arteries was described. Clinical cases of extensive auricular replantation however, suggested that a single artery could perfuse the entire flap. In our study, variants of this single pedicle approach have been studied, aiming to develop a more versatile replantation technique, in which the question of venous drainage has also been addressed.

Methods. For arterial perfusion study, we harvested 11 auricular grafts, either on a single STA pedicle (n=3) or a double STA-PAA pedicle (n=8). We then proceeded to selective barium injections, in STA, PAA or both PAA-STA. Arteriograms were acquired with a Micro-CT scan and analyzed on 3D-reconstructed images. Venous drainage was investigated in eight hemi-faces, carefully dissected after latex injection.

Results. Observations showed a homogenous perfusion of the whole auricle in all arterial graft variants. Venous drainage was highly variable, with either a dominant superficial temporal vein (37.5%), dominant posterior auricular vein (12.5%) or co-dominant trunks (50%).

Conclusions. We demonstrated that auricular subunit VCA can be performed on a single artery, relying on the dynamic intra-auricular anastomoses between STA and PAA branches. Potentially, this vascular versatility is prone to simplify the subunit harvest and allows various strategies for pedicle selection. Venous drainage, however, remains inconstant and thus the major issue when considering auricular transplantation.

1. Introduction

In the first human ear VCA model description [8], the use of both superficial temporal artery (STA) and posterior auricular artery (PAA) pedicles as arterial supply was advocated, in accordance with the classical static concept that the auricle is anatomically divided into two neighbor vascular territories in which the PAA is seemingly predominant. Based on clinical observations of extensive ear replantation cases [40-43] however, it seems obvious that both territories overlap and may then be complementary. Consequently, we postulated that a single pedicle could be sufficient to perfuse an entire auricular subunit. This approach, especially regarding superficial temporal pedicle as donor and/or recipient vessels, would bring a simplified technique for harvesting and revascularizing an auricle allograft, with a reduced donor and recipient morbidity at both sites.

2. Material and methods

For the arterial study, 11 auricules from 9 caucasian cadaveric fresh heads were harvested as simple grafts, based on the STA pedicle only (n=3) or as combined grafts, with a double STA-PAA pedicle (n=8), dissected down to the external carotid artery (ECA). Two main harvesting protocols were defined as following: for the *STA-PAA group*, procurement was adapted from Ulusal et al. [8]: briefly, incision was performed around the auricle and lengthened in the temporal and cervical regions. ECA collaterals and maxillary artery were then all ligated and transsected, STA and PAA excepted. Frontal (FB) and parietal (PB) STA branches were followed up to a 3-cm distance. Then, proximal STA exposure was carried through the parotid gland. Finally, the whole graft was elevated by blunt subfascial undermining. *For the STA group*, only temporal exposure of ST vessels was performed. Transplants were cannulated through ECA (STA/PAA group) or either distal STA (STA group). Perfusion of normal saline was performed to rinse clots. Total harvesting time was recorded for each group.

Three groups of injections were established (**Figure 1**): selective retrograde injection in STA (n=3); or selective prograde injection in PAA (n=3), achieved by

an ECA injection done in STA-PAA grafts after proximal STA ligation; and non-selective prograde ECA injection done in STA-PAA grafts (n=5). Arterial injections were performed with a mixture of normal saline with gelatin powder (Gelatin, Merck Millipore, Billerica, MA) and barium sulfate (MICROPAQUE®, Guerbet, Villepinte, France) heated at 40°C. After their acquisition with a helical CT scanner (NanoSPECT/ CT, Bioscan Inc., Washington D.C., USA), images were analyzed with Osirix© software (Pixmeo, Switzerland) [18].

For the venous study, four fresh heads were injected with a blue-colored latex solution (Latex and Latex color, Mida, Brussels, Belgium), as previously described [44]. Eight auriculo-temporal regions were then dissected, and venous configuration classified as established by Legre et al. [45].

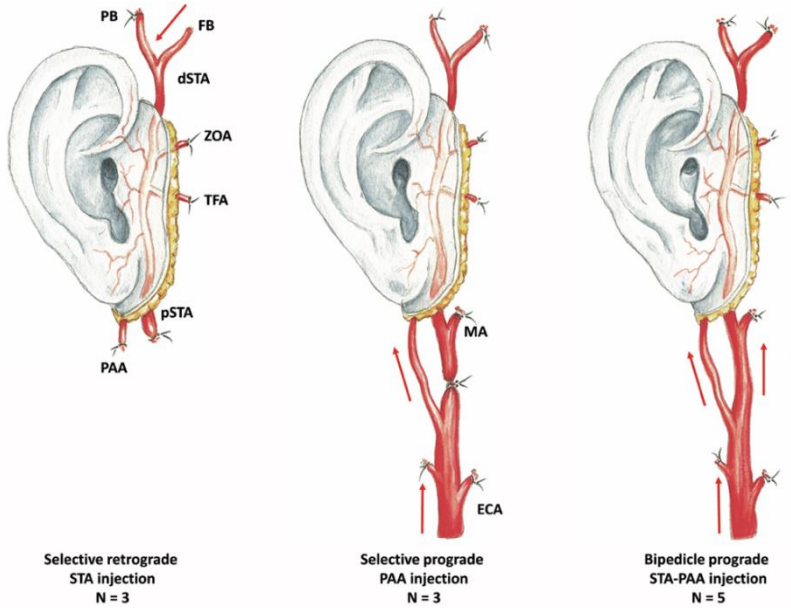

Figure 1: *Arterial injection groups for micro-CT. Schematic graft on the left shows the STA group, with selective distal STA retrograde injection. Schematic graft on the middle shows the PAA group, with selective PAA prograde injection through ECA; distal ECA is ligated to allow unidirectional flow. Schematic graft on the right shows STA/PAA group, with simultaneous STA and PAA injection through ECA. Red arrows: selective injections pathways. Abbreviations: STA, superficial temporal artery; PAA, posterior auricular artery; ECA, external carotid artery; pSTA, proximal STA; TFA, transverse facial artery; ZOA, zygomatico-orbital artery; dSTA: distal STA; FB, frontal branch; PB, parietal branch.*

3. Results

Mean harvesting time for STA grafts was 195 ± 21 min, compared to 254 ± 67 min in STA-PAA grafts. Maximum Intensity Projection (MIP) vascular analysis showed a bi-axial filling of PAA and STA territories in all groups and in every specimen (**Figure 2**).

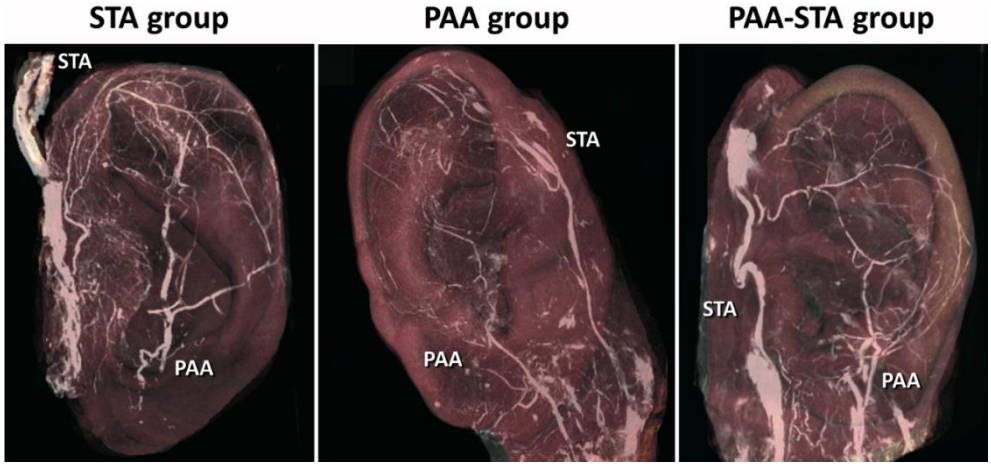

***Figure 2**: Micro-CT Maximum Intensity Projection (MIP) overview in each group. The figure shows a representative image from each STA (left), PAA (middle) and PAA-STA (right) graft injected groups, resulting from the fusion between 3D-volume rendering on the corresponding MIP.*

None of the vascular analysis showed evidence of one axis perfusion without the other. Intraauricular anastomoses between STA and PAA networks could clearly be observed at four different levels of the auricle: in the triangular fossa, the cymba conchae, the intertragic incisure and between both lobular arteries of the STA and PAA **(see Figure, Supplemental Digital Content 1, which shows the micro-CT aspect of intraauricular arterial anastomotic levels).**

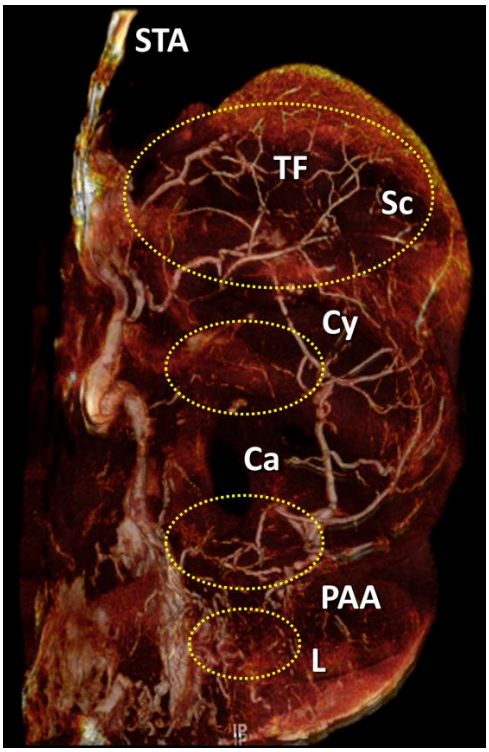

Figure, Supplemental Digital Content 1: *Micro-CT aspect of intra-auricular PAA-STA anastomoses. Upper right typical levels of anastomoses between PAA and STA (dotted circles). The four anastomotic areas are located in the triangular fossa (TF), in the scapha (Sc), in the cymba (Cy), in the concha (Ca), and in the peri-lobular (L) area.*

Venous dissections confirmed the existence of numerous significant variations in periauricular veins, even intra-individually. We found type I dominant superficial temporal vein in 37.5% cases, type II with dominant posterior auricular vein in 12.5% cases, and a type III co-dominant configuration in 50% cases **(see Figure, Supplemental Digital Content 2, which exposes the venous dissection results from the latex-injected specimen)**. Interestingly, the middle temporal vein and transverse facial vein were found consistently.

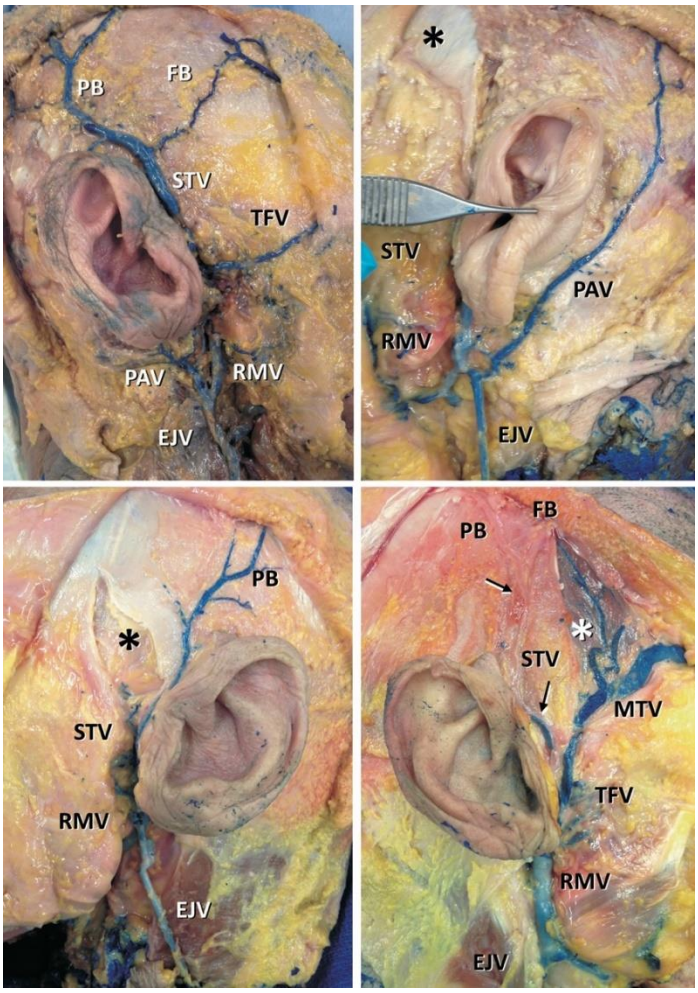

***Figure, Supplemental Digital Content 2**: Latex venous dissection. Upper left image shows the most frequent type III venous drainage, with co-dominant STV and PAV; TFV appears clearly in the anterior view. Upper right image shows a type II drainage, with dominant PAV; interestingly frontal and parietal branches are not visible, contrary to large PAV extension to temporal area. Lower left image shows a type I drainage, with dominant STV and developed PB. Lower right image shows a type I drainage, with hypoplastic temporal extension compensated by largely developed MTV. * MTV location on temporalis muscle after temporalis fascia division. Abbreviations: STV, superficial temporal vein; PAV, posterior auricular vein; TFV, transverse facial vein; PB, parietal branch from STV ; FB, frontal branch from STV; MTV, middle temporal vein; RMV, retro-mandibular vein; EJV, external jugular vein.*

4. Discussion

Our data confirmed the biaxial vascular perfusion findings, as proposed by Ulusal et al. [8], but demonstrated that bipedicle revascularization is not, contrary to previous affirmation, mandatory for whole graft perfusion: a reliable intraauricular anastomotic network allows monoaxial auricle perfusion either on the STA or PAA. Although it has been clearly established that the ear is supplied by PAA and STA distinct angiosomes [46,47], our results confirm former experimental predictions [48] and clinical observations on ear replantation hypothesizing active connections between both angiosomes [40,42,43,49,50]. This dynamic anastomotic behavior is due to the opening of the choke vessels [46,51,52]. In cadaveric studies, selective dye injections may challenge the existence of this *in vivo* dynamic phenomenon.

The STA is an interesting arterial axis for both donor and recipient vessel management. A temporal approach indeed provides an easy vascular access with minimal conspicuous scarring [53-55]. The use of a STA retrograde pedicle spares a long-lasting parotid dissection [56,57]. PAA pedicle exclusion should then be considered, as it aims to avoid deep cervical dissection which is time-consuming and somewhat challenging because of its small caliber and long length. Furthermore, clinical cases of ear replantation have demonstrated positive outcomes, even if the venous pedicle was missing [40,41].

During our dissections, we did not preserve any described extraauricular temporal anastomoses [46], which did not compromise either monoaxial or biaxial perfusion. Due to the extent of numerous strong and constant intraauricular connections, the entire graft supply is unlikely to be compromised during monobloc graft elevation, whichever pedicle should be selected for revascularization. Moreover, due to potential anatomical variations in the recipient, graft pedicle procurement should be extended as much as possible, for both arterial and venous pedicles. As recommended by some authors [44,58], a systematic angiographic assessment should probably be performed preoperatively.

The existence of a reliable auricular subunit model may be of major experimental interest, with its simple but unique association of different tissues. Arterial perfusion of all these tissues may be easily achieved on a single pedicle. As a matter of fact, ST vessels provide the optimal vascular access to a simple model for a basic skin-elastic cartilage association, designed for both immunological studies and first attempts in facial tissue engineering, prefiguring the more extensive application to the nose.

Chapter 3: Porcine ear transplant model

Porcine ear: a new model in large animals for the study of facial subunit VCA.

JPRAS Open – DOI 10.1016/j.jpra.2017.01.004.

Duisit J

Debluts D

Behets C

Gerdom A

Vlassenbroek A

Coche E

Lengelé B

Gianello P.

Summary

In the context of experimental development of VCA, the auricular model has been described in rats and humans, but not in pigs. A porcine ear transplant however, represents an interesting experimental composite facial subunit allotransplant, because of its reduced morbidity, its translational nature but mostly because it is composed of very different tissues. In this perspective, we have studied the anatomical and surgical aspects of an ear subunit VCA in pigs.

Our study was performed on 18 pigs: auricular and cervical regions were dissected without preparation (n=12) or after latex injections (n=2) in the common carotid artery. The angiosomes of the caudal auricular artery and superficial temporal artery were studied with selective injections (n=2). The surgical harvesting protocol was established using the caudal auricular artery as arterial pedicle and tissue perfusion was studied with injection of indian ink (n=1) and angio-CT (n=1). Finally, two *in vivo* orthotopic allotransplantations in four pigs were performed, followed by a short observation period.

The caudal auricular artery was shown to be the dominant artery to the auricle, able to ensure complete ear perfusion. Venous drainage relied on the caudal and rostral auricular veins, dissected down to the maxillary and external jugular veins. *In vivo* allotransplantations confirmed proper auricular vascularization on the sole caudal auricular artery under physiologic conditions.

We have described a new subunit model for experimental face VCA in large animals. Our study reports a reliable harvesting method and easily performed transplantation, with a single-based arterial pedicle.

1. Introduction

Since the first historical limb and face clinical applications in Vascularized Composite tissue Allotransplantation (VCA) [2,59], the experimental field has presented an exponential growth [60-62]. In particular, several facial animal models for VCA have been developed, from full face transplants [63] to subunit models, mainly regarding the auricle, in a few small [64] and large [65,66] animals. Subunit models indeed allow studying of new immunosuppressive regimens, with a complete set of different tissues, while reducing surgical morbidity to the animal [64]. However, small animals are lacking both a pre-clinical dimension and a close-to-human immunological system: the swine on contrary offers these advantages among large animal models [67], resulting in several experimental studies already having been conducted in this species [68-70]. The vascularized pig ear subunit model, therefore represents a relevant model for VCA research in large animals and other isolated-organ studies, concerning elastic cartilage-related subunits. Moreover, the auricle possesses a highly characteristic shape and contains, except bone and mucosa, all the main tissue types involved in facial architecture: skin, cartilage, adipose tissue and even muscle. Furthermore, its harvest and transplantation is associated to less morbidities than more extensive face transplants. Accurate knowledge in specific anatomy however, is lacking for this subunit in current literature [71], because thus far, all surgical anatomy studies have mostly been dedicated to the anterior part of the face and facial nerve distribution [72]. In addition, to simplify transplantation protocols, we hypothesized that a reliable auricular flap could be harvested on the single caudal auricular artery. Therefore, we investigated the constitutive vascular anatomy and perfusion of the ear flap. Finally, we applied our anatomical findings to the design of an ear subunit, its harvesting technique, and followed with a pilot *in vivo* allotransplantation study.

2. Material and methods

Animals and specimens: All experiments were approved by a local ethical committee and carried out in accordance to EU Directive 2010/63/EU for animal experiments. The anatomical study was conducted in 14 pigs: 13 male Landrace piglets (5 to 7 kg) and one adult pig (50 kg) procured right after euthanasia for other experiments. Thereafter, two left auricular allotransplantations were performed *in vivo* using four female adult Landrace pigs (45 to 48 kg).

Latex-injection study: In two heads, red latex (Latex and latex color, Mida, Brussels, Belgium) injection was performed bilaterally in both common carotid arteries (CCA). Heads were then stored at -20 ° C and thawed at room temperature overnight before dissection. Arterial branching patterns were observed, with a particular interest for the caudal auricular artery (CAA). CCA, external carotid artery (ECA), CAA, superficial temporal artery (STA) and rostral auricular artery (RAA) lengths and calibers were recorded.

Angiosomes study: In two heads, STA and CAA were identified bilaterally and prepared for selective dye-injections, performed under constant manual pressure, with 70 ml of methylene blue (MB) mixed with saline in CAA (n=4), and with 70 ml scarlet eosin (EO) mixed with saline in STA (n=2). Stained ear and adjacent integuments were then evaluated for intensity and area of perfusion.

Auricular graft harvesting: A cervical incision line was drawn from the level of the intertragal notch down to a point located posterior to the mandibular angle, following the mandibular ramus and extending downwards to the midline. After superficial muscles section, parotid gland and *parotido-auricularis* (PA) muscle were exposed. Then, the lingo-facial vein, maxillary vein and external jugular vein (EJV) were exposed, with distal extension to the caudal auricular vein (CAV) and rostral auricular vein (RAV) (FIG1A). In this plane, sensitive branches of the great auricular neve could be found. Thereafter, the neurovascular bundle of the neck was exposed: CCA, internal jugular vein (IJV) and vagus nerve were identified laterally to the trachea and larynx. To achieve complete CCA exposure, ECA and

its collaterals, strap muscles, mandibular gland, thymus and hypoglossal nerve were transsected, completed by a paracondylar process osteotomy (FIG1B).

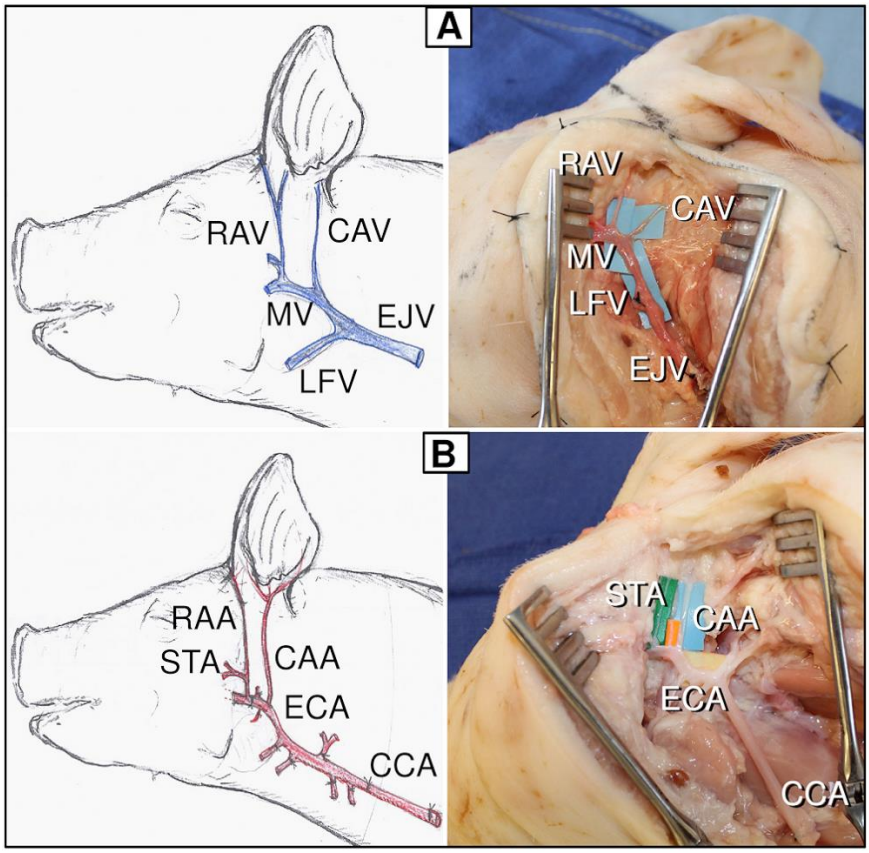

Figure 1: Surgical technique. ***A*** *Venous plane exposure with identification of rostral auricular vein (RAV), caudal auricular vein (CAV), maxillary vein (MV), linguo-facial vein (LFV) and external jugular vein (EJV).* ***B*** *Arterial plane exposure with superficial temporal artery (STA), rostral auricular artery (RAA), caudal auricular artery (CAA), external carotid artery (ECA) and common carotid artery (CCA).*

A circumferential incision at the base of the ear was then performed, including *the cartiligo scutiformis*. Next, starting clockwise from the PA muscle, extrinsic

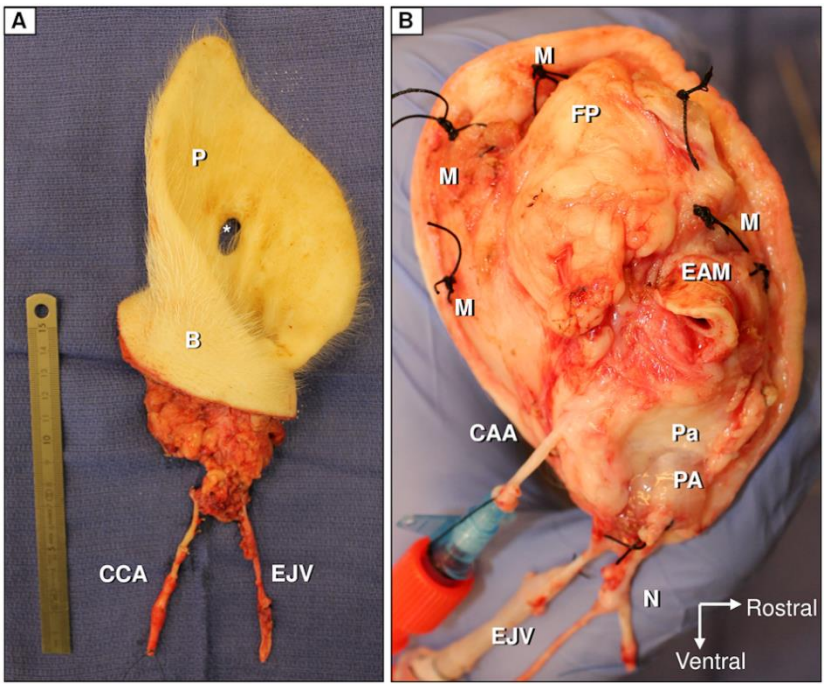

Figure 2: *Ear flap surgical anatomy*. ***A*** *Rostral view of the isolated ear flap with arterial pedicle (CCA) and venous pedicle (EJV). Pinna (P) and basis (B) are dividing the flap in two areas. In the pinna, the asterisk (*) indicates the hole created by animal badge scar.* ***B*** *Surgical anatomy of flap basal section: notice the peripheral distribution muscle stumps (M), with the parotido-auricular (PA) muscle as main ventral landmark, close to the parotid apex (Pa); the auricular fat pad (FP) is identified caudal and ventral to external auditory meatus (EAM). The vascular pedicle with cannulated caudal auricular artery (CAA), EJV, the latter coming with the great auricular nerve (N).*

auricular muscles were transsected. Carefully, annular and auricular cartilages were secured before section, with the CAA running just posteriorly to the external auricular meatus (EAM). Flap elevation was continued lateral to medial, including the deep temporalis fascia and the auricular fat pad. The pedicle was followed and protected down to the neck. Finally, EJV and CAA, eventually extended to CCA, were freed. On the isolated flap (FIG2), CAA was cannulated and perfused with heparinized saline, until observation of a proper and clear venous return.

Angio-CTs scan: Two piglets and one adult auricular flap were injected with 10-15 ml of contrast solution, obtained by mixing 100 ml of physiological saline with 3 g

of gelatin powder (Gelatin, Merck Millipore, Billerica, Massachusetts, USA) and 40 g of Barium Sulfate (MICROPAQUE®, Guerbet, Villepinte, France) in a water bath heated to a temperature of 40 ° C. Injected ears were preserved at 4°C. The computed tomography acquisition was performed on a 256-slice multi-detector CT scanner (iCT scanner, Philips Healthcare, Cleveland, Ohio, USA). Thereafter, reconstructed images were analyzed at the CT workstation (EBW workstation, Philips Healthcare, Cleveland, Ohio, USA) with standard 3D-visualization tools.

Ink perfusion and histology: In one head, an auricular flap was injected with 15 ml of black indian ink (FOUNT INDIA®, Pelikan, Schindellegi, Switzerland) diluted with saline (1:1). Full-thickness biopsies were harvested from the ear pinna, basis and fat pad. Fixed in 4% formaldehyde overnight, the samples were embedded in paraffin, sectioned and stained with Masson's Trichrome.

In vivo allotransplantation: After IM premedication with Tiletamine/Zolazepam (ZOLETIL® 100, Virbac S.A., Leuven, Belgium), 6 mg/kg, and Xylazine (ROMPUN™ Bayer, Shawnee Mission, Kansas, USA), 2 mg/kg, general anaesthesia (GA) was obtained by endotracheal intubation and Isofluran 2% administration (Vapor 19.3, Dräger, Lübeck, Germany). Rocuronium bromide (ESMERON®, Merck & Co. Inc., Kenilworth, New Jersey, USA) IV, 10 mg/ml, was given intra-operatively when required. All surgeries were performed by a single operator with 4.5x magnifying loupes.

Donor ear procurement: All surgical steps followed the previously described protocol, with the arterial pedicle extended to the CCA for the left ear in both donors. Systemic heparin (Heparin LEO®, LEO Pharma, Ballerup, Danmark), 400 UI/Kg, was given 40 minutes before clamping of the pedicle. After elevation, transplants were stored at 4°C until transplantation. Each animal was finally euthanized with Embutramide/Mebezonium iodide/Tetracaine hydrochloride (T-61®, Intervet, Boxmeer, Netherlands) IV injection.

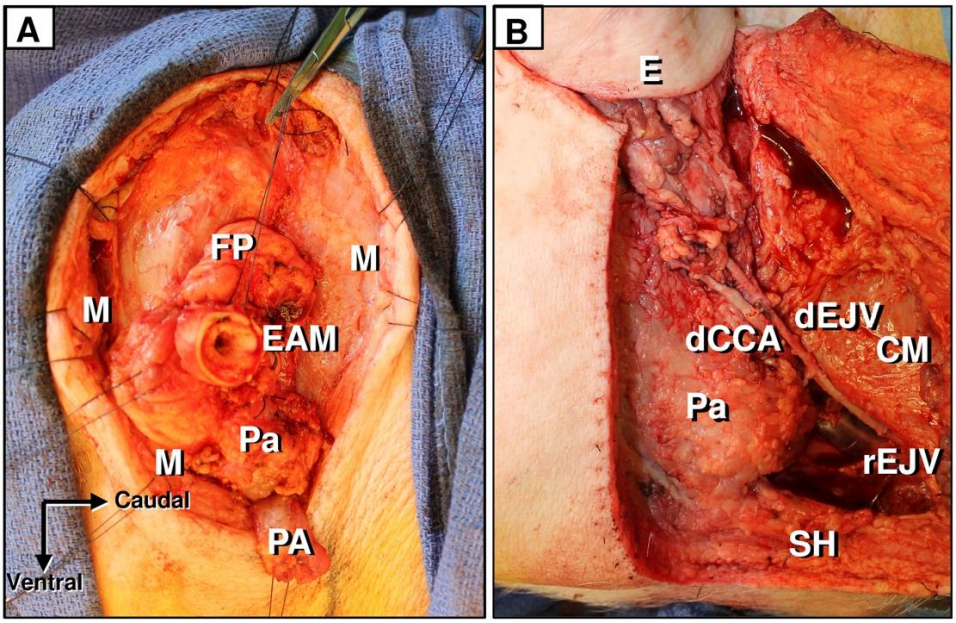

Figure 3: *Auricular allotransplantation procedure*. ***A*** *Lateral view of the left recipient site preparation and anatomy: identification of muscles stumps (M) including the parotido-auricularis (PA) muscle, auricular fat pad (FP) and external auditory meatus (EAM).* ***B*** *Ear flap (E) in position; end-to-side arterial anastomosis between donor CCA (dCCA) and recipient CCA (rCCA). End-to-end venous anastomosis between donor EJV (dEJV) and recipient EJV (rEJV). Anastomosis site is superficially delimited by the sterno-hyoideus (SH) muscle, the cleido-mastoideus (CM) muscle and posterior border of parotid gland (Pa).*

Recipient orthotopic preparation, transplantation and monitoring: After left native auricle explantation, preserving a cuff of *cartiligo scutiformis*, extra-auricular muscle sections and EAM were labelled with nylon sutures (FIG3A). Then, recipient EJV and CCA were exposed. A skin flap was elevated subcutaneously to reach the posterior border of the parotid gland. EJV was identified and secured with a vessel loop. The *sternomastoideus* muscle was identified then retracted medially to expose the CCA after division of the *omohyoideus* muscle. Thereafter transplant was fixed in to recipient cartilages.

Before clamping, systemic heparin was given. Arterial end-to-side CAA-CCA anastomosis was performed, followed by venous end-to-end EJV-EJV anastomosis (FIG3B). Additionally, a catheter was introduced in the transplant's auricular vein

and infused with 10 ml heparinized saline. Finally, skin flap closure was achieved by subcutaneous cutaneous nylon sutures. After unclamping, flap reperfusion was monitored for tegumental changes, congestion, and oximetry for one hour under general anesthesia (GA), before and after skin closure. Finally, both recipients were euthanized with a lethal T-61® IV injection.

3. Results

Piglet arterial morphometry and distribution: The CCA, with a mean caliber of 3±0.3 mm and length of 50±7 mm, presented constant collaterals, namely in a caudal to rostral direction: rostral laryngeal artery, rostral thyroid artery, occipital artery and internal carotid artery observed in a common trunk, ascending pharyngeal artery and rostral laryngeal artery (FIG4A). The ECA, had a mean caliber of 2.6±0.2 mm and length of 22±5 mm, was in direct continuity with the CCA and presented, after crossing the hypoglossal nerve, the following collaterals: lingual artery, facial artery, CAA and a branch to the parotid. The ECA terminated as STA and maxillary artery, shortly after crossing the mandibular ramus (FIG4A). STA, when present in an initial short trunk gave rise to a branch to the masseter muscle, a branch to the pre-auricular lymph node, the transverse facial artery and the RAA: the latter presented a mean caliber of 0.5±0.1 mm and length of 26±3 mm. CAA was found with a mean caliber of 1±0.2 mm and length of 27±6 mm; it presented branches to the parotid gland and pre-auricular lymph nodes. In the intra-auricular course of the CAA, several branches were observed to the pinna and basis, to the intrinsic and extrinsic auricular muscles (FIG4B). RAA course was parallel to the CAA, and more difficult to expose clearly. Distal CAA ran at the posterior side of the pinna cartilage and gave off several perforating branches to the anterior skin (FIG4B).

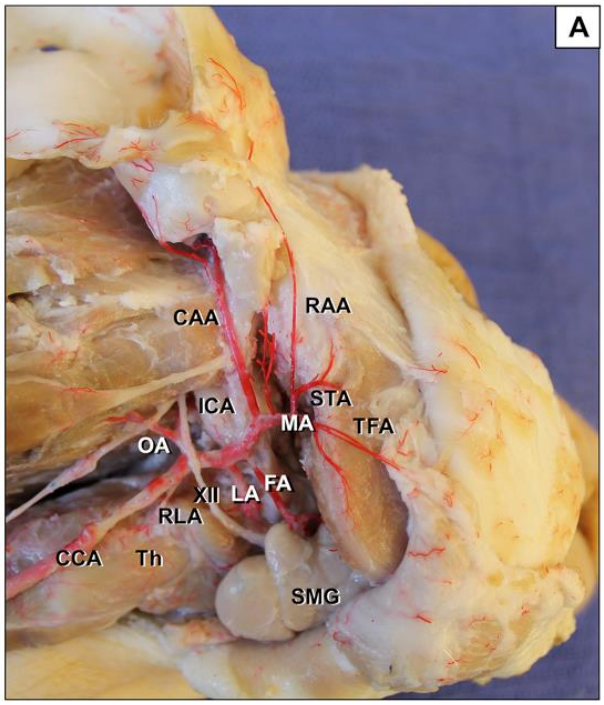

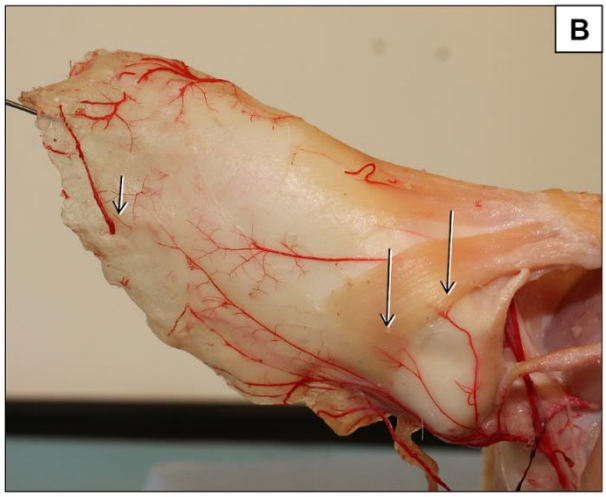

Figure 4: *Latex-injection. **A** Caudo-lateral view of cervico-auricular arterial network in latex-injected specimens: common carotid artery (CCA), recurrent laryngeal artery (RLA), occipital artery (OA), internal carotid artery (ICA), lingual artery (LA), facial artery (FA), caudal auricular artery (CAA), maxillary artery (MA), superficial temporal artery (STA), rostral auricular artery (RAA), transverse facial artery (TFA). The other important structures to consider are: the submandibular gland (SMG), hypoglossus nerve (XII) and the thyroid gland (Th). **B** CAA perforating branches (short arrow) and muscular branches (long arrows).*

Angiosomes: CAA perfusion territory included the whole ear area, with intense staining of the anterior and posterior sides of the pinna, and involved its whole basis of implantation (FIG5A). Additionally, staining undertook the posterior scalp

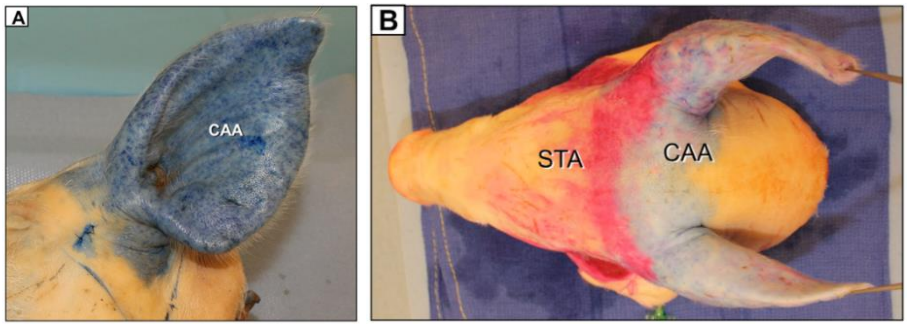

Figure 5: *Angiosomes*. ***A*** *Rostral auricular views of CAA angiosome territory after methylene blue perfusion.* ***B*** *Superior cephalic views of combined STA (eosin) and CAA (methylene blue) perfusion territories.*

area, with no midline crossing. STA perfusion area covered the whole ear but in a very less intense fashion than the CAA. Staining extended to the rostral facial area, without crossing the midline. In combined STA/CAA injections, CAA staining territory was predominant on STA regarding ear perfusion (FIG5B).

Harvested pedicled ear: Mean weight of grafts was 40.4±3.7 g. All harvested ears presented a satisfying venous drainage through EJV after saline perfusion, which appeared quickly clear and associated with whitening of the whole flap: later on, sufficient outflow was confirmed by emptiness of the large posterior auricular veins, demonstrating adequate wash of the vascular network.

Isolated ear CT imaging and histology: In all specimens, CT-scan 3D reconstruction showed a complete perfusion of the entire ear transplant vascular tree, with full extension to the whole parenchymal area (FIG6A). Indian ink-injected ears confirmed EAM staining. On histological sections, ink was detected in the lumen of the arteriolar capillary bed. On a biopsy of the lower half of the pinna, all major constituting tissues - skin, adipose tissue, cartilage and muscle - could easily be assessed at once (FIG6B).

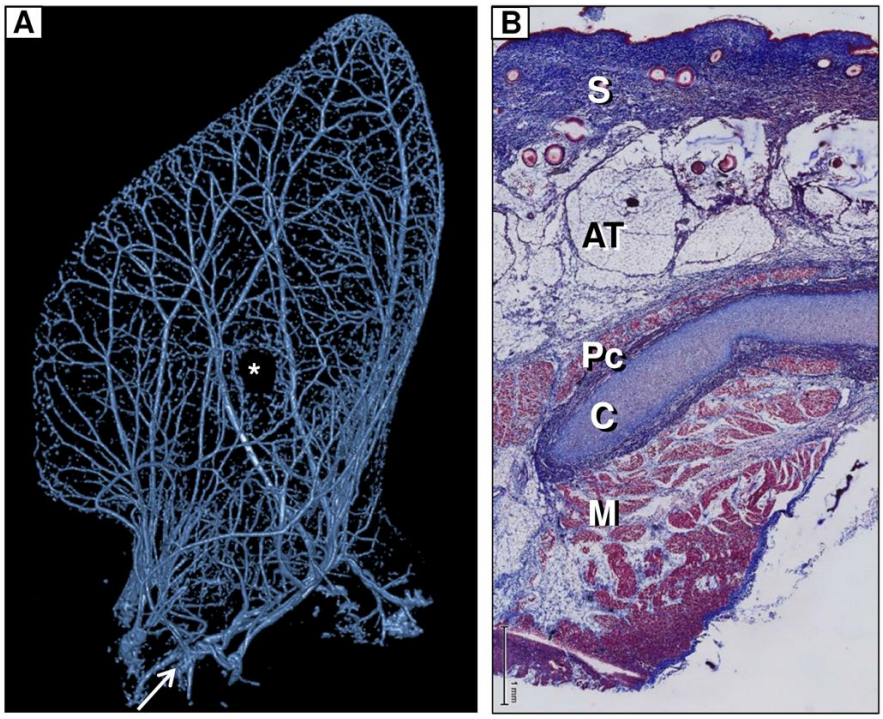

***Figure 6**: Perfusion imaging. **A** Angio-CT and 3D-volume rendering of barium sulfate injected ear flap, through caudal auricular artery (arrow). The asterisk (*) indicates the scar from animal labelling. **B** 10x Masson's Trichrom auricular base biopsy: all composite tissues can be obviously identified: skin and adnexes (S), adipose tissue layer (AT), perichondrium (Pc), auricular cartilage (C) and auricular muscle (M).*

In vivo allotransplantation study: Mean weight of donor versus explanted ears (recipient) was 200±10 g and 189.5±29.5 g. For the first transplantation couple: graft arterial pedicle total length was 94 mm, with 43 mm CCA, 21 mm ECA and 30 mm CAA. EJV length was 60 mm, between the maxillary vein and the anastomosis. Donor/recipient calibers were: 5.9 mm/6 mm for EJV, 3.8 mm/3.9 mm for CCA; flap CAA caliber was 1.6 mm. In the second transplantation couple: graft arterial pedicle total length was 100 mm, with 45 mm CCA, 20 mm ECA and 35 mm CAA.

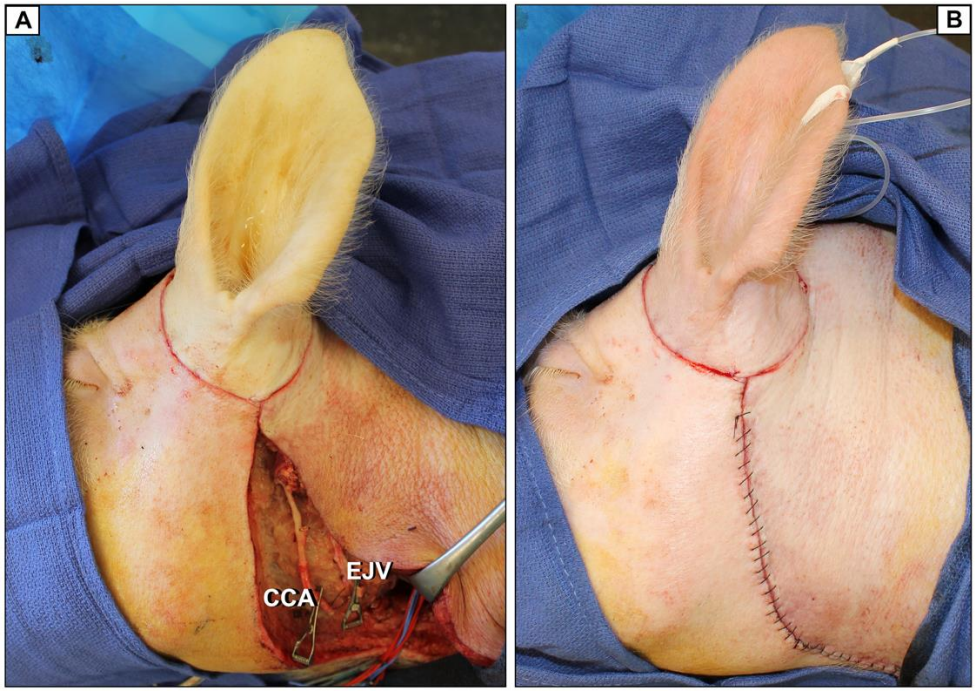

***Figure 7**: In vivo reperfusion of auricular allotransplant. **A** Flap fixed in position, before vascular anastomosis with prepared pedicle: common carotid artery (CCA) and external jugular vein (EJV). **B** Allotransplant aspect after 2 hours of reperfusion and skin closure. A peripheral catheter in the posterior auricular vein with slow heparinized saline instillation enhances optimal venous drainage.*

EJV length was 62 mm. Donor/recipient calibers were 5 mm/6 mm for EJV, 3.4 mm/ 3.5 mm for CCA; flap CAA caliber was 1.5 mm. Total time for venous and arterial anastomoses was respectively 33 and 29 min, with no particular technical difficulties. Warm versus cold mean ischemia time was 1.5/3 hours. Total surgical time was 210 ± 45 min for donor harvesting and 190±30 min for recipient implantation, at time of anastomosis completion. After unclamping in both recipient animals, transplanted ears presented a quick and homogeneous reperfusion, with good venous and arterial patency (FIG7A).

In the first following 20 minutes, the ear presented some congestion which resolved quickly, with additional perfusion of heparin through a catheter inserted

in a posterior auricular vein. Oxygen saturation was measured at 98%, with a pulsatile flow. Capillary refill was satisfactory. After peri-auricular and cervical skin closure, perfusion and venous drainage remained satisfactory (FIG7B). The transplant was easily sutured and positioned in the recipient site, with a good morphological outcome of the reconstructive transplantation.

4. Discussion

We have demonstrated that a vascularized pig ear subunit could be harvested and reliably perfused by the sole CAA, allowing a safe, quick and easy approach to a VCA subunit model in large animals, with a low-morbidity orthotopic transplantation. Given the size and location of the transplant, less per- and postoperative morbidities are inflicted on the animal, especially in a model that can be designed for unilateral or bilateral study, an advantage of a paired transplant. Moreover, this model is very preclinical compared to a small animal ear subunit transplantation model [64], for both adult and piglet ears. The adult pig ear transplantation presents the advantage of a better-suited and larger caliber of vessels for anastomosis and thus an easier surgical approach for a non-expert in microsurgery. In terms of perfusion, we have demonstrated that the main arterial auricular pedicle is the sole CAA. The STA represents a complementary but not necessary vascular supply. These anatomical features differ significantly from the descriptions made until now in human [8], sheep [66] and rat [64] auricular subunit transplant models, all referring to a bi-pedicle arterial description, contrary to ours which relies on a specific CAA/STA comparative study, with induced choke vessels opening and patency. In case of full face or half-face transplantation, harvesting both STA and CAA is the best approach, but tends to add more difficulties than for a single ear subunit: the RAA branch from the STA is very thin compared to the CAA and runs in a difficult area for a safe and easy dissection. Compared to humans, where the posterior auricular artery (PAA) and STA angiosomes are very complementary for perfusion [73], we observed a dominant PAA angiosome for this subunit: this could be explained by the larger pinna development in pigs. Interestingly, according to our results, STA alone could still

sustain isolated ear perfusion, if CAA was unavailable. During back-table preparation, the parotid apex should be removed to avoid postoperative morbidities related to salivary production, cyst formation and infections, described in larger face transplant models by Kuo et al [68]. Vascular anatomy and measurements were similar to other descriptions [74]. Interestingly, calibers presented similar values between latex-injected piglets and *in vivo* adult pigs, because of very strong vasocontrictive phenomena in pigs. This vasoactive phenomenon, together with the difficulty to achieve a direct CAA end-to-end anastomosis due to poor exposure and small arterial caliber, emphasizes the interest of a distal CCA end-to-side approach. Consequently, for reliable standard experimental surgery conditions, we advocate the harvest of a long pedicle for both EJV and CCA, with as much length as possible to reach a safe cervical anastomotic site, bridging over the parotid gland. Regarding motor nerve reattachment, besides its technical difficulty in this model and the limited functionality of auricular muscles, the absence of neural re-anastomosis will not highly impact ear motricity: during flap implantation, suturing distal muscle stumps to recipient proximal bellies whose innervation is intact, will probably lead to partial motor nerve regeneration through intramuscular growth and neurotisation [2]. The same features can justify the absence of sensitive nerve recovery, with reduced postoperative morbidity. Alternatively, nervous anastomosis could be performed in further studies, adding motor and sensitive recovery in the postoperative evaluation. When comparing adult versus piglet models, despite the previously described interest of the latter to match human ear mass, a larger animal model should be preferred to prevent technical issues in harvesting and anastomosis, considering distal end-to-end CAA anastomosis, in a more surgically dedicated model. Even if, as explained above, an adult pig model is preferable, piglet ears can represent a strategy to study VCA in newborns, as described by Solla et al [75]. For immunological studies, the model can be used with Massachusetts General Hospital (MGH) miniature swine models for discordant transplantation [76]. In the relative antigenicity concepts of VCA, as established by Lee et al in the rat [77], porcine ear represents an interesting broad composite tissue

association, combining skin, fat, muscle, cartilage and associated vessels and nerves, and could be studied on a single biopsy. The different types of tissues involved has a more relevant impact than the absolute mass of tissues: Lee et al. [77] for example, demonstrated that in the immunological outcomes of a primarily vascularized composite tissue allograft, muscle tends to be more immunogenic than skin; this relative antigenicity can also be different, when comparing simple tissue implantation versus a combination of tissues. Constitutive endothelial Swine Leucocyte Antigen (SLA) Class II expression, present in humans and pigs and absent in rodents [78], is another important aspect for considering pig ears as a primarily vascularized VCA model. This method thus offers the advantage of a common approach for animal labelling with few morbidities. The described subunit model is mostly used for immunological-based research but, in the rising era of facial subunits VCA and all related future fields of research, like tissue engineering, it has the potential for very large applications.

5. Conclusions

We provided an extensive description of the surgical anatomy and technique for auricular transplantation in the porcine model, representing a new subunit model for experimental VCA in large animals. Our study demonstrated a reliable pedicle based on the sole CAA and auricular veins, resulting in an easier and faster technique than in the previous models. The muscular component in this model provides an important value for immunological studies in large animals. The anatomical and surgical findings described in this study regarding pig auricular subunit transplantation are the first basic steps for further investigations on prolonged *in vivo* orthotopic allotransplantation, allowing testing of new experimental approaches for VCA tolerance induction and the development of innovative tissue engineering strategies.

Acknowledgements:

This work was financially supported by Fondation Saint-Luc and FSR-UCL (Fonds Spécial de la Recherche) grants. The content of the work is solely the responsibility of the authors.

We would like to thank M. Martial Vergauwen, M. Gwen Beaurin and M. Eric Legrand for technical assistance during animal anatomical preparation and dissection, Mrs Pascale Segers and M. Walter Hudders in manuscript and illustrations editing.

« Il n'y a pas de vérités premières, il n'y a que des erreurs premières. »

Gaston Bachelard

Section 2- Tissue Engineering studies: Non-motor subunits

Summary

In this section, we first applied the perfusion-decellularization/recellularization technique to a non-motor, cartilage-based, auricular subunit. The ear was selected, as a first model described in **Chapter 3**, because of its limited functionality, lower volume to treat and nearly complete spectrum of all elementary tissues involved in the facial VCA. In **Chapter 4**, a SDS detergent-based protocol for decellularization was used in our pig model in order to obtain a transplantable vascularized scaffold, which was extensively characterized through detailed histological, biochemical and mechanical analyses. The other primary aim of this inaugural study was to specifically investigate the allocompatibility of the decellularized composite graft, using a strong semi-identical porcine model. Thereafter, we developed an original set-up for scaffold recellularization and tested the feasibility of an efficient sterile cell-seeding in a bioreactor. At the end, we were able to produce a complex matrix, with an accessible vascular tree, which gained a full allocompatibility and was partially recellularized in a bioreactor.

In **Chapter 5**, we hypothesized that previous results obtained in the pig could be directly applied to human ear grafts, using cadaveric donors, according to a similar protocol. Actually, we demonstrated this work hypothesis, but also emphasized the mandatory addition of a polar solvent step to completely treat the adipose tissue.

Chapter 4: Porcine ear bioengineering

Decellularization Of The Porcine Ear Generates A Biocompatible, Non-Immunogenic Extracellular Matrix Platform For Face Subunit Bioengineering.

Annals of Surgery 2017 Mar 1.

Duisit J
Orlando G
Debluts D
Maistriaux L
Xhema D
Janssens de Bisthoven Y
Peloso A
Behets C
Lengelé B
Gianello P.

ABSTRACT

***Objective*:** The purpose of this study was to assess whether perfusion-decellularization technology could be applied to facial grafts.

Background Data: Facial allotransplantation remains an experimental procedure. Regenerative medicine techniques allow fabrication of transplantable organs from an individual's own cells, which are seeded into extracellular matrix (ECM) scaffolds from animal or human organs. Therefore, we hypothesized that ECM scaffolds also can be created from facial subunits. We explored the use of the porcine ear as a clinically relevant face subunit model to develop regenerative medicine-related platforms for facial bioengineering.

***Methods*:** Porcine ear grafts were decellularized and histologic, immunologic, cell culture studies done to determine whether scaffolds retained their 3D framework and molecular content; were biocompatible *in vitro* and *in vivo*, and triggered an anti-MHC immune response from the host.

***Results*:** The cellular compartment of the porcine ear was completely removed except for few cartilaginous cells, leaving behind an acellular ECM scaffold; this scaffold retained its complex 3D architecture and biochemical components. The framework of the vascular tree was intact at all hierarchical levels and sustained a physiologically relevant blood pressure when implanted *in vivo*. Scaffolds were biocompatible *in vitro* and *in vivo*, and elicited no MHC immune response from the host. Cells from different types remained viable and could even differentiate at the scale of a whole-ear scaffold.

***Conclusions*:** Acellular scaffolds were produced from the porcine ear, and may be a valuable platform to treat facial deformities using regenerative medicine approaches.

1. Introduction

Since the first groundbreaking report in 2005 [1,2], only 35 cases of partial to full facial transplantation (FAT) have been reported worldwide [79]. Continued issues include lack of consensus on indications, complexity of the procedure, and lack of suitable donors. Moreover, FAT raises major ethical concerns because disfigurement is not a life-threatening condition [80]. Such patients could significantly improve their quality of life and self-perception, but at the price of an expensive therapy and lifelong immunosuppression, whose cost-benefit balance remains unclear.

In the past two decades, regenerative medicine has shown great promise to meet the most urgent needs of modern organ transplantation, namely immunosuppression-free transplantation and the identification of a new, potentially inexhaustible source of organs [81]. Among the numerous technologies currently under development, so-called decellularization or cell-on-scaffold-seeding technology (CSST) [82] may be the quickest route to clinical application. In CSST, mammalian organs are decellularized through continuous perfusion of a detergent-based solution, to obtain extracellular matrix (ECM) scaffolds that will be reseeded with the individual's own cells [83].

This approach maintains the framework of the innate vasculature, which is critical for successful *in vivo* implantation [84-86]. ECM scaffolds can be successfully and consistently produced from all mammalian tissues, maintain their architecture and gross molecular composition, retain numerous growth factors within the 3D structure of the ECM, are non-immunogenic, relatively tolerogenic, and show physiologically necessary properties [87-91]. Importantly, when multipotent stem cells are seeded on such scaffolds, cells attach well, can migrate throughout the 3D framework of the scaffold, remodel the ECM, and can mount an inflammatory response in which a strong angiogenic response is obvious. Hence, acellular ECM scaffolds are frequently used as a biological template in regenerative medicine approaches to fabricate organs for transplantation [85,86].

Decellularization technology has been applied to composite tissues like the larynx in rabbits [92] and rats [93]. More recently, in an attempt to develop an appropriate model for limb bioengineering, acellular ECM scaffolds with preserved composite architecture were created through detergent-based decellularization of rat and primate forearms [94]. Promising results proved that composite tissues may be a valuable source of ECM scaffolds for bioengineering purposes, despite their anatomic complexity. We therefore inferred that CSST could be applied successfully for facial tissue reconstruction. We also hypothesized that decellularization techniques may be valuable for facial bioengineering research, with the ultimate goal of developing regenerative medicine-related therapies to treat facial deformities.

In this paper, we present our initial experiments with the porcine ear as a pre-clinical model for facial subunit CSST, as a first step towards total facial bioengineering.

2. Material and Methods

All experiments were approved by the local ethical committee at the Université catholique de Louvain (Brussels, Belgium) and were conducted in accordance to the EU Directive 2010/63/EU for animal experiments.

Ear graft preparation: Thirteen ear grafts were harvested from Massachusetts General Hospital (MGH) adult pigs and Landrace piglets under general anesthesia, with the caudal auricular artery (CAA) and external jugular vein as vascular pedicle (Fig. 1A-D), as previously described [95]. A 24G or 27G catheter was inserted into the CAA and the ear graft was flushed with heparinized saline until venous outflow became clear. Pigs were then euthanized by systemic infusion of T-61 Euthanasia Solution.

Ear graft decellularization: The arterial catheter was connected to a Masterflex L/S, easy load pump head and L/S 16G tubing (Cole-Parmer Instrument Co), with pressure remaining under 80 mm Hg. Following a previously published protocol [96],

heparinized serum (15 UI/ml) and 10 μM adenosine (Sigma-Aldrich) was perfused (1 liter). Subsequently, 1% SDS was perfused through the system (44.5 liters), during which time the graft was monitored for edema, epidermolysis, bullae formation, and for extra-auricular muscle stumps and adipose tissue bleaching at the base. At the end, deionized water was flushed (2 liters) to wash out SDS. Thereafter, scaffolds were rinsed with 1% Triton-X 100 solution (3.5 liters), followed by PBS (28 liters). Finally, type I DNAse from bovine pancreas (Roche, Sigma-Aldrich) was perfused at 37°C (1 liter), and briefly washed with PBS (2.5 liters). The porcine ear acellular scaffolds (peaECMs) were then stored at 4°C in PBS.

DNA and ECM proteins in native and decellularized samples: DNA was extracted with DNeasy Blood & Tissue Kit (Qiagen) and quantified using the Quant-it™ Picrogreen® dsDNA Reagents kit (Thermo Fisher Scientific). GAGs, elastin, and collagen proteins were quantified using the Blyscan™ sulfated glycosaminoglycan assay kit (Biocolor Ltd.), the Fastin™ elastin assay kit (Biocolor Ltd.) and the hydroxyproline assay kit (Chondrex, Inc.), according to each manufacturer's protocol.

Basic histology, immunohistochemistry (IHC) and immunofluorescence (IF): peaECMs and native ear (N-Ear) samples were fixed in 4% formalin for 24 hours, then paraffin-embedded, sectioned into 5μm-thick samples and mounted prior to staining. Slides were either digitized and analyzed with a slide scanner (SCN400, Leica Microsystems) or visualized using fluorescence microscopy (AxioImager Z1, Zeiss).

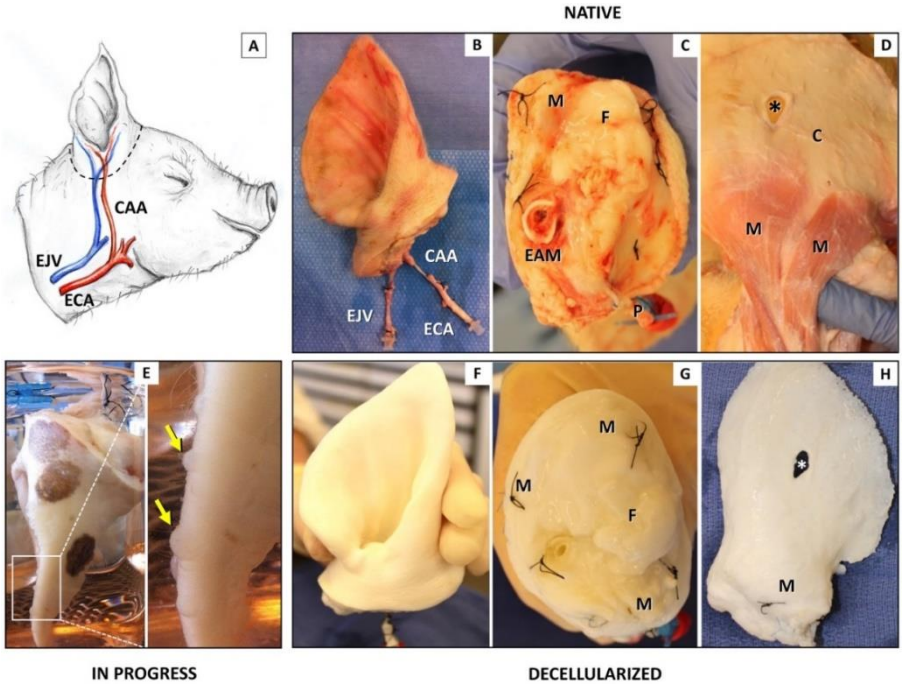

Figure 1. *Porcine ear graft procurement and decellularization.* ***(A)****: Anatomic landmarks for procurement of the porcine ear. Ears were procured starting with a cervical incision to expose the external jugular vein (EJV) and its branches to the auricle. Then, the vascular pedicle of the ear represented by the caudal auricular artery (CAA) was exposed and prepared until the external carotid artery (ECA).* ***(B)****: Ear graft with its vascular pedicle cannulated and prepared for decellularization.* ***(C)****: Basis of the graft: external auditory meatus (EAM), fat pad (F), pedicle (P) and extra-auricular muscle stumps (M).* ***(D)****: Ear cartilage (C) in the posterior auricular muscles after skin resection.* ***(E)****: Left image shows graft after 24 hours of SDS perfusion: skin is clearing and blisters are visible on pinna. Right image shows enlarged view of blisters (arrows); these will evolve into large bullae, indicating accurate epidermolysis induced by detergent perfusion.* ***(F)****: peaECMs with preserved shape and morphology, and cartilage able to sustain pinna erection.* ***(G)****: Basis of peaECMs: the fat pad (F) and muscular stumps (M) present the aspect of complete decellularization.* ***(H)****: Treated extra-auricular muscles (M) after removal of the cutaneous layer. (*) Hole from farm labeling device.*

For standard histology, we used hematoxylin and eosin, Masson's trichrome, and Safranin-O stains.

For IHC/IF, sections were processed as previously described [97], incubated with the following primary antibodies against: TGF-β1 (1:400; Abcam, ab92486), Swine

Leucocyte Antigen (SLA) class Ic (1:200; 16.7.E4.2: IgM), collagen type IV (1:500; Abcam, ab6586), fibronectin (1:200; Abcam, ab23751), laminin (1:50; Abcam, ab11575), van Willebrand factor (1:600; Abcam, ab6994), CD31 (1:50; Abcam, ab28364), vascular endothelial growth factor (VEGF, 1:200; Santa-Cruz, sc-53462). Nuclei were counterstained with 40-6-diamidino-2-phenylindole (DAPI) for IF, and hematoxylin for IHC. Negative controls lacked primary antibody.

Scanning electron microscopy (SEM): Tissues were prepared according to a previously described protocol [88] and analyzed with a field-emission scanning electron microscope (JSM-7600F, Jeol).

Mechanical testing: to test mechanical properties, we used a universal testing machine (Instron-5666, Instron Corporation). To assess cartilage rigidity, a ball burst test was performed. To do this, a 4-mm diameter steel ball with 1mm/min loading rate, with either 100N or 200N static load cells, was applied to decellularized (n=14) and native (n=9) disc samples. Skin elasticity was tested in decellularized (n=11) and native (n=8) dogbone-like shape samples, with a loading rate of 5 mm/min. Endpoints were the Young's modulus, failure stress, and failure strain.

***In vivo* allo-compatibility testing:** We used a well-defined semi-identical MGH miniature swine model [98] for implantation testing. Four SLA^{CD} (class $I^{C/D}$, class $II^{C/D}$) pigs were used as ear donors, while 3 SLA^{DD} (class $I^{D/D}$, class $II^{D/D}$) as recipients, in a one-haplotype mismatch allo-transplantation model. Samples of peaECMs skin (D-S), cartilage (D-C), and full-thickness (D-FT) skin were taken from each donor. Samples were placed into a pouch created in the pre-peritoneum. Identical tissue types from different donors were grouped and implanted in the same recipient; as a control, four native FT (N-FT) samples were implanted in a recipient. To monitor the development of a humoral immune response, we screened circulating anti-donor anti-SLA Ic/IIc alloantibodies (IgM and IgG) in blood samples collected from all recipients, at postoperative days 0, 10, 20, and 30. Alloantibodies were detected using FACS (BD FACSCalibur, BD Biosciences) driven by CellQuest Pro software (BD Bioscience), following previously described methods [99]. At day 30,

pigs were euthanized and implants were collected and processed for histology with Masson's Trichrome (MT), IHC for CD3 (1:300; Thermo-Scientific, RM-9107), and IF for CD31 staining.

AngioCT: To assess patency and integrity of the vascular tree, angioCT scanning was performed after contrast injection in peaECMs and controls, using a 256-slice multi-detector CT scanner (Philips Healthcare). Reconstructed images were analyzed with standard 3D-visualization tools.

***In vivo* revascularization of acellular porcine ear scaffolds:** To assess whether the preserved framework of the innate vasculature would sustain physiologically relevant blood pressure, we orthotopically replanted one acellular porcine ear scaffold in an adult pig, under general anesthesia. Systemic heparinization was achieved before beginning anastomosis (400 UI/Kg). End-to-side anastomosis was performed between scaffold artery and recipient common carotid artery, and again between the scaffold vein and recipient internal jugular vein. The vascular clamp was then removed and blood was allowed to flow within the acellular graft for three hours before euthanasia.

Disc seeding, biocompatibility and differentiation study: To assess whether the scaffolds would durably host new cells and allow them to differentiate, 1 cm^2 discs obtained from our peaECMS were sterilized with 0.1% peracetic acid (PCA) at 4°C, then statically seeded and cultured in a CO_2 bioreactor under standard conditions (5% CO_2, 37°C), with culture medium changed every 2 days.

Cos-7 cells were used to test attachment and proliferation of a fibroblastic cell lineage. Seeding was performed on skin, cartilage and muscle samples, at a density of $2.6x10^6$ cells per disc (n=13). Constructs were cultured in Dulbecco's Modified Eagle Medium (DMEM, Lonza), supplemented with 10% FBS, 1% L-Glutamine and 1% P/S, defined as proliferating medium. After 9 days, samples were processed for histology using H&E and anti-Ki67 (1:1; Abcam, ab21700) IHC staining. The ratio of Ki67+ cells to H&E-stained cells was used as a proliferation index.

***GFP+* porcine bone marrow mesenchymal stem cells** (pBM-MSC) from green fluorescent positive (GFP+) transgenic pigs (Avantea, Cremona, Italia) were isolated and cultured as previously established [100,101], to study ECM-based stem cell differentiation. Static seeding was performed on hypodermic side of samples, at a density of $1.5x10^5$ cells per disc. Discs were divided in two groups of cultures: proliferating medium (PM, n=8) or adipose differentiating medium (ADM, n=8) supplemented as previously described [102]. Discs without cells and cells alone were used as controls in each group. After 15 and 25 days, samples were examined either by direct, or whole-mount non-vital staining (Live/Dead Kit, Life Technologies), and subjected to GFP visualization under a fluorescence microscope.

Whole ear bioreactor seeding: We tested vascular cell seeding in whole piglet ears (n=2). After sterilization with 0.1% PCA and PBS perfusion, scaffolds were put in a sterile 1L bioreactor (Fig. 7I), placed in a CO_2 incubator under standard conditions, and continuously perfused with PM for 12 hours. We designed two types of cell seeding experiments:

pBM-MSC: To study distribution of stem cells throughout the scaffold and reproduction of ECM-based differentiation in whole graft bioreactor seeding conditions, $16x10^6$ pBM-MSCs were delivered through the arterial inlet, through four sequential injections of $4x10^6$ cells every 40 minutes. After each, an injection of medium was performed, with volume corresponding to the calculated dead space of tubing, followed by a limited static hold. Perfusion flow was set at 2 ml/min, then increased to 4 ml/min. After 2 weeks, biopsies were sent for IHC staining for collagen type I (1:250; Abcam, ab34710) with DAPI. Additionally, biopsies were embedded in OCT and frozen sections were stained with type IV Sudan for lipid detection.

NIH-3T3: In a different experiment, 70×10^6 NIH-3T3 cells (Sigma-Aldrich) were seeded with four intravascular injections of $17.5x10^6$ cells, with 30 minutes of static hold, after 0, 1, 20 and 22 hours. Flow was set at 1 ml/min and then increased to 4 ml/min. After 10 days, all culture medium was retrieved, samples were centrifuged to extract circulating cells outside the graft; a cell count was

proceeded to calculate an engraftment percentage. Biopsies (n=20) were treated with vital (Live/Dead) whole-mount staining or sectioned and stained with H&E.

Statistical analysis: All statistical analyses were performed using Prism version 7 (Graphpad Software). Significance was set at $p<0.05$ for unpaired Student's t-tests. All values were expressed as means ± standard error of the mean (SEM).

3. Results

Scaffold decellularization: cell removal and ECM preservation. Our perfusion method successfully and consistently cleared the cellular compartment of all ear grafts, while preserving their ECM. Macroscopically, epidermal bullae appeared in the first 24 hours (Fig. 1E); then porcine ears lost their epidermis and whitened within a few days, and they eventually became completely white after five days (Fig. 1F-H). H&E staining did not detect any cellular nuclear material (Fig 2A); this was confirmed by negative DAPI staining (Fig. 2B). These results, along with an overall 91.3% DNA reduction, were interpreted as indirect evidence of cellular clearance. However, we noticed some residual cell groups in cartilage biopsies, with a less significant difference compared to other tissues (Fig. 2C). Our scaffolds maintained the 3D framework and essential molecular composition of the innate ECM. Homogenous blue staining consistent with collagen was observed at all levels with MT staining (Fig. 3A). Safranin O staining showed architectural preservation of proteoglycans, with more reduction in the peripheral cartilage (Fig. 3B). IF for fibronectin (Fig. 3C), laminin and VEGF (Fig. 3D-E), and IHC for TGF-ß1 (Fig. 3F), a key factor in tissue remodeling and regeneration [103], confirmed preservation of essential components of the matrisome and ECM-associated proteins. SEM analysis showed a dense fibrous matrix and reticular fibers with preservation of functional structures such as dermal papilla (Fig. 3G-H). Laminin was preserved on the dermal side during epidermolysis (Fig. 3I), which is critical for epidermal reconstruction [104].

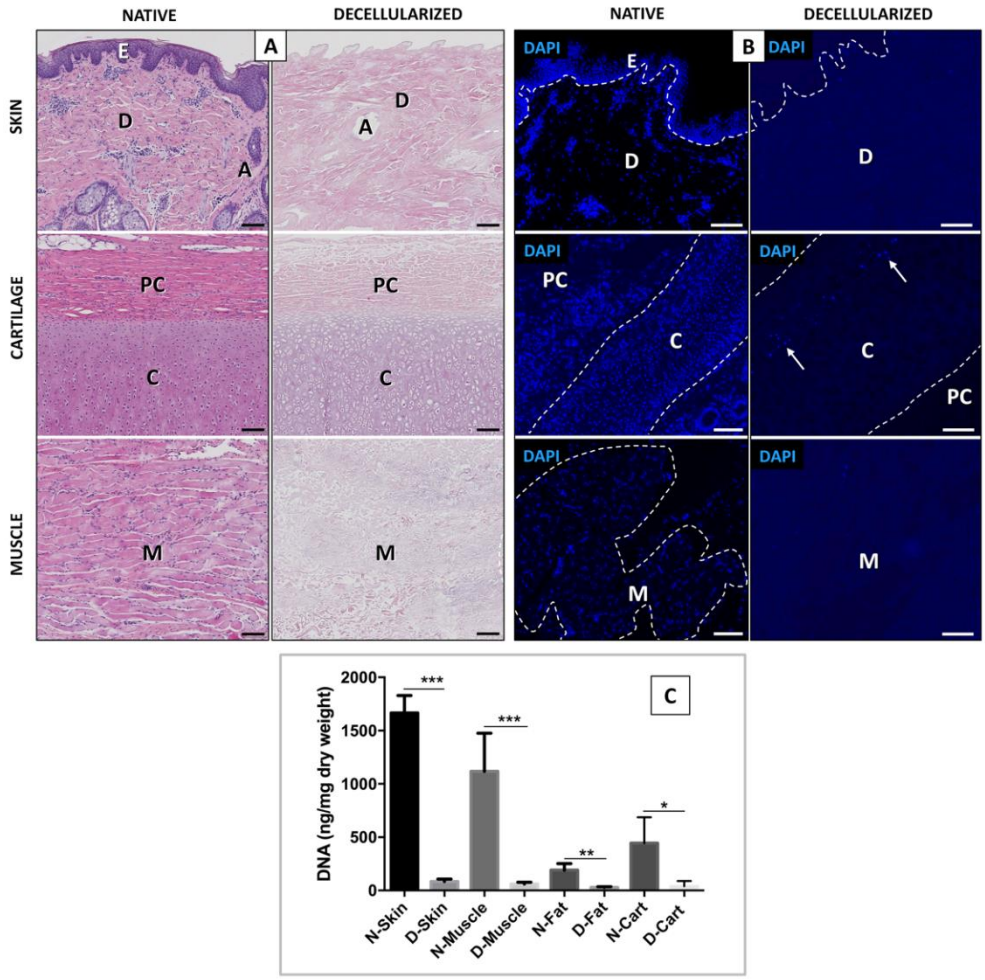

Figure 2. *Microscopic evaluation of peaECMs*. ***(A)***: *H&E staining of native (left) versus decellularized (right) tissues. All layers of the acellular ear scaffold –the epidermis (E), dermis (D) with adnexes (A), perichondrium (PC) and muscle (M) – were totally acellular, with the 3D framework of the ECM preserved; cartilage (C) shows some positive nuclei staining in the depths. Scale bars represent 100 μm.* ***(B)***: *DAPI staining of native (left) versus decellularized (right) tissues. The "starry sky" appearance typical of cellular tissues is absent, but some chondrocyte positivity is seen in some biopsies (white arrow).* ***(C)***: *DNA content in native (N-) versus decellularized (D-) porcine ear skin, muscle, and fat tissues (ng/mg dry weight tissue). Most DNA is cleared by the decellularization process. Mean ± SEM; *p<0.01, **p<0.001, ***p<0.0001.*

After decellularization of cartilage, collagen was highly preserved, elastin content was reduced by 50% in dermis, and GAGs content was reduced by 60% (Fig. 3J). This latter finding is consistent with another study [94] but in contrast to previous reports, in which GAGs were mostly cleared after decellularization [105-108]. In mechanical testing of cartilage, Young's modulus was 79.2±9.9 N/mm^2 in decellularized samples vs 91.9±27.8 N/mm^2 (p not significant) measured in the native tissue, correlating to a satisfactory preservation of the ECM framework. For skin, however, the elastic modulus in acellular tissue was significantly inferior to the native counterparts, with 24±4.9 versus 154.3±34.7 MPa ($p<0.05$) (Fig. 3K).

***In vivo* evaluation of the immunogenicity of peaECMs:** Implanted scaffolds were previously found negative for SLA antigen markers (Fig. 4A). Implantation was well tolerated and no adverse reactions were noticed. Importantly, no implanted scaffolds induced any relevant inflammatory processes, as demonstrated by the low inflammation at the implantation site, and by the lack of remodeling in the scaffolds themselves highly repopulated with signs of revascularization (Fig. 4B-E). Moreover, recipients did not produce anti-donor SLA specific antibodies throughout the 1-mo observation period (Fig. 4G-H) compared to controls (Fig 4F).

Imaging of the vasculature. Angio-CT of decellularized ear scaffolds revealed a nicely ramified, fully patent framework of the vasculature, and ruled out any leakage (Fig. 5A-B). Although scaffolds did not stain for CD31, they did stain for von Willebrand factor. Type IV collagen remained abundant in the vessels' ECM (Fig. 5C-E).

***In vivo* revascularization of a peaECM graft:** *In vivo* implantation of whole ECM scaffold grafts was technically feasible. The mechanical properties of the vasculature, deprived of the endothelial layer, supported the surgical reconnection of the vessel stumps of the scaffold to the recipient's neck vasculature (Fig. 6A). After clamp release, blood flowed well within the whole scaffold, which swelled gently and acquired a color similar to normal ear. When palpated, the reperfused scaffold was soft and the arterial pulse vigorous. Satisfactory blood flow throughout the whole acellular scaffold was observed for

180 minutes (Fig. 6B-D). No leaks were detected and no adverse events were recorded during surgery. Histologic staining demonstrated cellular engraftment and tissue preservation (Fig. 6E-F).

Cell viability and differentiation on discs: Cos-7 cells were well distributed and proliferated on the surface of all scaffolds, as assessed by positive H&E and Ki-67 staining (Fig. 7A-B), with a 51.4% proliferation index. The GFP+ pBM-MSCs seeded discs demonstrated macroscopic fat formation after 15 days (Fig. 7C-E), confirmed by GFP+ living cells with adipose cell morphology, for both PM and ADM (Fig. 7F-G), indicating a possible ECM-orientated stem cell fate. In controls, adipose cell formation was only observed with ADM (Fig. 7H).

Whole ear bioreactor vascular seeding: Ear graft seeded with pBM-MSC presented a yellowish aspect at time of sacrifice; type IV Sudan lipid staining confirmed increased lipid content (Fig. 7I-K). DAPI staining showed cell migration throughout the 3D framework of the scaffold (Fig. 7 L-M). For the ear graft seeded with NIH 3T3 cells, the cell count in culture medium indicated at least 94% cell engraftment. Whole-mount observation showed an important amount of living cells, equally distributed between extra- and intra-vascular compartments (Fig. 7N). For H&E (Fig 7 O-Q), 19 of 20 biopsies, with three different sections each, were positive for cells, either forming clusters in the parenchyma, or diffused cells in the ECM. Cells could be retrieved in both large vessels and capillaries. However, overall cell density remained fairly poor.

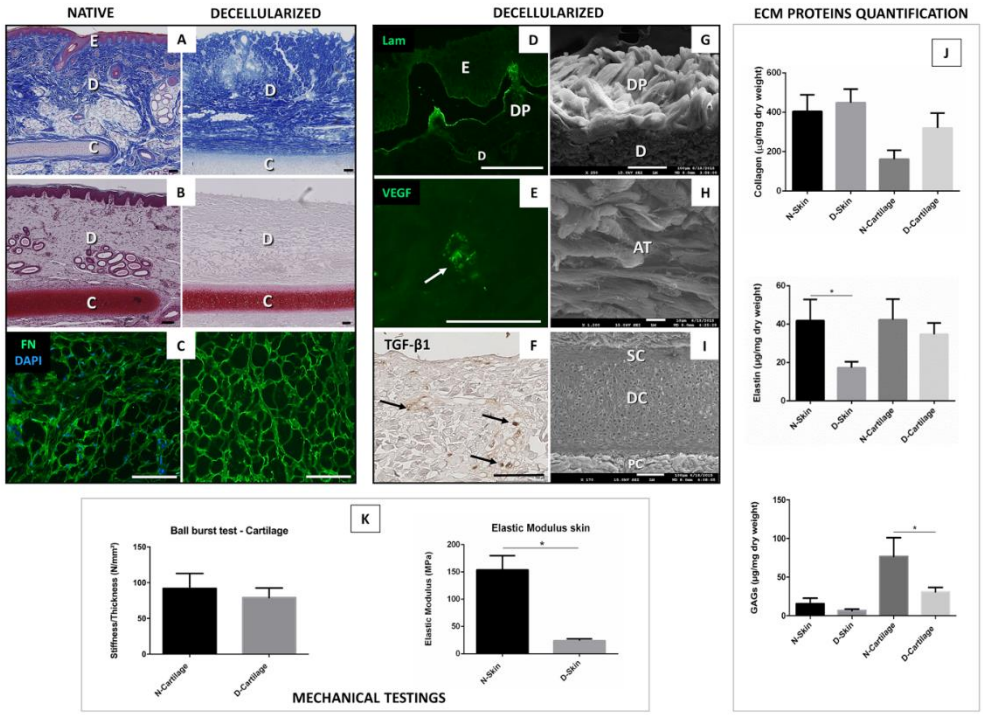

Figure 3: *Evaluation of preservation of ECM framework and molecular composition*. ***(A)***: *Masson's trichrome staining of peaECMs (right) versus the innate graft (left); connective tissue is stained blue and demonstrates high preservation of collagen structure and content.* ***(B)***: *Safranin O staining, where levels of proteoglycans can still be appreciated in the acellular cartilage.* ***(C)***: *IF staining for fibronectin in adipose tissue comparing native (left) versus decellularized (right) adipose tissue; in the latter, this important ECM protein appears very well preserved, along with absence of nuclei (DAPI) staining.* ***(D)***: *IF for laminin the dermal-epidermal junction during epidermolysis (see Fig. 1, panel E). Laminin is retained on the dermis side rather than the disrupted epidermis layer (E).* ***(E-F)***: *IF for VEGF and IHC for TGF-beta; positive staining was observed both within the parenchyma and around vascular structures (arrows). Scale bars represent 100 µm.* ***(G-I)***: *Decellularized skin, adipose tissue (AT) and cartilage on scanning microscopy. In the acellular skin* ***(G)***, *the dermis (D) shows extremely well preserved dermal papillae (DP). For the adipose tissue* ***(G)*** *the ECM reticular fibril structure is present. For the cartilage* ***(I)***, *the division between perichondrium (PC), superficial (SC) and deep cartilage (DC) is evident.* ***(J)***: *GAGs, elastin, and collagen quantification assays. Collagen is very well preserved in both cartilage and skin. Elastin is well preserved in cartilage and less in skin. GAGs are only partially preserved in cartilage, but much more than in all previous reports (see results).* ***(K)***: *Mechanical testing of skin and cartilage samples. Cartilage rigidity was assessed by ball burst testing, expressed in terms of stiffness normalized to thickness (N/mm²). Skin was evaluated for elasticity by elastic modulus (Mpa) and for resistance by maximum stress testing (Mpa). Mean ± SEM, *p<0.05, ***p=0.001.*

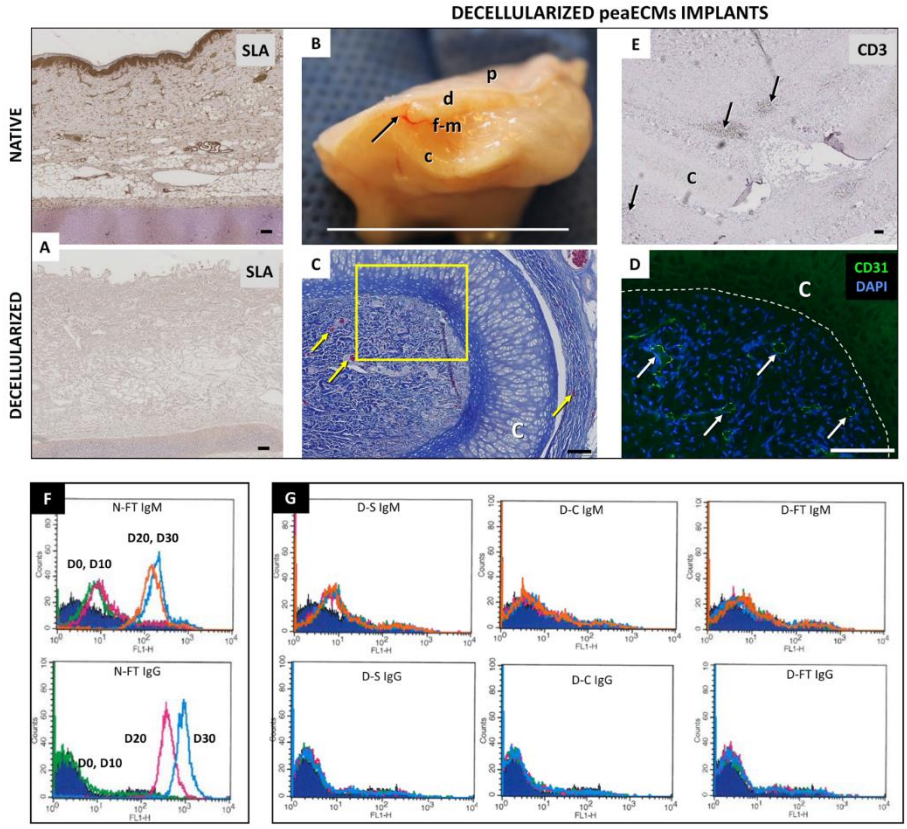

Figure 4. *In vivo immunogenicity evaluation of implanted acellular ECM porcine ear scaffolds.* ***(A)****: Anti-class I swine leucocyte antigen (SLA) IHC staining of native (up) and peaECM (down), demonstrating negativity of scaffolds for antigens prior to implantation.* ***(B)****: Macroscopic view of full-thickness scaffold explant, showing the peritoneum (P), dermis (D), fat (F), muscle (M) and cartilage (C) tissues, with a blood vessel (arrow).* ***(C)****: Masson's trichrome staining of the same explant; no signs of remodeling are observed and the framework of the scaffold maintains its essential and innate conformation, with evidence of blood cells within vessels (arrows).* ***(D, enlarged frame from panel C)****: Anti-CD31 staining of a portion of panel C, consistent with signs of micro-angiogenesis within the scaffold, or re-endothelialization of vessels (arrows).* ***(E)****: Anti-CD3 IHC staining of full-thickness implanted scaffold, with some lymphocytic foci at the level of dermis (arrows). Scale bars: macroscopic pictures, 2 cm; histology, 100 μm.* ***(F-G)****: Allogenicity study with FACS evaluation for anti-donor specific antibodies in the mismatched recipient at days 0, 10, 20, and 30 for the positive control* ***(F)*** *and the study group* ***(G)*** *of decellularized-skin (D-S), decellularized cartilage (D-C), decellularized full-thickness (D-FT), and control native full-thickness (N-FT) samples. IgM (upper row) and IgG (lower row) antibodies were detected in control samples at days 20 and 30, but not in recipients of acellular scaffold samples at any time.*

4. Discussion

This is the first study that assesses the efficacy of CSST for facial subunit reconstruction in a clinically relevant model. The primary endpoint of our investigations was the production of authentic biocompatible peaECMs, to be used in the future as a platform for bioengineering of facial subunits and then the whole face. We found that the cellular compartment of porcine ear can be almost completely removed, leaving behind an acellular ECM scaffold that retained its complex 3D architecture and biochemical components. Moreover, the framework of the vascular tree remained intact at all hierarchical levels and sustained physiologically relevant blood pressure after being implanted *in vivo*. As previously emphasized [84], this aspect is critical for organ grafts that are planned to be reconnected to the recipient's vasculature, e.g. auricular grafts.

The ear was selected as our model for several reasons. First, it is a non-essential, non-motor, and independent anatomic unit with a unique morphology. Second, it is extremely difficult to reconstruct with conventional reconstructive procedures in humans [109,110]. Third, despite the presence in the ear of all soft tissues constituting the anatomic framework of the face – i.e, skin, fat, muscles, elastic cartilage, and blood vessels – its anatomy and physiology are relatively simple. Thus, the ear has become an ideal platform for regenerative medicine applications [111,112]. The present features could then be directly applied to a nose subunit, which is central to face organization, and exhibits a very similar tissue association. Muscle, which was not a fundamental tissue in this model, allowed us to study its response in our decellularization protocol; this will be important when considering motor-based facial subunits, like eyelids and lips.

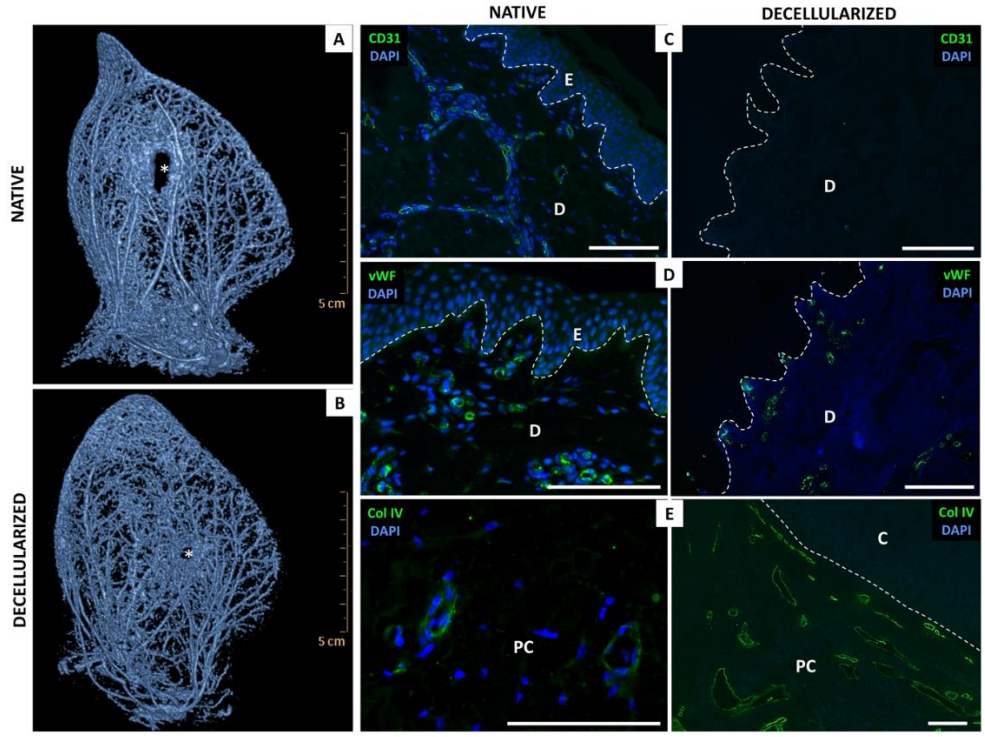

Figure 5. *Evaluation of the innate peaECMs vasculature.* ***(A-B)****: Angio-CT scan of native and decellularized grafts. Arteries were injected with contrast medium and 3D reconstruction performed for the vasculature of a native ear* ***(A)*** *and an acellular ear scaffold* ***(B)****. Both show a well-ramified vascular tree, with no signs of extravasation or blocks at any hierarchical level. (*) Hole from farm labeling device.* ***(C-E)****: IF evaluation of decellularization of the vascular compartment. We stained native (left) and acellular scaffolds (right) biopsies for: CD31* ***(C)****, von Willebrand factor* ***(D)*** *and type IV collagens* ***(E)****. E, epidermis; D, dermis; C, cartilage; PC, perichondrium. Scale bars represent 100 μm.*

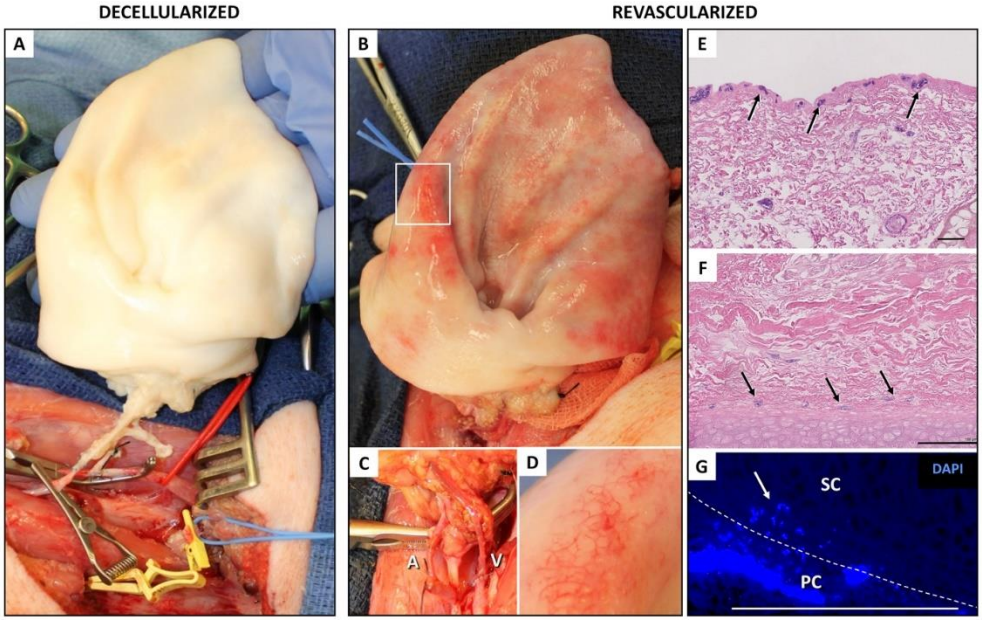

Figure 6. *In vivo revascularization of an acellular ECM ear scaffold*. ***(A)****: The scaffold's artery was anastomosed end-to-side to the recipient's CCA; the scaffold's vein was anastomosed end-to-end to the internal jugular vein.* ***(B-D)****: After clamp release and a 3-hour observation period before euthanasia, reperfusion could be observed in the whole scaffold* ***(B)***. *During this time, the artery (A) and vein (V) remained patent and showed no leakage* ***(C)***. *Subdermal plexus reperfusion, which showed a pink tinge immediately, was evident* ***(D, enlarged frame from panel B)***. ***(E-G)****: After euthanasia, the scaffold was procured and biopsied.* ***(E-F)*** *H&E staining of revascularized scaffold showing maintenance of structural compartments. Diffuse positivity for cells demonstrated their engraftment within the scaffold, in in vivo conditions with physiologically relevant blood pressure, at all levels of the vascular tree, such as the subdermal plexus* ***(E, arrows)*** *and perichondrium* ***(F, arrows)***. ***(G)*** *DAPI staining showing cells in the perichondrium (PC) and infiltration in the superficial cartilage (SC) area. Scale bars represent 100 μm.*

In the field of vascularized composite tissue allotransplantation, full facial transplants are considered the most immunogenic procedure in modern organ transplantation; therefore, developing technologies to minimize or abate inherent immunologic risks are of paramount importance. Consequently, the second purpose of this study was to produce a non-immunogenic, biocompatible scaffold.

Figure 7. *In vitro biocompatibility testing and attempted recellularization of the porcine ear graft*. ***Upper panel, static disc seeding***: ***(A)***: *H&E evaluation of Cos-7 seeded samples. Cells are on the cut surface of the ECM sample, and did not penetrate the 3D framework.* ***(B)***: *Ki67 IHC staining of Cos-7 seeded samples showing an important proportion of proliferating cells.* ***(C-E)***: *GFP+ pBM-MSC seeded discs showing macroscopic aspects of control disc* ***(C)****, or after 15* ***(D)*** *and 25* ***(E)*** *days of culture with non-differentiating proliferating medium, showing development of nodules of fat.* ***(F-G)***: *GFP+ BM-MSCs non-vital staining combined with GFP observed in fluorescence microscopy, for seeded discs at 15 days of culture with proliferating medium* ***(F)*** *and adipose differentiation medium* ***(G)****. Both show cells development of adipose morphology, negative for dead staining and GFP positive, differentiating them from original donor scaffold. We observed lipid globules that were not GFP positive, indicating that delipidation of the scaffold may be incomplete.* ***(H)***: *Control GFP+ BM-MSCs cell culture with proliferating medium and with adipose differentiation medium (insert). Morphologic differentiation of cells did not occur in normal medium. Scale bars represent 100 μm for Cos cells histology; 7.5 mm for macroscopic views and 200 μm for fluorescence for pBM-MSCs.* ***Lower panel, whole ear recellularization in a perfusion bioreactor***: ***(I-M)***: *We seeded 16x10^6 porcine bone marrow stem cells through vascular injection within the whole peaECM flap, and kept them into a bioreactor for 2 weeks.* ***(I)***: *peaECM in sterile perfusion-bioreactor apparatus, in culture medium before seeding.* ***(J)*** *Construct at sacrifice cut for deep tissue examination, showing a yellow aspect compatible with fat formation.* ***(K)*** *Type IV Sudan lipid staining of seeded construct (right), compared to non-seeded peaECM (left), confirming a significant increase in lipid content.* ***(L-M)****. Nuclei (arrows) are visible in adipose tissue* ***(L)*** *and in perichondrium* ***(M)****, indicating wide spreading of cells. Legend: D, dermis; F, fat; PC, perichondrium. Scale bars represent 100 μm.* ***(N-Q)***: *We seeded 70x10^6 NIH 3T3 fibroblastic cells through vascular injection within the whole peaECM flap, and kept them into a bioreactor for 10 days.****(N)***: *Whole-mount live/dead staining aspect of construct, with observation of copious living cells still circulating or in the extra-vascular space.* ***(O)***: *H&E staining showing cell cluster formation in the ECM.* ***(P)***: *In the vessels, significant numbers of cells were found in both large and micro-vessels* ***(Q)***: *Nuclei in the adipose tissue. Scale bars represent 1mm for Sudan IV staining; 500 μm for live/dead images; 100 μm for type I collagen IF and H&E staining.*

Our scaffolds were biocompatible, both *in vitro* and *in vivo*. In fact, peaECMs supported the growth of three different types of cells, when seeded on samples and even at the whole-organ scale. When peaECMs samples were implanted *in vivo*, recipients tolerated the implants, and never mounted a specific anti-SLA humoral response, as demonstrated by the lack of donor-specific antibodies.

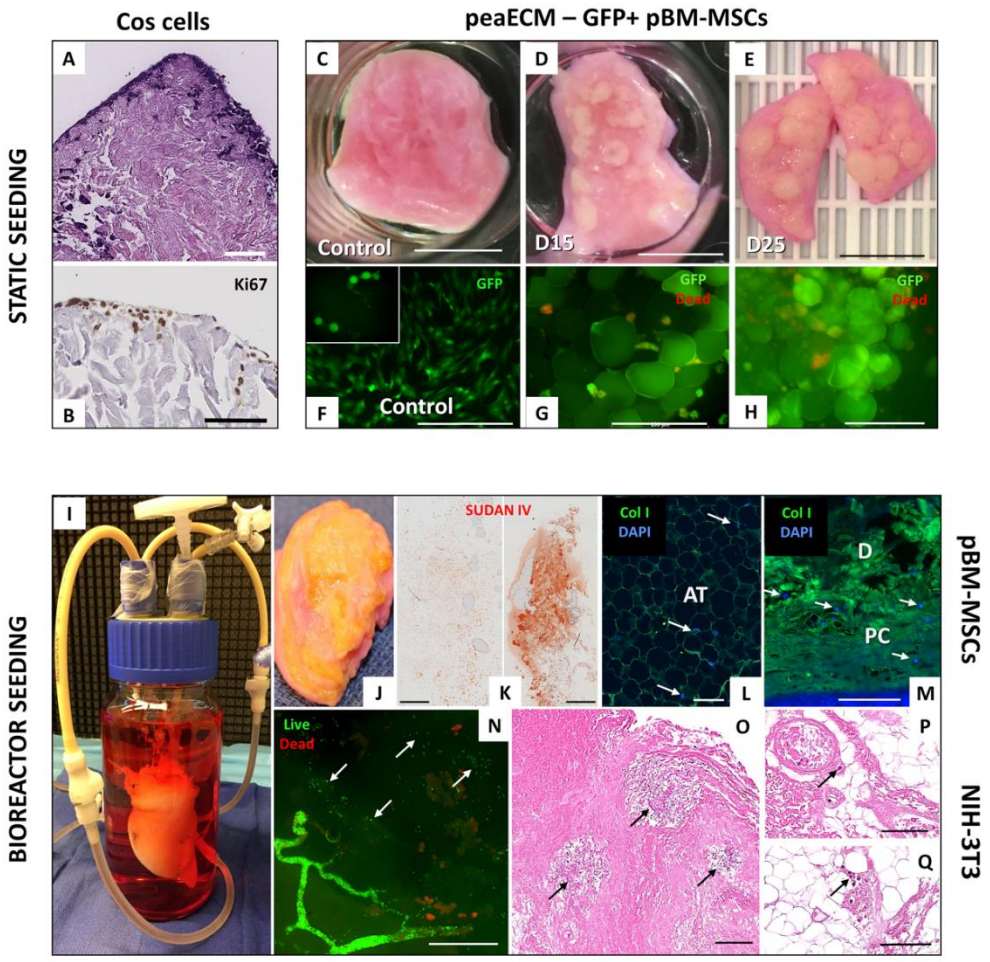

This was true although some cells remained within the cartilage, but apparently not enough to be immunogenic. This should probably be attributed to the intrinsic difficulty of delivering the detergent within this tissue due to its avascular nature, and is consistent with current literature [93]: this was observed by histology but not reflected in DNA quantification. Since examination of biopsies remains qualitative, testing *in vivo* implantation and targeted immune response, as we did, is a more complete assessment of cell removal and other characteristics. These findings are consistent with our previous data and those of others showing that the acellular ECM is not immunogeneic [87,91,113].

Relative perfusion and tissue behavior after exposure to decellularizing agents were acceptable using our protocol. This aspect is important when considering recellularization, since we demonstrated non-specific vascular relocation of cells within the scaffold. For the ear (and any vascularized composite tissue type) three compartments for further recellularization are involved: external, defined as tegmental; parenchymal, containing all the different non-tegmental tissue types; and finally, intra-vascular. Both vascular and tegmental compartments can be selectively recellularized; the inner parenchymal compartment can be recellularized by selective injections, but exposure will damage the skin and adipose layers.

For complex locations like the face, injection seeding is difficult to apply and skin damage is not acceptable. Thus, topical application for the external compartment, and vascular cell seeding for both parenchymal and intra-vascular compartments, appears to be the best strategy to consider. Due to its non-anatomic selectivity, ECM-guided differentiation of seeded stem cells could be significant for this type of regenerative procedure. Cartilage tissue, with its avascular nature and intra-graft location, will be a major issue in future recellularization attempts.

In our recellularization experiments, we finally obtained a diffuse cell engraftment, but still at a low density. The porcine ear, as a pre-clinical model, would thus need a major upscaling in cell production. This could also be solved experimentally by down-scaling the model, i.e. the rodent ear graft model [64]. But our model raises strategic questions for human applications, e.g. finding the right autologous cell reservoir, both for aspects of cell quantity and type. For a whole human face, the large amount of cells needed appears to preclude *in vitro* recellularization as a long-term strategy. Therefore, the *in vivo* cell engraftment we observed after our short revascularization study is promising, and should lead to induced autologous graft regeneration. The vascular compartment is the only site where *in vitro* recelullarization is essential. Current research in vascular regeneration offer only a few days of graft survival after replantation [114]. Thus,

longer survival is a high-priority goal for both organ and vascularized composite tissue bioengineering.

Author Contributions: JD conceived, designed, and wrote the study project, performed all investigations and all surgeries, collected results, interpreted data, and wrote the manuscript. He was responsible for the primary undertaking, completion, and supervision of all experiments. GO contributed to the study design, provided input on tissue engineering aspects, edited and revised the manuscript critically, and approved its final version. DD and LM performed tissue sampling and processing. DX performed porcine phenotyping and all FACS analysis. YB conceived and performed mechanical testing. CG provided GFP cells needed to demonstrate the stem cell engraftment in scaffolds and their orientated fate, supported methodology and results. CB reviewed the manuscript and provided technical support. BL contributed to the study design, provided input on aspects of facial anatomy and transplant surgery aspects, edited and revised the manuscript critically, and approved its final version. PG contributed to the study design, provided the pig model and expertise in transplant immunology, edited and revised the manuscript critically, and approved its final version.

Acknowledgments: The authors express gratitude to Christine de Ville de Goyet, Adeline Dedriche, Martial Vergauwen, Gwen Beaurin, Christophe de Terwangne, Eric Legrand, Marie Henry, Pascale Segers, Caroline Bouzin, Marc de Bournonville, Emmanuel Coche, Yannick Nizet, Corinne Lecuivre, Lauren Edgar, Vincent Destoop, Thomas Pardoen, Walter Hudders and Fatima Hammouch for their devoted technical assistance or logistic support. We also acknowledge the editorial assistance of Karen Klein, MA, in the Wake Forest Clinical and Translational Science Institute (UL1 TR001420; PI: McClain). We are thankful to Drs. Silvia Colleoni and Roberto Duchhi (Avantea, Cremona, Italy) for their advices about GFP+ porcine bone marrow stem cells. Finally, we would like to thank Pr. Ranieri Cancedda for providing tissue engineering expertise during manuscript revision.

Chapter 5: Human ear bioengineering

Perfusion-decellularization of human ear grafts enables ECM-based scaffolds for auricular vascularized composite tissue engineering.

Acta Biomaterialia, Under revision

Duisit J
Amiel H
Wüthrich T
Taddeo A
Dedriche A
Destoop V
Pardoen T
Bouzin C
Magee D
Vögelin E
Harriman D
Orlando G
Behets C
Rieben R
Gianello P
Lengelé

Abstract

Introduction: Human ear reconstruction is recognized as the emblematic enterprise in tissue engineering. Up to now, it has failed to reach human applications requiring appropriate tissue complexity along with an accessible vascular tree. We hereby propose a new method to process human auricles in order to provide a poorly immunogenic, complex and vascularized ear graft scaffold.

Methods: 12 human ears with their vascular pedicles were procured. Perfusion-decellularization was applied using a SDS/solvent protocol. Cell and antigen removal was examined by histology and DNA was quantified. Preservation of the extracellular matrix (ECM) was assessed by conventional and 3D-histology, proteins and cytokines quantifications. Biocompatibility was assessed by implantation in rats for up to 60 days. Adipose-derived stem cells seeding was conducted on scaffold samples and whole graft in a perfusion-bioreactor.

***Results*:** Histology confirmed cell and antigen clearance. DNA reduction was 97.3%. ECM structure and composition were preserved. Implanted scaffolds were tolerated *in vivo*, with acceptable inflammation, remodeling, and anti-donor antibody formation. Seeding experiments demonstrated cell engraftment and viability.

***Conclusions*:** Vascularized and complex auricular scaffolds can be obtained from human source to provide a platform for further functional auricular tissue engineered constructs, hence providing an ideal road to the vascularized composite tissue engineering approach.

Keywords: Human; Ear graft; Perfusion-decellularization; Extracellular matrix; Vascularized Composite tissue Engineering.

1. Introduction

Reconstruction of sizable auricular defects represents an enduring challenge in the field of plastic surgery, with variable clinical results despite extensive approaches and experimentation. Conventional autologous techniques[109,110,115,116] produce donor site morbidity and are limited by surgeon experience and expertise. The use of prosthetic cartilage implants has been reported, however the risk of extrusion has limited clinical applicability [117]. Vascularized Composite tissue Allotransplantation (VCA), whereby cadaver auricles are harvested and implanted into a recipient, are not available for single subunit reconstruction, since immunosuppressive (IS) treatment is not acceptable for such a small, non-life saving transplant [118]. In theory, tissue engineered (TE) autologous auricular implants may be able to overcome the limitations of current techniques [111,119,120], unfortunately the move from bench to bedside has yet to be achieved. Barriers to the success of TE auricles include the challenge of reproducing the biological complexity of human tissue along with the challenge of creating and accessing a vascular tree necessary for sustainment of seeded cells and implantation into a recipient. The perfusion-decellularization technique, as previously described in organs [81,84,96,121,122] and composite tissues [92-94], may represent the 'holy grail' of immunosuppression-free auricular transplantation. The basics of this technique involve circulating a mild detergent through a harvested organ/tissue via the native vascular system with the goal of removing cellular components, thus creating an extracellular matrix (ECM) scaffold retaining original tissue architecture and properties. The ECM scaffold could then be repopulated with autologous cells that would lead to a biological identity reassignment and immune tolerance once implanted. This technology appears ideally suited for the creation of a clinically useful bioengineered auricle. We previously reported the application of the perfusion-decellularization technique in porcine ear and human face models, with successful graft decellularization, preservation and accessibility of the vascular tree, suitable for repopulation with new cells and allocompatibility [38,39]. We hypothesized that this technology can be applied to human ear grafts. We hereby propose here a method to process cadaveric human auricles, in order to

provide a poorly immunogenic, complex and vascularized ear graft scaffold. Indeed, the relatively robust nature of composite tissues to post-mortem degradation could allow successful transplant processing, defining the new auricular synthesis approach of Vascularized Composite tissue Engineering (VCE).

2. Materials and Methods

2.1 Specimens. Twelve ear grafts were harvested from eight human cadaveric donors at the Université catholique de Louvain human anatomy department (Brussels, Belgium). Prior to passing, all donors had consented to research and teaching on their body. Donors were aged 68 to 104 years at the time of death. Bodies were preserved at 4°C for 1 to 4 days prior to graft procurement. All animal experiments were approved by the Université catholique de Louvain Animal Ethics Committee and following the EU Directive 2010/63/EU for animal experiments.

2.2 Ear graft procurement and perfusion-decellularization. According to previously described surgical protocol [8,9], ears were harvested with their corresponding vascular and nervous pedicles. Briefly, a peri-auricular incision was made within 1 cm around auricular implantation and continued to the temporal and cervical regions. In the cervical region, the common carotid artery, external carotid artery, posterior auricular artery (PAA), proximal superficial temporal artery (STA), external jugular vein and great auricular nerve were isolated. All other arterial branches and collaterals were ligated. After temporal incision, distal STA and vein were identified and dissected distally to frontal and parietal branches. Pre-auricular STA dissection and exposure was completed through the parotid gland. Superficial temporalis fascia was incised circumferentially, then elevated by blunt subfascial undermining down to the zygomatic arch of the temporal bone aiming to reach the external acoustic meatus and posteriorly, to the external aspect of the mastoid process. During this retrograde dissection, the PAA was protected. Finally, the ear completely elevated, along with its pedicle. Contralateral ear was either harvested identically or simply explanted as control.

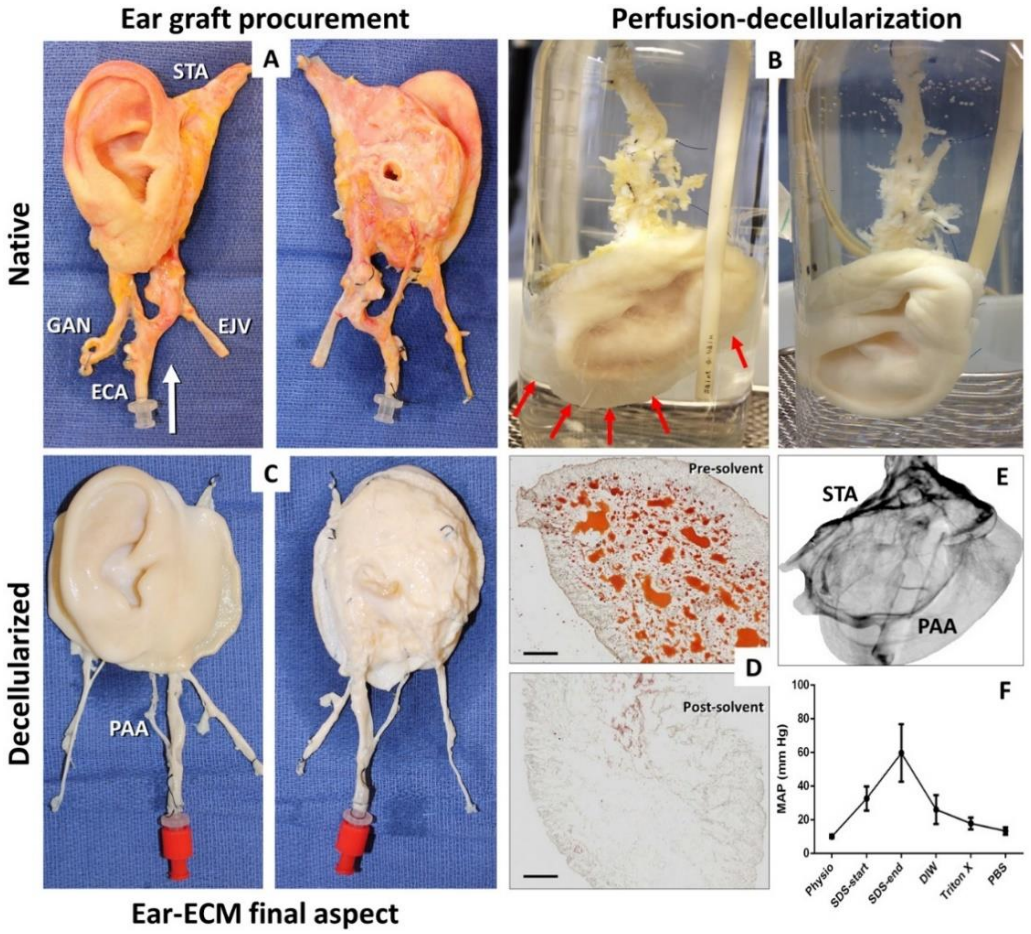

Figure 1: *Cadaveric ear graft perfusion-decellularization*. ***A*** *Native ear flap after procurement, with arterial (external carotid artery ECA, posterior auricular artery PAA, superficial temporal artery STA) and venous (external jugular vein EJV) pedicle, with anterior (left) and posterior (right) views; the arrow indicates the flow direction.* ***B*** *Perfusion-decellularization: left, after 24 hours perfusion, with evidence of epidermolysis and large bullae formation (arrows); right, final aspect.* ***C*** *Decellularized ear anterior (left) and posterior (right) views, with evidence of morphology preservation and oil cysts removal, after 2-propanol solvent treatment. GAN Great Auricular Nerve.* ***D*** *Ear lobe section and staining with type IV Sudan fat staining prior (up) and after (down) polar solvent treatment. Scale bars 1 mm.* ***E*** *Arterial fluoroscopy of decellularized ear: STA and PAA are opacified.* ***F*** *Mean arterial pressure (MAP) evolution during process, at constant output. MAP expressed in mm Hg.*

A luer was inserted in the arterial pedicle for heparinized saline (15 UI/ml) irrigation of the graft. This solution was infused until clear return was identified, in veins left free.

Complementary vascular control was performed with either suture ligation or microclips. Remaining parotid tissue was excised then each ear was weighted.

The arterial catheter was then connected to a Masterflex L/S peristaltic pump with L/S easy load pump head and L/S 16G tubing (Cole-Palmer Instrument Co, Vernon Hills, IL, USA) after final immersion in a 1L glass jar filled with the same solution as perfused. Perfusion-decellularization sequence, in an open circuit fashion, followed by eight steps: (1) 1000 ml of heparinized saline (15UI/ml), containing 10 μM adenosine (Sigma-Aldrich, St. Louis, MO), 4°C; 1% sodium dodecyl sulfate (SDS, VWR, Radnor, PA) in deionized water (DIW) was perfused for 88 hours (36500 ml), room temperature (RT). This treatments leads to epidermolysis and bullae formation, tissue bleaching and edema formation, while shape is preserved; (3) DIW was then perfused for 3 hours (1200 ml), RT; (4) Triton-X 100 1% (VWR) in DIW for 25 hours (10000 ml), RT; (5) Phosphate buffered saline (PBS) for 38 hours (16000ml), RT; (6) Polar solvent step, as previously described [123,124], whereby the flap was perfused for 4 hours (1000 ml), until critical increase of vascular resistances, then transferred to a stirring bath of 100% 2-propanol (VWR) overnight at RT, changed once, then rinsed in DIW bath for 2 hours, and finally perfused with PBS for 30 hours (16000 ml). This treatment removes oil from adipose tissue layer; (7) Type I Bovine DNAse (Roche I, Sigma), 50 UI/ml in PBS with 203.3 M magnesium chloride (Sigma), for 6 hours (900 ml), 37°C; (8) brief wash of the auricle with PBS, RT. Decellularized human ears (HE-ECM) were stored at 4°C in PBS. Before tissue analysis, each HE-ECM was weighted, examined for epidermis and hair remnants, bleaching and morphology.

2.3 Arterial pressure monitoring. During all steps of perfusion-decellularization, with exception of polar solvent perfusion, the mean arterial pressure (MAP) was recorded with a central line connected to a Datex-Ohmeda S/5 anesthesia monitor and M-Prestin module (GE Healthcare Life Sciences, Chicago, IL, USA) for a selected pump inflow. A MAP profile was established for a constant flow of 8 ml/min.

2.4 Fluoroscopic vascular assessment. Contrast agent (Visipaque, GE Healthcare) mixed with normal saline (1:2) was injected in the arterial pedicle by a constant manual pressure. Image acquisition was performed with a Powermobil C-Arm (Siemens, Munich, Germany). Images were exported in DICOM format and visualized with Osirix© software (Pixmeo, Bernex, Switzerland).

2.5. Histology, immunohistochemistry (IHC), immunofluorescence (IF)

Paraffin-embedding. Tissues were fixed in 4% formalin for 24 hours, transferred in successive toluene and alcohol baths prior to dehydration, then embedded in paraffin and sectioned into 5µm slices.

Histological staining. Sections were deparaffinized and rehydrated. We used hematoxylin and eosin (H&E), Masson's trichrome (MT), alcian blue and safranin O stains according to standard protocols. Miller's elastin/alcian blue/sirius red stains were also performed as described [125] in order to stain elastic fibers (purple), sulfated glycosaminoglycans (GAGs) (blue) and collagen (red).

IHC. After deparaffinization, slides were subjected to antigen retrieval by heating at 98°C for 60 min in 10 mM citrate buffer, at pH 5.7. Endogenous peroxidases were inhibited using 1% H_2O_2 and non-specific antigenic sites were neutralized with 1:50 goat serum. Samples were incubated at 4°C overnight, using the primary antibodies: anti-type I HLA (ab134189, 1:200, Abcam, Cambridge, UK) and anti-CD31 (ab28364, 1:50, Abcam). Next, the sections were successively incubated with 1:50 biotinylated secondary antibody, stained with streptavidin-HRP (Sigma) and 3,3'-diaminobenzidine (DAB) peroxidase substrate (Vector laboratories, Burlingame, Ca, USA), followed by counterstaining in Mayer's hematoxylin for 1minute, dehydration in alcohol and toluene baths and finally mounting with Entellan medium. PBS containing 1% bovine serum albumin (BSA) was used to rinse sections after each step.

IF. Deparaffinized, formalin-fixed sections were quenched with NaBH4 (1:100), then subjected to antigen retrieval by heating at 98°C for 60 min in 10 mM citrate buffer, pH 5.7. Samples were incubated at 4°C overnight with the following

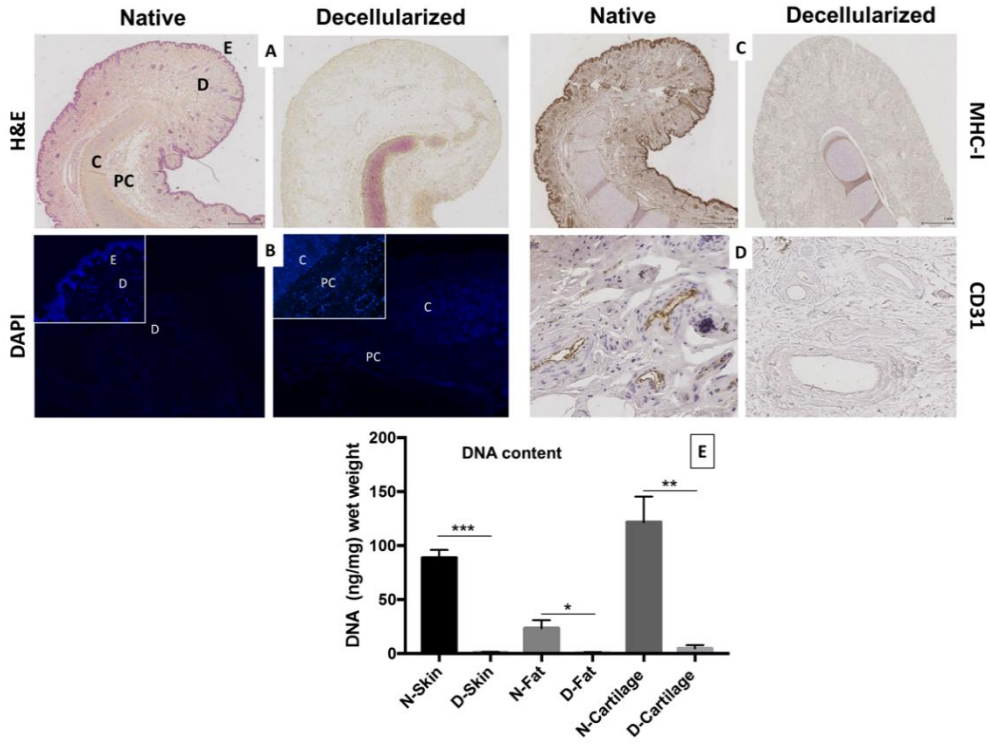

***Figure 2**: Cells and antigens removal. **A** H&E staining comparing native (left) and decellularized (right) ear grafts. E epidermis, D dermis, PC perichondrium, C cartilage. **B** DAPI staining showing native (left) and decellularized (right) ear sections. **C** anti-type I HLA staining in native (left) versus decellularized (right) tissues. **D** Anti-CD31 staining in native (left) versus decellularized (right) tissues. **E** DNA content in native (N-) versus decellularized (D-) tissues, expressed in ng/mg wet weight. Statistics were performed using unpaired student t-test, mean ± SEM, ***p<0.001, ** p<0.01, * p<0.05. Scale bars: upper raw 1 mm; lower raw 100 µm.*

primary antibodies: anti-type I collagen (ab34710, 1:250, Abcam), anti-type II collagen (ab34712, 1:200, Abcam) and anti-type IV collagen (ab6586, 1:500, Abcam). Neutralization of nonspecific sites was done with PBS containing 5%BSA. For fluorescence staining, secondary antibody labeled with Alexa Fluor 488 (goat anti-Rabbit or anti-mouse IgG, 1:300, ThermoFisher Scientific, Whaltam, MA), was used and the nuclei were stained with 4'-6-diamindino-2-phenyl-indole (DAPI, 1:1000) and mounted with DAKO fluorescent mounting medium (Agilent, Santa Clara, CA, USA).

Lipid droplet evaluation on frozen sections. Tissue-Tek O.C.T. Compound (Sakura Finetek, Alphen aan den Rijn, The Netherlands) embedded biopsies were cut on a Microm HM 560 cryostat (ThermoFisher). Sections were cut to 5µm thickness and processed for the staining. Type IV Sudan (Sigma) staining was then performed, following standard protocol.

Histology and IHC sections were digitalized at 40x magnification with a SCN400 slide scanner (Leica, Wetzlar, Germany) and visualized using Digital Image Hub (Leica Biosystems, Dublin, Ireland). Images of IF sections were acquired on a Zeiss AxioImager.z1fluorescence microscope (Zeiss).

2.6 3D-histology serial reconstruction and analysis: Full-thickness biopsies were taken from a native ear and a HE-ECM graft. For each sample, 50 serial sections of 5 µm thickness were prepared with Miller's elastin/alcian blue/sirius red stains. Slides were scanned using the SCN400 slide scanner (Leica) with a 40x objective. Damaged sections were discarded after visual examination (2-3 sections per sample) and 3D-reconstruction was performed using the HeteroGenius MIM 3D Pathology add-on (HeteroGenius Ltd, Leeds, UK) with 4 levels of non-rigid alignment (1.25X, 2.5X, 5X and 10X) and a final B-Spline size of 12x12mm, subsequent to automatic rigid alignment of sections performed at 1.25X. Whole sample 3-D visualization of original data (~1000x1000x50 voxels) was produced, with a total volume of 7.61 mm^3 and 8.21 mm^3 in the native ear and HE-ECM graft samples respectively. Subvolume analysis data, defined by volumes of interest in the cartilage, skin and connective tissue, from both native and decellularized samples, was annotated manually on a single slide, using a box of approximately 1 x 1 x 0.25mm. Animated Graphics Interchange Format (GIF) images of the whole stack were produced by exporting the aligned stack volumes from HeteroGenius MIM and using ImageJ software [126] for volume rendered examples.

Quantitative analysis of porosity was performed on tissue samples using the HeteroGenius MIM Colour Analysis add-on. A 3-class (collagen, elastin and background) probabilistic model was built by manually labelling examples of each class. Pixel counting for each class was performed for a single annotated sub-

region per image, by classifying a pixel as belonging to the class if the probability of class membership was 0.75 or larger ("QuantifyByColour" analysis method). Annotation of the tissue region was performed automatically at 0.625X resolution, which uses a greyscale threshold (value=200), plus morphology, hole filling and boundary tracing to annotate tissue pieces with a Bezier curve. Porosity was obtained by the ratio between non-stained and stained volumes. Additionally, annotations excluding the cartilage were produced manually for a subset of 2 images per sample.

2.7 Scanning Electron Microscopy (SEM). Native and decellularized biopsies were fixed with 2.5% glutaraldehyde overnight at 4°C. Samples were then washed with PBS and gradually dehydrated by successive immersion in increasing concentrations of ethanol for 15 min each. Before SEM imaging, tissues were critical-point dried and coated with an 8-nm gold layer. SEM measurements were performed at 15 keV. Samples were observed with a field-emission scanning electron microscope (JSM-7600F, Jeol, Akishima, Tokyo, Japan) according to standard protocols.

2.8 DNA quantification. DNA from skin, fat and cartilage samples of native ear (n=9) and HE-ECM (n=9) was extracted, with DNeasy Blood & Tissue Kit (Qiagen, Hilden, Germany), processing up to 25 mg biopsies. Briefly, tissues were incubated overnight at 56°C with proteinase K solution. After adding buffer and ethanol, the mixture was transferred to a spin column filled with buffers and repeated elution was performed. Extracted DNA content was assessed by Quant-it™ Picrogreen dsDNA assay kit (ThermoFischer Scientific), according to manufacturer's protocol. Final value was expressed in ng DNA per mg tissue wet weight.

2.9 ECM protein quantification. Biopsies from native (n=9) and decellularized (n=9) samples were used. Collagen content was evaluated using a Chondrex hydroxyproline assay kit (Chondrex, Inc., Redmond, WA) according to manufacturer's protocol. Briefly, samples were hydrolyzed in 10M hydrochloric acid for 24 hours at 100°C, and mixed with standards. Chloramine-T was added to solution from samples and standards, then incubated 20 min at room temperature.

DMAB was added to standards and samples solutions, then incubated at 60°C. Absorbance was read at 570 nm. GAGs content was evaluated using the Blyscan Sulfated-GAG assay kit (Biocolor LTD, Carrickfergus, Northern Ireland) according to manufacturer's recommendations; samples extraction was proceeded with papain overnight at 65°C. After centrifugation, supernatant was collected and color reactant was added to precipitate S-GAGs, followed by repeated centrifugation until dissociation was completed. Absorbance was read at 630 nm. Elastin content was measured with the Fast Elastin Assay kit (Biocolor) according to manufacturer's recommendations. 0.25M oxalic acid was added to samples, and digested for one hour at 100°C before supernatant collection. This extraction was repeated two times for skin and fat and three times for cartilage and muscle. Final extraction volume was mixed with equal reactant volume for elastin precipitation until complete elastin digestion and centrifuged. Colored reactant was added in the remaining solution, stirred and centrifuged prior to supernatant elimination. Absorbance was read at 510 nm. All results were expressed as µg/mg wet weight.

***Figure 3**: ECM major proteins and 2D structure preservation. **A-F** Histology stainings by **A** Masson's trichrome of skin, **B** Type I collagen of skin, **C** type II collagen of cartilage, **D** type IV collagen in dermis, **E** Alcian blue and **F** Safranin O in cartilage, of native (upper raw) and decellularized (lower raw) tissues; DEJ, dermo-epidermal junction. **G-J** SEM evaluation of **G** dermal surface with preserved dermal papillae (DP), **H** dermal section with appreciation of DEJ, **I** cartilage section and **J** adipose tissue, from acellular scaffolds; insert represent native samples. **K-M** Major ECM content quantification: **K** Collagen, **L** Elastin and **M** GAGs; expressed in µg/mg wet weight of tissue. Statistics were performed using unpaired student t-test, mean ± SEM, ** p<0.01, * p<0.05. Scale bars: 100 µm.*

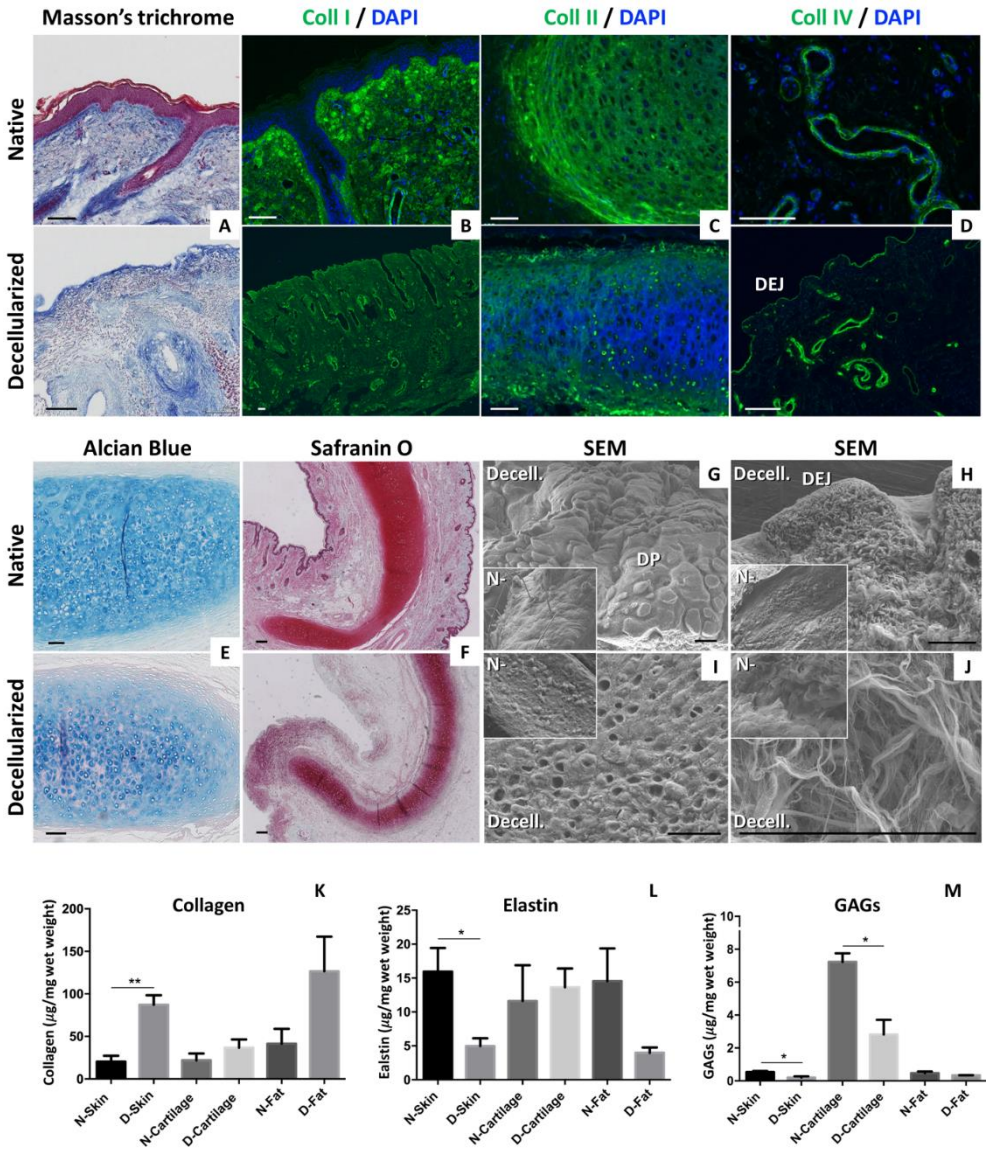
Masson's trichrome
Coll I / DAPI
Coll II / DAPI
Coll IV / DAPI
Native
Decellularized
A
B
C
D
DEJ
Alcian Blue
Safranin O
SEM
SEM
E
F
G
H
I
J
Decell.
DP
N-
K
Collagen
Collagen (μg/mg wet weight)
L
Elastin
Ealstin (μg/mg wet weight)
M
GAGs
GAGs (μg/mg wet weight)
N-Skin
D-Skin
N-Cartilage
D-Cartilage
N-Fat
D-Fat

2.10 Mechanical properties. A ball burst test was performed to determine the stiffness of the cartilage. We used an Instron-5666 universal testing machine (Instron Corporation). A 4-mm diameter steel ball with 1mm/min loading rate, and a 100N load cell, was applied to decellularized (n=5) and native (n=5) disc samples, clamped in 5-mm diameter O-rings. Endpoint was the maximum force. Stiffness was expressed as the ratio between the maximum force and the corresponding crosshead displacement. Values were divided by sample thickness and expressed as N/mm^2.

2.11 Cytokines quantification

Protein extraction. Skin, cartilage and fat tissue biopsies were collected from native (n=4) and decellularized ear grafts (n=3). Samples were kept at 4°C until processing. Biopsies were weighed on an analytical scale and cut into small pieces with a surgical knife. The pieces were transferred into M tubes (Miltenyi Biotec GmbH, Bergisch Gladbach, Germany) containing RIPA buffer (50mM Tris-HCl, pH 8.0, with 150mM sodium chloride, 1.0% Igepal CA-630 (NP40), 0.5% sodium deoxy cholate and 0.1% sodium dodecyl sulfate) laced with protease inhibitor cocktail (P8340, 1:100, SIGMA). M tubes were promptly inverted and put on a gentle MACS Dissociator (Miltenyi Biotec GmbH), then homogenized using the program specific for protein extraction. After termination of the program, homogenates were incubated on ice and underwent sonication.

After a short spin down, the supernatant was transferred to smaller tubes for centrifugation at 13'000 rpm for 1 hour at 4°C. Again, the supernatant was transferred to a new tube for further analysis. For protein quantification, a classical Bicinchoninic acid (BCA) assay was performed. A bovine serum albumin standard (2.0mg/ml in 0.9% aqueous NaCl containing sodium azide, 23209, Thermo Fisher Scientific) was prepared and transferred to a flat transparent 96-well plate (Thermo Fisher Scientific). 5µl of sample were added to the wells and the assay was performed according to the DC Protein Assay kit instructions (Bio-Rad,

Hercules, CA, USA). The OD was measured at 750nm on a plate reader (Infinite M1000 PRO) and interpolated by Prism 7 (GraphPad Software, La Jolla, CA, USA).

Cytokine measurement. Protein levels of 42 different cytokines were measured by Bio-Plex multiplex immunoassays. The Bio-Plex Pro Human Chemokine 40-Plex Panel (Bio-Rad) and the Bio-Plex Pro TGF-ß 3-Plex kit (Bio-Rad) were used to analyze the supernatants of the protein extraction (above) and run on a FLEXMAP 3D system (Luminex, Austin, CA, USA). The procedure was performed based on the original manufacturer instruction manual. Growth factor content was normalized to the mass of starting tissue and expressed as pg of analyte per mg of tissue. After log2 transformation, concentrations above or below the limit of detection were eliminated from the analysis.

2.12 *In vivo* biocompatibility study. 16 adult Wistar rats (all females, mean weight = 208±15 g) were implanted subcutaneously with 2 biopsies from either native ear (n=8) or HE-ECM (n=8), previously sterilized by 0.1% peracetic acid (PCA). General anesthesia was performed using intra-peritoneal injection of 50 mg/ml Ketamine with 20mg/ml Xylazin in saline. After disinfection, a median incision was performed on the abdomen and two subcutaneous pockets were created. For serum collection, 1ml blood puncture was performed at time of implantation and sacrifice; collected blood was then centrifuged 15 min at 3000 rpm, and serum preserved at -80°C. Euthanasia was performed at postoperative day (POD)15 (n=6), POD30 (n=6) and POD60 (n=4); then implants were retrieved, paraffin-embedded, sectioned and stained with H&E, MT and CD68 (ab31360, Abcam) IHC. For inflammatory quantification, CD68-stained sections were digitalized with the slide scanner and analyzed using the image analysis tool (Author version 6.6.3, Visiopharm, Hørsholm, Denmark).

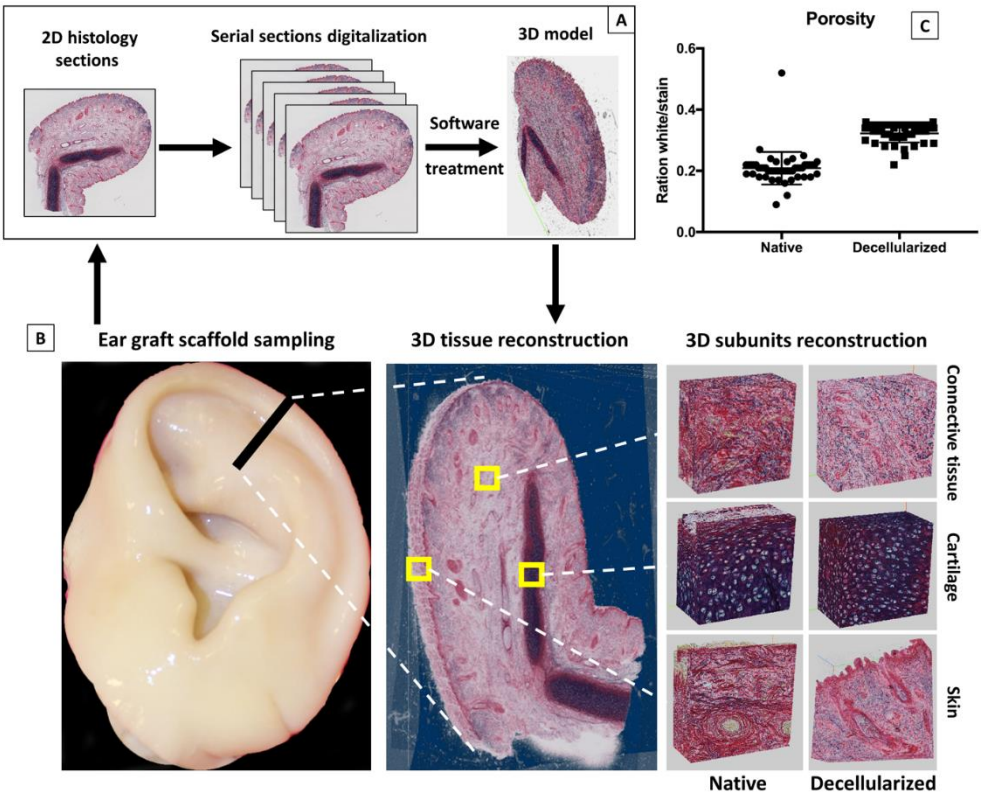

Figure 4: *ECM 3D-histology reconstruction*. ***A*** *Methodology: native and decellularized ear samples are serial sectioned, then digitalized and treated for 3D alignment and reconstruction with a specific software.* ***B*** *Biopsy location (left), 3D-histology volume reconstruction and virtual sampling locations (middle) for 3D subunit elementary tissue reconstruction: connective tissue, cartilage and skin, from native and decellularized samples (right).* ***C*** *Porosity value calculated from the ratio between non-stained and stained area in the whole 3D biopsy volume from native and decellularized samples, with inclusion of cartilage layer.*

The implant in each section was delineated manually and care was taken to exclude tissue folds and artefacts from the analysis. CD68-positive pixels were then detected within the previously delineated tissue at high resolution (20x) using a classification based on image feature highlighting the DAB staining (HDAB-DAB matrix of the software). Threshold was adjusted on representative stained vs non-stained tissue areas. The results were expressed as CD68-stained area percentages and calculated as CD68-stained area/total tissue area ×100. The parameters were kept constant for all slides.

Detection of anti-donor alloantibody (IgG) by flow cytometry. Human peripheral blood mononucleated cells (PBMC) were incubated with recipient serum for 30 min at room temperature. Before incubation, the serum was decomplemented for 30 min at 56°C. After washing with fluorescence-activated cell sorting buffer (Hanks balanced salt solution – HBSS – containing 0.5% fetal bovine serum and 0.1% sodium azide), saturating amounts of Alexa Fluor 488 goat anti-rat IgG polyclonal antibody (Thermo Fisher Scientific, Merelbeke, Belgium) was added and incubated for 30 min at room temperature, then washed twice. Each analysis included the appropriate Alexa Fluor 488-conjugated antibody with only PBMCs, for nonspecific reaction. Cells were acquired and analyzed with BD FACSCalibur (BD Bioscience Benelux NV, Erembodegem, Belgium) driven by CellQuest Pro software (BD Bioscience). A positive reaction was defined as a shift of more than 10-channels in mean fluorescence intensity when testing donor lymphocytes with post-transplantation (Day 15, 30 and 60) serum and comparing with pre-transplant serum (Day 0).

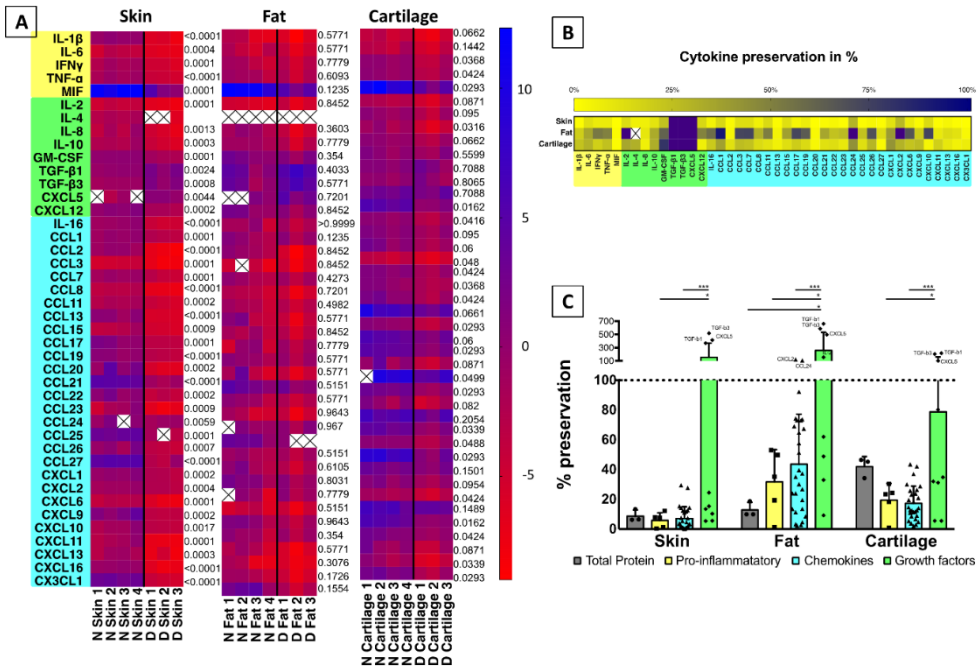

Figure 5: *Cytokines quantification.* ***A*** *Heatmap showing changes in abundances of 42 absolutely quantified cytokines in skin, fat and cartilage biopsies from four native (N-) and three decellularized (D-) scaffolds. Individual protein pictogram abundance per milligram of tissue was log2 transformed. Red boxes correlate with lower protein concentration and blue boxes with higher protein concentration. Crossed boxes indicate samples under the detection limit. Numbers represent the P value of two-sample t-tests with Benjamini, Krieger and Yekutieli correction to compare native and decellularized values.* ***B*** *Heatmap showing cytokine preservation after decellularization in skin, fat and cartilage as percentage of native tissues abundance. Yellow boxes correlate with lower preservation and blue boxes with higher cytokine preservation. Purple boxes indicate increased cytokine levels as compared to native tissues (≥ 100 %).* ***C*** *Relative preservation of total protein extract (grey), pro-inflammatory cytokines (yellow), chemokines (green) and growth factors (blue) in decellularized skin, fat and cartilage. Highly preserved cytokines (>100%) are indicated. Data presented as mean±SD. *p<0.05; *** p<0.001 by one-way ANOVA with Tukey's correction.*

2.13 Disc seeding with human and rodent adipose-derived stem cells

Rat Adipose-derived Stem Cells (rASCs). rASCs were isolated as previously reported [102]: briefly, we retrieved fresh inguinal fat from one adult rat, right after euthanasia for other experiments. Fat was digested with type II collagenase (LS004176, Worthington, Lakewood, NJ, USA), reconstituted in HBSS, and incubated for 1h at 37°C with continuous agitation for 60 min. After digestion, the collagenase was inactivated in Dulbecco's Modified Eagle's Medium (DMEM, Westburg, Leusden, The Netherlands) supplemented with 10% FBS, 2 mM L-glutamine, penicillin 100 U/mL, and streptomycin 100 µg/mL. Collected tissue was centrifuged for 10 min at 1500 rpm, at room temperature. The supernatant was aspirated and cells pellet was suspended with DMEM with 10% FBS, 2 mM L-glutamine, penicillin 100 U/mL, and streptomycin 100 µg/mL. After filtration through a 500-µm mesh screen, the collected tissue was centrifuged for 10 min at 1500 rpm, at room temperature and the pellet was suspended in proliferation medium and identified as the stromal vascular fraction (SVF). After 24-48 h of incubation at 37°C in 5% CO2, the cultures were washed with PBS and maintained in proliferation medium, and trypsinized when reaching 80% confluence, up to 4 passages.

Human adipose-derived stem cells (hASCs). hASCs were purchased (Promocell, Heidelberg, Germany) and cultured up to 7 passages, as detailed above for rASCs.

Disc seeding: Decellularized 1cm^2 samples (n=12) of external carotid artery pedicle (D-Artery, n=2), skin (D-Skin, n=2) and full-thickness auricles (D-FT, n=8) were sterilized: briefly, 0.1% PCA, Sigma) was prepared with DIW, and sterilized with a filtration unit. Samples were then washed overnight in PCA, using an orbital stirrer. Samples were then rinsed with DIW and repeated PBS washes on orbital-shaker, and finally preserved in sterile PBS/AA. Scaffolds were positioned in a 48-well plate, then impregnated with supplemented DMEM. hASCs were seeded at a density of 2x10^5 /cm^2 on the 5 D-FT; rASCs were seeded at a density of 3.6x10^4 cells/ cm^2 on the remaining scaffolds. All seeded HE-ECM were then placed in a CO2 incubator, and cultivated under standard conditions. Medium was changed

every 48h for 14 days. At retrieval, biopsies were first treated as whole-mounts with vital staining then Vybrant MTT (4,5-Dimethylthiazol-2-yl)-2,5-Diphenyltetrazolium Bromide) Cell Proliferation Assay Kit (Life Technologies) was used, mixing 12mM MTT with PBS. Next, specimens were incubated with scaffold for 4 hours at 37°C observed under a binocular microscope, and with Live/Dead Viability/Cytotoxicity Kit (Life Technologies, L3224), incubating 2mM ethidium homodimer and 4mM calcein-AM with samples for 40 min at room temperature. The rest of the constructs were paraffin-embedded, sectioned and stained with H&E.

2.14 Bioreactor HE-ECM whole-graft Stromal Vascular Fraction (SVF) seeding

Scaffold preparation. A whole HE-ECM graft was sterilized using 0.1% PCA protocol of alternating bath-stirring and perfusion, under sterile conditions, as previously described [38]. The HE-ECM was then mounted in a sterile perfusion-bioreactor, in closed circuit with the arterial pedicle connected to the tubing and the veins left free in the jar. The perfusion chamber was filled with 900 ml DMEM and graft conditioned for 2 hours with perfusion set at 5 ml/min, in a CO2 incubator, set at 37°C and 5%CO2.

Porcine SVF isolation. Concurrently, adipose tissue (weight 20 g) was procured from an adult landrace pig, right after euthanasia for other approved experiments. The SVF extraction was proceeded as described in the rASCs protocol. $56.6x10^6$ cells could be extracted and suspended in 100 ml supplemented DMEM.

SVF vascular seeding and culture. The cell reservoir was connected to the main bioreactor tubing and vascular seeding was perfused at 1 ml/min for 100 min. After a static period of 45 minutes, the flow was restored and set at 5 ml/min. After 3 days, the seeded scaffold was retrieved, biopsied and analyzed by MTT whole-mount and H&E staining.

2.15 Statistical analysis. Graphic presentation and statistical analysis was performed on Prism 7 (GraphPad Software). For GAGs, elastin and collagen content, unpaired student t-tests were performed between native and decellularized ear samples. For cytokines, two-sample t-tests with Benjamini, Krieger and Yekutieli correction were performed to quantitatively compare their abundance in native and decellularized tissues. One-way ANOVA with post-hoc Tukey's multiple comparison correction was used to compare the relative preservation of the different cytokine groups within the analyzed tissues. Data are presented as mean ± SEM for all analysis with exception of cytokines quantification expressed as mean ± SD. $P < 0.05$ was considered statistically significant.

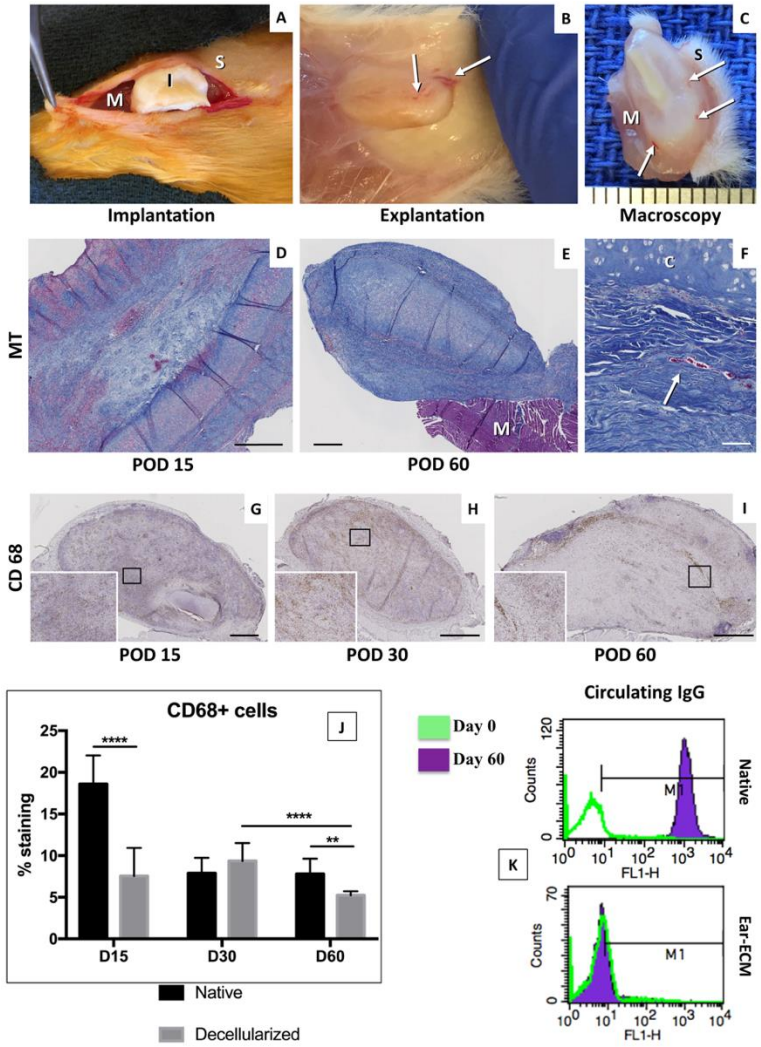

Figure 6: *In vivo study, subcutaneous implantation in rat.* ***A-C*** *Macroscopic assessment: HE-ECM implant (I) at time of* ***A*** *implantation,* ***B*** *explantation with no signs of capsular formation and evidence of growing vessels (arrows);* ***C*** *explant cross-section and integration between layers of skin (S) and muscle (M) of the recipient's abdominal wall.* ***D-F*** *HE-ECM Masson's trichrome assessment at* ***D*** *postoperative day (POD)15 and* ***E*** *POD60, with diminution of cellular infiltration, limited remodeling and* ***F*** *patent blood vessels (arrow). C Cartilage, M Muscle.* ***G-I*** *Macrophage infiltration CD 68 IHC staining at* ***G*** *POD15,* ***H*** *POD30,* ***I*** *POD60; windows enlarged views in the inserts.* ***J*** *CD68 quantification at POD15, POD30 and POD60 in native (black) and decellularized (grey) implants. **** p<0.0001; **p<0.001. Scale bars: 1 mm (with exception of F: 100 µm).* ***K*** *Flow cytometry of anti-human circulating IgG antibodies in the rat recipient at D0 (green curve) and POD60 (purple curve), in native (above) and decellularized (below) implant recipients. Selected curves originate from the most representative positive (control) and negative (decellularized) flow cytometries.*

3. Results

3.1 Perfusion-decellularization. Blistering was observed within the first 12h of SDS perfusion, first affecting the posterior surface followed by the anterior surface of the graft. The blisters evolved into large bullae which led to complete epidermis removal (**FIG 1A-B**). After completion of the Triton-X step, a yellowish aspect of the adipose tissue remained, demonstrating scattered oil cysts. Adipose tissue was satisfyingly treated after the supplementary 2-propanol step, as confirmed by macroscopic observation and type IV Sudan staining (**FIG 1C-D**). After the final PBS step, the cartilage layer retained the original auricular morphology. Vascular patency was confirmed by fluoroscopy (n=2), with opacification of ECA, PAA and STA axis and their distal parenchymal branches, without signs of contrast extravasation (**FIG 1E, supplementary material 1 video**). Regarding MAP evolution during protocol, SDS perfusion was associated with an important increase of arterial vascular resistances, macroscopically associated with edema of the fat layer; MAP decreased as steps were followed, and finally came back to initial MAP value after decellularization completion (**FIG 1F**).

3.2 Cell clearance. H&E and DAPI confirmed cellular clearance in skin and adnexa, with a few remnant chondrocyte nuclei visible in the deep cartilage, associated with negativity of type I MHC markers in treated grafts (**FIG 2A-C**). CD31 markers of endothelial cells were also completely removed (**FIG 2D**). DNA quantifications in D-Skin, D-Fat and D-Cartilage were found to be respectively 0.99±0.75, 0.84±0.56 and 4.82±3.95 ng/mg wet weight compared to 88.7±9.6, 28.2±15.7 and 121.7±31.1 ng/mg wet weight in native samples; this represented an overall 97.3% DNA reduction in HE-ECM ($p<0.001$) (**FIG 2E**).

3.3 ECM structural preservation. MT, type I and type II collagen stains confirmed the high-quality preservation and structural organization of major collagen proteins (**FIG 3A-C**). Type IV collagen, which is fundamental for basal membranes and critical for further epidermal reconstruction strategies, was well-observed in the vessels, glands and especially in the dermis, at the level of the dermo-

epidermal junction (DEJ) (**FIG 3D**). Alcian blue and safranin O stains demonstrated GAG preservation in the cartilage layer, with some reduction in peripheral areas more exposed to the decellularizing flow agents through the perichondrium (**FIG 3E-F**).

SEM examination reveals the preservation of the HE-ECM ultrastructure with dermal papillae, cartilage with emptied chondrocyte lacunae, and fat with fibrillary organization and absence of oil cysts. No detergent crystal could be detected in examined samples, revealing the efficiency of PBS perfusion to remove them (**FIG 3G-J**).

The tridimensional structural preservation of specific elements of the composite tissue is appreciated (elastin, collagen, GAGs), by the 3D-ECM histological reconstructions. From these samples, we extracted a volume of subunits for 3D reconstructions (**FIG 4A-B**), enabling a better targeted structural assessment. The 3D cartilage subunit evaluation confirmed the 2D histology observation and quantification, with a better characterization of the cartilage lacunae density and staining preservation. For the skin, the 3D volume confirmed the presence of intact dermal papillae and adnexal removal. The connective tissue, including deep dermis, adipose tissue, vessels and glands appeared at a lesser density. On the 3D volumes quantification, the porosity of whole-biopsy volume was increased in the decellularized sample, with a mean non-stained ratio to stained areas of 32.2±2.2%, compared to 20.8±2.6% in the native samples (**FIG 4C**). When excluding the cartilage, the porosity in HE-ECM was even higher, with 46%, signifying the loss of structural volumes mainly located in the non-cartilaginous areas.

3.4 ECM protein quantification. The qualitative ECM assessment was correlated to the preservation of its major protein content (**FIG 3K-M**). Collagen was highly preserved in D-Skin, D-Fat and D-Cartilage (87.2±14.3, 126.5±52.5 and 36.7±12.3 μg per mg wet weight respectively) compared to controls (20.3±8.2, 41.2±23.2 and 21±8 μg per mg wet weight respectively), representing a mean relative increase in collagen content of 300 % compared to native tissues. The global content increase is explained by collagen preservation following perfusion-decellularization, as well

as by the reduction of cell content and other ECM proteins, leading to an important relative mass increase in all ear scaffold tissues. Mean elastin content in D-Skin, D-Fat and D-Cartilage was 4.96±1.5, 3.96±0.99 and 34.7±10.3 μg per mg wet weight respectively, compared to 16.68±4.41, 14.53±6.44 and 14.98±6.92 μg per mg wet weight respectively in controls. Reduction of elastin was significant in skin ($p<0.05$), with 41.3% relative preservation of elastin content while in cartilage 82% of native elastin content was preserved with non-significant difference. For GAGs, D-Skin, D-Fat and D-Cartilage was 0.2±0.1, 0.33±0.01 and 2.82±1.2 μg per mg wet weight respectively, compared to 0.53±0.01, 0.47±0.11 and 7.23±0.65 μg per mg wet weight respectively in controls. D-Skin preserved 42.6% of native GAG content while GAG value represented 40% of native content preservation for D-Cartilage ($p<0.05$). It is vitally important that both elastin and collagen content are preserved in cartilage, as they are primarily responsible for the mechanical properties of cartilage: indeed, preservation of the morphological support is one of the most important feature for auricular graft functionality.

3.5 Mechanical properties. Mechanical testing of cartilage revealed an overall reduction of stiffness in decellularized (9.3+/-8.4 N/mm^2, range 1.5-21.3) compared to native samples (18.4+/-9.3 N/mm^2, range 4.4-30.2). This result demonstrates an overall reduction of the stiffness in the decellularized group, remaining however in the same order of magnitude as for the native.

3.6 HE-ECM preservation of cytokines. The cytokine analysis revealed that essentially all 42 tested cytokines were measurable in skin, cartilage and fat samples. In order to quantitatively characterize cytokine preservation in the different tissues of the scaffold, we analyzed the degree of change of growth factors in each biological sample. As shown (**FIG 5A**), all the measured cytokines in skin samples collected from the decellularized scaffold decreased significantly compared to native skin samples. Conversely, none of the measured cytokines decreased significantly by decellularization in fat tissue, with the exception of IL-4 which was below detection level. Cartilage presented a middle behavior with 22/44 cytokines significantly decreased after decellularization compared to

controls. To better understand how the decellularization process affected cytokines in HE-ECM, we calculated the relative proportion of preservation for each cytokine in decellularized tissues expressed as percentage of the native mean abundance (**FIG 5B**). In order to investigate whether different cytokine subclasses were differentially affected by the decellularization process, the following cytokine groups were created according to cytokine function: 1) pro-inflammatory cytokines (IL-1ß, IL-6, IFNγ, TNF-α, MIF), 2) Chemokines (IL-16, CCL1, CCL2, CCL3, CCL7, CCL8, CCL11, CCL13, CCL15, CCL17, CCL19, CCL20, CCL21, CCL22, CCL23, CCL24, CCL25, CCL26, CCL27, CXCL1, CXCL2, CXCL6, CXCL9, CXCL10, CXCL11) and 3) Growth factors (IL-2, IL-4, IL-8, IL-10, GM-CSF, TGF-ß1, TGF-ß2, TGF-ß3, CXCL5, CXCL12). Although many cytokines exhibit pleiotropy, we classified each cytokine into one of the three groups. No double classifications were allowed. As shown (**FIG 5C**), in decellularized skin total protein preservation was 8.75±4.07% with similar preservation of pro-inflammatory cytokines and chemokines (5.88±5.0% and 7.13±7.87%, respectively). Growth factors showed a much higher percentage of preservation (152.68±213.84) compared to pro-inflammatory cytokines and chemokines. Similar results were observed in cartilage (41.99±6.73%, 19.48±11.21%, 17.30±11.53% and 78.77±80.37 of preservation of total protein, pro-inflammatory cytokines, chemokines and growth factor, respectively) and in fat (12.9±5.09%, 31.74±21.65%, 43.63±33.52%, 255.94±275.28% of preservation of total protein, pro-inflammatory cytokines, chemokines and growth factor, respectively). Interestingly, only three of the forty-two cytokines (i.e., TGF-beta1, TGF-beta3 and CXCL5) showed an increase in expression levels when comparing decellularized and native tissues. This is likely due to more efficient protein extraction in the cell-empty ECMS and the increase in the ratio of pg cytokine per total ECMS dry weight in the decellularized tissues. In fat tissue, three cytokines displayed relative increase as compare to native tissue (i.e., IL-2, CXCL2 and CCL24), confirming the higher capacity of the adipose tissue to retain growth factors during the decellularization process. Apart from TGF-ß1, TGF-ß3 and CXCL5 the most preserved cytokines across tissues were IL-2, GM-CSF, CCL1, CCL24 and CXCL2 (**Figure 5B**).

3.7 *In vivo* implantation – biocompatibility study. There was no adverse event encountered at the time of graft implantation. During scaffold retrieval, the surrounding abdominal wall skin appeared healthy, and after incision and direct implant observation, no obvious capsular formation could be identified. The integration with recipient tissues was satisfying in all groups with signs of macroscopic vascular infiltration present. At histology, the cellular infiltration was diffuse at POD15 and POD30, but less important at POD60, with signs of micro-vascular permeability in the deep scaffold (**Figure 6A-C**). Remodeling was globally limited. CD68+ macrophage infiltration was important and located exclusively within the scaffold, being less intense and more peripheral at POD60 (**Figure 6G-I**); this correlates to the CD68 staining quantification, in which the % stained area was significantly ($p<0.0001$) higher in the control native group at POD15, with reduction at POD30 so that there was now no difference between groups. At POD60, the native group was significantly more infiltrated than the decellularized group (**$p<0.001$). Interestingly, the decellularized group was significantly less infiltrated at POD60 compared to the same group at POD30 (**Figure 6J**). Flow cytometry of circulating rat anti-human IgG antibodies showed the following positive recipient immunization: 2/3 POD15 and POD30, 2/2 POD60 in control group, compared to 0/3 POD15, 1/3 POD30 and 0/2 POD60 (**Figure 6K**).

3.8 Cell viability study. For rASCs-seeded discs, MTT staining revealed homogeneous engraftment of viable cells on all scaffolds. On the full-thickness scaffolds, cells were located on all tissue layers including the epidermal side (**FIG 7A-B**). Cell viability was confirmed by live/dead staining, with a few dead cells identified (**FIG 7C-D**). For hASCs-seeded discs, MTT showed a similar pattern of distribution as with rASCs, with confirmed viability (**FIG 7E-G**). On H&E sections, examination established the cell layers at the surface of seeded scaffold, with no deep migration **(FIG 7F)**.

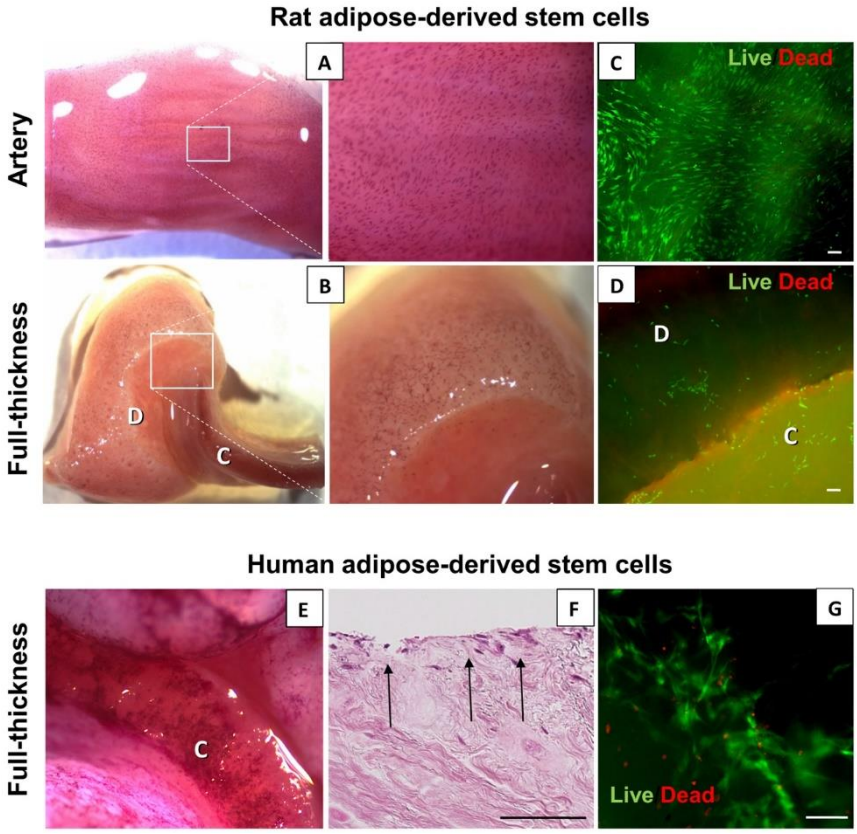

Figure 7: ***<u>Cell-compatibility testing</u>****. A-D* ***Static seeding*** *with rat adipose-derived Stem Cells (ASC) 3.6x10^4 cells/ cm^2 for 14 days:* ***A-B*** *Seeded scaffold and enlarged view, and observation of MTT staining,* ***C-D*** *Live/dead vital staining examination on whole-mount, of arterial pedicle (upper raw) and full-thickness (lower raw) samples from acellular ear; D dermis, C cartilage.* ***E-G*** *seeding of ear scaffold section with human ASCs, at a density of 20x10^4 cells/ cm^2 for 14 days:* ***E*** *MTT staining observation with positivity in the different layers;* ***F*** *H&E section showing cells (arrows) at the scaffold surface;* ***G*** *Live/dead vital staining observation. Scale bars: 100 µm.*

3.9 Whole-ear perfusion-bioreactor seeding. No sign of contamination was recorded during the experiment. At retrieval, the culture HE-ECM appeared diffusely pink, indicating perfusion and impregnation of the culture medium (**FIG 8A-D**). Viable cells were found in the parenchyma based on light density. The most important cell clusters were located in the superficial dermis, at seen on the H&E sections (**FIG 8E-F**).

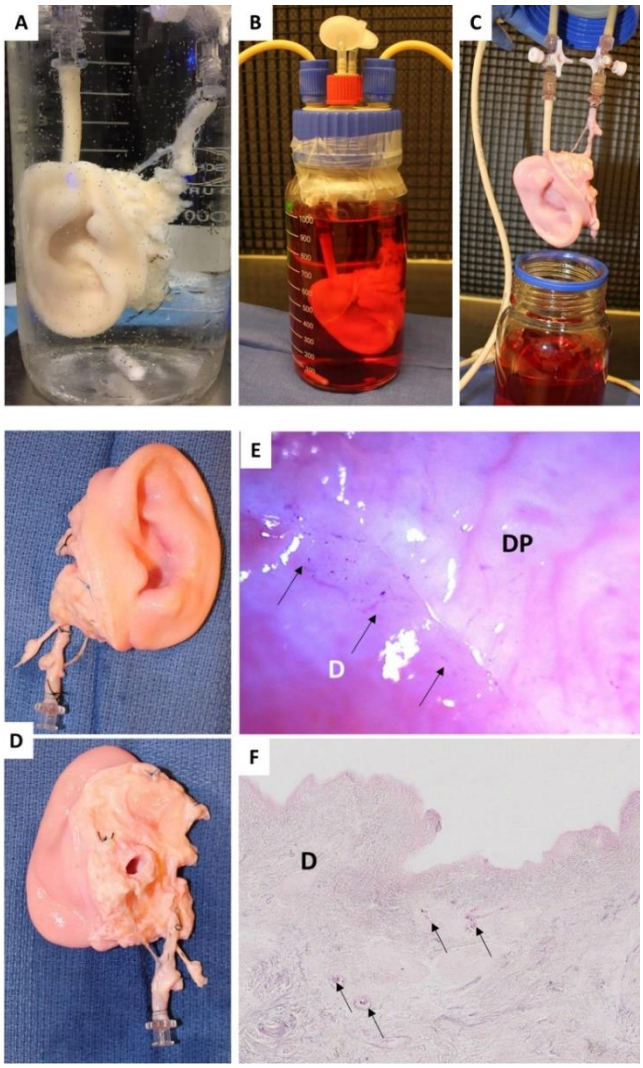

***Figure 8**: Whole-ear scaffold perfusion-bioreactor seeding. **A** Perfusion-sterilization with 0.1% peracetic acid and PBS rinsing. **B** Sterile mounting in perfusion-bioreactor, and immersion with culture medium, prior to cell seeding **C-D** Ear graft scaffold at time of retrieval, with pinky aspect as sign of proper culture medium perfusion and ECM impregnation. **E** Whole-mount staining and direct observation after MTT vital staining and cell positivity (arrows) in the superficial dermis (SD), under the basal membrane; DP dermal papillae. Scale bar: 100 µm.*

4. Discussion

A functional, implantable and clinically applicable engineered auricle is our ultimate objective. This study takes important steps in achieving this goal. We were able to produce whole acellular human ears with route for access to the vascular tree utilizing the approach of Vascularized composite Tissue Engineering. We demonstrated that early findings from porcine ear engineering [38] could be applicable to a human auricular graft model, confirming the relevance of the pig model in a preclinical experimental approach for composite tissue engineering. The feasibility of using elderly postmortem human donors, even several days after death, was shown. This is possible because of high collagen content of composite tissue ECM that seems to better handle cell necrosis and proteolytic enzymes, likely due to the presence of cell populations with low metabolic activity and less aggressive enzymatic content, as compared to exocrine pancreas cells involving complex organ engineering challenges [87]. Finally, vascular tree patency was displayed at all levels throughout the auricular ECM scaffold. It is however important to highlight that a diseased vascular tree, with extensive arteriosclerosis, can compromise perfusion and thus success in the decellularization.

An important difference when comparing the present data with our porcine ear study concerned the adipose tissue defatting: the ability to remove nuclei was efficient with detergents, as confirmed by DAPI staining, but a high content of scattered oil cysts persisted, requiring an additional treatment with polar solvent, as recommended in non-perfused isolated human adipose tissue engineering [123]. Our polar solvent step resulted in successful fat removal, although DAPI staining showed nuclei removal prior to the step, without impairment of the vascular tree. Even if considered as a minor issue for organ bioengineering, the ability to completely treat the adipose tissue is critical when dealing with composite tissue engineering, as fat represents a major component for this type of graft, in both qualitative and quantitative aspects. The real question however is whether adipose tissue needs to be fully treated or not, as the use polar solvent is not

straightforward. When considering *in vivo* application, persistence of lipid droplets can trigger a significant inflammatory reaction that may be deleterious to scaffold implantation. Moreover, even for *in vitro* application only, native adipose tissue persistence results in reduced engraftment of new adipocyte and thus poorer adipose tissue regeneration [124]. This illustrates the need for combination of decellularizing agents in VCE. Indeed, other tissues were successfully treated, with only some donor cells observed in the cartilage. These few remaining cells should not be an issue considering the significant reduction of total DNA observed in this tissue and its poor immunogenicity due to its avascular nature and ECM density [92]

Following processing, the auricular ECM structural components and 3D organization were well-preserved, which is critical for body parts in which function is directly related to the preservation of its form. The stiffness of the decellularized cartilage was maintained in an acceptable manner in our study, which applies directly to the target function of shape preservation of TE auricles, but may not be universally applicable to other tissue such as knee articular cartilage which experiences repetitive strain as its main function. Due to the cadaveric origin and the variability of the donors in this study, such results provide an overall appreciation of such an assessment. In order to further determine the structural organization of the auricular VCE, we performed a 3D characterization. This innovative tool brings a new level of resolution to scaffold analysis, allowing for precise comprehension of the spatial organization of both native and decellularized tissue with accurate reproduction of ECM in tissue engineering. As a quantitative measurement, porosity was calculated based on 3D volume, which is a more accurate assessment than conventional 2D analysis can provide. Still, new 3D analytic tools need to be developed for soft tissue and organ engineering evaluation, so as to mimick the success of 3D bone tissue evaluation [127].

Perfusion-decellularization with SDS-based protocol seems to be suitable for protection of innate cytokines of skin, fat and cartilage in the human ear. We showed that cytokines of different function and nature are preserved to a measurable extent and therefore may contribute to the favorable characteristics

of natural ECM in the decellularized ECM scaffold. Overall, growth-inducing cytokines were preserved most frequently, followed by the cell-guiding chemokines then inflammatory cytokines. This balance of cytokines demonstrates preservation of "protective" growth factors and a more pronounced depletion of pro-inflammatory cytokines across all analyzed tissues. In addition to the positive cytokine profile, we also observed distinct responses to the perfusion process of individual tissue ECMs in terms of protein preservation, with cartilage and fat being the most preserved tissues. Taken together, these findings suggest that newly colonizing cells in the ECM scaffold will come across a cell-friendly environment, akin to physiologic conditions. ECM obtained via perfusion-decellularization are therefore very likely to increase the success rate of cell-reseeding.

We observed an overall increase of vascular resistances during scaffold production, especially during SDS perfusion. This phenomenon of increasing vascular pressure during perfusion-decellularization has been described for other organs [94,128] with a subsequent decrease in resistance after re-endothelialization. In contrast to these findings, MAP was already back to normal values after PBS rinsing in our study. Considering adaptation of perfusion inflow, we question the need to adapt flow to follow constant ideal vascular resistance, as recommended for solid organs preservation and engineering. Indeed, during the initial steps, a high pressure increases the risk of damage to microcirculation and of edema formation. Furthermore, vascular resistances after cellular depletion likely reflect extra-vascular rigidity with subsequent increased pressures against flow. Thus, maintaining adequate flow, against increased vascular resistances, should be the goal to allow distal perfusion.

During the *in vivo* part of our study, the decellularized scaffolds were well tolerated even when significant remodeling was observed, with an important CD68+ macrophage infiltration during the first 8 weeks post-implantation. This remodeling is well-known [129,130] and part of a necessary integration period of the ECM by the recipient, with a related ECM mass decrease. In our study, we observed a preservation of the ECM structure at POD60, with less remodeling than expected

for an ECM rich in collagen. The discrepancies observed when screening anti-donor circulating IgG may rely on the immunogenicity of the treated ECM itself, along with the use of cadaveric donors. For the control, the immune response was mild, explained by the need to use non-fresh controls from human cadavers, with reduced allogenic properties. Moreover, the need to sterilize native tissues with 0.1% PCA participated in reducing allogenicity further, as PCA itself has been described as a decellularizing agent on its own [131]. This appears to be the downside of using human grafts from cadaveric sources, and further studies should investigate the effect of procurement delay and conditions on the overall outcome and immune response *in vivo*. Nevertheless, this model is a very useful tool to study and establish VCE protocols at a direct human scale, with readily accessible donor supply.

When dealing with future whole-graft scaffold recellularization strategies, it is of paramount importance to consider the ear as a complex 3D anatomical structure at all scales, with multilayered tissues including skin, cartilage, fat, nerves and blood vessels. This conceptual framework highlights the challenges of creating a clinically useful auricle based on conventional TE approaches. Even if we had an efficient protocol readily available to adequately treat all the tissues at once to produce a decellularized ECM scaffold with a single vascular access, recellularization remains an important problem to solve. As demonstrated in this study, vascular access to facilitate seed dissemination and preservation of basal membranes are prerequisite factors to allow dermal perfusion of culture medium with subsequent cell engraftment; non-perfused TE skin construct approaches are limited in their ability to recellularize a scaffold [132]. Apart from skin and vessels, which can be approached in a direct manner for seeding, other tissue types, such as cartilage and adipose, are buried deep in the scaffold, making it almost impossible for any selective seeding like topical, vascular injection, or cell infusion. For these tissues, the ideal option relies on a single-type stem cell approach, that differentiates and replicates when in contact with specific ECM tissues, as demonstrated by other groups [133,134]. For the cartilage, combined to a whole composite scaffold, like ear or nose, the difficulty will be important, by its

deep location it the graft and the absence of vascular access. The current strategies in cartilage engineering have successfully treated isolated scaffolds [119,135], but cannot be directly applied to our cadaveric auricular ECM scaffold model at this time. Perichondrium and peripheral cartilage enhanced porosity could allow seeded cells to repopulate the decellularized cartilage adequately with further research efforts

5. Conclusions

Complex auricular scaffolds with preserved vasculature can be obtained from human delayed postmortem sources to provide a platform for further functional tissue engineered constructs. Access to an auricular vascular tree, for which preservation and accessibility has been obtained for the first time in this study, is the key step required to translate experimental science to clinical usage. Overall, perfusion-decellularization application to body parts show great promise in generating suitable composite tissue scaffolds for body reconstruction. The goal of future experiments should be to improve the efficiency of the decellularization protocol and to improve recellularization by enhancing vascular seeded engraftment and density, as well as epidermal regeneration on a perfused acellular dermis.

Author Contributions. JD designed study, performed all procurements, set up and performed all decellularizations and scaffolds seeding, interpreted data, wrote article. HA and DA participated extensively to specimen collection and treatment, performed analysis. TW, AT, EV and RR performed all cytokines quantifications. CBo performed all histological processing and quantifications. DM was responsible for 3D histology reconstruction and quantification. VD and PD performed all mechanical testings. DH and GO participated to study design and data interpretation. CBe, PG and BL participated to study design, supported all analysis. All authors interpreted data, revised manuscript and gave their final approval.

Acknowledgments. The authors express gratitude to Erick Montoya, An Catherine Hoang Le Thien, Sarah El Hathout, Daela Xhema, Marc de Bournonville, Darren

Treanor, Chantal Fregimilicka, Michele De Beukelaer, Christine de Ville de Goyet, Marie Henry, Bernard Caelen, Pascale Segers and Walter Hudders for their devoted technical assistance or logistic support.

Conflict of interest/disclosure. HG-MIM Software is produced by HeteroGenius Limited, UK, of which Derek Magee is a director. All authors approved the final version of the article.

Funding source. This work was supported by a Fondation Saint-Luc Grant, FSR-UCL (Fonds Spécial de la Recherche) and Fonds Dr. Gaëtan Lagneaux.

« L'Homme influence sa propre évolution, ce n'est déjà plus depuis longtemps une évolution darwinienne au sens classique. »

Jacques Monod

Section 3- Tissue Engineering studies: motor subunits

Summary

In this section, we extend the experiments to motor subunits, characterized by the inclusion of cutaneous muscle and their subsequent functionality to restore. In addition to the cartilage-based nose subunit, previously explored through the ear in a same morphological subunit group, our next goal was thus to simultaneously study the lips and eyelids for the motor subunits group.

In **Chapter 6**, a preliminary study was performed on the rat hemi-face: apart from studying a compound muscle-bearing graft, the secondary aim of this research was to assess the relevance of the rat face model for VCE, knowing its description as an experimental model in VCA. Our observations have shown that the intravascular perfusion was not mandatory for decellularization in this model, because of the very small volumes of tissue, which could also be efficiently treated by passive penetration of decellularizing agents. However, we claimed the relevance of this widespread laboratory model for further recellularization studies, due to the smaller number of cells required, to repopulate the entire scaffold.

In **Chapter 7**, we applied all findings from previous studies to the implementation of the PDR technique to the historical human segmental lower face allograft, then

extended to the whole human face soft tissues. For the recellularization study, we isolated lip subunits scaffolds, as described in the first chapter, following the experimental rationale for subunits selection. Our results demonstrated the complete decellularization of a segmental graft, then extension to the full-face could be successfully achieved with a preserved ECM and a patent and perfusable vascular tree. Furthermore, the morphological identity of the face image was restored when the ECM was replaced on its original bony support. Isolated lip scaffold seeding was successful for muscle progenitor cells and endothelial cells, both critical for further transplantation approaches.

Chapter 6: Rat face bioengineering

Face scaffold production in a rat model.

Plast Reconstr Surg. 2017 Sep 14;

doi: 10.1097/PRS.0000000000003910. [Epub ahead of print].

Duisit J
Amiel H
Dedriche D
Behets C
Orlando G
Gianello P
Lengelé B

ABSTRACT

Background. As a route towards face bioengineering, our group previously reported the production of a complete scaffold production by perfusion-decellularization of a porcine ear subunit graft and partial recellularization. In order to extend the scaffold to the whole face and to down-scale it, we applied our findings to a rodent hemi-facial graft model.

Methods. After euthanasia, seven full-thickness rat hemi-face grafts were harvested with the CCA and the EJV as pedicle, and cannulated. Grafts were decellularized by a detergent-based protocol: either by perfusion through the CCA, or by mechanical agitation. After decellularization, samples were analyzed for DNA quantification and histology by H&E, Masson's Trichrome, Sirius red or Safranin O staining. Vascular tree patency was assessed by Micro-Angio CT after contrast injection. Cell-friendly ECM was assessed by seeding of human adipose-derived stem cells and vital staining after 7 days of culture.

Results. Decellularization was effective in both groups, with a cell clearance at all levels, with the exception of cartilage areas in the agitation treated groups. Microscopic assessment found a well-preserved ECM in both groups. Vascular contrast was found in all regions of the scaffolds. After sacrifice, seeded cells were found viable and well distributed on all scaffolds.

Conclusions. We successfully decellularized face grafts in a rodent model, with a preserved vascular tree. Perfusion-decellularization led to better and faster results than with mechanical agitation, but is not mandatory in this model. The rat face is an interesting scaffold model for further recellularization studies, in the final goal of human face bioengineering.

1. Introduction

Restoration of extensive facial defects is one of the most challenging goals in reconstructive surgery. Since World War I, the use of autologous tissues has allowed significant progress in facial surgery, which however is often inefficient at restoring the exact missing morphology and function. Face vascularized composite tissue allotransplantation (VCA), from its experimental description in a small animal rodent model [136-138] to its first clinical application in 2005 [1,2] offers a revolutionary therapeutic option for the treatment of severely disfigured patients. However, its applicability remains very limited, due to the technical challenges, the need for lifelong immunosuppression (IS) and the still limited lifespan of the graft [37]. Investigations undertaken to induce immune tolerance have not yet succeeded in providing strong outcomes, both experimentally and clinically [139,140]. In the era of tissue engineering, perfusion-decellularization technology has been successfully applied to nearly all organs of clinically relevant species [81,85,86], enabling the production of complex extra-cellular matrix (ECM), while preserving an accessible vascular tree. By repopulating the produced scaffold with autologous cells, this approach could lead to IS-free transplantation [81,141]. In this emerging field of vascularized composite engineering (VCE), applications have already been described for the trachea, larynx and limb models [38,93,94,142,143]. We recently reported for the first time the applicability of a detergent-based perfusion-decellularization technique for facial subunits, namely the porcine ear [38], that was chosen for its relatively low anatomical and functional complexity. We demonstrated that the porcine ear can be successfully and consistently decellularized to obtain acellular scaffolds that are biocompatible and non-immunogenic, and as such, may be used as a template for the bioengineering of a missing ear. On the wake of these promising results, we planned on scaling up to the whole face but, given the extremely challenging anatomical and functional complexity of the whole face, we opted for a smaller and more approachable model, namely the rat. This manuscript reports the results of these studies that aimed to provide the proof of concept that decellularization technology can be

applied to the whole face in order to produce acellular ECM-based scaffolds for the bioengineering of the whole face.

2. Materials and methods

Specimens: The study was conducted on seven hemi-face grafts, procured from ten adult Wistar rats, sacrificed following other experiments approved by Université catholique de Louvain local Ethical committee, and in accordance with the EU Directive 2010/63/EU for animal experiments.

Face graft procurement and decellularization : Perfusion-decellularization (Perf-D) group: shortly after euthanasia, four full soft tissue thickness hemifacial grafts (RAF-G) were harvested as described by Climov et al.[144], with the vascular pedicle being extended to the external carotid artery (ECA), cannulated with a 27G catheter, and the external jugular vein (EJV), left free. All grafts were weighed and measured. RAF-G were immersed in a 500-ml glass jar, filled with phosphate buffered saline (PBS, VWR international, Radnor, PA, USA). The arterial pedicle was then connected to a peristaltic pump (Masterflex L/S, Cole-Palmer Instrument Co, Vernon Hills, IL, USA), via a 16G silicone tubing (Cole-Parmer) (**Figure 1**). Perfusion flow was set from 2 to 4 ml/min, to ensure mean arterial pressure to remain under 100 mmHg. The following mean perfusion sequence was applied: normal heparinized (15 UI/ml) saline for 1 hour; 1% sodium dodecyl sulfate (SDS, VWR) for 100 hours, based upon the evolution of decellularization; and finally, PBS rinsing for 24 hours. Agitation decellularization (Agi-D) group: As a control to perfusion, three RAF-G were harvested without pedicle preparation, immersed in a 500-ml jar and decellularized by constant mechanical agitation, set to medium speed, following the same decellularization steps as previously described: heparinized saline for 1 hour; 1% SDS for 140 hours, changed every 48 hours; and finally, PBS rinsing for 72 hours. All decellularization steps were performed at room temperature in both groups, and RAF-G monitored for bleaching, epidermolysis and edema formation. After the final step, all produced rat face extracellular

matrix (RAF-ECM) scaffolds were preserved at 4°C in PBS, until further analysis. Group comparison was performed for the macroscopic and microscopic assessment of decellularization.

Tissue sampling: For both histology and DNA quantification, full-thickness sampling was performed at the level of mystacial pads, lips, eyelids, cheeks and ears, for native, Perf-D and Agi-D groups.

Histology, Immunofluorescence: Tissues were fixed in formalin for 24 hours, transferred in successive alcohol baths prior to dehydration and then embedded in paraffin and sectioned into 5µm slices. Sections were deparaffinized and rehydrated to allow staining with histochemical dyes for either hematoxylin and eosin (H&E), Masson's Trichrome (MT), sirius red (Picrosirius red stain kit, Polysciences, Warrington, PA, USA) or Safranin O (Sigma-Aldrich, St. Louis, MO, USA), according to standard protocols. After dehydration, sections were mounted with Entellan mounting medium (Merck, Billerica, MA, USA). For immunofluorescence (IF), sections were deparaffinized and quenched with NaBH4, then unmasked in bain-marie at 98°C for 30 minutes in a 10% citrate buffer solution containing triton X-100. Neutralization of nonspecific sites was done with PBS/BSA 5%. Sections were then incubated at 4°C overnight with the following primary antibody: collagen I (1:250, Abcam, Cambridge, UK), then incubated with an anti-rabbit secondary antibody (1:300, Thermo Fisher Scientific, Waltham, MA, USA). Finally, nuclei were counterstained with 4',6-Diamidino-2-Phenylindole, Dihydrochloride (DAPI) (1:1000, Sigma-Aldrich) and mounted with fluorescence medium (Dako, Glostrup, Denmark). Histology sections were digitalized at a 40x magnification with a SCN400 slide scanner (Leica Biosystems, Wetzlar, Germany). IF Images were acquired with an AxioImager Z1 (Zeiss, Oberkochen Germany) and treated with Axiovision microscope software (Zeiss).

DNA quantification: In order to assess cell reduction, DNA was quantified from native and RAF-ECM samples. First, DNA was extracted with DNeasy® Blood & Tissue Kits (Qiagen, Milan, Italy): RAF-ECM samples were incubated overnight at 56°C with proteinase K solution, followed by several elutions in columns, following

the manufacturer's instructions. The concentration of the extracted DNA was assessed by Quant-it Picrogreen DsDNA assay kit (Thermo Fischer Scientific), according to the manufacturer's protocol; Fluorescence was read at 480/520 nm on a plate reader and final DNA concentration was expressed in ng/mg (wet weight).

Micro-angioCT: RAF-ECM arterial filling from the Perf-D group was performed with 2 ml injection of a barium-gel solution, obtained by mixing 100 ml of physiological saline with 3 g of gelatin powder (Merck Millipore, Billerica, MA, USA) and 40 g of barium sulfate (Micropaque, Guerbet, Villepinte, France) in a water-bath heated to a temperature of 40 ° C. After injection, gel was allowed to solidify at 4°C, for at least 24 hours. The vascular tree was then studied by acquisition on a helical micro-CT scanner (NanoSPECT/ CT, Bioscan Inc., Washington D.C., WA, USA). The projections were reconstructed and 3D analysis was performed with Osirix© software (Pixmeo, Bernex, Switzerland).

Human adipose-derived stem cell seeding: In order to verify if the produced ECM scaffolds were non-toxic and allow cell engraftment and survival, human adipose-derived stem cells (hASCs) were purchased from manufacturer (Promocell, Heidelberg, Germany). The hASCs were cultured until passage 9 and then collected. RAF-ECM was sterilized using a 0.1% peracetic acid (PCA) solution (Lonza, Basel, Switzerland): briefly, samples were agitated overnight in PCA at 4°C, then rinsed with several sterile PBS baths and finally stored at 4°C in PBS with Penicillin and Streptomycin (P/S). $5x10^5$ hASCs were statically seeded on $1cm^2$ scaffold discs (n=4), either on the dermal or internal surface side, in a 24-well plate (Greiner Bio-one, Kremsmunster, Austria) for 7 days, after immersion in Dubelcco's Modified Eagle Medium (DMEM, Lonza) supplemented with 10% FBS (Thermo Fischer Scientific), 1% Glutamine (Lonza), 1% P/S (Lonza), changed every two days. At the end of the experiment, seeded scaffolds were processed, either as whole-mounts with the vital Live/Dead staining kit (Thermo Fischer Scientific), according to manufacturer's protocol, or formalin-fixed, sectioned and stained for collagen I by IF and with DAPI.

Statistics: Statistical analysis was performed using GraphPad Prism version 7 (GraphPad Softwares, La Jolla, CA, USA) and unpaired student t-tests. All data are presented as mean value ± standard error of the mean (SEM) and significance was set at $p<0.05$.

3. Results

Macroscopic aspect: In Perf-D group, a quick epidermolysis associated to blistering was obtained on the ear, midface and mystacial pad, within 24 hours of SDS perfusion, with an easy removal of hairs and vibrissa on the extrados. On the intrados, bleaching of the muscular structures was observed. After completion of the perfusion protocol, a satisfying "acellular" aspect was obtained (**Figure 1**), with the preservation of the facial structure and appearance. The morphology of the ear and nose was intact, indicating the preserved ability of the underlying cartilage to support the specific form of these subunits. Compared to Perf-D group, Agi-D grafts obtained a similar aspect, with however the absence of blistering of the epidermal cell layer and a slower effect on the epidermolysis and the treatment of the mystacial pad and facial muscles. Moreover, some auricular tears could be observed, as a result of the shear stress during mechanical agitation (**see Figure, Supplemental Digital Content 1, showing an auricular tear, from a scaffold belonging to the agitation group**).

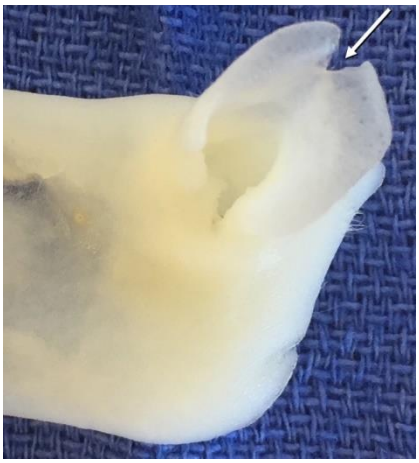

***Supplemental Digital content 1**: Auricular tear (arrow), in a rat face scaffold belonging to the agitation group.*

Cellular clearance: DNA quantification showed a dramatic reduction of cellular content of RAF-ECM in Perf-D and Agi-D groups compared to native samples, with respectively a mean 18.16 ng/mg ECM and 28.48 ng/mg ECM (wet weight) compared to 213.85 ng/mg in native tissues, achieving a 91.5% ($p<0.0001$) and 86.7% ($p=0.0001$) reduction (**Figure 1**). Although differences between both groups were not significant, the mean trend was higher for the agitation treated grafts, especially in the auricular area. H&E and DAPI staining confirmed cellular clearance, with absence of nuclear stain, and preservation of ECM structures at the different biopsies locations, with the exception of the cartilage in the agitation group, demonstrating areas of remaining chondrocytes (**Figure 2**) and some persisting cells observed in the dermis, from glands and hairs.

ECM preservation: Masson's trichrome stain of the RAF-ECM showed an excellent preservation of the collagen fibers in the different face labial and auricular subunit areas and for their different constituting composite tissues: dermis, cartilage, adipose tissue and muscle (**Figure 3**). Sirius red staining confirmed the high preservation of type I/III collagen in non-cartilaginous tissues, and proteoglycans in the cartilage as shown by the Safranin O staining (**see Figure, Supplemental**

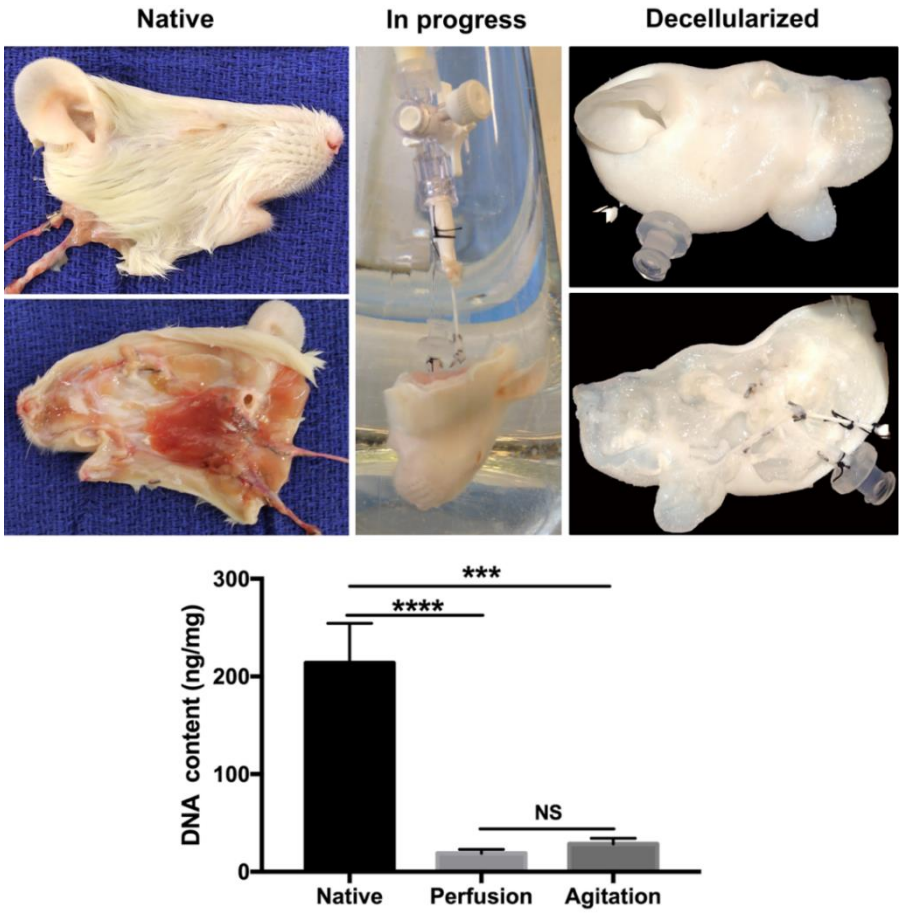

***Figure 1**: Superior panel: native hemi-face graft with cannulated pedicle (left); graft in perfusion-decellularization jar, with arterial catheter connected to a peristaltic pump (middle); final aspect of the face scaffold (right). Inferior panel: DNA quantification in native, perfusion-decellularized (Perfusion) and immersion-agitation decellularized (Agitation) samples; expressed in ng/mg (dry weight), error bar representing the standard error from the mean, **** $p<0.0001$, *** $p=0.0001$, NS non-significant.*

Digital Content 2, which shows special histology of native (*left panel*) and decelllularized (*right panel*) tissues of the auricular cartilage, with Safranin O staining to demonstrate proteoglycans preservation, and of the lip, with Sirius red staining to highlight type I/III collagens fibers. Scale bar 100 μm). Among these tissues, acellular nerve fibers could be well distinguished, especially in the MP area, with its rich nervous innervation (**Figure 3**).

Vascular bed preservation: the RAF-ECM micro-Angio CT (**Figure 4)** demonstrated a homogeneous arterial contrast distribution in all subunit areas: in the auriculo-temporal region, with intact vascular channels to the ear, cheek and scalp, and in the central face, with the observed continuity of the facial artery and collateral branches distributed to the superior and inferior lips, to the mystacial pad and to the nose.

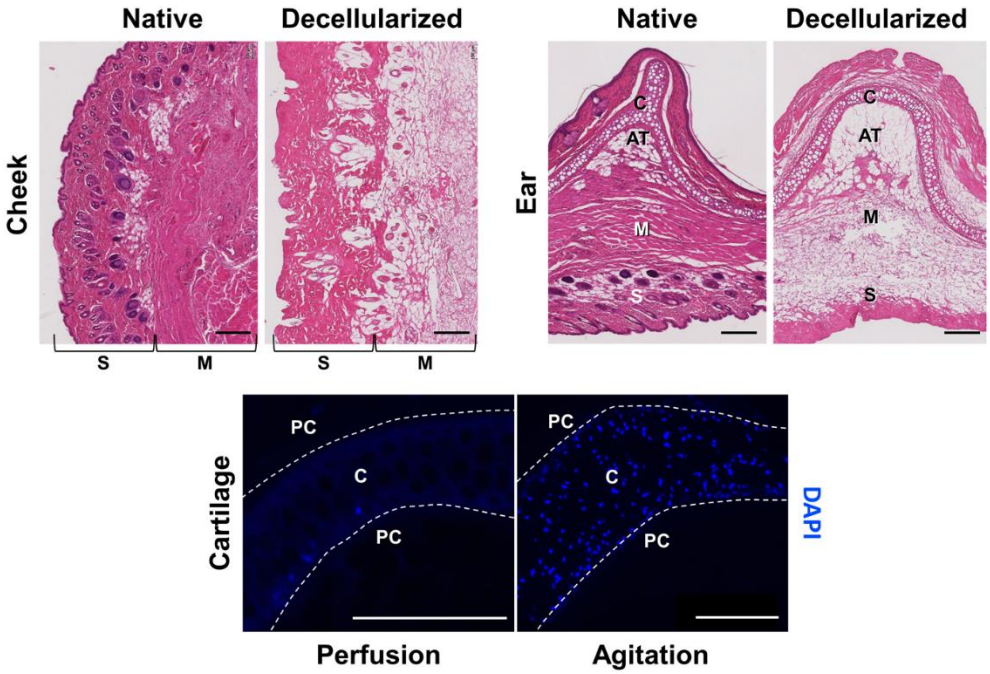

***Figure 2**: Histologic assessment of cell removal. Superior panels: H&E staining of native and decellularized samples from cheek (upper left) and ear (upper right); skin (S), muscle (M), cartilage (C), adipose tissue (AT). Inferior panel: DAPI nuclear fluorescence from decellularized ear samples. Aspect of cartilage (C) compared in perfusion and agitation groups; the perichondrium (PC) is very well treated in both groups but more cells are observed in the cartilage of agitation group. Scale bars represent 200 μm.*

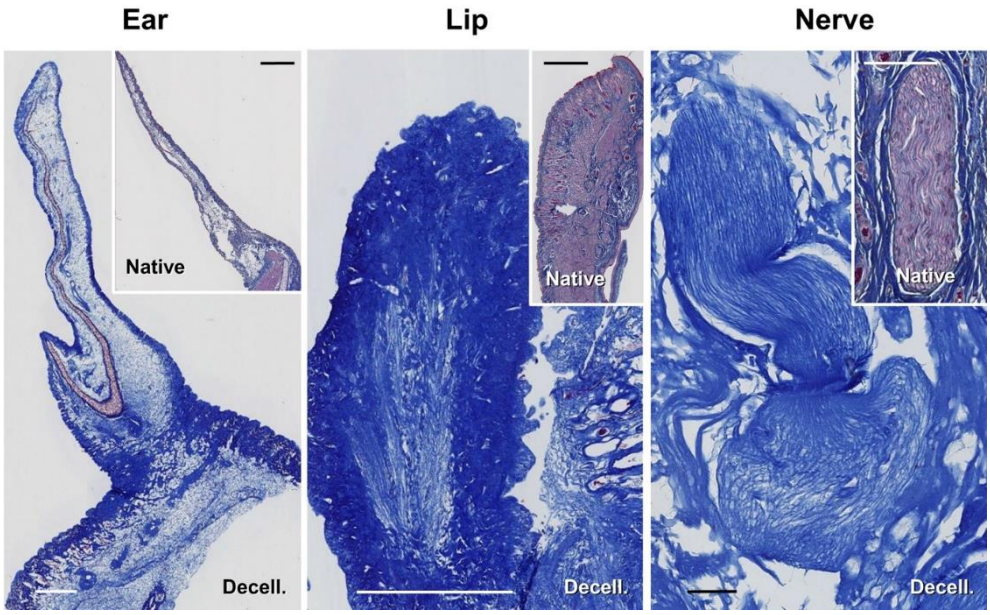

Figure 3: *Masson's trichrome staining of RAF-ECM (main box), compared to native tissue (insert), of the ear (left, scale bar 1 mm), inferior lip (middle, scale bar 1 mm), and trigeminal nerve fibers (right, scale bar 100 μm).*

Cell seeding: a predominant amount of seeded HASCs were found alive and well-distributed on all scaffolds, as demonstrated by vital staining (**Figure 5**), on both dermal and internal sides. The cells demonstrated some migration in the ECM, as shown by positive nuclei on the surface and within the dense collagen of the ECM (**Figure 5**).

4. Discussion

We have demonstrated that decellularization technology can be applied in the rat model, to a whole hemi-face graft to obtain acellular ECM-based scaffolds for face bioengineering purposes.

Perfusion in this model presents several advantages: it is faster, epidermolysis is more effective, the endothelium of the vascular tree is completely and more thoroughly cleared. Moreover, continuous perfusion allows for a more efficient clearance of cell debris and proteolytic enzymes. Interestingly, epidermolysis is obtained very efficiently by blistering at the level of the dermoepidermal junction, due to the subdermal plexus perfusion. Keratinocytes' debris are then swept out without being trapped in the 3D framework of the remaining ECM.

Interestingly, in the rodent, the perfusion method is not the only option because successful decellularization could also be accomplished with the sole mechanical agitation method. More than on the complexity of the tissues involved, this relies on the relatively high exposed surface of the intrados of the graft. More particularly with the face, the skin represents only a half of the total graft area, and the harvested surface facing the bone support offers an ideal surface for agent penetration, with interrupted basal membranes; indeed, the preservation of basal membranes is an obstacle to solution penetration on the dermal side. This phenomenon is not observed in whole-solid organ decellularization, even in a small model, because of existing continuous basal membranes and a true capsule, which represent a barrier to agent prenetration leading to a poor penetration of the solution agents, as observed classically in conventional histology fixation. Moreover, the specific soft face configuration offers a relative limited thickness with a maximum of 5 mm at the level of the cheek, as recorded in our study.

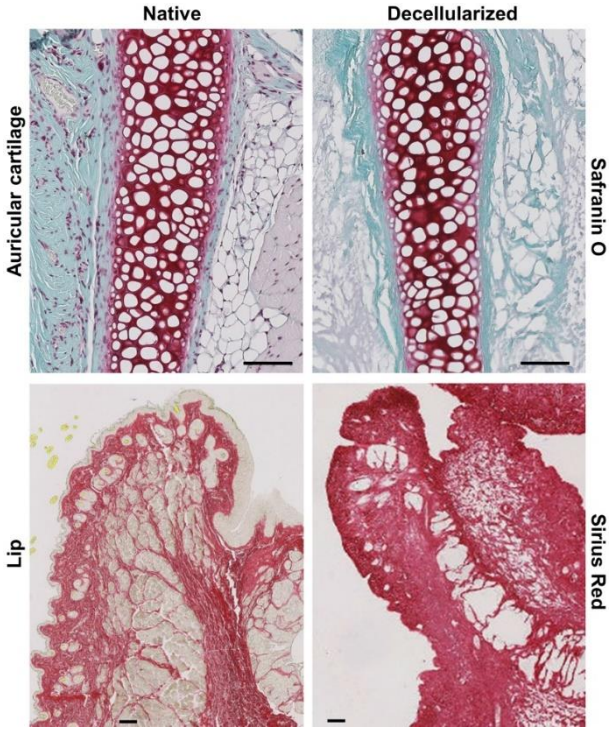

Supplemental Digital content 2: *Special histology of native (left panel) and decelllularized (right panel) tissues, of the auricular cartilage with Safranin O staining, to demonstrate proteoglycans preservation, and of the lip, with Sirius red staining, to highlight type I/III collagens fibers. Scale bar 100 μm.*

This explains the need for perfusion as observed for other body part engineering in small animal studies, like the rat hind limb [94] whose configuration is totally different: a relatively large dermal surface and a small basis section. In fact, the interrupted basal membrane surface, and thus the surface for penetration, is far less important in limbs compared to the face, because of the dermal barrier and the additional muscular fascia. As confirmation, we report a study using agitation only for decellularization of a rat skin flap [145]. The disadvantages of a non-perfusion method were reflected in a less efficient cartilage treatment, requiring an active solution washout in the perichondrium, and for the skin: even if epidermolysis occurs naturally with cell necrosis, annexes like glands and hairs appendages can be trapped in the natural dermal convolutions in the absence of blistering and bullae formation, leading to trap allogenic elements in the dermal ECM.

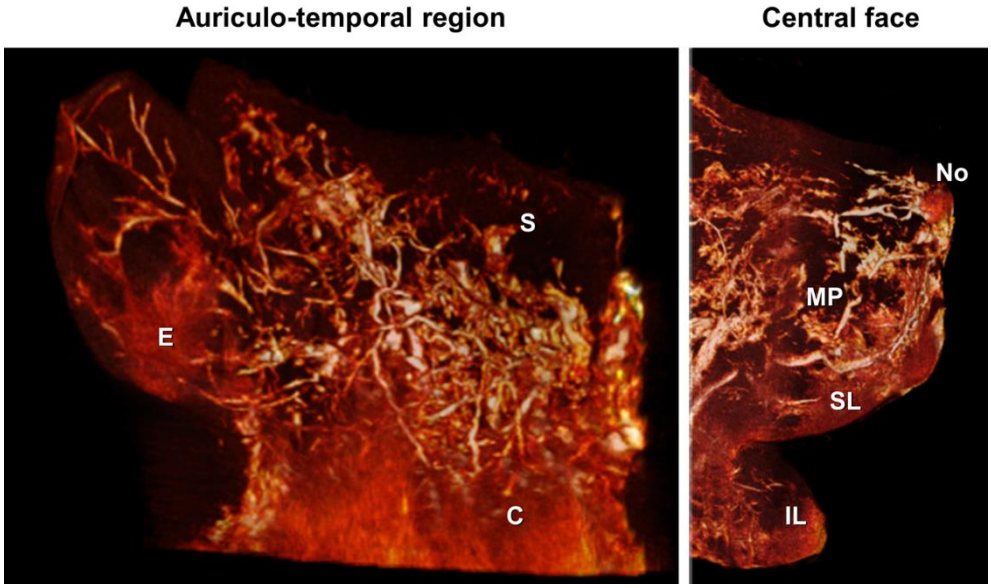

***Figure 4**: Micro-angio CT of a hemi-face scaffold, after barium sulfate gel arterial injection. 3D rendering of the auriculo-temporal (left) and central face (right) regions. E, ear ; S, scalp ; C, cheek ; IL, inferior lip ; SL, superior lip ; MP, mystacial pad ; No, nose.*

The drawback of an open circuit perfusion design, in comparison with decellularization by immersion and agitation, is the larger volume of solutions wasted. In our study, agitation consumed ten times less volumes compared to perfusion. This difference is acceptable for cheap solutions like SDS, but could represent a major experimental issue for more expensive solution types. For example, sodium deoxycholate was found less efficient to treat cartilage and resulted in the near destruction of the ear (*Duisit J et al, unpublished data*), with however a good effect on the skin and muscle, as previously described [146,147]. It is indeed both difficult to handle and relatively expensive. SDS-based detergent protocols, whose use has been largely documented for organs [87,90,96] and composite tissues [38,93,94], have the advantage of an overall efficiency on all tissues, despite a known poor effect on the preservation of growth factors and chemokines [131]. As a direct advantage of a lesser volume of solutions needed and of a very simple

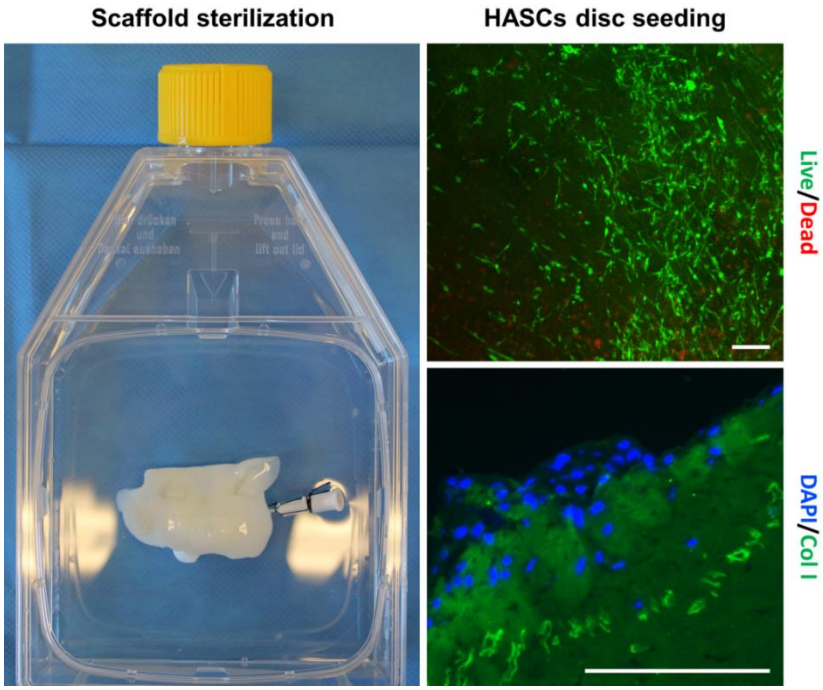

***Figure 5**: Left panel, acellular face graft after sterilizarion with peracetic acid, stored in sterile PBS prior to seeding. Right panel, whole-mount imaging with vital staining, for living (green) or dead (red) human adipose-derived stem cells (upper raw) ; immunofluorescence staining of cell nuclei (DAPI, blue) and matrix (green) type I collagen (lower raw). Scale bars 200 μm.*

apparatus, agitation could be used to test more easily the action of new agents on composite tissues prior to its transposition in a perfusion model in the same or higher scale.

However, for both VCE methods, the treatment of very broad tissue associations and the absence of selective targeting is a major issue to address, with a unique pedicle and vascular access. Thus, a validated protocol should interest all tissues with an overall and balanced outcome for the different tissues. As of relevance to these precise experimental concerns, facial subunits could provide models with more specific tissue associations, i.e. the ear for cartilage and the lip for facial muscle.

When recellularization is considered, in addition to static (i.e. keratinocytes) or injection (i.e. muscle, cartilage) cell seeding, a preserved vascular access is

mandatory for accurate recellularization. Thus, perfusion represents a pathway to seed cells either to the whole parenchyma, or to treat the vasculature itself by endothelial and related cells, in order to obtain a transplantable engineered graft. This could enable the development of a know-how at a small scale, with an affordable number of cells to cultivate and seed, that could be later on, translated to larger models. As a native allograft, the rat face model shows limitations into its direct transposition to a human model in terms of both surgery and immunology. Indeed, it is not a pre-clinical model but could be a very valuable tool as a tissue engineering experimental model because of the smaller mass to be decellularized and consequently, the fewer cells needed for its recellularization.

5. Conclusions

VCE represents an alternative to current VCA strategies and paradigms, by adding an *in vitro* step before donor graft harvesting and re-implantation in the recipient. In this application to the face, the rat model represents an interesting platform to prove feasibility of tissue engineering principles and applicability to a challenging field like face subunit and whole face reconstruction. Regarding decellularization, it has the advantage of an easy exploration of the very different tissues associated to a composite face graft, with the possible use of mechanical agitation to simplify the process and the apparatus. However, the absence of a true need of perfusion-decellularization, represents the translational limit of this model, compared to large animal and human models. This is different however for the recellularization and *in vivo* replantation, in which the vascular access will be of great matter for cell seeding and reperfusion.

In conclusion, even if not a true pre-clinical model, the rat face model offers a conceptual approach and a platform for the future approaches in whole human face bioengineering, especially for the recellularization aspects. This role of small models in tissue engineering acts in the same manner as in the research history of

face allotransplantation, and provides in an interesting manner, a new application to the classical VCA experimental models.

Chapter 7: Human face bioengineering

Bioengineering a human face graft: the matrix of Identity.

Annals of Surgery 2017. In Press

IF (2017): 8.980

Duisit J
Maistriaux L
Taddeo A
Orlando G
Joris V
Coche E
Behets C
Lerut J
Dessy C
Cossu G, R
Vögelin E
Rieben R
Gianello P
Lengelé B

ABSTRACT

Objective: During the last decade, face allotransplantation has been shown to be a revolutionary reconstructive procedure for severe disfigurements. However, offer to patients remains limited due to lifelong immunosuppression. In order to move forward in the field, a new pathway in tissue engineering is proposed.

***Summary Background Data*:** Our previously reported technique of matrix production of a porcine auricular subunit graft has been translated to a human face model.

Methods: Five partial and one total face grafts were procured from human fresh cadavers. After arterial cannulation, the specimens were perfused using a combined detergent/polar solvent decellularization protocol. Preservation of vascular patency was assessed by imaging, and cell and antigen removal by DNA quantification and histology. The main extra-cellular matrix proteins and associated cytokines were evaluated. Lip scaffolds were cultivated with dermal, muscle progenitor and endothelial cells, either on discs or in a bioreactor.
Results: Decellularization was successful in all facial grafts within 12 days revealing acellular scaffolds with full preservation of innate morphology. Imaging demonstrated a preservation of the entire vascular tree patency. Removal of cells and antigens was confirmed by reduction of DNA and antigen markers negativation. Microscopic evaluation revealed preservation of tissue structures as well as of major proteins. Seeded cells were viable and well distributed within all scaffolds.

Conclusions: Complex acellular facial scaffolds were obtained, preserving simultaneously a cell-friendly extra-cellular matrix and a perfusable vascular tree. This step will enable further engineering of postmortem facial grafts, thereby offering new perspectives in composite tissue allotransplantation.

1. Introduction

At the dawn of the 21st century, conventional facial reconstructive techniques, based on the use of autologous tissues, have shown their limitations and inability to simultaneously restore the morphological identity, cosmetic appearance and expressive function devoted to the human face. In 2005, the first successful facial transplantation [1,2] was applied to the highly complex three-dimensional framework of the face, relying on the vascularized composite tissue allotransplantation (VCA) principles learned from limb transplantation [59]. The success of face transplantation raised a lot of hopes for a significant improvement of the surgical treatment of severe disfigurement. A decade later, however, face transplantation remains of limited clinical applications with an overall of 35 cases reported worldwide [79]. While ethical concerns have been overcome by the outstanding superiority of the clinical results [148], the cost-benefit balance of the procedure remains questioned, because of need for a lifelong immunosuppression (IS) [149]. Initially, the reluctance to accept the procedure relied mostly on the risk of acute rejection, whereas nowadays the main concern regarding the future of this technique is chronic rejection. Like in other types of VCA, chronic rejection [37,150] induces distal vascular impairment, which results in a mean graft survival of 10-15 years. Hence, the need to open up new therapeutic pathways arose, with two different strategic options: the first one is aimed at reaching the ultimate goal of a long-term graft tolerance [151,152], the second one relies on the *de novo* creation of new grafts, that will naturally be tolerated, through the new original pathway of regenerative medicine [141]. In regenerative medicine, the so-called Cell Seeding on Scaffold Technology (CSST), in which cells from a patient can be grown on extra-cellular matrix (ECM) scaffolds to produce functional organs, has been previously investigated in solid organs [85,88,96,121,129] and limbs [94] with very promising results. In a previous report [38], we demonstrated the successful application of CSST in a porcine ear graft model, designed as an emblematic initial experimental platform to start face bioengineering. The so-obtained results on the auricular facial subunit led us to draw three hypotheses for the present study: first, can we extend CSST to other types of facial subunits, such as the nose, lips, cheeks or even a whole face? Then,

can we transpose it to a human model? And finally, can we extend the donor criteria for face graft procurement, through the resistance of composite tissues from cadaveric donors to biological degradation?

2. Material and Methods

Our study was conducted on five segmental lower face grafts (SF-G) and one full face graft (FF-G), procured from fresh human cadavers from body donation at Université catholique de Louvain, within a median delay of fifty hours (range 12 to 96) from death. Median age was 82 years (range 63-96). The cadavers were stored in a cold room at 4°C until graft procurement. All experiments were approved by the local ethical committee.

Surgical technique: SF-G involving the nose, lips and cheeks subunits, were elevated as previously described [5] after facial artery (FA) and vein isolation, with the facial, mental and infra-orbital nerves.

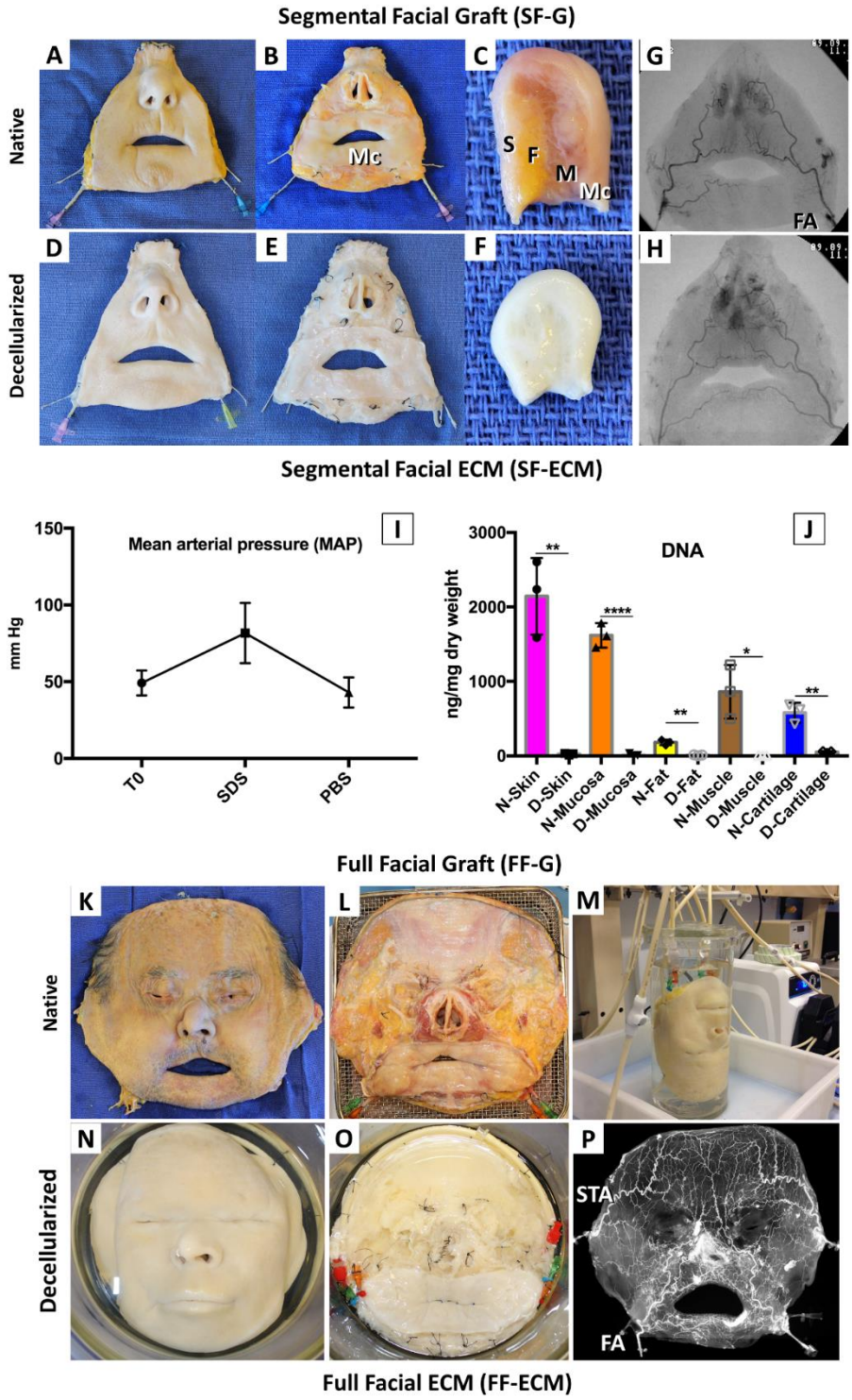
Segmental Facial Graft (SF-G)
A
B
C
G
Native
Mc
S
F
M
Mc
FA
D
E
F
H
Decellularized
Segmental Facial ECM (SF-ECM)
I
Mean arterial pressure (MAP)
150
100
50
0
mm Hg
T0
SDS
PBS
J
DNA
3000
2000
1000
0
ng/mg dry weight
**
****
**
*
**
N-Skin
D-Skin
N-Mucosa
D-Mucosa
N-Fat
D-Fat
N-Muscle
D-Muscle
N-Cartilage
D-Cartilage
Full Facial Graft (FF-G)
K
L
M
Native
N
O
P
Decellularized
STA
FA
Full Facial ECM (FF-ECM)

***Figure 1**. Segmental and full face grafts perfusion-decellularization. **A-C** Native segmental (SF-G) nose-lip face graft with its associated vascular pedicle, in **A** anterior and **B** posterior views. **C** represents the lower lip cross section with the associated tissue layers of skin (S), fat (F), orbicularis ori muscle (M) and oral mucosa (Mc). **D-F** Decellularized segmental face graft (SF-ECM) demonstrating a satisfying superficial aspect of **D** the acellular skin, mucosa, fat and **E** muscle stumps labelled with a nylon suture; **F** deep thickness examination of the lip, demonstrating treatment of all layers. **G-H** Fluoroscopy demonstrates that patency of the facial artery (FA) and branches is preserved when comparing **G** native SF-G with **H** produced acellular SF-ECM vascular tree. **I** Mean arterial pressure (MAP) during the main decellularization steps of SF-G expressed in mm Hg: baseline (T0), at the end of sodium dodecyl sulfate (SDS) perfusion, and after final rinsing (PBS). **J** DNA content in native (N-) and decellularized (D-) tissues: skin (S), oral mucosae (Mc), fat (F), facial muscles (M) and cartilage (C). Results expressed in ng/mg ECM and native tissue (dry weight). Data presented as mean ± SEM, *p<0.05, **p<0.01, ***p<0.0001 by two-tailed unpaired T-test. **K-L** Native full-thickness face graft (FF-G), in **K** anterior and **L** posterior views. **M** Decellularization apparatus and graft in process **N-O** Decellularized full-thickness face graft (FF-ECM), exhibiting obvious skin and annexes treatment as well as tissues on the inner side. **P** Radiogram of the barium-gel injected decellularized FF-ECM; contrast injection through superficial temporal arteries (STA) and facial arteries (FA) demonstrates a very well preserved vascular tree after decellularization.*

Both FAs were cannulated and muscles labelled (**Fig. 1A-C**). In case of the FF-G, procurement was extended to the upper face, adding both superficial temporal arteries (STA) (**Fig. 1K-L**).

Perfusion-decellularization technique: All grafts were immersed in a glass jar, and the arterial cannulas were connected to a Masterflex L/S peristaltic pump with 16G tubing (Cole Parmer, Vernon Hills, IL). Mean arterial pressure (MAP) was recorded with a Datex-Ohmeda S/5 monitor (GE Healthcare Life Sciences, Chicago, IL). Perfusion of both FAs, keeping the MAP below 80 mm Hg, was divided into three sequences, respecting volumes load indicated for SF-G. In the first sequence, adapted from Ott et al. [121], the solution consisted of heparinized saline (15 UI/ml, 1.5L), 10 μM adenosine (A-4036, Sigma-Aldrich, St. Louis, MO); 1% SDS (70L); de-ionized water (6L); 1% Triton-X 100 (9L) and PBS (30L). During the second sequence, defatting was achieved using 2-propanol (ISO) (VWR, Radnor, PA). After a first overnight stirring-bath (1L), ISO was perfused in closed circuit perfusion (2L) for 12 hours. After a second overnight ISO stirring-bath (1L), grafts were rehydrated, with de-ionized water (1L) and PBS perfusion (26L). During the third

sequence, type I bovine DNAse (Sigma-Aldrich) (25 mg/L, 1.5L PBS) was perfused at 37°C, washed with PBS (10L). During all three steps, MAP as well as the graft were monitored with respect to edema, blistering of facial skin and mucosae, fat and muscle bleaching. For FF-G, perfusion was done alternatively in STAs and FAs. Produced segmental (SF-ECM) and full (FF-ECM) face ECM scaffolds were either processed for analysis or stored at 4°C in PBS.

In vitro vascular assessment, mock transplantation and in vivo reperfusion study: SF-ECM vascular patency was assessed by fluoroscopy, acquired with a Powermobil C-Arm (Siemens, Munich, Germany). FF-ECM were injected with a barium sulfate-gel solution (40 ml), as previously described [95], then imaged with a Senograph Essential (GE Healthcare, Chicago, IL). To mimic transplantation, the FF-ECM was replaced on the original donor head and images acquired with a CT scanner (Philips Healthcare, Cleveland, OH), and analyzed using Osirix software (Pixmeo, Bernex, Switzerland). To assess if the innate vasculature of the scaffold would support a physiological blood pressure, we heterotopically reperfused an SF-ECM graft under general anaesthesia in a porcine recipient.

Figure 2. *FF-ECM, mock transplantation and SF-ECM in vivo reperfusion.* ***A-F*** *Mock transplantation of the FF-ECM and angio-CT* ***A-C*** *Anterior, lateral and upper view of FF-ECM replaced and sutured on the original donor head defect; preservation of facial morphology in all areas, including cartilaginous support of the nasal framework, as well as transition with original native areas.* ***D-E*** *corresponding angio-CT views from previous panel, showing the perfect anatomical and plastic congruence of the acellular graft, and its opacified vasculature, with the underlying bone support of the recipient.* ***G-K*** *In vivo reperfusion of SF-ECM in a porcine recipient. External view* ***G*** *before and* ***H*** *after vascular clamp release; the general recoloration is obvious, especially on the lip vermillion.* ***I*** *Internal aspect of the revascularized scaffold, with signs of oral mucosa reperfusion and capillary bleeding on the graft's section.* ***J-K*** *Similar observations on* ***J*** *lip section and* ***K*** *nasal septum.*

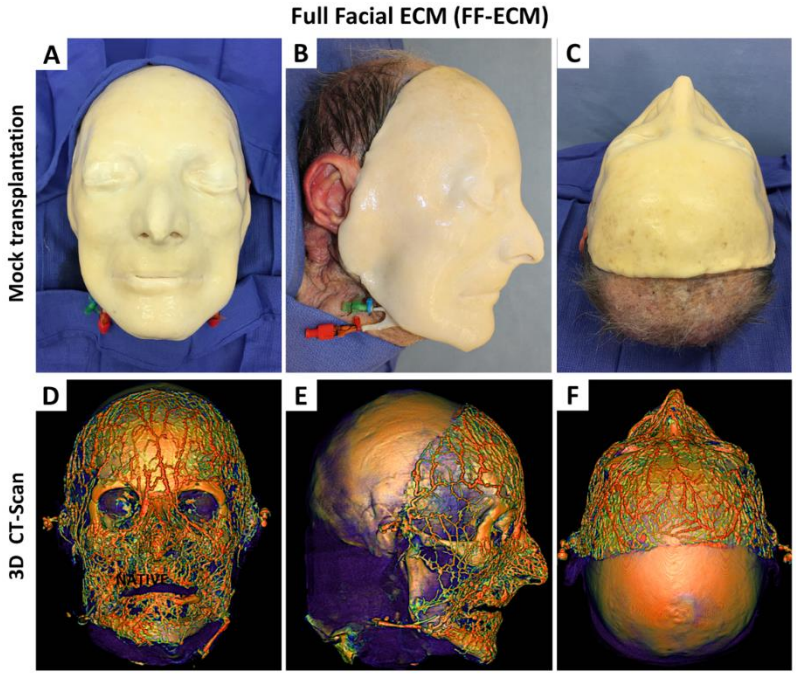
Full Facial ECM (FF-ECM)
A
B
C
Mock transplantation
D
E
F
3D CT-Scan

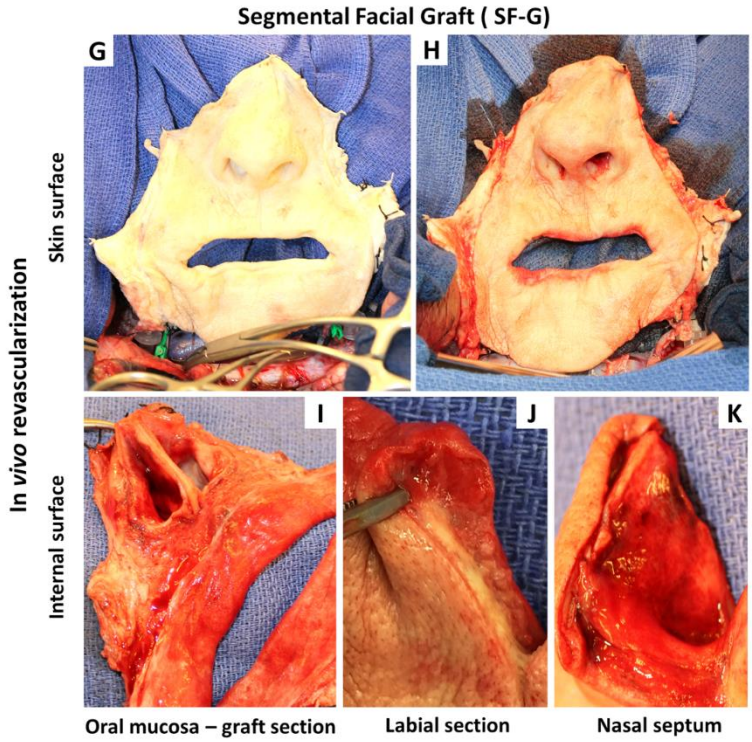
Segmental Facial Graft (SF-G)
G
H
Skin surface
In vivo revascularization
I
J
K
Internal surface
Oral mucosa – graft section
Labial section
Nasal septum

Both FAs were anastomosed to abdominal aorta and the inferior mesenteric artery. After systemic heparinization, reperfusion was observed for four hours.

Tissue sampling: SF-G and SF-ECMs were sampled for histology, quantification of DNA and proteins, at various locations and in triplicate (**Fig. 2A**).

Histology, Immunohistochemistry and Immunofluorescence: Samples were processed according to standard protocols, including 5μm-thick sectioning and staining with H&E and Masson's trichrome. Methods followed previously described protocols [97]. For immunohistochemistry (IHC), sections were incubated with anti-MHC class I antibody (1:200, ab198376, Abcam, Cambridge UK) and anti-CD31 (1:100, ab28364, Abcam). Nuclei were counterstained with hematoxylin. For immunofluorescence (IF), incubation was performed with anti-collagen IV (1:500, ab6586, Abcam), anti-laminin (1:50, ab11575, Abcam), and nuclei were counterstained with 4-6-diamidino-2-phenyl-indole (DAPI).

DNA quantification: DNA was extracted from samples with a DNeasy kit (Qiagen, Hilden, Germany) and quantified using the Quant-it Picrogreen dsDNA assay kit (ThermoFischer Scientific, Waltham, MA), according to manufacturer's instructions. To determine the remaining DNA fragments size, samples were analyzed by gel electrophoresis, as previously described [153]

Quantification of ECM proteins, growth factors and cytokines: In order to understand how the decellularization process affected the ECM and their presence, major ECM proteins, several growth factors and cytokines were quantified. Collagen was quantified using a Chondrex hydroxyproline assay kit (Chondrex, Inc., Redmond, WA); Glycosaminoglycan (GAGs) content was evaluated using the Blyscan Sulphated-GAG assay kit (Biocolor LTD, Carrickfergus, Northern Ireland) and elastin content was quantified using the Fast Elastin Assay kit (Biocolor), according to manufacturer's protocols. Concentration of growth factors and cytokines were quantified using the Bio-Plex Pro Human Chemokine 40-plex Panel and Bio-Plex Pro TGF-ß assays (Bio-Rad, Hercules, CA) according to the manufacturer's guidelines.

Static disc cell-seeding: 1cm^2 discs acellular lips (Lip-ECM) obtained from SF-ECM were sterilized with 0.1% peracetic acid (PCA). Sixteen discs were seeded with 50x10^4 NIH-3T3 dermal fibroblast (Sigma-Aldrich) and 4x10^6 C2C12 (Sigma-Aldrich) myoblast progenitor cell lines, placed in 24-well plates, and allowed to grow in supplemented Dulbecco's Modified Eagle Medium (DMEM), changed every 2 days. For C2C12 cells, we used 1% FBS as differentiation medium. After 14 days, biopsies were either processed according to standard protocols as whole-mount for Live/Dead Cell Viability assays (ThermoFisher Scientific), prepared for analysis with a field-emission scanning electron microscope (JSM-7600F, Jeol, Akishima, Tokyo, Japan), or processed for H&E staining.

Whole lip bioreactor cell-seeding: Two upper Lip-ECM, were procured with their artery from SF-ECM, sterilized with 0.1% PCA, set-up in a 500ml perfusion-bioreactor and conditioned through medium perfusions for 4 hours at 37°C/5% CO_2 conditions (**fig. 5I-J**).

C2C12 cells: The bioreactor was filled with DMEM differentiation medium supplemented with 1% FBS. 70x10^6 cells were collected and delivered into the scaffold by twenty 0.1ml injections (**Fig. 5K**). Perfusion flow was set at 2ml/min for 4 hours and increased thereafter to 4ml/min. After two weeks, the recellularized scaffolds were examined by Live/Dead and H&E stainings.

Human Aortic Endothelial Cells (HAEC): After immersion in Endothelial Cell Growth Medium MV2 (Bio-Connect, Toronto, Canada), 25x10^6 HAEC (304-05A, Sigma-Aldrich) were slowly injected through the arterial line. A static period was observed for 4 hours, to allow cell attachment. Then flow was restarted at 1ml/min for 48 hours; thereafter, biopsies were processed for Live/Dead, H&E and CD31 IHC stainings.

Statistical analysis: All statistical analyses were performed using Prism 7.00 (GraphPad Software, La Jolla, CA). Values were expressed as means ± standard error of the mean, and significance was set at $p<0.05$, using two-tailed unpaired t-test.

3. Results

Macroscopic decellularization, vascular patency and DNA reduction: The used perfusion method successfully and consistently resulted in complete cell clearance of the face grafts, while preserving their ECM. Macroscopically, epidermal blistering appeared in the first 24 hours of SDS perfusion; epidermolysis was complete and muscle became whitish within a few days, with remaining lipidic content; fat became completely white after the polar solvent sequence (**Fig. 1A-F**). Fluoroscopy demonstrated the patency of the FA main axis and branches of the SF-ECM (**Fig. 1G-H**). During the decellularization process, the MAP was increased during the SDS perfusion step, associated with graft diffused edema which resolved after the final perfusion (**Fig. 1I**). This phenomenon was principally located in the fat layer. The DNA content was significantly reduced in all tissues, with a mean reduction of 97% ($p<0.001$) in decellularized biopsies compared to native ones (**Fig. 1J**). The remaining DNA fragments size was found heterogeneous, with some long fragments especially observed in cartilage and muscle. When extending the process to a full-face graft (**Fig. 1K-M**), we also observed a satisfying aspect in all graft tissues (**Fig. 1N-O**). The arterial radiogram revealed an extremely well-preserved vasculature (**Fig. 1P**).

Mock transplantation and CT of a FF-ECM, in vivo reperfusion of a SF-ECM graft : The replacement of the produced FF-ECM on the original donor harvesting site enhanced the quality of morphological preservation of the face in all anatomical areas (**Fig. 2 A-C**) and integration to the native environment. The CT-scan examination of the mock transplantation showed an excellent integration of the graft and vessels in 3D, with a perfect plastic congruence on the underlying facial bone support (**Fig. 2D-F**).

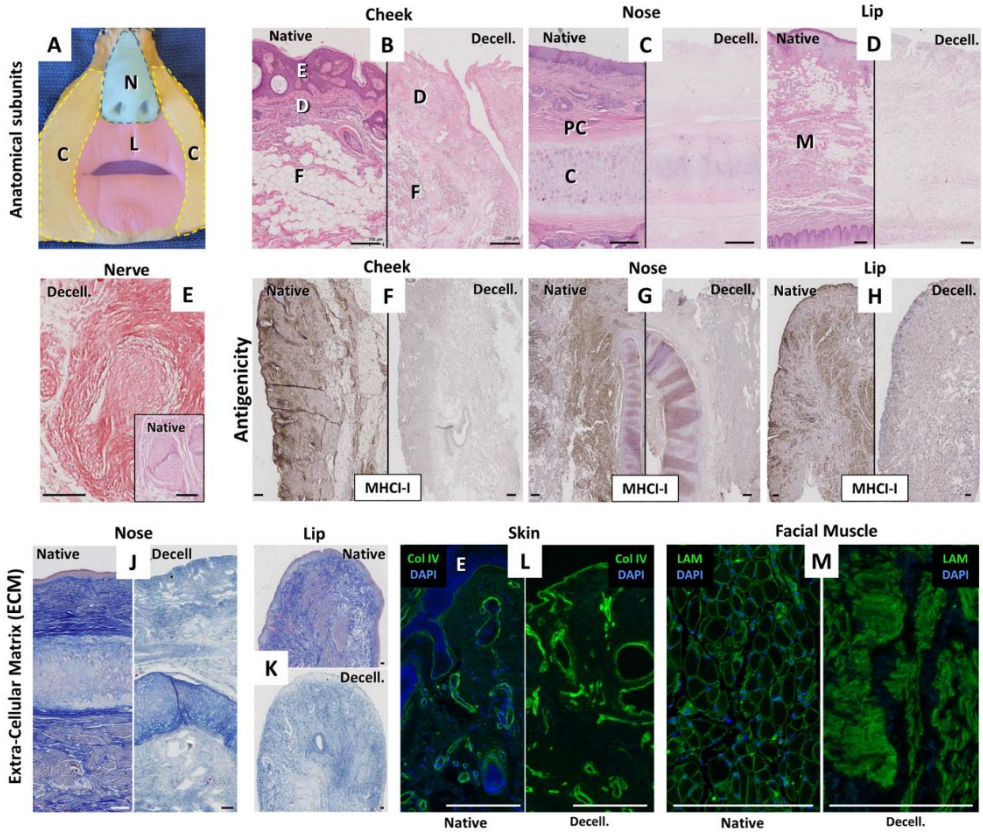

Figure 3. *Microscopic assessment of SF-ECM.* ***A*** *The mapping for SF-ECM biopsies is defined on the subunits division of this segmental face graft: nose (N), cheek (C), lips (L).* ***B-E*** *H&E staining of the three different subunits, from native and decellularized grafts, with cell removal at all levels, confirming the DNA content analysis (see Fig. 1J), with preservation of the ECM structure.* ***B*** *In the cheek, epidermis (E) and skin appendages exhibit clear cell clearance, leaving an acellular dermis (D); this anatomical location allows a more important observation of the adipose tissue (fat, F).* ***C*** *The nose allows a more specific study of the elastic cartilage (C) tissue layer, demonstrating structural preservation after decellularization. Remaining cell nuclei can be observed in the deep layer, but not correlated to high remaining DNA.* ***D*** *In the lip, facial muscle (M) can be specifically studied and exhibits complete cell clearance with structural preservation.* ***E*** *Decellularized nerve compared to native (insert).* ***F-H*** *Anti-MHC class I IHC staining in the cheek, nose and lip biopsies, comparing native (left) and decellularized (right) tissues, with absence of staining in the latest.* ***J-M*** *Examination of specific ECM structural proteins.* ***J-K*** *Masson's Trichrome stain demonstrates collagen preservation in the nose and lip areas.* ***L*** *Anti-type IV collagen IF staining in native (left) and decellularized skin (right): the staining is positive for both vessels, glands and dermal basal membranes.* ***M*** *Anti-laminin IF staining in native (left) and decellularized (right) facial muscles, with evidence of its preservation in the scaffold. Scale bars represent 200 μm.*

During *in vivo* reperfusion, the SF-ECM arteries could be easily anastomosed to the recipient vessels. A restored flow was immediately observed in the lips, then on the nasal septum and graft margins and was patent for the 4-hours observation period (**Fig. 2G-K**).

Cell and antigen clearance: H&E staining performed in all anatomical subunits did not identify any basophilic staining indicative of cell nuclei (**Fig. 3B-E**). This was confirmed by negative MHC-I antigen staining (**Fig. 3F-H**). These findings indirectly indicate the cellular clearance. However, the cartilage did retain some cells, as we reported in the porcine ear engineering [38] and in the literature [93] with a negligible impact on DNA content.

Preservation of ECM proteins and growth factors: Masson's trichrome showed a structural preservation of whole collagen (**Fig. 3J-K**), and especially type IV collagen (**Fig. 3L**), involved in basal membrane preservation, for dermal junction, vessels and glands. For the muscle, laminin was very well preserved, as confirmed by laminin staining (**Fig. 3M**), a positive factor for subsequent muscular regeneration [154]. Regarding the major ECM protein content (**Fig. 4A**), collagen was found important in all tissues, with a high relative increase. For elastin, the reduction was significant in all tissues with exception of fat. For the GAGs, a significant decrease was observed in skin, mucosa and muscle; for fat and cartilage they were relatively well-preserved. Regarding decellularization effect on cytokines and growth factors **(Fig. 4B)**, we observed in skin a significant decrease of IL-8 and GM-CSF; SDF-1alpha, IL-10, TNF-alpha and IL6 did not decrease significantly due to their high variation in the native tissues. In mucosa, a significant decrease of all analyzed cytokines was observed with the exception of IL-8 and IL-6, which nevertheless showed a clear tendency to decrease. The fat presented the highest grade of preservation, with a significant decrease of GM-CSF, IL-10 and TNF-alpha. In facial muscles, a significant decrease of GM-CSF and IL-10, a tendency to decrease of IL-8, TNF-alpha and IL-6 with partial preservation of SDF-1alpha was observed. Finally, cartilage presented a significant decrease of all analyzed cytokines but SDF-1alpha.

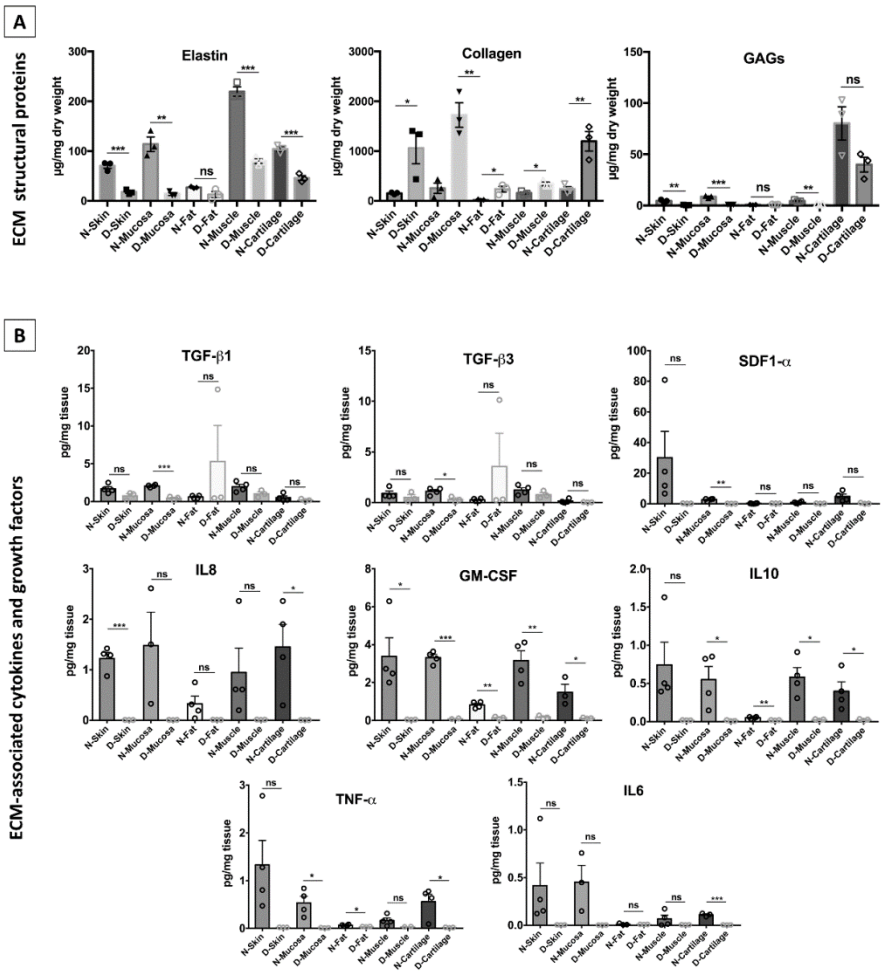

Figure 4. *Evaluation of the decellularized process on the preservation of collagen, elastin, glycosaminoglycans, growth factors and cytokines*. ***A*** *Quantification of elastin, collagen and GAGs in native (N-) and decellularized (D-) skin, oral mucosa, fat, muscle and cartilage tissue biopsies from native segmental face grafts and decellularized segmental face ECM. Elastin, even with a certain degree of preservation, is significantly reduced in all tissues, with exception of the adipose tissue. The collagen is highly preserved, and even demonstrates an important increase after decellularization, due to its relative gain with decrease of the other ECM proteins. GAGs are significantly reduced in skin, mucosa and muscle, whilst relatively preserved in the fat and cartilage tissues.* ***B*** *Cytokine concentrations of TGF-beta1, TGF-beta3, SDF1-alpha, IL-8, GM-CSF, IL-10, TNF-alpha and IL-6 in biopsies collected from native and decellularized tissues, analyzed by Luminex-like multiplex assay. Preservation of the analyzed cytokines ranged from 57.4±31.1 for TGF-beta3 to 0.4±0.1 for IL-8 in skin, from 71.5±13.9 for TGF-beta3 to 0.1±0.03 for IL-8 in mucosa; from 178.3±15.6 for SDF-1alpha to 4.8±0.4 for IL-8 in fat; from 62.7±16.9 for TGF-beta3 to 2.0±0.4 for IL-8 in muscle and from 38.6±17.3 for TGF-beta1 to 0.2±0.05 for IL-8 in cartilage. Data presented as mean ± SEM, ns=not significant, *p<0.05, **p<0.01, ***p<0.001 by two-tailed unpaired T-test. The content is expressed in µg/mg dry weight for ECM proteins and in pg/mg for cytokines.*

Cell compatibility and distribution on discs: For both NIH-3T3 and C2C12 cell-seeded constructs showed viability, attachment and proliferation of the cells on the scaffold surface in all samples. Cells remained at the surface of the scaffolds with a limited deep migration, relying on the passive aspect of cell seeding and on the high density of the ECM. For C2C12, cells adopted a different muscular phenotype (**Fig. 5E-H**).

*Whole-lip bioreactor vascular seeding (***Fig. 5I-P***):* C2C12-injected lip demonstrated cell groups at different superficial and deep levels, mainly located in the parenchyma, forming clusters and infiltrating the matrix with some migration. Cell viability was confirmed by live/dead staining (**Fig. 5K-M**). HAEC, observed homogenously in vessels, throughout the scaffold whole-thickness, were viable (**Fig. 5N**) and exhibited vascular attachment. Cells with a typical endothelial morphology were located on the vessel wall, in both large and small vessels, rather than remaining in the lumen (**Fig. 5O**). CD31 staining was observed on the vascular wall similar to normal endothelium phenotype (**Fig. 5P**). Some cell clusters could be found at the border of the graft, as vascular leakage.

4. Discussion

This report describes matrix production from human cadaveric face grafts. Our protocol successfully decellularized segmental and total faces, whilst keeping their morphology, sustaining vascular perfusion and allowing cell engraftment.

Previous work by our group on the porcine ear model has allowed scaling up to the entire face in the human model, with the main difference of adding a polar solvent step, as described for isolated adipose tissue decellularization [123,147]. Indeed, contrary to solid organs, adipose tissue is a true anatomical and functional compartment in the face [155]. Finally, we confirmed that deceased donors from even several days can be used: this resistance to degradation of composite tissues

could be explained by their low metabolic cell activity, and a high collagen content.

Growth factor preservation in matrix is a key factor, as investigated in organ CSST [90]. Our decellularization method allowed for a partial preservation of growth factors, which were still detectable in skin, mucosa, fat, muscle and cartilage. Interestingly, in all the analyzed tissues TGF-beta1 and TGF-beta3 were only minimally decreased with a significant decrease only in mucosa. Other detectable cytokines have a role in stem cell chemotaxis and survival (SDF-1alpha), in differentiation and migration of monocytes and neutrophils (GM-CSF and IL-8), and in modulation of the inflammatory process (TNF-alpha, IL-6 and IL-10). Although we found some remaining long DNA fragments, discussed as a possible negative predictive factor in the host [153,156,157], this observation was balanced by a very small DNA matrix content, by the modulated content of inflammatory cytokines, and finally the negative HLA markers in our scaffolds.

Face is a very unique anatomical and functional organ, consisting in a very complex association of different tissues, which must be uniformly treated. Further studies in facial CSST should concentrate on a subunit approach, as we did with the lip in the present study, in order to allow an anatomical selectivity of tissue associations and a discrimination of specific tissues: nose and ear for cartilage; lips and eyelids, for muscle; cheeks for adipose tissue and muscle. Moreover, given the importance of the neuromuscular component in the facial function, research on face bioengineering should also focus on this aspect, to ultimately warrant the motility of the construct. Restoration of face discriminative expressivity is indeed the ultimate goal of any reconstructive procedure, especially in the lower and midface areas. Applied to VCA in general, this technology could result in functional developments, critical for bioengineering of other highly complex body parts, like hands.

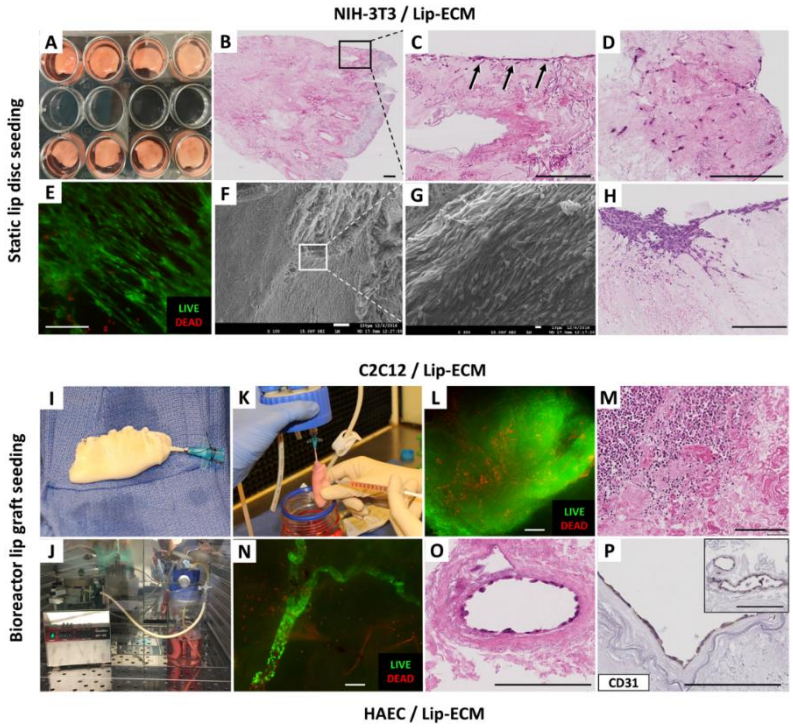

Figure 5. *Acellular lip (Lip-ECM) disc culture and bioreactor recellularization after 14 days of culture.* ***A-H*** *Static NIH-3T3 and C2C12 cells seeding.* ***A*** *Acellular lip discs in the 24-well plate and conditioned with medium prior to seeding.* ***B-D*** *NIH-3T3 dermal fibroblast cell line seeding result on the acellular lip side section.* ***B*** *Cells are found on the whole section, as seen on panel* ***C****, enlarged view from* ***B****, remaining mainly at the scaffold surface (arrows).* ***D*** *In some locations, a certain degree of cell migration in the scaffold can be seen.* ***E-H*** *C2C12 myoblast progenitor cell seeding results.* ***E*** *Live/Dead whole-mount staining revealing a majority of living cells; C2C12 cells have taken an elongated morphology, typical of ongoing muscular differentiation.* ***F-G*** *SEM observation of the cultured discs, showing an important contact of the cells with the scaffold ECM.* ***H*** *H&E observation of cells forming proliferative conglomerates at the surface, with a limited degree of migration into the scaffold.* ***I-P*** *Perfusion-recellularization of a whole upper-lip acellular graft in a perfusion-bioreactor.* ***I*** *Lip-ECM with the cannulated labial artery, extracted from a segmental face scaffold.* ***J*** *Perfusion-bioreactor apparatus in a* CO_2 *incubator, with pre-conditioning of the lip with medium.* ***K-M*** *C2C12 cells injection seeding.* ***K*** *Seeding through twenty 0.1 ml injections of cells and cultured for two weeks.* ***L*** *Live/dead of recellularized lip, with observation of a large proportion of living cells, organized in clusters.* ***M*** *H&E examination of the cell clusters showing signs of cell contact with the ECM.* ***N-P*** *Human Aortic Endothelial Cells (HAEC) vascular seeding and culture for 48 hours.* ***N*** *Live/Dead observation shows living cells, located in the vessels.* ***O*** *H&E examination demonstrates attachment of endothelial cells on the intimal vessel wall, with excellent endothelial morphological aspect.* ***P*** *Anti-CD31 IHC staining demonstrates positivity of the seeded cells, at all vessels calibers, from arterial pedicle to distal vessels (insert). Scale bars represent 200* μ*m.*

Contrary to solid organs [158], xenotransplantation can't be applied to face which is species-specific, and CSST techniques must apply to human models. Ideally, facial ECM should reproduce the exact missing morphology of the patient, and serve as template for the *ex novo* bioengineering of the new face to implant. As current state-of-the-art synthetic technologies [111] have not yet reach this step, due to the unfeasibility of replicating the complexity of the matrisome and 3D framework of the innate human ECM, human organs are being proposed as source of ECM. Since the first report on discarded human kidneys as a platform for organ bioengineering and regeneration [141], numerous studies have corroborated the idea that ECM scaffolds obtained from the decellularization of human organs may represent a valuable template for organ biofabrication [87,88,90,159-164] Importantly, these studies have shown that partial regeneration of the cellular compartment of the 3D innate ECM can be obtained, but to an extent that it is still not compatible with physiological functional needs.

Our experience confirms these findings, as our cells were not able to diffusely migrate within the 3D framework of the ECM. As stigmatized by the experiences with kidney bioengineering, major physical barriers remain in CSST that limit *in vitro* recellularization of acellular scaffolds, and numerous are the obstacles that must be investigated to effectively advance this strategy for regenerative medicine [165].

While the regeneration of the endothelium should be considered the *sine qua non* condition for bedside application, research should aim at identifying alternative regenerative strategies to solve the high complexity of recellularizing acellular ECM scaffolds of composite grafts, possibly using the recipient as its own bioreactor, as intelligently suggested by others [166].

In the history of surgery, solid organ transplantation preceded VCA. This sequence also occurred for tissue engineering. The two domains, however, are now merging in an unprecedented synergetic effort in the whole field of transplantation surgery [81].

AUTHOR CONTRIBUTIONS:

JD conceived, designed, and wrote the study project, performed all investigations and surgeries, collected results, interpreted data, and wrote the manuscript. He was responsible for the primary undertaking, completion, and supervision of all experiments, and gave final approval to the version to be published. **LM** participated to the study project, assisted all investigations, collected results, interpreted data, and reviewed the manuscript, and gave final approval to the version to be published. **AT, RR and EV** were responsible for the growth factor and cytokines analysis in the native and decellularized grafts, performed all related experiments, interpreted data, reviewed the whole manuscript, and gave final approval to the version to be published. **GO** contributed to the study design, provided input on tissue engineering aspects, edited and revised the manuscript critically, and gave final approval to the version to be published. **EC** performed radiogram and CT-Scan of the face graft, reconstructed and interpreted images, reviewed manuscript and gave final approval to the version to be published. **VJ and CD** were responsible for endothelial cell culture choice and production, participated to the re-endothelialization methodology and results interpretation, reviewed manuscript, and gave final approval to the version to be published. **JL** reviewed the manuscript and provided strong insights on tissue engineering and organ transplantation aspects, edited and revised the manuscript critically, gave final approval to the version to be published. **CB** provided technical support, reviewed the manuscript and gave final approval to the version to be published. **GC** Provided support in muscular regeneration conception for the study design, reviewed and interpreted data, reviewed the manuscript, and gave final approval to the version to be published. **PG** contributed to the study design, provided input on tissue engineering aspects, supported analysis and review data, edited and revised the manuscript critically, and gave final approval to the version to be published. **BL** contributed largely to the study design, provided strong input on aspects of face anatomy, transplant surgery, tissue engineering, edited and revised the manuscript extensively, and approved its final version to be published.

ACKNOWLEDGMENTS:

The authors express gratitude to Adeline Dedriche, Erick Montoya, Tsering Wüthrich, Christine de Ville de Goyet, Caroline Bouzin, Marie Henry, Jean Philippe Hastir, Fabienne Bertulot, Aurélie Jooris, Maite Van De Woestijne, Bernard Caelen, Pascale Segers and Walter Hudders for their devoted technical assistance or logistic support. CD is a Senior Research Associate of the FNRS.

Section 4- Tissue Engineering studies: Skeletal subunits

Summary

In this last experimental section, we explored the application of the PDR technology to the human finger subunit as a model for a skeletal-based subunit TE **Chapter 8**. Our investigations were then extended to the whole hand.

Our previous studies on the face indeed, involved only soft tissues. The inclusion of the mandible, the maxilla or the temporo-mandibular joint in our experimental graft models would have raised some technical issues, both in terms of processing and analysis. Considering our subunit approach concept however, similar tissue associations should be considered identical in terms of TE, independently from their anatomical location. As a matter of fact, we thus focused our attention on the limbs, in which the finger constituted the perfect subunit model to investigate the specific behavior of hard tissues in the PDR technology. Moreover, the limb engineering itself, especially like the hand in VCA, is also critical to be developed in VCE: a previous study about PDR application to the rat upper limb confirmed the relevance of this experimental approach. However, this study was focused on the forearm musculo-skeletal engineering, in a small animal model. We then decided to carry on additional studies on human hand and fingers, including their entire skin cover. Our well-documented PDR protocol derived from human face studies was successfully applied to the elementary human finger graft, and then extended to whole hands. Interestingly, a significant difference with facial grafts was noticed, in terms of epidermolysis and reperfusion efficiency. Strikingly also, the bone content was not altered and could provide a stable structural support to the scaffold. Moreover, the biomechanical properties of flexor and extensor tendons, as well as those of PIP and DIP joints, were preserved in the scaffolds.

As very last outcomes and ultimate achievement of this PhD work, we finally used this hand scaffold model to validate the use of our patented perfusion-bioreactor (**Appendix**), developed in close collaboration with the Louvain School of Engineering (Dr B. Herman). It was designed with two compartments, in order to allow a separate seeding of the internal parenchymal compartment of the scaffold, recellularized through an intravascular perfusion pathway, and the vascular compartment itself, independently from the external tegmental compartment, involving the dermis peripheral surface of the scaffold, seeded topically with epidermal cells.

Chapter 8: Human finger subunit and hand bioengineering

Vascularized human finger decellularization: a subunit approach to hand tissue engineering – *Manuscript in preparation.*

Presented at :

- 13th Congress of the Internation Society of Vascularized Composite Allotransplantation (ISCVCA, Salzburg, 26-27/10/2017). Poster presentation.
- 18th congress of the European Society for Organ Transplantation (ESOT, 24-27/9/2017). Oral presentation.
- 27 European Tissue Repair Society meeting (ETRS, 13-15/9/2017). Oral presentation (invited speaker).
- 6th European Association of Plastic Surgerons (EURAPS) Research Council Annual Meeting (Pisa,24-25/5/2017). Oral presentation. **Best paper award**
- French National Academy of Surgery – Research forum (Paris, 15/12/2017). **2017 Laboratory research award.**

Duisit J

Debluts D

Maistriaux L

Roels T

Behets C

Orlando G

Gianello P

Lengelé B

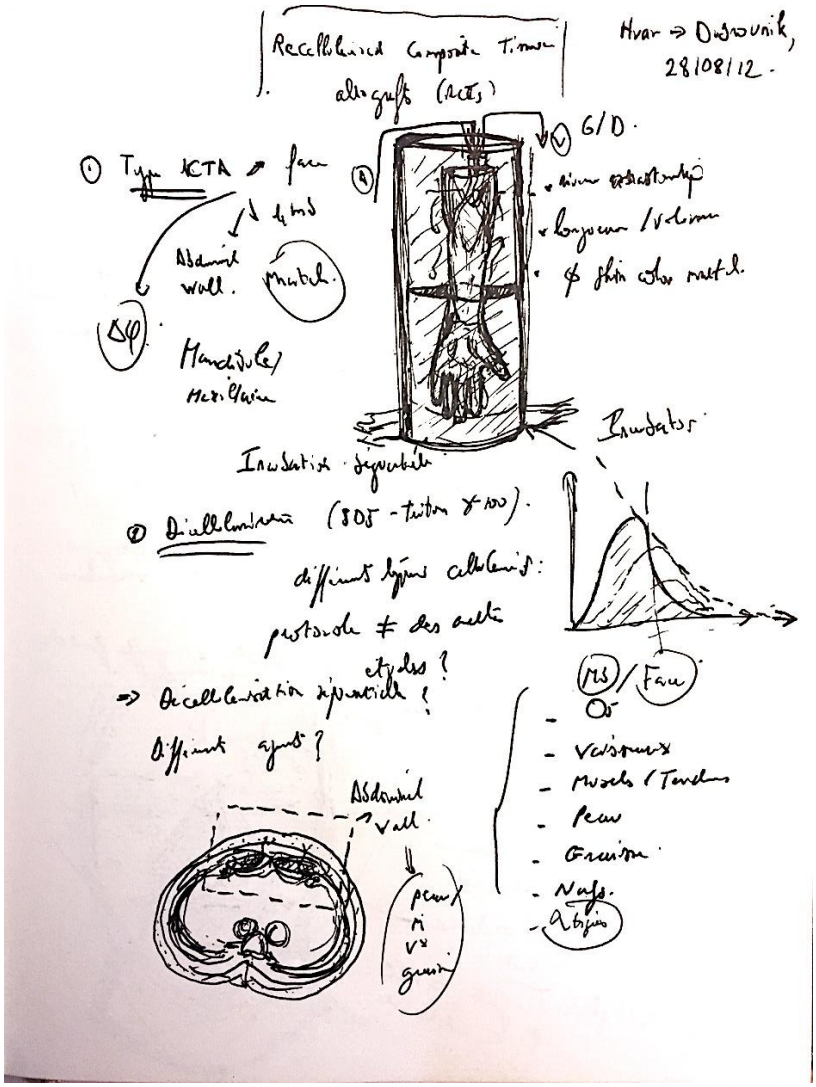

Author's notes (Hvar 28.08.2012)

ABSTRACT

***Background*:** Hand allotransplantation breakthrough is still highly limited by the need for immunosuppression. From our previous results in the porcine ear and human face tissue engineering, we hypothesized an application to human finger and hand scaffold production.

***Methods*:** Nine long-digit grafts were procured postmortem from four fresh human donors, and decellularized by sequential arterial perfusions of detergent/polar solvent solutions. Cellular clearance was assessed by DNA quantification and H&E staining. Extra-cellular matrix preservation was assessed by Masson's Trichrome (MT) for soft tissues and bone mineral density (BMD) for phalangeal bones. Acellular samples were cultured with fibroblastic cell lines, and examined with vital staining. To challenge *in vivo* the vasculature, a short reperfusion study was performed in a pig recipient. Finally, decellularization was applied to three whole human hand, and vascular tree assessed by angio-CT scan.

***Results*:** Digital grafts were successfully decellularized, with a quick epidermolysis, nail loss and complete bleaching. Cell clearance was demonstrated on H&E sections, associated to 95.3 % DNA reduction, compared to native tissues ($p<0.0001$). MT staining showed microscopic structural preservation. Decellularized phalanx mean BMD was 510 mg hydroxyapatite/cm3, similar to control. Seeded cells were viable and homogeneously distributed on all scaffolds. *In vivo*, blood quickly reperfused the whole scaffold; after three hours, the vascular tree was still patent, as demonstrated by fluoroscopy, fingertip pulse and 93% oxygen saturation. The extension to a whole-hand graft decellularization was achieved successfully, with an excellent preservation of the superficial and deep vascular tree.

***Conclusion*:** We could produce finger and hand extracellular matrix scaffolds from human cadaveric source, with a preserved and perfusable vascular tree. These results could represent a true alternative to upper extremity allotransplantation.

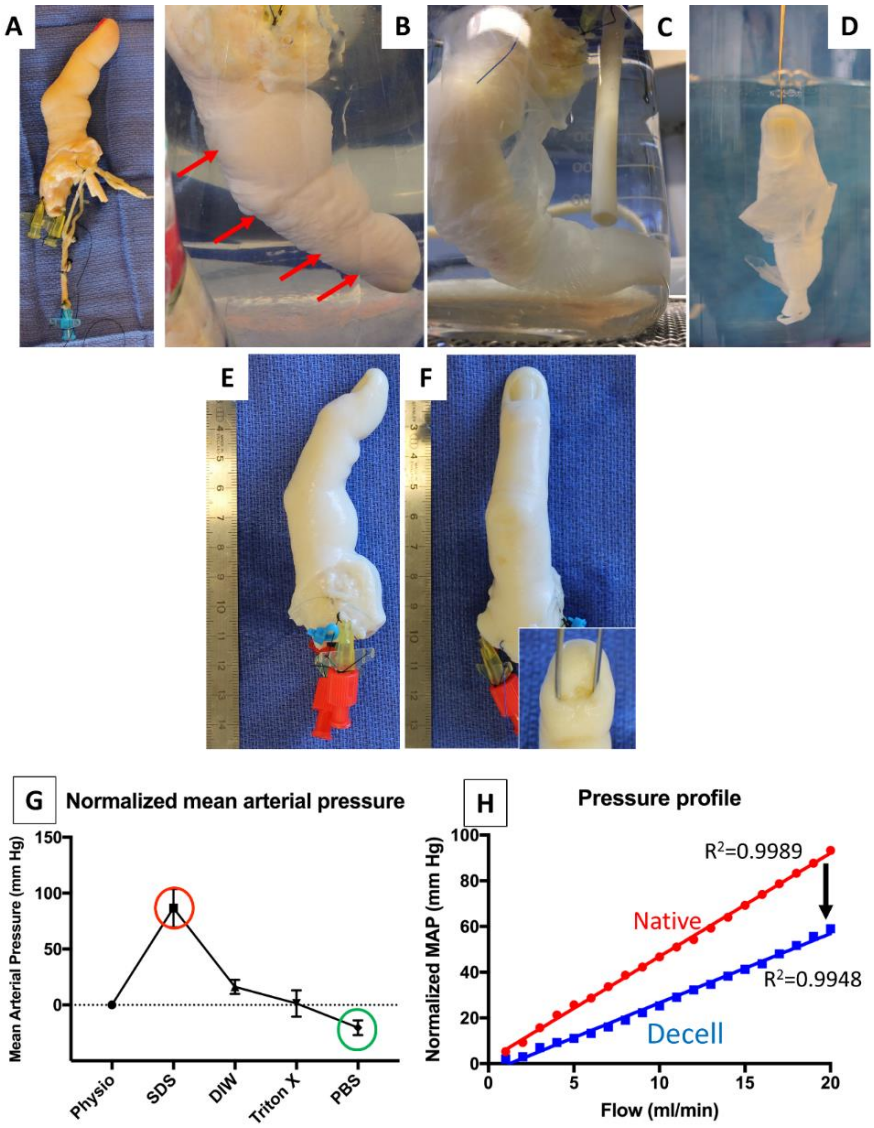

Figure 1: *Human finger graft perfusion-decellularization. **A-D** Decellularization process: **A** Procured native graft prepared for detergent perfusion; **B** Early epidermolysis and blistering (arrows); **C-D** Late epidermolysis and complete epidermis and nail degloving. **E-F** Final aspect, with examination and adequate defatting after finger tip incision and examination (insert). **G** Mean arterial pressure at constant flow: SDS step is associated with a high vascular resistance, resolving at final rinsing step. **H** Arterial pressure profile comparing native and decellularized graft at final stage: both curves present a linear correlation and enhanced compliance for decellularized graft.*

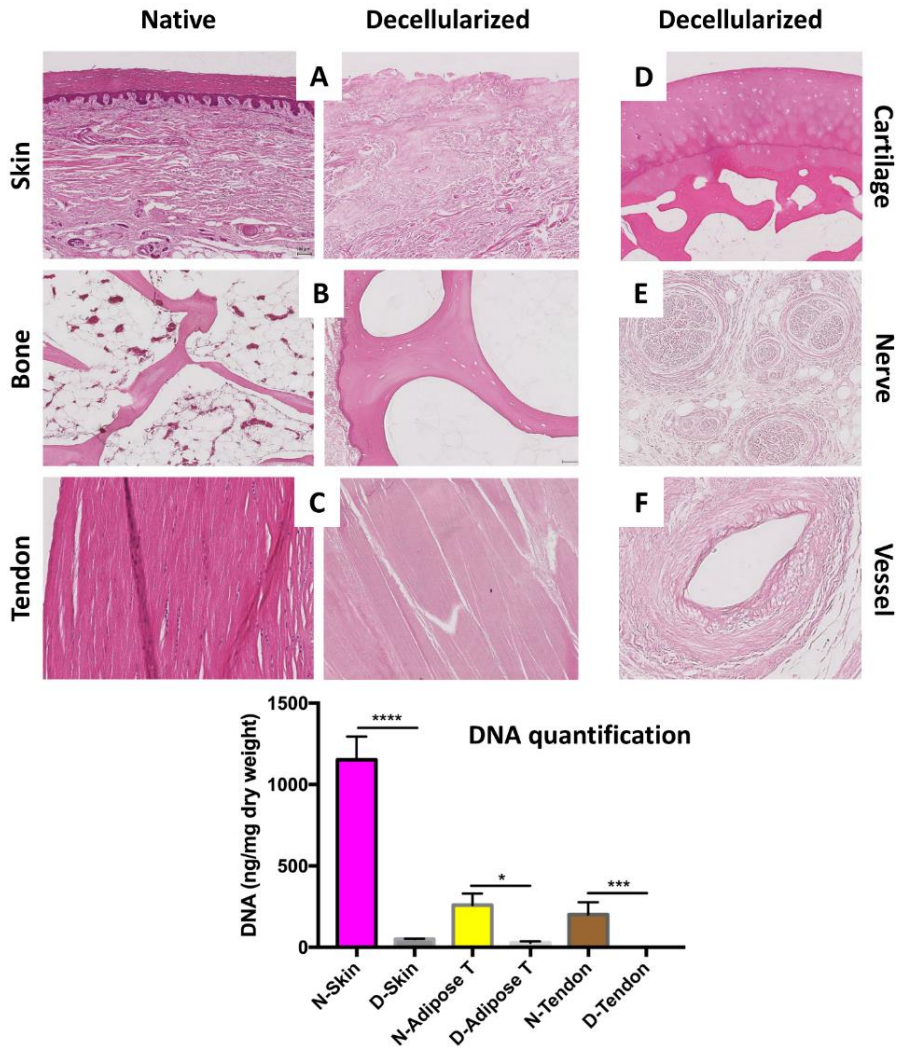

Figure 2: *<u>Cell clearance</u>. **A-F** Skin, bone, tendon, articular joint cartilage, collateral nerve and vessel H&E examination, confirming negative cell staining in decellularized. **G** DNA quantification in native versus decellularized samples for skin, adipose tissue and tendons: reduction is significant in all tested samples.*

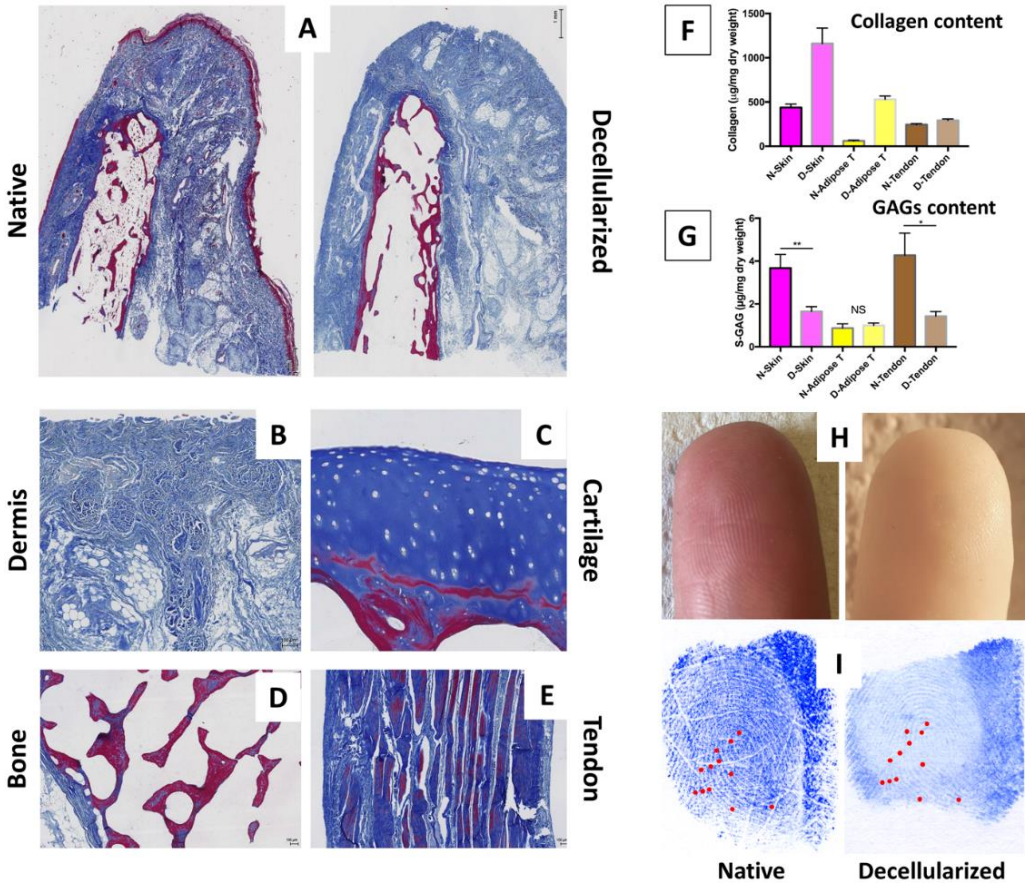

Figure 3. *ECM structural preservation*. ***A-E*** *Masson's Trichrome evaluation of decellularized graft:* ***A*** *Finger Tip,* ***B*** *Dermis,* ***C*** *Cartilage,* ***D*** *Trabecular bone and* ***E*** *tendon.* ***F-G*** *ECM collagen (****F****) and GAGs (****G****) proteins quantification.* ***H-I*** *Finger print examination of native compared to decellularized scaffold, retrieved 12 matching points.*

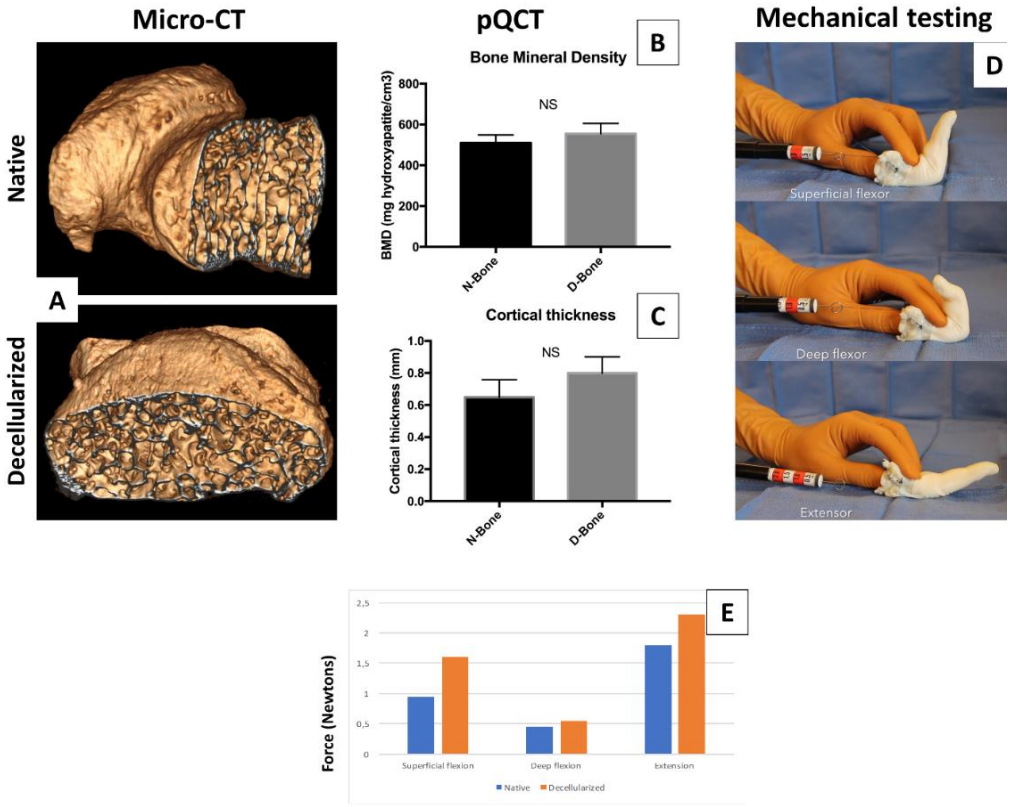

Figure 4. *<u>Bone density assessment and mechanical testing on whole-finger scaffold.</u>* ***A*** *Micro-CT reconstruction of phalangeal bone and qualitative observation of trabecular bone in native and decellularized specimens.* ***B-C*** *pQCT for assessment of bone mineral density (**B**) and cortical thickness (**C**), not significant between native and decellularized.* ***D*** *Whole-graft mechanical testing. Superficial (upper image), deep flexor (middle image) and extensor (lower image) tendons were tested for complete flexion and extension, in native and decellularized grafts; force applied on tendons was recorde.* ***E*** *Forces quantitative results from digits flexion/extension in native (blue) versus decellularized (orange) for the three types of movement, namely superficial flexion, deep flexion and extension. Expressed in Newtons.*

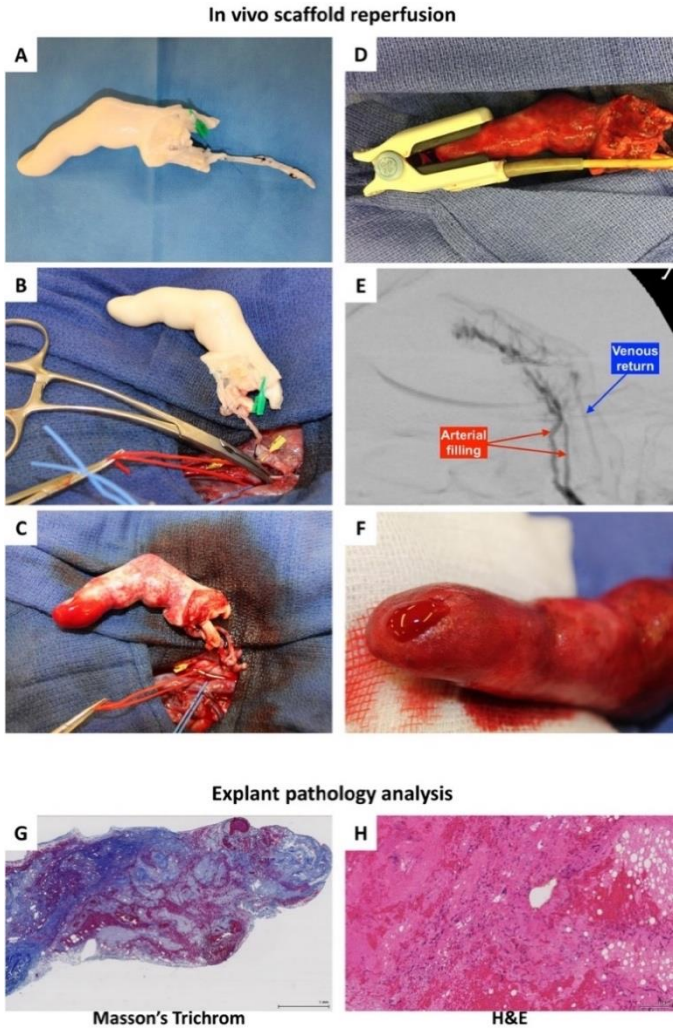

Figure 5. *In vivo reperfusion of a digital scaffold*. ***A*** *Digital scaffold with long arterial pedicle for anastomosis.* ***B*** *Arterial anastomosis on the external iliac artery (vein left free), before clamp release.* ***C*** *Early reperfusion aspect, with signs of dermal perfusion and bleeding at the section.* ***D*** *Oxygen saturation measurement at 93% after a 4-hours observation period.* ***E*** *Corresponding angioscopy demonstrating filling of both collateral arteries and venous return.* ***F*** *Incision at the tip of the finger showing a persisting bleeding.* ***G-H*** *Masson's trichrome (G) and H&E stainings of reperfused scaffold, with important blood extravasation and ECM filling with a high density of blood and nucleated cells, as a future route for in vivo regeneration.*

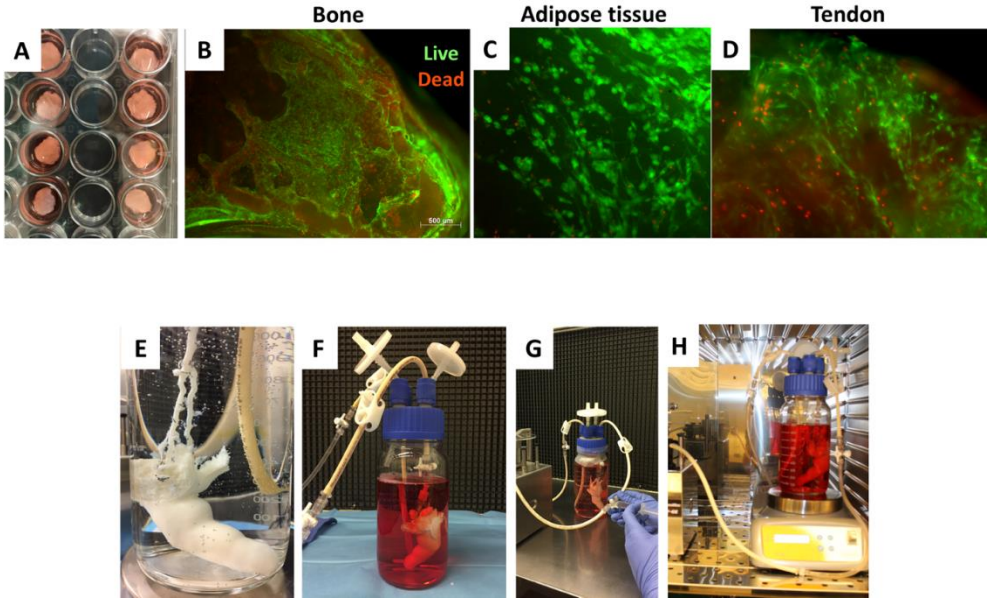

Figure 6. *<u>Fibroblast disc seeding and whole-digit scaffold preparation for perfusion-bioreactor cell seeding.</u>* ***A-D*** *MBone, tendon and adipose tissue scaffold preparation and seeding with NIH-3T3 fibroblasts, further examined with Live/dead vital staining. Scale bar.* ***E-F*** *Scaffold sterilization in 0.1% peracetic acid (**E**), mounted in sterile perfusion bioreactor (**F**); Cells seeding though vascular infusion (**G**); culture in a C02 incubator under normal conditions (5% C02, 37˚C).*

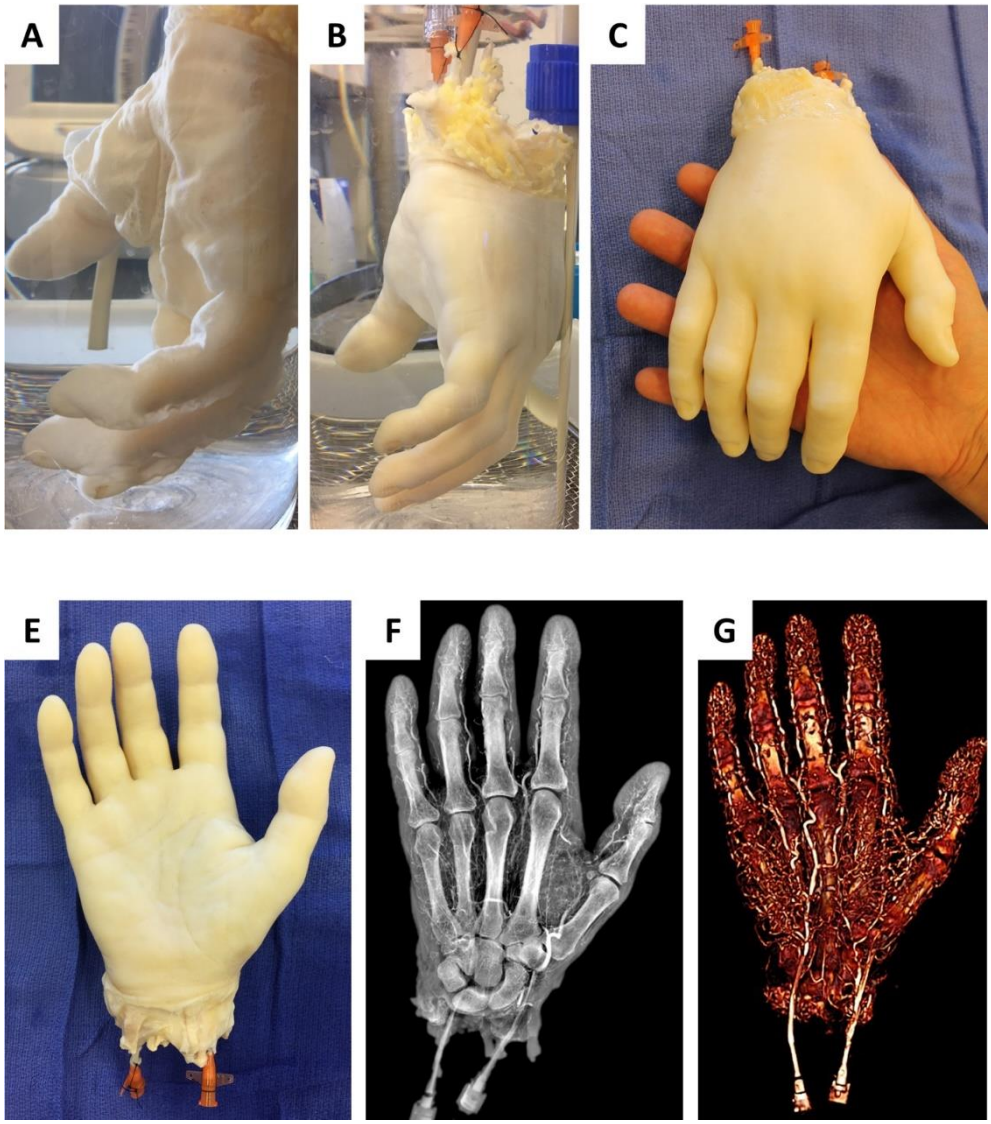

Figure 7. ***<u>Human hand graft decellularization</u>.*** ***A*** *Epidermolysis and bullae formation occurring in all fingers during SDS perfusion step, with total nail and epidermis degloving.* ***B*** *Appearance before defatting and persistence of untreated adipose tissue oil cysts.* ***C*** *Final aspect and comparison with a normal human hand.* ***E-F*** *Imaging assessment: anterior view of the decellularized hand (****E****), corresponding X-ray of the specimen, confirming osseous density (****F****); Angio-CT scan performed after contrast gel vascular injection and showing preservation and access to the graft vascular tree (****G****).*

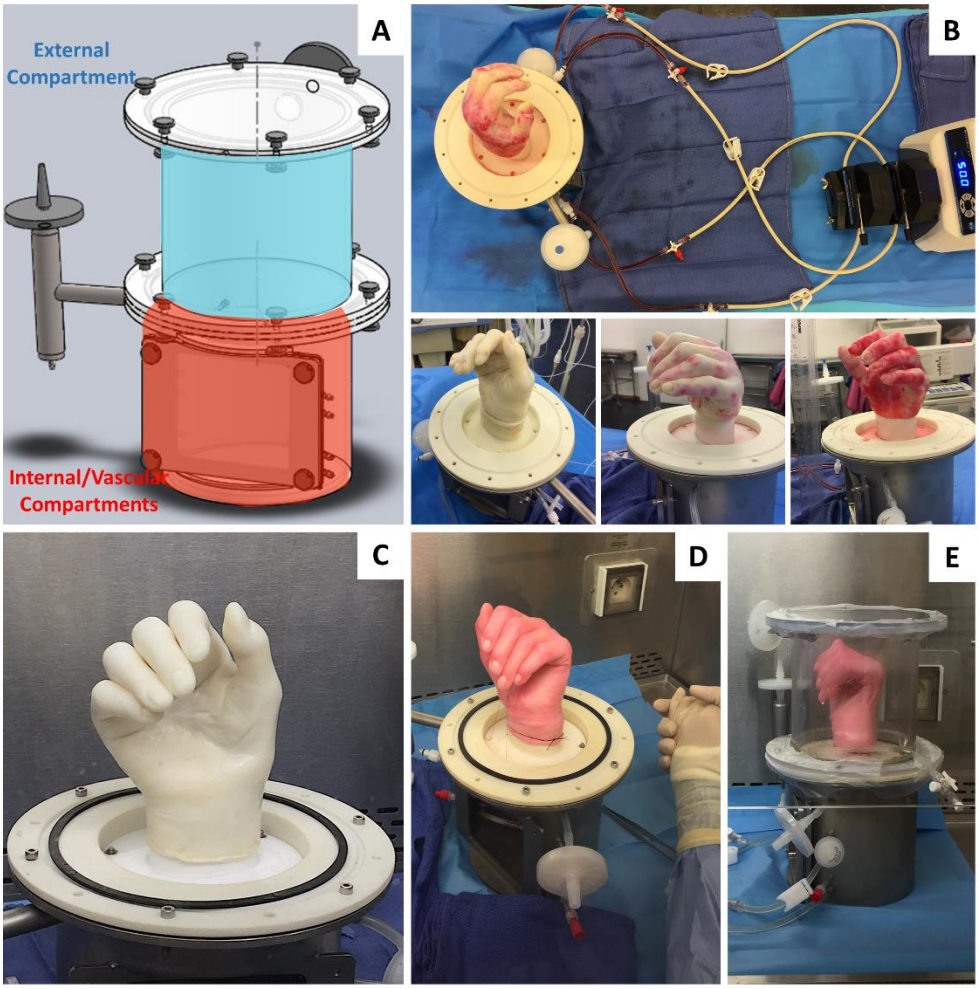

Figure 8. ***<u>Hand scaffold mounting in specific bi-compartmental bioreactor</u>***.
A *Schematic aspect of the bicompartmental bioreactor, demonstrating separation between the external compartment chamber (blue) the internal/vascular compartments chamber (red), by the mean of a specific support.* ***B*** *Validation of perfusion flow and arterial pressure to ensure a correct perfusion of colored serum, by the team of tubing and peristaltic pump connected to the arterial pedicle in a close-circuit fashion* ***C,D*** *Sterile mounting in bioreactor:* ***C*** *Previously sterilized hand graft mounted on the specific bioreactor support and exposing the tegmental surface.*
D *Aspect after culture medium pre-conditioning.* ***F*** *Final sterile mounting of the human hand graft scaffold in the bicompartmental bioreactor and ready for subsequent compartments culture (see Appendix for more details).*

References

1. Devauchelle B, Badet L, Lengelé B et al. First human face allograft: early report. Lancet. 2006;368:203-209.
2. Dubernard JM, Lengelé B, Morelon E et al. Outcomes 18 months after the first human partial face transplantation. N Engl J Med. 2007;357:2451-2460.
3. Siemionow M, Papay F, Alam D et al. Near-total human face transplantation for a severely disfigured patient in the USA. Lancet. 2009;374:203-209.
4. Dorafshar AH, Bojovic B, Christy MR et al. Total face, double jaw, and tongue transplantation: an evolutionary concept. Plast Reconstr Surg. 2013;131:241-251.
5. Lengele BG. Current concepts and future challenges in facial transplantation. Clin Plast Surg. 2009;36:507-521.
6. Mathes DW, Edwards JA, Anzai Y, Neligan PC. A functional periorbital subunit allograft: vascular, anatomic, and technical considerations for future subunit facial transplantation. J Plast Reconstr Aesthet Surg. 2014;67:1371-1377.
7. Rodriguez-Lorenzo A, Audolfsson T, Wong C, Saiepour D, Nowinski D, Rozen S. Vascular Perfusion of the Facial Skin - Implications in Allotransplantation of Facial Aesthetic Subunits. Plast Reconstr Surg. 2016;
8. Ulusal BG, Ulusal AE, Lin JY et al. Anatomical and technical aspects of harvesting the auricle as a neurovascular facial subunit transplant in humans. Plast Reconstr Surg. 2007;120:1540-1545.
9. Duisit J, Amiel H, Debluts D et al. Single-artery human ear graft procurement: a simplified approach. Plast Reconstr Surg. 2017;140:599-603.
10. Vasilic D, Barker JH, Blagg R, Whitaker I, Kon M, Gossman MD. Facial transplantation: an anatomic and surgical analysis of the periorbital functional unit. Plast Reconstr Surg. 2010;125:125-134.
11. Dorafshar AH, Mundinger GS, Robinson B et al. Nasal Unit Transplantation: A Cadaveric Anatomical Feasibility Study. J Reconstr Microsurg. 2017;33:244-251.
12. Burget GC, Walton RL. Optimal use of microvascular free flaps, cartilage grafts, and a paramedian forehead flap for aesthetic reconstruction of the nose and adjacent facial units. Plast Reconstr Surg. 2007;120:1171-1207.
13. Chepeha DB, Malloy KM, Moyer JS, Chanowski EJ, Khariwala SS. Maxillomandibular-labial reconstruction: an autogenous transplant as an alternative to allogenic face transplantation. Plast Reconstr Surg. 2010;126:2007-2011.
14. Lengele BG, Testelin S, Bayet B, Devauchelle B. Total lower lip functional reconstruction with a prefabricated gracilis muscle free flap. Int J Oral Maxillofac Surg. 2004;33:396-401.
15. Rohrich RJ, Gunter JP, Friedman RM. Nasal tip blood supply: an anatomic study validating the safety of the transcolumellar incision in rhinoplasty. Plast Reconstr Surg. 1995;95:795-799.

16. Rohrich RJ, Muzaffar AR, Gunter JP. Nasal tip blood supply: confirming the safety of the transcolumellar incision in rhinoplasty. Plast Reconstr Surg. 2000;106:1640-1641.

17. Lohn JW, Penn JW, Norton J, Butler PE. The course and variation of the facial artery and vein: implications for facial transplantation and facial surgery. Ann Plast Surg. 2011;67:184-188.

18. Rosset A, Spadola L, Ratib O. OsiriX: an open-source software for navigating in multidimensional DICOM images. J Digit Imaging. 2004;17:205-216.

19. Banks ND, Hui-Chou HG, Tripathi S et al. An anatomical study of external carotid artery vascular territories in face and midface flaps for transplantation. Plast Reconstr Surg. 2009;123:1677-1687.

20. Nakajima H, Imanishi N, Aisb o S. Facial artery in the upper lip and nose: anatomy and a clinical application. Plast Reconstr Surg. 2002;109:855-861.

21. Park C, Lineaweaver WC, Buncke HJ. New perioral arterial flaps: anatomic study and clinical application. Plast Reconstr Surg. 1994;94:268-276.

22. Jayakumar R, Zachariah JR, Senthilkumar M, Guild AJ, Cyriac A, Nair G. Composite facial part replantation. Plast Reconstr Surg. 2013;131:296e-298e.

23. Kayikcioglu A, Karamursel S, Kecik A. Replantation of nearly total nose amputation without venous anastomosis. Plast Reconstr Surg. 2001;108:702-704.

24. Sun W, Wang Z, Qiu S, Li S. Successful microsurgical replantation of the amputated nose. Plast Reconstr Surg. 2010;126:74e-76e.

25. Hammond DC, Bouwense CL, Hankins WT, Maxwell-Davis GS, Furdyna J, Capraro PA. Microsurgical replantation of the amputated nose. Plast Reconstr Surg. 2000;105:2133-2136.

26. Koh KS, Kim HJ, Oh CS, Chung IH. Branching patterns and symmetry of the course of the facial artery in Koreans. Int J Oral Maxillofac Surg. 2003;32:414-418.

27. Lee JG, Yang HM, Choi YJ et al. Facial arterial depth and relationship with the facial musculature layer. Plast Reconstr Surg. 2015;135:437-444.

28. Edizer M, Magden O, Tayfur V, Kiray A, Ergur I, Atabey A. Arterial anatomy of the lower lip: a cadaveric study. Plast Reconstr Surg. 2003;111:2176-2181.

29. Taylor HO, Andrews B. Lip replantation and delayed inset after a dog bite: a case report and literature review. Microsurgery. 2009;29:657-661.

30. Yang HM, Lee JG, Hu KS et al. New anatomical insights on the course and branching patterns of the facial artery: clinical implications of injectable treatments to the nasolabial fold and nasojugal groove. Plast Reconstr Surg. 2014;133:1077-1082.

31. Schulte DL, Sherris DA, Kasperbauer JL. The anatomical basis of the Abbe flap. Laryngoscope. 2001;111:382-386.

32. James NJ. Survival of large replanted segment of upper lip and nose. Case report. Plast Reconstr Surg. 1976;58:623-625.

33. Holtje WJ. Successful replantation of an amputated upper lip. Plast Reconstr Surg. 1984;73:664-670.

34. Walton RL, Beahm EK, Brown RE et al. Microsurgical replantation of the lip: a multi-institutional experience. Plast Reconstr Surg. 1998;102:358-368.

35. Duroure F, Simon E, Fadhul S, Fyad JP, Chassagne JF, Stricker M. Microsurgical lip replantation: evaluation of functional and aesthetic results of three cases. Microsurgery. 2004;24:265-269.

36. Nichter LS, Haines PC, Edgerton MT. Successful replantation in the face of absent venous drainage: an experimental study. Plast Reconstr Surg. 1985;75:686-691.

37. Morelon E, Petruzzo P, Kanitakis J et al. Face transplantation: partial graft loss of the first case ten years later. Am J Transplant. 2017;17:1935-1940.

38. Duisit J, Orlando G, Debluts D et al. Decellularization of the porcine ear generates a biocompatible, nonimmunogenic extracellular matrix platform for face subunit bioengineering. Ann Surg. 2017;[Epub ahead of print].

39. Duisit J, Maistriaux L, Taddeo A et al. Bioengineering a human graft: the matrix of Identity. Ann Surg. 2017;[Epub ahead of print].

40. Sullivan SR, Taylor HO. Images in clinical medicine. Ear replantation. N Engl J Med. 2014;370:1541.

41. Momeni A, Liu X, Januszyk M et al. Microsurgical ear replantation-is venous repair necessary?-A systematic review. Microsurgery. 2016;36:345-350.

42. Finical SJ, Keller KM, Lovett JE. Postoperative ramifications of total ear replantation. Ann Plast Surg. 1998;41:667-670.

43. Kind GM, Buncke GM, Placik OJ, Jansen DA, D'Amore T, Buncke HJ, Jr. Total ear replantation. Plast Reconstr Surg. 1997;99:1858-1867.

44. Lopez R, Benouaich V, Chaput B, Dubois G, Jalbert F. Description and variability of temporal venous vascularization: clinical relevance in temporoparietal free flap technique. Surg Radiol Anat. 2013;35:831-836.

45. Legre R, Sandre J, Jallut Y et al. [Use of a free superficial temporalis flap. Apropos of 14 cases]. Annales de Chirurgie Plastique et Esthétique. 1987;32:333-343.

46. Houseman ND, Taylor GI, Pan WR. The angiosomes of the head and neck: anatomic study and clinical applications. Plast Reconstr Surg. 2000;105:2287-2313.

47. Whetzel TP, Mathes SJ. Arterial anatomy of the face: an analysis of vascular territories and perforating cutaneous vessels. Plast Reconstr Surg. 1992;89:591-603.

48. Pinar YA, Ikiz ZA, Bilge O. Arterial anatomy of the auricle: its importance for reconstructive surgery. Surg Radiol Anat. 2003;25:175-179.

49. Pereira O, Bins-Ely J, Lobo GS, Lee KH, Eickhoff D. Successful replantation of an almost-amputated nose. Plast Reconstr Surg. 2010;125:249e-251e.

50. Park C, Lineaweaver WC, Rumly TO, Buncke HJ. Arterial supply of the anterior ear. Plast Reconstr Surg. 1992;90:38-44.

51. Taylor GI, Chubb DP, Ashton MW. True and 'choke' anastomoses between perforator angiosomes: part i. anatomical location. Plast Reconstr Surg. 2013;132:1447-1456.

52. Chubb DP, Taylor GI, Ashton MW. True and 'choke' anastomoses between perforator angiosomes: part II. dynamic thermographic identification. Plast Reconstr Surg. 2013;132:1457-1464.

53. Park C, Lew DH, Yoo WM. An analysis of 123 temporoparietal fascial flaps: anatomic and clinical considerations in total auricular reconstruction. Plast Reconstr Surg. 1999;104:1295-1306.

54. Kim BS, Jung YJ, Chang CH, Choi BY. The anatomy of the superficial temporal artery in adult koreans using 3-dimensional computed tomographic angiogram: clinical research. J Cerebrovasc Endovasc Neurosurg. 2013;15:145-151.

55. Tilotta F, Lazaroo B, Laujac MH, Gaudy JF. A study of the vascularization of the auricle by dissection and diaphanization. Surg Radiol Anat. 2009;31:259-265.

56. Dakpe S, Lengelé B, Willemart G, Gbaguidi C, Testelin S, Devauchelle B. The reverse helical chondrocutaneous free flap in distal nose reconstruction : technical refinements, extended indications and anatomical limits. J Craniomaxillofac Surg. 2004;32:120.

57. Devauchelle B, Testelin S, Wolff V, Sinna R, Lengelé B. Microsurgical miniflaps in facial reconstruction. J Craniomaxillofac Surg. 2002;30:19.

58. Kobayashi S, Nagase T, Ohmori K. Colour Doppler flow imaging of postauricular arteries and veins. Br J Plast Surg. 1997;50:172-175.

59. Dubernard JM, Owen E, Herzberg G et al. Human hand allograft: report on first 6 months. Lancet. 1999;353:1315-1320.

60. Brandacher G, Grahammer J, Sucher R, Lee WP. Animal models for basic and translational research in reconstructive transplantation. Birth Defects Res C Embryo Today. 2012;96:39-50.

61. Siemionow M, Kulahci Y. Experimental models of composite tissue allograft transplants. Semin Plast Surg. 2007;21:205-212.

62. Siemionow M, Klimczak A. Advances in the development of experimental composite tissue transplantation models. Transpl Int. 2010;23:2-13.

63. Ulusal BG, Ulusal AE, Ozmen S, Zins JE, Siemionow MZ. A new composite facial and scalp transplantation model in rats. Plast Reconstr Surg. 2003;112:1302-1311.

64. Ulusal AE, Ulusal BG, Hung LM, Wei FC. Establishing a composite auricle allotransplantation model in rats: introduction to transplantation of facial subunits. Plast Reconstr Surg. 2005;116:811-817.

65. Barth RN, Bluebond-Langner R, Nam A et al. Facial subunit composite tissue allografts in nonhuman primates: I. Technical and immunosuppressive requirements for prolonged graft survival. Plast Reconstr Surg. 2009;123:493-501.

66. Uygur S, Ozturk C, Kwiecien G, Djohan R, Siemionow M. Sheep hemifacial and auricular transplantation models: an anatomic study. Ann Plast Surg. 2014;72:469-474.

67. Dehoux JP, Gianello P. The importance of large animal models in transplantation. Front Biosci. 2007;12:4864-4880.

68. Kuo YR, Shih HS, Lin CC et al. Swine hemi-facial composite tissue allotransplantation: a model to study immune rejection. J Surg Res. 2009;153:268-273.

69. Nguyen JT, Ashitate Y, Buchanan IA et al. Face transplant perfusion assessment using near-infrared fluorescence imaging. J Surg Res. 2012;177:e83-e88.

70. Santiago GF, Susarla SM, Al Rakan M et al. Establishing cephalometric landmarks for the translational study of Le Fort-based facial transplantation in Swine: enhanced applications using computer-assisted surgery and custom cutting guides. Plast Reconstr Surg. 2014;133:1138-1151.

71. Sack, W.O., Hamilton, W.P. Essentials of pig anatomy. Ithaca, N.Y.: [Published and distributed by] Veterinary Textbooks, 1982.

72. Sasaki R, Watanabe Y, Yamato M, Aoki S, Okano T, Ando T. Surgical anatomy of the swine face. Lab Anim. 2010;44:359-363.

73. Parkhouse N, Evans D. Reconstruction of the ala of the nose using a composite free flap from the pinna. Br J Plast Surg. 1985;38:306-313.

74. Dondelinger RF, Ghysels MP, Brisbois D et al. Relevant radiological anatomy of the pig as a training model in interventional radiology. Eur Radiol. 1998;8:1254-1273.

75. Solla F, Pan H, Watrelot D, Leveneur O, Dubernard JM, Gazarian A. Composite tissue allotransplantation in newborns: a swine model. J Surg Res. 2013;179:e235-e243.

76. Gianello P, Fishbein JM, Sachs DH. Tolerance to primarily vascularized allografts in miniature swine. Immunol Rev. 1993;133:19-44.

77. Lee WP, Yaremchuk MJ, Pan YC, Randolph MA, Tan CM, Weiland AJ. Relative antigenicity of components of a vascularized limb allograft. Plast Reconstr Surg. 1991;87:401-411.

78. Sachs DH, Germana S, el-Gamil M, Gustafsson K, Hirsch F, Pratt K. Class II genes of miniature swine. I. Class II gene characterization by RFLP and by isolation from a genomic library. Immunogenetics. 1988;28:22-29.

79. Devauchelle BL, Testelin SR, Davrou J et al. Face graft? Extrapolation of facial allotransplantation to children. J Craniomaxillofac Surg. 2016;44:925-933.

80. Khalifian S, Brazio PS, Mohan R et al. Facial transplantation: the first 9 years. Lancet. 2014;384:2153-2163.

81. Orlando G, Soker S, Stratta RJ. Organ bioengineering and regeneration as the new Holy Grail for organ transplantation. Ann Surg. 2013;258:221-232.

82. Salvatori M, Peloso A, Katari R et al. Semi-xenotransplantation: the regenerative medicine-based approach to immunosuppression-free transplantation and to meet the organ demand. Xenotransplantation. 2015;22:1-6.

83. Hynes RO. The extracellular matrix: not just pretty fibrils. Science. 2009;326:1216-1219.

84. Orlando G, Farney AC, Iskandar SS et al. Production and implantation of renal extracellular matrix scaffolds from porcine kidneys as a platform for renal bioengineering investigations. Ann Surg. 2012;256:363-370.

85. Badylak SF, Taylor D, Uygun K. Whole-organ tissue engineering: decellularization and recellularization of three-dimensional matrix scaffolds. Annu Rev Biomed Eng. 2011;13:27-53.

86. Badylak SF, Weiss DJ, Caplan A, Macchiarini P. Engineered whole organs and complex tissues. Lancet. 2012;379:943-952.

87. Peloso A, Urbani L, Cravedi P et al. The Human Pancreas as a Source of Protolerogenic Extracellular Matrix Scaffold for a New-generation Bioartificial Endocrine Pancreas. Ann Surg. 2016;264:169-179.

88. Orlando G, Booth C, Wang Z et al. Discarded human kidneys as a source of ECM scaffold for kidney regeneration technologies. Biomaterials. 2013;34:5915-5925.

89. Petrosyan A, Zanusso I, Lavarreda-Pearce M et al. Decellularized Renal Matrix and Regenerative Medicine of the Kidney: A Different Point of View. Tissue Eng Part B Rev. 2016;22:183-192.

90. Peloso A, Petrosyan A, Da SS et al. Renal Extracellular Matrix Scaffolds From Discarded Kidneys Maintain Glomerular Morphometry and Vascular Resilience and Retains Critical Growth Factors. Transplantation. 2015;99:1807-1816.

91. Petrosyan A, Da SS, Tripuraneni N et al. A step towards clinical application of acellular matrix: A clue from macrophage polarization. Matrix Biol. 2016;

92. Hou N, Cui P, Luo J, Ma R, Zhu L. Tissue-engineered larynx using perfusion-decellularized technique and mesenchymal stem cells in a rabbit model. Acta Otolaryngol. 2011;131:645-652.

93. Ma R, Li M, Luo J et al. Structural integrity, ECM components and immunogenicity of decellularized laryngeal scaffold with preserved cartilage. Biomaterials. 2013;34:1790-1798.

94. Jank BJ, Xiong L, Moser PT et al. Engineered composite tissue as a bioartificial limb graft. Biomaterials. 2015;61:246-256.

95. Duisit J, Debluts D, Behets C et al. Porcine ear: a new model in large animals for the study of facial subunit VCA. JPRAS Open. 2017;[Accepted].

96. Ott HC, Clippinger B, Conrad C et al. Regeneration and orthotopic transplantation of a bioartificial lung. Nat Med. 2010;16:927-933.

97. Gerard AC, Humblet K, Wilvers C et al. Iodine-deficiency-induced long lasting angiogenic reaction in thyroid cancers occurs via a vascular endothelial growth factor-hypoxia inducible factor-1-dependent, but not a reactive oxygen species-dependent, pathway. Thyroid. 2012;22:699-708.

98. Sachs DH, Leight G, Cone J, Schwarz S, Stuart L, Rosenberg S. Transplantation in miniature swine. I. Fixation of the major histocompatibility complex. Transplantation. 1976;22:559-567.

99. Scalea JR, Villani V, Gillon BC et al. Development of antidonor antibody directed toward non-major histocompatibility complex antigens in tolerant animals. Transplantation. 2014;98:514-519.

100. Colleoni S, Donofrio G, Lagutina I, Duchi R, Galli C, Lazzari G. Establishment, differentiation, electroporation, viral transduction, and nuclear transfer of bovine and porcine mesenchymal stem cells. Cloning Stem Cells. 2005;7:154-166.

101. Colleoni S, Bottani E, Tessaro I et al. Isolation, growth and differentiation of equine mesenchymal stem cells: effect of donor, source, amount of tissue and supplementation with basic fibroblast growth factor. Vet Res Commun. 2009;33:811-821.

102. Schubert T, Xhema D, Veriter S et al. The enhanced performance of bone allografts using osteogenic-differentiated adipose-derived mesenchymal stem cells. Biomaterials. 2011;32:8880-8891.

103. Naba A, Clauser KR, Ding H, Whittaker CA, Carr SA, Hynes RO. The extracellular matrix: Tools and insights for the "omics" era. Matrix Biol. 2016;49:10-24.

104. De Rosa L, Carulli S, Cocchiarella F et al. Long-term stability and safety of transgenic cultured epidermal stem cells in gene therapy of junctional epidermolysis bullosa. Stem Cell Reports. 2014;2:1-8.

105. Luo L, Eswaramoorthy R, Mulhall KJ, Kelly DJ. Decellularization of porcine articular cartilage explants and their subsequent repopulation with human chondroprogenitor cells. J Mech Behav Biomed Mater. 2015;55:21-31.

106. Elder BD, Kim DH, Athanasiou KA. Developing an articular cartilage decellularization process toward facet joint cartilage replacement. Neurosurgery. 2010;66:722-727.

107. Kheir E, Stapleton T, Shaw D, Jin Z, Fisher J, Ingham E. Development and characterization of an acellular porcine cartilage bone matrix for use in tissue engineering. J Biomed Mater Res A. 2011;99:283-294.

108. Canal GC, Hung CT, Ateshian GA. Electrostatic and non-electrostatic contributions of proteoglycans to the compressive equilibrium modulus of bovine articular cartilage. J Biomech. 2010;43:1343-1350.

109. Firmin F, Marchac A. A novel algorithm for autologous ear reconstruction. Semin Plast Surg. 2011;25:257-264.

110. Nagata S. A new method of total reconstruction of the auricle for microtia. Plast Reconstr Surg. 1993;92:187-201.

111. Kang HW, Lee SJ, Ko IK, Kengla C, Yoo JJ, Atala A. A 3D bioprinting system to produce human-scale tissue constructs with structural integrity. Nat Biotechnol. 2016;34:312-319.

112. Griffin MF, Premakumar Y, Seifalian AM, Szarko M, Butler PE. Biomechanical Characterisation of the Human Auricular Cartilages; Implications for Tissue Engineering. Ann Biomed Eng. 2016;44:3460-3467.

113. Fishman JM, Lowdell MW, Urbani L et al. Immunomodulatory effect of a decellularized skeletal muscle scaffold in a discordant xenotransplantation model. Proc Natl Acad Sci U S A. 2013;110:14360-14365.

114. Ren X, Moser PT, Gilpin SE et al. Engineering pulmonary vasculature in decellularized rat and human lungs. Nat Biotechnol. 2015;33:1097-1102.

115. Kasrai L, Snyder-Warwick AK, Fisher DM. Single-stage autologous ear reconstruction for microtia. Plast Reconstr Surg. 2014;133:652-662.

116. Baluch N, Nagata S, Park C et al. Auricular reconstruction for microtia: A review of available methods. Plast Surg (Oakv). 2014;22:39-43.

117. Giot JP, Labbe D, Soubeyrand E et al. Prosthetic reconstruction of the auricle: indications, techniques, and results. Semin Plast Surg. 2011;25:265-272.

118. Lengelé BG. Current concepts and future challenges in facial transplantation. Clin Plast Surg. 2009;36:507-521.

119. Cao Y, Vacanti JP, Paige KT, Upton J, Vacanti CA. Transplantation of chondrocytes utilizing a polymer-cell construct to produce tissue-engineered cartilage in the shape of a human ear. Plast Reconstr Surg. 1997;100:297-302.

120. Cervantes TM, Bassett EK, Tseng A et al. Design of composite scaffolds and three-dimensional shape analysis for tissue-engineered ear. J R Soc Interface. 2013;10:20130413.

121. Ott HC, Matthiesen TS, Goh SK et al. Perfusion-decellularized matrix: using nature's platform to engineer a bioartificial heart. Nat Med. 2008;14:213-221.

122. Uygun BE, Price G, Saedi N et al. Decellularization and recellularization of whole livers. J Vis Exp. 2011;

123. Flynn LE. The use of decellularized adipose tissue to provide an inductive microenvironment for the adipogenic differentiation of human adipose-derived stem cells. Biomaterials. 2010;31:4715-4724.

124. Wang L, Johnson JA, Zhang Q, Beahm EK. Combining decellularized human adipose tissue extracellular matrix and adipose-derived stem cells for adipose tissue engineering. Acta Biomater. 2013;9:8921-8931.

125. Sarathchandra P, Smolenski RT, Yuen AH et al. Impact of gamma-irradiation on extracellular matrix of porcine pulmonary valves. J Surg Res. 2012;176:376-385.

126. Schneider CA, Rasband WS, Eliceiri KW. NIH Image to ImageJ: 25 years of image analysis. Nat Methods. 2012;9:671-675.

127. Chappard D, Legrand E, Haettich B et al. Fractal dimension of trabecular bone: comparison of three histomorphometric computed techniques for measuring the architectural two-dimensional complexity. J Pathol. 2001;195:515-521.

128. Song JJ, Guyette JP, Gilpin SE, Gonzalez G, Vacanti JP, Ott HC. Regeneration and experimental orthotopic transplantation of a bioengineered kidney. Nat Med. 2013;19:646-651.

129. Uygun BE, Soto-Gutierrez A, Yagi H et al. Organ reengineering through development of a transplantable recellularized liver graft using decellularized liver matrix. Nat Med. 2010;16:814-820.

130. Badylak SF, Gilbert TW. Immune response to biologic scaffold materials. Semin Immunol. 2008;20:109-116.

131. Crapo PM, Gilbert TW, Badylak SF. An overview of tissue and whole organ decellularization processes. Biomaterials. 2011;32:3233-3243.

132. Bannasch H, Stark GB, Knam F, Horch RE, Fohn M. Decellularized dermis in combination with cultivated keratinocytes in a short- and long-term animal experimental investigation. J Eur Acad Dermatol Venereol. 2008;22:41-49.

133. Ng SL, Narayanan K, Gao S, Wan AC. Lineage restricted progenitors for the repopulation of decellularized heart. Biomaterials. 2011;32:7571-7580.

134. Cui L, Wu Y, Cen L et al. Repair of articular cartilage defect in non-weight bearing areas using adipose derived stem cells loaded polyglycolic acid mesh. Biomaterials. 2009;30:2683-2693.

135. Fulco I, Miot S, Haug MD et al. Engineered autologous cartilage tissue for nasal reconstruction after tumour resection: an observational first-in-human trial. Lancet. 2014;384:337-346.

136. Gordon CR, Nazzal J, Lozano-Calderan SA et al. From experimental rat hindlimb to clinical face composite tissue allotransplantation: historical background and current status. Microsurgery. 2006;26:566-572.

137. Yazici I, Unal S, Siemionow M. Composite hemiface/calvaria transplantation model in rats. Plast Reconstr Surg. 2006;118:1321-1327.

138. Demir Y, Ozmen S, Klimczak A, Mukherjee AL, Siemionow M. Tolerance induction in composite facial allograft transplantation in the rat model. Plast Reconstr Surg. 2004;114:1790-1801.

139. Siemionow M, Klimczak A. Chimerism-based experimental models for tolerance induction in vascularized composite allografts: Cleveland clinic research experience. Clin Dev Immunol. 2013;2013:831410.

140. Fryer M, Grahammer J, Khalifian S et al. Exploring cell-based tolerance strategies for hand and face transplantation. Expert rev clin immunol. 2015;11:1189-1204.

141. Orlando G, Soker S, Stratta RJ, Atala A. Will regenerative medicine replace transplantation? Cold Spring Harb Perspect Med. 2013;3:

142. Elliott MJ, De Coppi P, Speggiorin S et al. Stem-cell-based, tissue engineered tracheal replacement in a child: a 2-year follow-up study. Lancet. 2012;380:994-1000.

143. Mommaerts MY, Michiels ML, De Pauw GA. A 2-year outcome audit of a versatile orthodontic bone anchor. J Orthod. 2005;32:175-181.

144. Climov M, Maciuceanu Zarnescu MB, Stefanescu A, Zamfirescu D, Lascar I. Learning curve in hemifacial transplantation in rats. Chirurgia-Bucharest. 2013;108:234-240.

145. Henderson PW, Nagineni VV, Harper A et al. Development of an acellular bioengineered matrix with a dominant vascular pedicle. J Surg Res. 2010;164:1-5.

146. Totonelli G, Maghsoudlou P, Garriboli M et al. A rat decellularized small bowel scaffold that preserves villus-crypt architecture for intestinal regeneration. Biomaterials. 2012;33:3401-3410.

147. Porzionato A, Sfriso MM, Macchi V et al. Decellularized omentum as novel biologic scaffold for reconstructive surgery and regenerative medicine. Eur J Histochem. 2013;57:e4.

148. Aycart MA, Kiwanuka H, Krezdorn N et al. Quality of Life after Face Transplantation: Outcomes, Assessment Tools, and Future Directions. Plast Reconstr Surg. 2017;139:194-203.

149. Giatsidis G, Sinha I, Pomahac B. Reflections on a Decade of Face Transplantation. Ann Surg. 2016;265:841-846.

150. Petruzzo P, Testelin S, Kanitakis J et al. First human face transplantation: 5 years outcomes. Transplantation. 2012;93:236-240.

151. Siemionow M, Klimczak A. Tolerance and future directions for composite tissue allograft transplants: part II. Plast Reconstr Surg. 2009;123:7e-17e.

152. Gajanayake T, Olariu R, Leclere FM et al. A single localized dose of enzyme-responsive hydrogel improves long-term survival of a vascularized composite allograft. Sci Transl Med. 2014;6:249ra110.

153. Keane TJ, Londono R, Turner NJ, Badylak SF. Consequences of ineffective decellularization of biologic scaffolds on the host response. Biomaterials. 2012;33:1771-1781.

154. Vracko R, Benditt EP. Basal lamina: the scaffold for orderly cell replacement. J Cell Biol. 1972;55:406-419.

155. Rohrich RJ, Pessa JE. The fat compartments of the face: anatomy and clinical implications for cosmetic surgery. Plast Reconstr Surg. 2007;119:2219-2227.

156. Gilbert TW, Freund JM, Badylak SF. Quantification of DNA in biologic scaffold materials. J Surg Res. 2009;152:135-139.

157. Wong ML, Griffiths LG. Immunogenicity in xenogeneic scaffold generation: antigen removal vs. decellularization. Acta Biomater. 2014;10:1806-1816.

158. Dehoux JP, Gianello P. Xenotransplantation. Commun Agric Appl Biol Sci. 2003;68:21-29.

159. Gifford S, Zambon JP, Orlando G. Recycling organs - growing tailor-made replacement kidneys. Regen Med. 2015;10:913-915.

160. Gilpin SE, Ren X, Okamoto T et al. Enhanced lung epithelial specification of human induced pluripotent stem cells on decellularized lung matrix. Ann Thorac Surg. 2014;98:1721-1729.

161. Katari R, Peloso A, Zambon JP et al. Renal bioengineering with scaffolds generated from human kidneys. Nephron Exp Nephrol. 2014;126:119.

162. Mazza G, Rombouts K, Rennie HA et al. Decellularized human liver as a natural 3D-scaffold for liver bioengineering and transplantation. Sci Rep. 2015;5:13079.

163. Sanchez PL, Fernandez-Santos ME, Costanza S et al. Acellular human heart matrix: A critical step toward whole heart grafts. Biomaterials. 2015;61:279-289.

164. Sanchez PL, Fernandez-Santos ME, Espinosa MA et al. Data from acellular human heart matrix. Data Brief. 2016;8:211-219.

165. Remuzzi A, Figliuzzi M, Bonandrini B et al. Experimental Evaluation of Kidney Regeneration by Organ Scaffold Recellularization. Sci Rep. 2017;7:43502.

« La décision morale est le lieu où l'homme joue son autonomie, le lieu où, en définitive, il joue sa propre destinée »

J.F. Malherbe

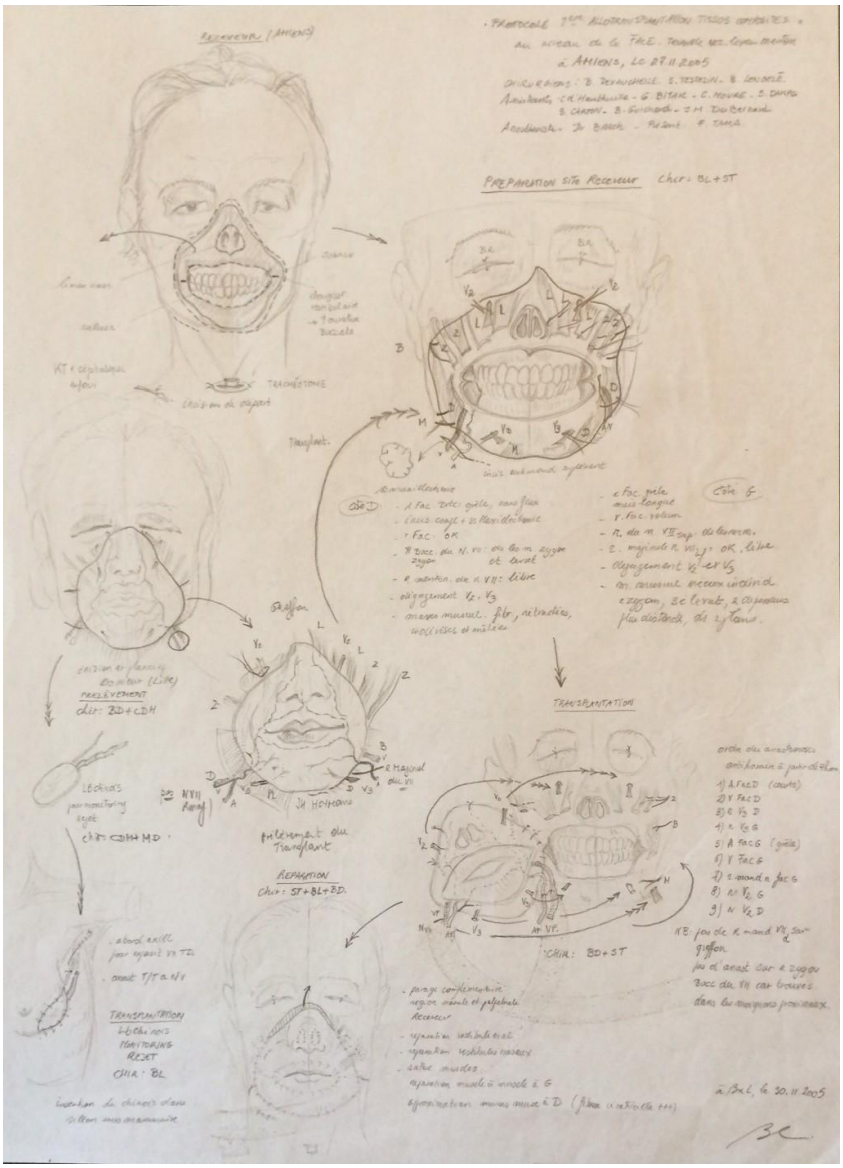

Operation's note of the first face transplant surgery (B. Lengelé, 30.11.2005)

Part III- General discussion, perspectives and conclusion - From "VCA" to "VCE"

The data collected from our various reported investigations have demonstrated that subunit models were relevant as an experimental strategy to initiate human face and hand engineering. Furthermore, they have emphasized that the PDR technology could be applied to a large spectrum of vascularized composite tissues. By exploring face, hand and their subunits for VCE, we could cover almost the entire scope of possibilities in terms of tissue associations validation models. The few remaining specific models, because of their unique tissue associations and/or functions are: the penis, for the corpus cavernosum and spongiosum tissues and the erectile function; the breast for the mammary gland and lactation; the tongue (**Figure 1**) for the association of a skeletal muscle and oral mucosa, with very particular functions, mixing a highly complex motricity with the sense of taste. Tongue [1], breast [2] and penis [3] engineering attempts have already been reported, but never in a vascularized approach, just focusing on small tissue samples, which do not authorize any clinical translation.

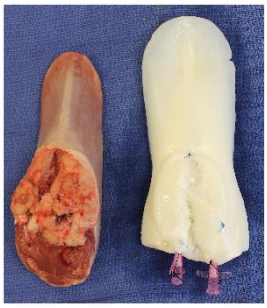

***Figure 1**: Native and decellularized porcine tongue graft (UCL)*

Choice of models. The use of large animals and human cadavers allowed us to work at a very preclinical scale, which was fundamental for such a set-up.

However, it was, with current means and technology, more adapted for decellularization steps, than to the recellularization process. This justified to develop also smaller models, such as the rat for face and limb described by other teams [4]. Similarly in the history of VCA, small animal models were useful laboratory and conceptual tools [5,6], but they remained limited in their relevance by the inability to bridge directly clinical applications.

Decellularization protocol. The use of a combined detergent/solvent perfusion protocol was a very useful and versatile tool to walk through all the steps of the process, from decellularization to reperfusion, which was mandatory in such an exploratory work, in order to develop a know-how and associated technologies. But certainly, the protocols will need to be refined, in both experimental and clinical approaches: we know the limitations related to detergents, especially SDS [7], in the preservation of the ECM and its growth factors. However, this agent is very suitable in an early experimental phase, because of its efficiency on all tissues and its low-cost. The main long-term problem of detergents will be the effect of residual traces on new cells seeded on the ECM scaffold, then becoming at risk of undergoing oncogenic evolution; this critical aspect should thus be studied for any protocol. We explored (**unpublished data**) other, unsuccessful, decellularization techniques: SDS at different concentrations, 0.1, 0.5, 1%, the latest being the more efficient; Triton X-100 only, unable to treat correctly the graft; Sodium Deoxycholate, successful in intestine engineering [8], was very performing in epidermolysis but was too aggressive for cartilage, leading to a complete loss of morphology, a yellowish stain of tissues and a poor efficiency regarding muscle, compared to other tissues; the freeze-thaw technique, destroying the microcirculation. Different elegant and more efficient approaches however have been described [9], and could be of great interest when getting closer to clinical applications, even though not relevant in the experimental field for the moment. On our side of the bench, we introduced a polar solvent step to classical detergent-based protocols, in order to treat specifically the adipose tissue and to remove scattered oil cysts, as described for isolated adipose tissue decellularization [10], but

not for organs. The explanation is that adipose tissue is not fundamental in solid organs, contrary to composite tissues, in which the fat plays frequently, as in the face, a prominent role for gliding tissue or for volumetric expressive function. Questions remain about the need to remove all the facial fat for future regeneration and about the effect of several solvent steps on the integrity of ECM and the vascular tree, even if our treated scaffolds demonstrated excellent properties in both these dimensions.

Finally, a radically transversal approach in this thesis, through different models considered at the same time, despite their various types and origins, and analyzed at all levels of the process, allowed us to draw the very fundamental concepts to consider research in VCE, and determine how to combine VCE with the current VCA field.

Experimental models and strategies

Defining accurately a composite scaffold

Due to the large spectrum of possible combinations of composite tissues in grafts, a first approach is required to characterize properly the grafts as experimental models. Actually, three dimensions are fundamental to define a VCE model:

- Layers of Tissues involved**:** Layer composition will guide protocols for the decellularization and directly condition the bioreactor specifications and the functions to restore (motor, non-motor) during recellularization. A single layer vascularized scaffold (with exception of the avascular cartilage) represents an elementary VCE model: i.e.: a skin flap, a muscle flap, a bone flap. The intermediate step of investigating subunit grafts is the only practical approach, to follow when testing new protocols for new tissues associations.
- Mass, dimensions/Surface: These biomimetic data are relevant in absolute

and relative values for the different components. Inside the subunit under study, as for any recipe, knowing the quantitative tissue composition and the relative contribution of every tissue is necessary (**Figure 2**). It will be predictive and guide protocols for decellularization (duration, type) and recellularization (number of

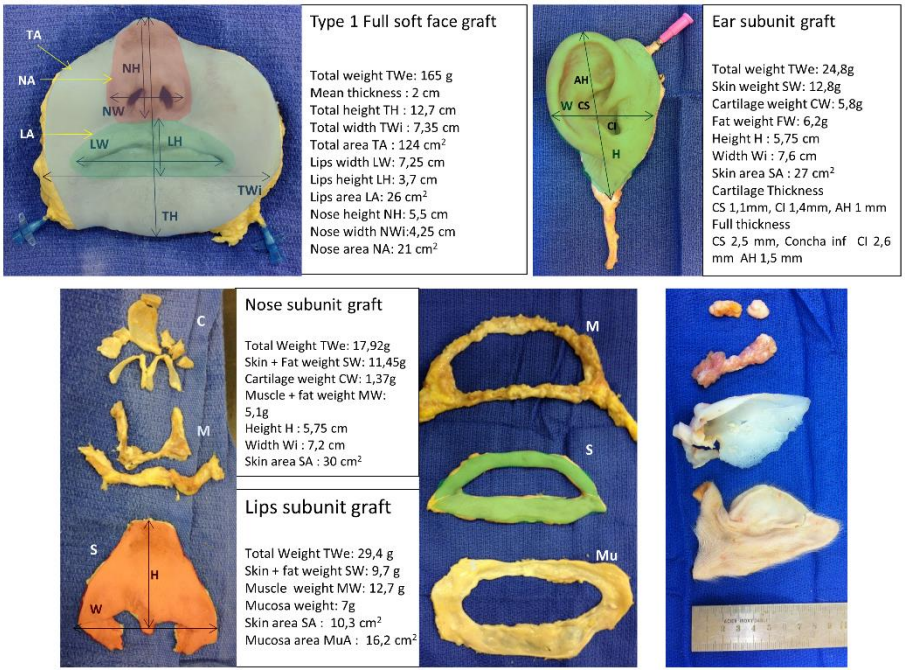

***Figure 2**: Division and characterization of different tissues from a facial graft.*

cells needed, type of bioreactor and culture sequence). For a same graft type, the (important) variations are directly related to the donor: small or large animal, human.

- <u>Functions to restore</u>:
    - *Non-motor*: optimal morphology and sensitivity restoration.
    - *Motor*: i.e. the cutaneous animation is part of face expressivity; skeletal mobility in limbs is mandatory for locomotion or prehension; breathing is essential for thoracic or diaphragmatic rehabilitation.
    - *Others*: erection, lactation.

The following dimensions are not critical for VCE model definition.

Vascular and nervous pedicle: Contrary to conventional flaps, the type of vascularization (perforator, direct branch, etc.) is not determinant in VCE. What is relevant is the number of vessels, to be connected to the pump, and the function associated to the nerve pedicle: sensory for skin, motor for musculature.

Topography: This is also not determinant if the tissue composition is similar. In VCE, what matters is the tissue association rather than the anatomical location.

Recellularization concepts

As previously described, composite tissues contain very different structures and thus bear several functions to restore. The rationale and techniques to reach this goal are similar in numerous ways as those previously addressed to approach organs bioengineering, but with very important specificities. Like for organs, the main factors to consider will be the choice of cell types, their quantity and the seeding pathways, probably different for each type of tissue to be regenerated, in respect with their location, function and targeted level of regeneration. Being highly specific in VCE, like the need for versatile protocols to achieve an optimal decellularization, recellularization of composite scaffolds is an equation with multiple unknown variables to solve: numerous potential cell types for seeding, multiple tissues with few selective accesses, multiple sequences of differentiation and the need for adapted bioreactors. A previously stated, cell seeding can be performed through three ways: needle injections, topical deposition or vascular infusion. Closely associated to these pathways, scaffolds must be divided in three distinct recellularization compartments (**Figure 3**):

- The **External compartment**: bounded by skin or mucosa.
- The **Internal compartment**: comprising the parenchyma and the graft section.
- The **Vascular compartment**: subdivided into the extra- (pedicle) and intra-scaffold vascular trees.

a- The external compartment (EC). Composite scaffolds offer an external compartment/environment (mucosal/cutaneous lining), unique when comparing with organs. Access to the dermis is direct and simple for topic seeding and culture. Dermal basal membrane preservation is essential to allow epidermal reconstruction and isolation of the Internal Compartment. A specific bioreactor should then provide the isolation of the external graft envelope allowing a guided skin layer culture on its surface.

b- The internal compartment (IC). This compartment contains all other composite tissue layers with exclusion of the vascular tree. The cell seeding can be performed either by injection or vascular spread. The IC is present in organs, but is there usually bounded by a closed capsule, which does not exist in VCE grafts. These latter constructs always exhibit a more or less extensive parenchymal section, deprived of any coverage layer.

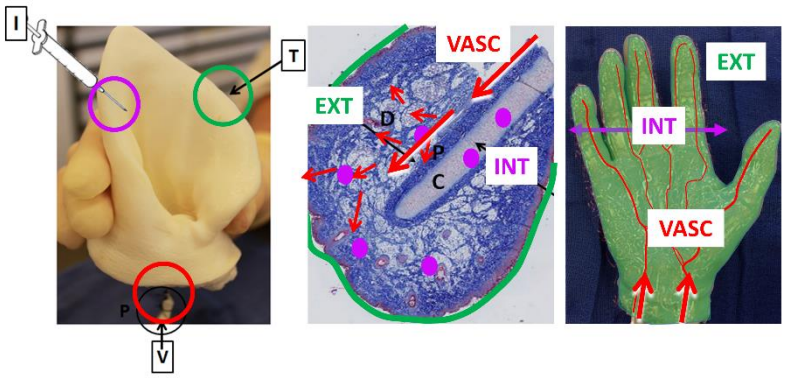

***Figure 3**: Recellularization compartments and cell seeding pathways of a vascularized composite tissue scaffold. Cell seeding pathways in a composite tissue: injection (I), topical (T) and vascular (V) (left); seeding pathways and related compartments, external (EXT), internal (INT) and vascular (VASC) as represented on an ear scaffold auricular histological section (middle; same divisions, illustrated on a hand scaffold (right).*

c- The vascular compartment (VC). This compartment has to be considered critical for VCE: first, it constitutes a route to regenerate the vasculature itself, with an easy access to the vascular framework of the scaffold, lined by intact basal lamina, and a direct exposure to culture medium and cells. Second, it also

constitutes an intermediate access before re-endothelialization, to spread cells in the deep tissues of the internal compartment. The VC is present and large in organs.

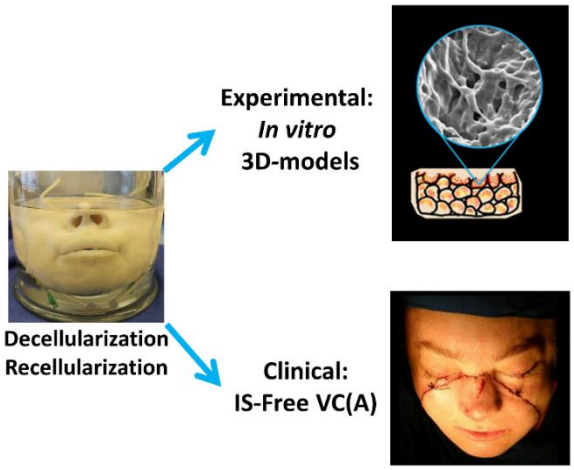

***Figure 4**: Main application types of the perfusion-decellularization/recellularization technology.*

For each compartment, 3 questions need to be considered:

- **The targeted application**: experimental versus clinical.
- **The cell seeding method**: pathways, engraftment yield and sequence of seeding and culture.
- **The cell choices**: type, differentiated or undifferentiated, quantity.

Targeted application

The various objectives of the recellularization process are very different, according the fact that they are aiming to reach human applications in reconstructive surgery, or are, on the opposite, targeted to produce specific recellularized matrices for *in vitro* experiments (**Figure 4**). Scaffolds indeed can be used as complex 3D-culture i.e. for *in vitro* cancer study, or for toxicology applications [1,11]. In this particular case, the vascular compartment does not need to be regenerated and cells can be originated from totally different types than

those in the normal tissues. For clinical applications, recellularization studies should be performed first by tissue type, depending on the main tissue of interest. Thereafter, different approaches can be developed, knowing that, **in engineering, a composite tissue is not equivalent to the sum of isolated tissues**.

Cell seeding method

As previously explained, the cell seeding pathway will depend on the selected compartment to be regenerated, either isolated or combined. But for this purpose, there is a critical **need for new and specific types of perfusion-bioreactors.** There are several drawbacks indeed with current bioreactor devices, adapted to organs but obviously not fully suitable for the skin-lined composite scaffolds, with the need to: isolate the external compartment (EC); provide a specific handling of the graft protecting a very fragile pedicle; manage the scaffold parenchymal section. Contrary to solid organs, composite tissue grafts, especially the soft face without bone support, are prone to lose their shape after harvest, deprived from their structural support. A specific bioreactor will thus have to provide a support and allow the adjunct of special functions like i.e. electro-mechanical stimulation for muscular regeneration. None of the existing bioreactors is fulfilling the various needs listed above, specific to VCE. We developed adapted solutions, implemented in a new bioreactor prototype (**see Appendix, patent**), illustrated in the last experiments of human hands scaffolds culture set-up (Chapter 8).

Given the different recellularization compartments and the very different cell types to consider for seeding (with their specific culture medium and conditions), a true challenge in VCE will be to find the most effective culture sequences.

For the vascular seeding, an important issue is to define the right perfusions pressures and flow, either to allow endothelial cells engraftment only in the VC (achieved by a low-flow infusion, and a long static period); or, at the opposite, to promote the vascular seeding of the IC (requiring high perfusion pressure and flow, aiming to force cell extravasation in the ECM and enhance engraftment yield). Interestingly, we found in our *in vivo* experiments that the blood pressure was very efficient to drive IC seeding.

Cells choices: types and quantity in clinical applications

Cells types. In order to enter the clinical practice, it is essential to identify a suitable cell source, which could be isolated under minimally invasive conditions and thereafter quickly expanded in culture, while maintaining the capacity to subsequently generate functional tissues with reproducible properties.

Apart from general strategies and cell types limitations, the appropriate selection of cell lines for a first set of experiments already raises tissue-specific questions to be solved, in order to enable clinical applications.

Adult differentiated cells versus stem cells. Differentiated cells should be considered for the EC and VC, like i.e. keratinocytes for epidermis or endothelial cells for vessels. Similarly differentiated cells have to be used in any situation when the seeding is selective and/or is required for experimental studies. For the self-renewal of the constructs, especially for tissues with a quick turnover, like the skin, it is important in any cases, to add a certain proportion of progenitor cells. Stem cells will be critical for the IC of composite tissues. Indeed, needle-injection is discriminative enough to target buried specific tissue among close layers, like the thin cutaneous muscle in the lips, resulting in disparate and isolated clusters of cells (Chapter 7). On the contrary, the vascular route is ideal to seed cells in the whole scaffold IC; however, it will not be tissue-selective: perfused cells will spread in all tissues, without specificity. This apparent drawback is not an issue for widely spread cells like fibroblasts, but is not an option for specialized cells like myocytes, osteocytes or chondrocytes, because potentially leading to ectopic tissue formation. Then, the only solution for IC regeneration, in VCE, is the use of multipotent (like adipose-derived stem cells or bone-marrow mesenchymal stem cells) or pluripotent stem cells (like IPS cells), then relying on the ECM's ability to orientate the cell fates and to regenerate properly the tissue layers, as a natural result of its specific 3D-structure and chemical composition (**Figure 5**). Growth factors, cytokines and differentiation molecules preserved in the ECM should trigger stem cells differentiation in a right way, at the right place.

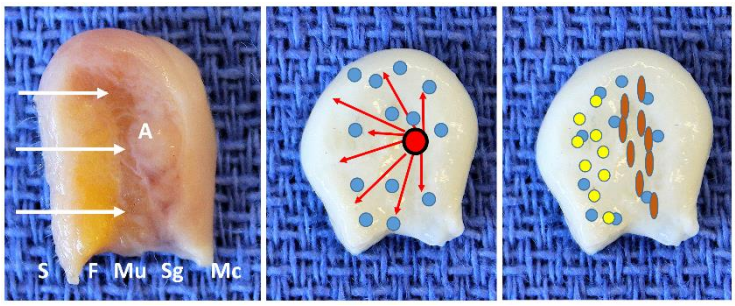

***Figure 5**: Cell types and seeding strategies of the internal compartment. Native lip with visible different tissue layers: skin (**S**), fat (**F**), muscle (**Mu**), accessory salivary glands (**SG**), mucosa (**Mc**), labial artery (**A**); injection from the surface (white arrows) results in a difficult targeting of the muscle specific layer (left). Vascular seeding of a lip scaffold through the labial artery (red dot) leads to a multidirectional spread (red arrows) of cells (blue dots), with a homogeneous but non-selective distribution (middle). Ideal stem cell differentiation fate (right), leading to a specific tissue regeneration with the adequate topography, like for adipose cells (yellow dots) and muscular cells (brown dots).*

Cells quantity and origin. The main issue is not the type but the number of cells needed for regeneration (**Figure 6**). The total number of cells in the body is estimated to 3.72×10^{13} [12]. In the skin, the total cells are estimated 2.03×10^{12} for $1.85 m^2$. As defined above, the morphometrics (weight, surface) of the scaffold are critical to estimate the number of cells to culture and to seed, the relative mass proportion of each tissue being of great importance. For example, the muscular cells needed to regenerate the few grams of thin cutaneous muscles in the face, are not comparable with the number of cells required for the recellularization of skeletal muscle in a whole-limb scaffold, up to kilograms. Such a requirement is questioning as well as the origin of cells, when the cell type is not easily lab-grown. If very large amounts of cells need to be harvested from the recipient, when dealing with large defects, this may result in significant donor-site morbidity. However, such morbidities created to obtain enough cells are not acceptable in tissue engineering strategies.

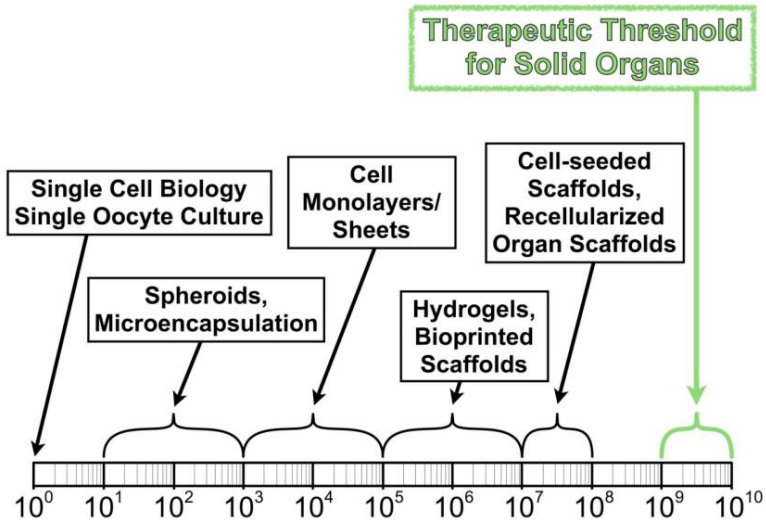

***Figure 6**: Number of cells needed per construct, from Bianconi et al.* [12]

Targeting re-endothelialization first and in vivo regeneration. The number of cells, the culture length and the conditions required to fully regenerate *in vitro* an organ scaffold are prohibitive and should not be an objective *per se*. As stated by S. Badylak [13], we have to rely on the *in vivo* contribution of the recipient, as its own bioreactor, to achieve the final scaffold regeneration (**Figure 7**). In bioreactors, we shall only target critical sectors: vascular, to allow replantation and *in vivo* regeneration. We observed during our short *in vivo* reperfusion experiments that a large cell density engraftment was obtained after only a few hours, compared to the poor density in our scaffolds seeded with millions cultured cells and during up to three weeks. Back to the general Regenerative Medicine considerations, the future will have to consider a balance for the restoration of body parts and organs, resulting from an adequate combination of purely *in vitro* tissue engineering and a complementary *in vivo* maturation and healing.

Here again we join a common effort with organ engineering, establishing the need to restore a functional vascular tree: the completion of this step will enable clinical applications for the whole fields of solid organs and vascularized composite tissues engineering.

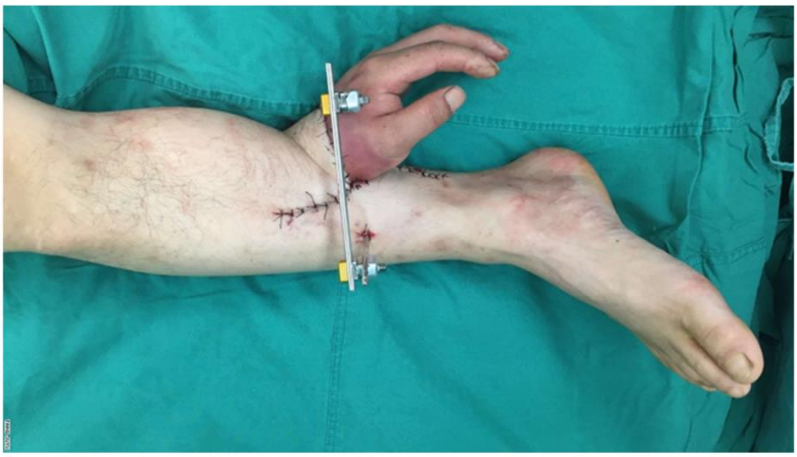

***Figure 7**: Illustration of possible heterotopic in vivo regeneration prior to orthotopic transplantation. (credits Dr Juyu Tang)*

Implication for VCE immunology

Apart from allogenicity, carried by cell membranes, we will have to closely consider immune response to the ECM proteins themselves, decellularization creating *de facto* new epitopes. This explains the negative allo-immune response to scaffolds, but with non-specific inflammation and remodeling. This true immunological assessment will only be obtained when long-term reperfusion of scaffolds will be possible, to expose a whole graft to circulating blood and recipient immune system.

Principal tissue-specific approaches and challenges

Skin. Culture of a few cm^2 biopsies from the recipient will provide enough epidermis to cover large surfaces. Total Body Surface Area (TBSA) classification is there useful for a quick estimation of cells needed. To restore the epidermis, keratinocytes will have to be seeded adequately on 3D surfaces, by means of sprays or epidermal sheets grafting. For this tissue, the preservation of the basal membrane at the dermo-epidermal junction will be critical. Dermis regeneration will be obtained through a vascular seeding, demonstrated with our perfusion-

seeding studies, with the distribution of dermal fibroblasts right under the dermo-epidermal junction contrary to conventional skin equivalent culture. Moreover, culture medium will be continuously perfused.

Adipose tissue. As a morphological and functional layer on its own, a correct restoration of the adipose tissue will be very important for composite tissues engineering. Fortunately, the adipose tissue in the recipient will represent an important source of adipocytes and progenitor cells. This cell-therapy field is also well explored already, in both experimental and clinical domains.

Cartilage (elastic). Nasal and auricular cartilage recellularization is challenging. Facial cartilage is deep, buried under the skin cover: this is a totally different feature from larynx engineering, where the cartilage scaffold is directly accessible. Moreover, since cartilage is avascular, the repopulation should occur from the perichondrium vascularized layer; due to the high density of a cartilage scaffold, compared to the surrounding tissues, migration of cells towards the cartilage rather than the external layers is not evident. Chondrocytes could be harvested from the nasal septum or the ear cartilage. Alternative cell sources could be chondrocytes from other origin such as articular or costal chondrocytes, or stem cells from bone marrow or adipose tissue committed *in vitro* to chondrogenic differentiation.

Muscle. Along with the vascular tree, it is critical to ensure a correct muscular regeneration and training *in vitro*, to properly orientate muscular fibers during their growth, control their mechanical efficiency and avoid an *in vivo* fibrosis formation, waiting for motor nerves regrow within the nerve scaffold. This will rely on the use of the adequate cell types and on specific dynamic bioreactors to train and control muscular formation. Once the musculature is regenerated, the main risk to avoid is a damage by hypoxia. At this stage, we will be back to the classical VCA concerns with muscle (limb, face) and need for accurate preservation and acceptable revascularization timing. We will have to explore if a stimulation/pacing needs to be continued *in vivo* after replantation and prior to re-innervation. As explained before, the main challenges for the cell sources (i.e.

myoblasts, mesoangioblasts, pericytes) will concern large skeletal muscle regeneration, in terms of amount needed.

Nerves. Apart from Schwann cells seeding, there is not much that can be done *in vitro* for nerves; we will have to wait for the recipient axons to grow through the scaffold, as in VCA. This is not a major issue for sensitive nerves, but more probably for motor nerves, as explained in the muscle section.

Endothelium and vessels. Unlocking long-term reperfusion is the KEY for any clinical application in vascularized composite tissue and organ engineering. However, despite various strategies [14,15], graft survival is still limited to a few days after reperfusion in the host. Re-endothelialization is important but a combination of endothelial cells, smooth muscle cells and satellite cells is critical to restore a functional proximal and distal microvascular bed. Is a complete regeneration necessary before reconnection to the host circulation, so as to be completed *in vivo*? The VC recellularization is facilitated by its direct access, like in the EC. This compartment is less quantitative in VCE compared to solid organs, with a lower circulating volume. The adequate sources have to be identified in the recipient (i.e. radial artery, saphenous vein), but avoiding additional morbidities.

Likelihood of engineered composite tissues clinical applications

Justifying combined study of face and hand VCE for clinical research. Face and hand being the only visible body parts with critical functionalities and nearly impossible to restore with conventional reconstructive techniques, it makes sense to investigate both models at the same time, aiming to develop further clinical applications based on lessons learnt from one to another, from the bench to the bedside. These body parts indeed have a symbolic importance, are highly relevant of human identity and therefore they targeted and stimulated the most radically new technologies for reconstruction, as observed in the history of both allotransplantation and TE. Considering the fact that, in case of failure, a non-

vital organ does not immediately expose the recipient patient to any life-threatening risk, the probability is quite high that the first transplantation of TE organs will be carried on composite tissue subunits like lips or fingers rather than on solid organs. On the other hand, VCA is the crucial field where immunosuppression is so limiting, and thus significantly impairs the extension of the potential clinical indications for disfigured or amputated patients. In terms of engineering indeed, it is not harder, contrary to what may be thought, to work on VCT body parts as limbs, face or abdominal wall than a solid organ. Basically, what is critical is the tissue association type with specific amounts of each tissue. Although described for VCA in terms of allogenic response, proportional and absolute amounts of different tissues encountered in a VCT are nevertheless crucial for TE aspects. In allotransplantation, the amount of tissues is not directly correlated to the intensity of the allogenic response, but more relying on the variety of tissues implanted. Successful complex grafting through a successful handling of transplant in VCA and surgical justification for IS treatment have led to consider the evolution towards larger and larger transplants as a positive evolution of the technique. The recent observations reporting a probably limited lifetime and long-term failure of VCA grafts due to a chronic vascular rejection despite IS treatment, should however moderate the unrealistic enthusiasm about VCA, which lead some teams to perform potentially devastating extensive face transplantation.

Principle of reversibility. In the quest to move engineered organs from bench to bedside, the best candidate for a "first in human" is the kidney: indeed, and contrary to heart, lung and liver, there is an alternative option in case of graft failure with dialysis. There is also the possibility for an *in vivo* maturation, contrary to an organ like the heart, which has to be fully functional when transplanted: as discussed before, building a fully functional organ *in vitro* is a huge challenge.
Regarding VCE, and according to the "less is more" principle, subunit grafts will be more secure for first clinical applications and very likely be performed before organs, precisely for the exact same reasons of their contra-indications in

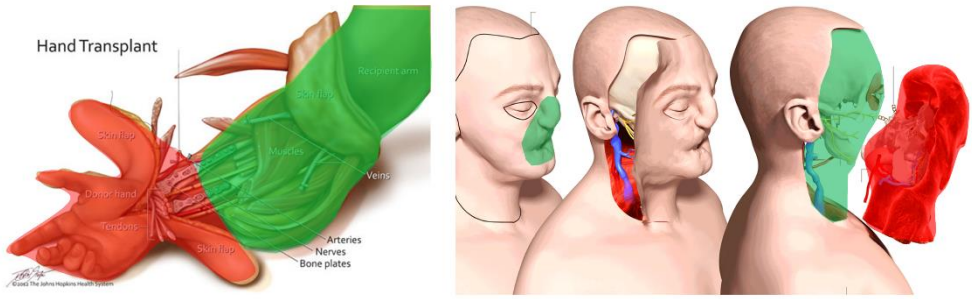

***Figure 8**: The reversibility principle in hand and face grafts. The green area represents the remaining defect after explantation, when compared with the preoperative defect. Similar in limb and back to the original amputation level in case of transplant failure. Significantly larger than the original central face defect in case of extensive transplantation techniques.*
(credits J. Hopkins, Dr E. Rodriguez, with adaptation)

allotransplantation: being non-vital, from cancer resection or traumatic, but interesting relatively small parts of the body, in a mixed adult and pediatric population. Small constructs will be indeed easier to engineer and also better accepted by the population at first. Actually, in VCE, the conceptual evolution is rather towards down-scaling than up-scaling: engineering a whole face or a whole limb will obviously be less frequent than engineering smaller subunits, like finger or lips, in terms of number of potential indications and patients to treat. Furthermore, like kidney, subunits can finish maturation after implantation, after the minimum *in vitro* vascular and muscular regeneration.

Still following the principle of reversibility in case of failure, limbs engineering will be more likely implemented as a "first in man", before the face, as in VCA development. However, the limited face graft lifespan, as recently reported [16], and the important pre-implantation defects created by an increased removal of soft tissues to perform the full-face transplants, will be later on associated with a dramatic situation at the expected time of graft chronic failure and removal (**Figure 8**). Of course, re-transplantation should then be an option, but finding in emergency a perfect matching VCA donor will be nearly impossible. Going back to autologous reconstructive options techniques will at this stage represent the most reliable rescue option, if not exhausted by prior serial reconstructions.

VCA-VCE shared synergy: the surgeon's role

VCE and VCA are closely-related and complementary fields. Allotransplantation was justified to create models, inspire, treat already patients, even with its limitations. It will then remain justified, as long as VCE will not be safely applied as a therapeutic tool. Without development of face transplantation techniques, acting as an intermediate step, there should not be, at present, any model for engineering, and no future clinical applications of VCE technology

But, contrary to solid organ transplantation, studied and performed for decades, the VCA field lacks clinical and experimental developments, although critical for engineering approaches, like organ maintenance and physiology or *ex vivo* perfusion. Preliminary to laboratory bench work, surgical procurement, graft preparation, maintaining the cells alive, transferring the graft to a patient, performing surgery with patent anastomoses, managing postoperative follow-up, all these tasks and challenges requiring new synergistic efforts with basic life scientists will be almost the same for VCA and VCE. Then, basic research, anatomical and technological developments are required in both fields, for the specific engineering applications, and are lacking even in VCA science. As a direct impact of potential clinical applications of engineered body parts, the number of cases will rise importantly, and so will require further research.

The surgeons will then stand in a leading position, at the forefront of scientific collaborations. The surgeon's role in VCE will at least remain the same, as defined in VCA: to take care of the graft procurement and to perform recipient's preparation and transplantation, in addition to achieve a new *in vitro* intermediate laboratory step, relying on an in-depth knowledge and expertise in cell biology. The mastership in conventional reconstructive surgery techniques, however, will remain, as in all fields of plastic and cosmetic surgery (i.e. for vascular and morphological revisions), a mandatory tool in VCE. The aim of a better integration of the transplant to the recipient site is central. Although some new revolutionary horizons seem arising, the other techniques will preserve their strength and position in clinical practice: in many cases, the conventional techniques are the

most relevant. All the art of therapeutics is to choose between different available treatment options; the art of clinical research and innovation is to offer new options, among, above and far beyond existing others. The lessons learnt from the pioneers is the only ground for the next generation of researchers.

Other Perspectives

Cryopreservation and banking. The development of cryopreservation techniques and banking, like for cells and simple tissue, of complex vascularized scaffolds will be fundamental to develop both experimental and clinical applications [17].

3D printing – restoration of all lost identities. Modern reconstructive surgery should allow a restoration *ad integrum* of defects, form and function, without secondary morbidities (donor site morbidity with autologous tissues; IS treatment with allografts). As explained in the introduction, facial prosthesis represents the ideal "static" and conservative approach to address a loss of substance, but remains inert and prosthetic materials are perceived by patients as foreign bodies. The 3D-bioprinting approach in VCE shares the concepts and technical steps of prosthetic reconstruction, but based on living tissues.
In this synthetic approach, perfusion-decellularization also represents a way to study and modelize the ECM, hoping later on to become able to reproduce the Nature's genius, by the adequate technologies. The 3D-tools demonstrated in our ear ECM analysis can therefore be seen as pre-analytic models or as blueprints, to later on proceed to a "reverse engineering" technology. For the face, such a customized reconstruction should be performed like a "living" facial prosthesis, that should allow to restore both biological and morphological identities of the disfigured patient (**Figure 9**).

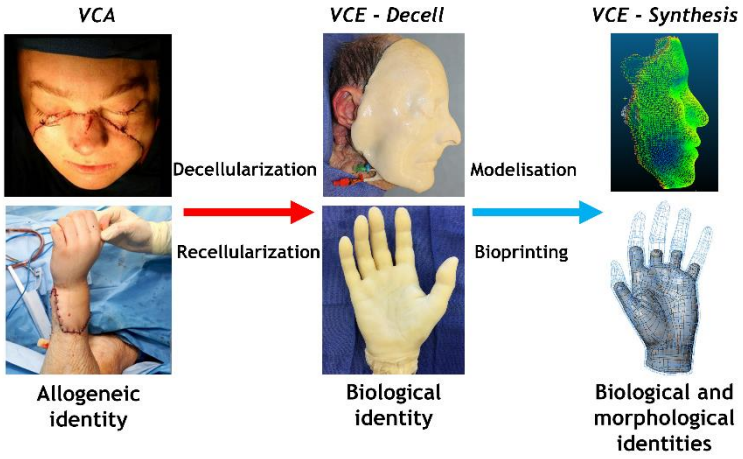

***Figure 9**: Restoring the "lost identities" through VCE: the roads of innovations.*

We are already entering this new era, when any body part will be replaced and designed in a custom-made fashion. What ethical challenges will society have to face, when the technology will be able to modelize and create *de novo* entire organs and body parts? If those body parts may carry on a specific morphological identity, the question of creating a new identity on demand will arise. Should we then be ready to customize VCE face looking to a specific idealized pattern of the human face? Or should we, on contrary, stay on the basic principle of restoring the lost identities, including it disgraces? This belongs to the public debate.

General conclusion: the shifting paradigms

We demonstrated the feasibility of applying the perfusion-decellularization and recellularization technique to vascularized composite tissues of several types, including face and its subunit parts, as well as the finger and the hand, from various sources: small (rat) and large (pig) animal models, and cadaveric human bodies. VCE changes the original allotransplantation scheme, consisting in a direct transfer of the graft from the donor to a recipient, with the addition of an *in vitro* laboratory step, in order to treat the allograft, to switch off its original biological identity, then to reset its new cellular characteristics, aiming to input in the scaffold the recipient's biological identity. VCE is thus a new combination of TE and VCA. By following these new pathways, modern reconstructive surgery should be able to strictly restore the loss of substance/function, through an "on-demand" and customized reconstruction, which should on its counterpart not necessarily integrate the reconstructive ladder at a non-terminal level (with exception to the large defects).

As allotransplantation enabled our tissue engineering approach, the decellularization/recellularization technique will act as a comprehensive step, and an intermediate clinical solution for the patient, waiting for, later on, an accurate full synthesis technology, suitable to efficiently restore all lost identities. The goal of facial reconstruction is to restore all the morphogenetic relationships between each embryonic subunits of the brain and each soft tissue subunits deriving from it, through segmental migrating pathways of neural crest cells. The restoration of the fundamental relation between the face and the brain, expressed in the mimics and requiring to restore the nervous continuity of the Vth and VIIth cranial nerves is the critical factor for the successful functional re-integration of the face graft in the recipient's body scheme. This concept is totally different from the first developed during the pre-history of the face transplantion misconcept, on this time built on describing the transplantation of a cutaneous mask, unsensate and inanimated, on a burn face.

As a matter of fact, VCE may be considered the potential ultimate achievement of Sir Harold Gillies's principle of replacing "like tissue with like tissue". Should a VCE engineered face or hand become possible to be constructed on demand, then transferred and revascularized on the recipient's underlying framework, and finally connected to his brain, trough recellularized nerve scaffolds within the ECM construct, then Science-fiction as dreamed in fantastic books or movies, should become, at last, a true science fact.

More than ever, the surgeon will remain, among all these new technologies, at a central and leading position. He will, following his devoted mission to the patient, be the guardian of the next ethical challenges, to make these scientific and biomedical revolutions remain humanistic progresses.

References

1. Zhao L, Huang L, Yu S, Zheng J, Wang H, Zhang Y. Decellularized tongue tissue as an in vitro model for studying tongue cancer and tongue regeneration. *Acta Biomater*. 2017;58:122-135.
2. Findlay MW, Dolderer JH, Trost N et al. Tissue-engineered breast reconstruction: bridging the gap toward large-volume tissue engineering in humans. Plast Reconstr Surg. 2011;128:1206-1215.
3. Patel MN, Atala A. Tissue engineering of the penis. ScientificWorldJournal. 2011;11:2567-2578.
4. Jank BJ, Xiong L, Moser PT et al. Engineered composite tissue as a bioartificial limb graft. Biomaterials. 2015;61:246-256.
5. Siemionow M, Klimczak A. Advances in the development of experimental composite tissue transplantation models. Transpl Int. 2010;23:2-13.
6. Siemionow M, Kulahci Y. Experimental models of composite tissue allograft transplants. Semin Plast Surg. 2007;21:205-212.
7. Crapo PM, Gilbert TW, Badylak SF. An overview of tissue and whole organ decellularization processes. Biomaterials. 2011;32:3233-3243.
8. Totonelli G, Maghsoudlou P, Garriboli M et al. A rat decellularized small bowel scaffold that preserves villus-crypt architecture for intestinal regeneration. Biomaterials. 2012;33:3401-3410.
9. Bourgine PE, Pippenger BE, Todorov A, Jr., Tchang L, Martin I. Tissue decellularization by activation of programmed cell death. Biomaterials. 2013;34:6099-6108.
10. Choi YC, Choi JS, Kim BS, Kim JD, Yoon HI, Cho YW. Decellularized extracellular matrix derived from porcine adipose tissue as a xenogeneic biomaterial for tissue engineering. Tissue Eng Part C,Methods. 2012;18:866-876.
11. Maxwell GP, Gabriel A. Bioengineered Breast: Concept, Technique, and Preliminary Results. Plast Reconstr Surg. 2016;137:415-421.
12. Bianconi E, Piovesan A, Facchin F et al. An estimation of the number of cells in the human body. Ann Hum Biol. 2013;40:463-471.
13. Badylak S. Perspective: Work with, not against, biology. Nature. 2016;540:S55.
14. Ren X, Moser PT, Gilpin SE et al. Engineering pulmonary vasculature in decellularized rat and human lungs. Nat Biotechnol. 2015;33:1097-1102.
15. Jackson JR, Abolbashari M, Huling J et al. CD31 Antibody Conjugation Improves Re-Endothelialization of Acellular Kidney Scaffolds for Whole Organ Engineering. J Am Coll Surg. 2014;219:S141.
16. Morelon E, Petruzzo P, Kanitakis J et al. Face transplantation: partial graft loss of the first case ten years later. Am J Transplant. 2017;17:1935-1940.
17. Giwa S, Lewis JK, Alvarez L et al. The promise of organ and tissue preservation to transform medicine. Nat Biotechnol. 2017;35:530-542.

APPENDIX

Academic production during thesis period (2013-2017)

GRANTS AND AWARDS

2017: **Annual award for surgical research, sponsored by Brothier Laboratories.** French National Academy of Surgery (ANC), Paris, France.

2017: The Transplantation Society (TTS) Young Investigator Scientific Award. International Society for Vascularized Composite Allotransplantation (ISVCA), Salzburg, Austria.

2017: **Best paper award.** European Association of Plastic Surgeons-Research Council (EURAPS-RC), Pisa, Italy.

2017: **Travel grant.** Prize of the Banque Transatlantique Belgium (CIC).

2015: **Nominative private research grant.** Fonds Dr Gaëtan Lagneaux.

2013-2014: **Nominative private research grant.** Fondation Saint-Luc.

SOCIETIES MEMBERSHIP

Since 2017: The Transplantation Society (TTS), trainee membership.

Since 2017: International Society for Vascularized Composite Allotransplantation (ISVCA), trainee membership.

SCIENTIFIC ARTICLES

Duisit J, Amiel A, Wüthrich T, Taddeo A, Dedriche A, Destoop V, Pardoen T, Bouzin C, Magee D, Vögelin E, Harriman D, Orlando G, Behets C, Rieben R, Gianello P, Lengelé B. Perfusion-decellularization of human ear grafts enables ECM-based scaffolds for auricular vascularized composite tissue engineering –*Under revision.*

Cravedi P, Farouk S, Angeletti A, Edgar L, Tamburrini R, **Duisit J**, Perin L, Orlando G. Regenerative immunology: the immunological reaction to biomaterials. Transpl Int. 2017 Dec;30(12):1199-1208. IF: 3.079

Duisit J, Amiel H, Dedriche D, Behets C, Orlando G, Gianello P, Lengelé B. Face scaffold production in a rat model. Plast Reconstr Surg. 2017 Sep 14; doi: 10.1097/PRS.0000000000003910. [Epub ahead of print]. IF: 3.789

Duisit J, Maistriaux L, Gerdom A, Vergauwen M, Gianello P, Behets C, Lengelé B. Nose and lips graft variants: a subunit anatomical study. Plast Reconstr Surg. 2017 Nov 11; doi: 10.1097/PRS.0000000000004116. [Epub ahead of print]. IF: 3.789

Duisit J, Maistriaux L, Taddeo A, Orlando G, Joris V, Coche E, Behets C, Lerut J, Dessy C, Cossu G, R, Vögelin E, Rieben R, Gianello P, Lengelé B. Bioengineering a human face graft: the matrix of Identity. Ann. Surg. 2017 Nov;266(5):754-764. IF: 8.980

Duisit J, Amiel H, Debluts D, Maistriaux L, Gerdom A, Bol A, Gianello P, Behets C, Lengelé B. Single-artery human ear graft procurement: a simplified approach. Plast Reconstr Surg. 2017 Sep;140(3):599-603. IF: 3.789

Duisit J, Debluts D, Behets C, Gerdom A, Vlassenbroek A, Coche E, Lengelé B, Gianello P. Porcine ear: a new model in large animals for the study of facial subunit VCA. JPRAS Open – DOI 10.1016/j.jpra.2017.01.004.

Duisit J, Orlando G, Debluts D, Maistriaux L, Xhema D, Janssens de Bisthoven Y, Peloso A, Behets C, Lengelé B, Gianello P. Decellularization Of The Porcine Ear Generates A Biocompatible, Non-Immunogenic Extracellular Matrix Platform For Face Subunit Bioengineering. Ann Surg. 2017 Mar 1. doi: 10.1097/SLA.0000000000002181. [Epub ahead of print]. IF: 8.980

Van Steenberghe M, Schubert T, Xhema D, Bouzin C, Guiot Y, Abdelhamid K, Henry M, **Duisit J,** Sinnaeve M, Gianello P. Enhanced biocompatibility and vascular regeneration of bovine/human pericardium after combined chemical/physical treatment in rodents. Journal of Surgical Research. 2018; 222:167-179. [Epub ahead of print]. IF: 2.187

de Beco G, **Duisit J**, Poncelet AJ. Heart transplantation using a donor with partial anomalous pulmonary venous connection and atrial septal defect. Interact Cardiovasc Thorac Surg. 2017 Jun 1;24(6):978-979. IF: 1.857

Peloso A, Katari R, Tamburrini R, **Duisit J**, Orlando G. Glycosaminoglycans as a measure of outcome of cell-on-scaffold seeding (decellularization) technology. Expert Rev Med Devices. 2016 Dec;13(12):1067-1068. IF: 1.784

Delaey P*, **Duisit J***, Behets C, Duprez T, Gianello P, Lengelé B. Specific branches of hypoglossal nerve to genioglossus muscle as a potential target of selective neurostimulation in obstructive sleep apnea: anatomical and morphometric study. Surg Radiol Anat. 2016 Nov;39(5):507-515.* Contributed equally. IF: 1.051

Vanthournhout L, Herman B, **Duisit J**, Château F, Szewczyk J, Lengelé B, Raucent B. Requirements analysis and preliminary design of a robotic assistant for reconstructive microsurgery. Conf Proc IEEE Eng Med Biol Soc. 2015 Aug;2015:4926-30.

INTERNATIONAL PATENT (UCL owner)

Duisit J., Herman B., Gianello P., Lengelé B. (Inventors). WO 2017/202908 A1 - Perfusion-bioreactor and method for processing vascularized composite tissue. Deposit: 25/05/2016. International publication date: 30/11/2017.

ORAL PRESENTATIONS, POSTERS AND CONFERENCE PAPERS

Duisit J, Debluts D, Maistriaux L, Roels T, Behets C, Orlando G, Gianello P, Lengele B. Vascularized human finger decellularization: subunit approach to hand tissue engineering.
Oral presentation: French National Academy of Surgery, Research forum (Paris, 15/12/2017). **Annual award for Surgical Research.**

Duisit J, Maistriaux L, Taddeo A, Tsering Wüthrich, Orlando G, Joris V, Coche E, Behets C, Lerut J, Dessy C, Cossu G, R, Vögelin E, Rieben R, Gianello P, Lengelé B. Bioengineering a human face graft: the matrix of identity.
Poster presentation: ISVCA annual *meeting (Salzburg, 26-27/10/2017).*
The Transplantation Society (TTS) travel grant.

Duisit J, Debluts D, Maistriaux L, Roels T, Gianello P, Lengele B. Vascularized human finger decellularization: subunit approach to hand tissue engineering.
Poster presentation: ISVCA annual meeting (Salzburg, 26-27/10/2017).

Duisit J, Debluts D, Maistriaux L, Roels T, Behets C, Orlando G, Gianello P, Lengele B. Vascularized human finger decellularization: subunit approach to hand tissue engineering.
Oral presentation: 18th congress of the European Society for Organ Transplantation (ESOT, 24-27/9/2017).

Duisit J, Debluts D, Maistriaux L, Roels T, Behets C, Orlando G, Gianello P, Lengele B. Vascularized human finger decellularization: subunit approach to hand tissue engineering.
Oral presentation (Invited speaker): 27th meeting of the European Tissue Repair Society (ETRS, 13-15/9/2017).

Duisit J, Vanthournout L, Herman B, Lengelé B, Raucent B. First steps towards specific robotic assistance in microsurgery: requirements analysis on a rat model and primary design.
Oral presentation:Association Française des Chirurgiens de la Face (AFCF, Honfleur, 22-24/6/2017).

Duisit J, Maistriaux L, Orlando G, Behets C, Gianello P, Lengele B. Bioengineering a human face graft: the matrix of identity.
Oral presentation: Association Française des Chirurgiens de la Face (AFCF, Honfleur,22-24/6/2017).

Duisit J, Maistriaux L, Orlando G, Joris V, Dessy C, Behets C, Gianello P, Lengele B. Bioengineering a human face graft: the matrix of identity.
Oral presentation: 6th triennial congress of the Advanced Digital Technology in Head and Neck reconstruction (ADT) conferences (Amiens, 31/5 – 3/6/2017).

Duisit J, Maistriaux L, Orlando G, Behets C, Gianello P, Lengele B. Bioengineering a human face graft: the matrix of identity.
Oral presentation: 28th annual meeting of the EURAPS (Pisa,25-27/5/2017).

Duisit J, Debluts D, Maistriaux L, Roels T, Gianello P, Lengele B. Vascularized human finger decellularization: subunit approach to hand tissue engineering.
Oral presentation: 6th EURAPS Research Council Annual Meeting (Pisa,24-25/5/2017). **Best Paper Award**

Duisit J, Maistriaux L, Orlando G, Behets C, Gianello P, Lengele B. Bioengineering a human face graft: the matrix of identity.
Oral presentation:24th annual meeting of the European Surgical Association (ESA) (Bucharest,4-6/5/2017).

Duisit J, Orlando G, Behets C, Gianello P, Lengele B. Bioengineered vascularized ear.
Oral presentation: 27th annual meeting of the European Association of Plastic Surgeons (EURAPS, Brussels, 26-28/5/2016).

Duisit J, Orlando G, De Terwangne C, Behets C, Gianello P, Lengelé B. Porcine Ear Extracellular Matrix Scaffolds as a platform for the Bioengineering and Regeneration of Face Subunits.
Poster: EMBO meeting - cell therapy today, hypes and hopes (Manchester, 9-12/9/15).

Vanthournhout L., Herman B., **Duisit J.**, Château F., Szewczyk, J., Lengelé, B., Raucent B. Requirements analysis and preliminary design of a robotic assistant for reconstructive microsurgery.
Conference paper: Proceedings of the 37th Annual International Conference of the IEEE Engineering in Medicine and Biology Society (Milan, 25-28/8/2015).

Debluts D, **Duisit J**, Coche E, Vlassenbroek A, Gianello P, Behets C, Lengelé B. Bases anatomiques et chirurgicales du modèle d'allotransplant auriculaire porcin.
Oral presentation: 97ème Congrès de l'Association des Morphologiste – session jeunes morphologistes (Brussels,31/01/15).

Maistriaux L, **Duisit J**, Gerdom A, Behets C, Lengelé B. De la vascularisation naso-labiale : bases anatomiques de l'allotransplant sous-unitaire du nez.
Oral presentation : 97ème Congrès de l'Association des Morphologiste – session jeunes morphologistes (Brussels,31/01/15).

Delhaye P, **Duisit J**, Mashiach A, Behets C, Gianello P, Lengelé B. Thérapie des apnées obstructives du sommeil : bases morphologiques pour une stimulation ciblée du muscle génioglosse.
97ème Congrès de l'Association des Morphologiste – session jeunes morphologistes (Brussels,31/01/15).

Vanthournhout L, Château F, **Duisit J**, Herman B, Szewczyk, J, Lengelé, B, Raucent B. First steps towards robotic assistance to reconstructive microsurgery.
Conference paper: 13th Belgian Day on Biomedical Engineering (Brussels, 28/11/14).

Vanthournhout L, Herman B, **Duisit J**, Château F, Szewczyk, J, Lengelé, B, Raucent B. Toward user-friendly robotic assistance for enhancing accuracy and safety of reconstructive microsurgery.
Conference paper: 4th Joint Workshop on New Technologies for Computer/Robot Assisted Surgery (Genova, 14-10/10/2014).

SUPERVISED MASTER THESES

Medical students (supervisor): H. Amiel, D. Debluts, L. Maistriaux, P. Delaey.

Louvain School of Engineering students (co-promotor): A. Springuel, J. Legrand, C. Faes.

Institut Paul Lambin (supervisor): S. Lefèvre, M. Célis, A-C Hoang Le Thien, E. Montoya, S. El Hathout.

Haute Ecole Louvain en Hainaut student (co-promotor): V. Keil.

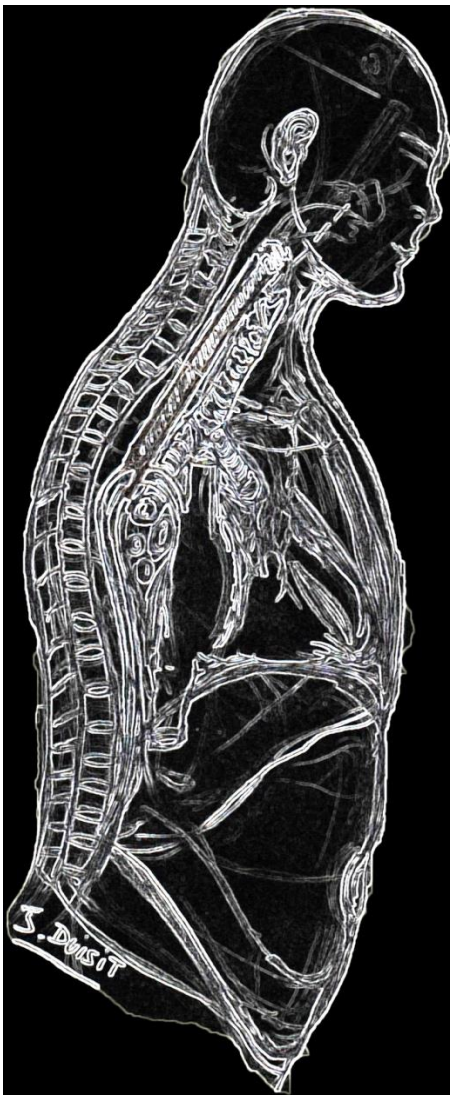
S. DUSIT

(12) INTERNATIONAL APPLICATION PUBLISHED UNDER THE PATENT COOPERATION TREATY (PCT)

(19) World Intellectual Property Organization
International Bureau

(43) International Publication Date
30 November 2017 (30.11.2017)

WIPO | PCT

(10) International Publication Number
WO 2017/202908 A1

(51) International Patent Classification:
C12M 3/00 (2006.01) *A61L 27/36* (2006.01)
A01N 1/02 (2006.01) *C12M 1/00* (2006.01)

(21) International Application Number:
PCT/EP2017/062538

(22) International Filing Date:
24 May 2017 (24.05.2017)

(25) Filing Language: English

(26) Publication Language: English

(30) Priority Data:
16171339.1 25 May 2016 (25.05.2016) EP

(71) Applicant: **UNIVERSITÉ CATHOLIQUE DE LOUVAIN** [BE/BE]; Place de l'Université 1, 1348 Louvain-la-Neuve (BE).

(72) Inventors: **DUISIT, Jérôme**; 4 rue Henri Vandermaelen, 1150 Brussel (BE). **HERMAN, Benoît**; Boterbloemenlaan 14, 3080 Tervuren (BE). **GIANELLO, Pierre**; 9, avenue de la Rochefoucauld, 1330 Rixensart (BE). **LENGELÉ, Benoît**; 8-10 rue de l'ancienne gare, 1380 Lasne (BE).

(74) Agent: **GYI, Jeffrey** et al.; E. Gevaertdreef 10a, 9830 Sint-Martens-Latem (BE).

(81) Designated States *(unless otherwise indicated, for every kind of national protection available)*: AE, AG, AL, AM, AO, AT, AU, AZ, BA, BB, BG, BH, BN, BR, BW, BY, BZ, CA, CH, CL, CN, CO, CR, CU, CZ, DE, DJ, DK, DM, DO, DZ, EC, EE, EG, ES, FI, GB, GD, GE, GH, GM, GT, HN, HR, HU, ID, IL, IN, IR, IS, JP, KE, KG, KH, KN, KP, KR, KW, KZ, LA, LC, LK, LR, LS, LU, LY, MA, MD, ME, MG, MK, MN, MW, MX, MY, MZ, NA, NG, NI, NO, NZ, OM, PA, PE, PG, PH, PL, PT, QA, RO, RS, RU, RW, SA, SC, SD, SE, SG, SK, SL, SM, ST, SV, SY, TH, TJ, TM, TN, TR, TT, TZ, UA, UG, US, UZ, VC, VN, ZA, ZM, ZW.

(84) Designated States *(unless otherwise indicated, for every kind of regional protection available)*: ARIPO (BW, GH, GM, KE, LR, LS, MW, MZ, NA, RW, SD, SL, ST, SZ, TZ, UG, ZM, ZW), Eurasian (AM, AZ, BY, KG, KZ, RU, TJ, TM), European (AL, AT, BE, BG, CH, CY, CZ, DE, DK, EE, ES, FI, FR, GB, GR, HR, HU, IE, IS, IT, LT, LU, LV, MC, MK, MT, NL, NO, PL, PT, RO, RS, SE, SI, SK, SM, TR), OAPI (BF, BJ, CF, CG, CI, CM, GA, GN, GQ, GW, KM, ML, MR, NE, SN, TD, TG).

Declarations under Rule 4.17:
— *of inventorship (Rule 4.17(iv))*

Published:
— *with international search report (Art. 21(3))*

(54) Title: PERFUSION-BIOREACTOR AND METHOD FOR PROCESSING VASCULARIZED COMPOSITE TISSUE

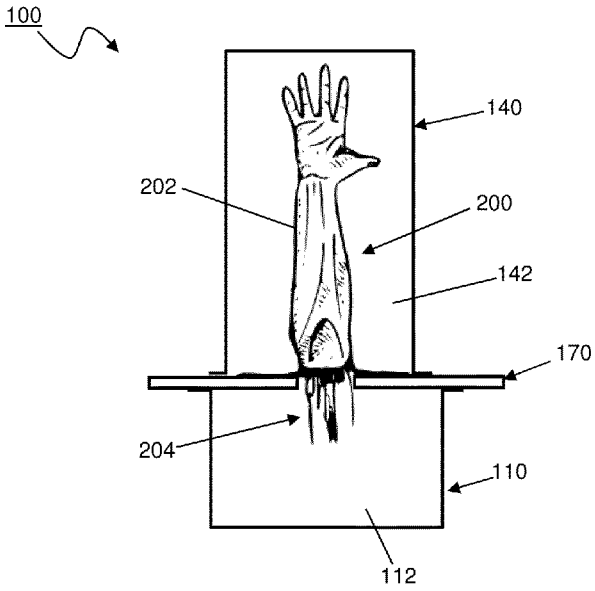

FIG. 4

(57) Abstract: A bioreactor (100) for a vascularized structure (200) is provided comprising a vasculated portion (202) and a vascular pedicle (204), the bioreactor (100) comprising a first void space (112) configured to receive the vascular pedicle (204) optionally contained in a first vessel (110) having a first opening (114), a second void space (142) in fluid contact with at least part of the vasculated portion (202), and a support element (170) for supporting the vascularized structure (200) and fluidly separating the first void space (112) from the second void space (142), comprising an aperture region (176) comprising one or more apertures configured to receive at least part of the vascular pedicle (204).

WO 2017/202908 A1

PERFUSION-BIOREACTOR AND METHOD FOR PROCESSING VASCULARIZED COMPOSITE TISSUE

Field of the invention

Described herein is a perfusion-bioreactor for processing tissue and organs, in particular for a vascularized structure applicable especially in the field of tissue engineering.

Background to the invention

Perfusion-Bioreactors are principally designed for *in vitro* perfusion and regeneration ((re)cellularization) by culturing cells in acellular organs scaffolds such as a heart, liver, kidney and the like for eventual transplantation into a subject. Existing bioreactors typically comprise a liquid vessel and a plurality of ports for exchange of perfusion fluids, however, they have been found to be unsuitable for body parts, such as vascularized composite tissue (VCT, or synonym Composite Tissue Allograft (CTA)), for instance those having multiple layers and interfaces, in particular a skin layer. There is a substantial need for processing VCT, such as limbs, trunk, face and scalp in its larger association, uterus or addressing single layers: simples like skin flap, muscle flap; or complex associations in targeted areas like subunits: ear, nose, lips, eyelids, tongue, fingers, breast, genitalia– for preservation, for perfusion decellularization/recellularization technology or cellularization of synthetic scaffolds. Decellularization is a process of removing native cells from a donor tissue with preserving its extracellular matrix (ECM) and associated biochemical components, generating matrix that can be repopulated (recellularized) with cells from the transplant recipient. This approach avoids or reduces the possibility of transplant rejection by the recipient. The present invention aims to provide a solution to the problem of vascularized composite tissue bioengineering.

Summary of the invention

Described herein is a bioreactor (100) for a vascularized structure (200) comprising a vasculated portion (202) and a vascular pedicle (204), the bioreactor (100) comprising:

- a first void space (112) configured to receive the vascular pedicle (204) optionally contained in a first vessel (110) having a first opening (114),
- a second void space (142) in fluid contact with at least part of the vasculated portion (202),
- a support element (170) for supporting the vascularized structure (200) and fluidly separating the first void space (112) from the second void space (142),

comprising an aperture region (176) comprising one or more apertures configured to receive at least part of the vascular pedicle (204).

The bioreactor (100) may be provided wherein:

- the support element (170) comprises a body provided with a first side (172) adjoining the first void space (112) and a second side (174) adjoining the second void space (142), and wherein the aperture region (176) connects the first side (172) with the second side (174),
- the second void space (142) is contained in a second vessel (140) having a second opening (144) or contained in a gap between the support element (170) and a covering plate.

The support element (170) may further comprise a clamp or more suture anchors configured to fixedly attach at least part of the vasculated portion (202) around a periphery of the aperture region (176) thereby fluidly sealing the aperture region (176).

The first (110) vessel and second vessel (140) or covering plate may be each dismountably attachable to the support element (170). They may be mutually fluidly isolated when the aperture region (176) is sealed.

The first vessel (110) may be further disposed with a sealable access opening (111), for manual access to the vascular pedicle (204).

The first vessel (110) may be further disposed with one or more ports (113) in fluid connection with the first void space (112) for inlet and/or outlet of fluid, of one or more electrically conducting cables, or of one or more flexible cords, optionally some ports being arranged at different distances from the first opening (114) or a different peripheral positions around first vessel.

The second vessel (140) may be further disposed with one or more ports (113) in fluid connection with the second void space (142) for inlet and/or outlet of fluid, of one or more electrically conducting cables, or of one or more flexible cords, optionally some ports on the second vessel (140) being arranged at different distances from the second opening (114) or a different peripheral positions around second vessel.

The support element (170) may be configured to position the aperture region (176) within the first void space (112), and optionally to provide a gap between a wall (118) of the first vessel (110) and the support element (170), optionally the gap having an annular form.

The bioreactor (100) may further comprise a third void space (192) separated from the first (112) or second (142) void space by the support element (170), configured to receive at least a part of the vasculated portion (202) not received by the received by the second void space (142).

Further provided is a use of a bioreactor (100) as described herein, for perfusion of a vascularized structure (200), for decellularization of a vascularized composite tissue, recellularization of a vascularized composite tissue scaffold or for preservation of vascularized composite tissue.

The use may be provided wherein:
- the first void space (112) is configured to contain liquid, and the second void space (142) is configured to contain a gaseous atmosphere or *vice versa*, or
- the first void space (112) and the second void space (142) are each configured to contain a liquid, or
- the first void space (112) and the second void space (142) are each configured to contain a gaseous environment.

Further provided is a method for perfusion of a vascularized structure (200), comprising the steps:

- providing a bioreactor (100) according to any of claims 1 to 9,
- attaching the vascularized structure (200) to the support element (170) such that at least part of the vasculated portion (202) is in fluid connection with the second void space (142) and at least part of the vascular pedicle (204) is disposed in the first void space (112),
- whereby a part of the vascularized structure (200) is sutured and/or clamped over the aperture region (176) to seal it, thereby isolating the first void space (112) from the second void space (142), and
- perfusing the vascularized structure (200) through vasculature of vascular pedicle (204).

Further provided is a kit comprising a bioreactor (100) according to any of claims 1 to 9, wherein there are at least two interchangeable support elements (170), each having a different aperture region (176) size and/or shape.

The kit may further comprise at least two different drawing templates, one for each different support element (170) for marking skin of a donor for harvesting such that the size and shape of the skin harvested is suitable for suturing and/or clamping over the corresponding aperture region (176) size and/or shape of the support element (170).

The vascularized structure (200) according to the use, the method according or the kit according may be a vascularized composite tissue or a vascularized composite tissue scaffold.

Figure Legends

FIG. 1 is a schematic illustration of a cross-section through a first vessel and second vessel of a bioreactor described herein.

FIG. 2 panels **A** and **B** depict respectively plan and side views of a support element as described herein.

FIG. 3 depicts a vascularized structure exemplified as a part of an arm.

FIG. 4 illustrates an assembled bioreactor disposed with a vascularized structure.

FIG. 5 illustrates cross-sectional view of a support element comprising a clamp mating body.

FIG. 6 is a photograph of part of a bioreactor showing the second vessel disposed with the vasculated portion of vascularized structure that is a hand.

FIG. 7 is a photograph of part of a bioreactor showing the first vessel disposed with the vascular pedicle of a vascularized structure that is a hand.

FIG. 8 is an isometric view of an exemplary bioreactor described herein

FIG. 9 is a schematic illustration of a cross-section through an exemplary bioreactor as described herein comprising three void spaces.

FIG. 10 panels **A to D** depict different sizes of drawing template.

FIG. 11 panel **A** depicts a vascularized structure that is a skin flap. Panel **B** depicts the vascularized structure that is the skin flap of panel **A** provided in a bioreactor.

FIG. 12 panel **A** depicts a vascularized structure that is a face comprising a vasculated portion and a vascular pedicle. Panel **B** depicts the vascularized structure that is the face of panel **A** provided in a bioreactor.

FIG. 13 depicts a vascularized structure that is a vagina and uterus comprising a vasculated portion (uterine, vaginal) and a vascular pedicle provided in a bioreactor

FIG. 14 panel **A** depicts a vascularized structure that is an arm disposed in a bioreactor as shown in **FIG. 4**, together with an ancillary support structure that is a cylindrical cage and a further ancillary support structure that is hollow cylindrical projection.

FIG. 14 panel **B** is a section through region B of **FIG. 14** panel **A** depicting a further ancillary support structure that is hollow cylindrical projection around the aperture region and extending from the second side.

FIG. 15 panels **A** to **D** show photographs of a vascularized structure that is a skin flap comprising a vasculated portion and a vascular pedicle mounted on a supporting element.

FIG. 16 panels **A** and **B** show photographs of a vascularized structure (vasculated portion side) that is a nose and surrounding skin mounted on a support element, second side.

FIG. 17 panels **A** and **B** show photographs of a vascularized structure (vasculated portion side) that is an ear and surrounding skin mounted on a support element, second side.

FIG. 18 panels **A** and **B** show photographs of two ancillary support structures that are cylindrical cages.

FIG. 19 panels **A** to **C** show photographs of harvesting a mouth and nose using a drawing template.

Detailed description of invention

Before the present system and method of the invention are described, it is to be understood that this invention is not limited to particular systems and methods or combinations described, since such systems and methods and combinations may, of course, vary. It is also to be understood that the terminology used herein is not intended to be limiting, since the scope of the present invention will be limited only by the appended claims.

As used herein, the singular forms "a", "an", and "the" include both singular and plural referents unless the context clearly dictates otherwise.

The terms "comprising", "comprises" and "comprised of" as used herein are synonymous with "including", "includes" or "containing", "contains", and are inclusive or open-ended and do not exclude additional, non-recited members, elements or method steps. It will be appreciated that the terms "comprising", "comprises" and "comprised of" as used herein comprise the terms "consisting of", "consists" and "consists of".

The recitation of numerical ranges by endpoints includes all numbers and fractions subsumed within the respective ranges, as well as the recited endpoints.

The term "about" or “approximately” as used herein when referring to a measurable value such as a parameter, an amount, a temporal duration, and the like, is meant to encompass variations of +/-10% or less, preferably +/-5% or less, more preferably +/-1% or less, and still more preferably +/-0.1% or less of and from the specified value, insofar such variations are appropriate to perform in the disclosed invention. It is to be understood that the value to which the modifier "about" or “approximately” refers is itself also specifically, and preferably, disclosed.

Whereas the terms “one or more” or “at least one”, such as one or more or at least one member(s) of a group of members, is clear *per se*, by means of further exemplification, the term encompasses *inter alia* a reference to any one of said members, or to any two or more of said members, such as, *e.g.,* any ≥3, ≥4, ≥5, ≥6 or ≥7 etc. of said members, and up to all said members.

All references cited in the present specification are hereby incorporated by reference in their entirety. In particular, the teachings of all references herein specifically referred to are incorporated by reference.

Unless otherwise defined, all terms used in disclosing the invention, including technical and scientific terms, have the meaning as commonly understood by one of ordinary skill in the art to which this invention belongs. By means of further guidance, term definitions are included to better appreciate the teaching of the present invention.

In the following passages, different aspects of the invention are defined in more detail. Each aspect so defined may be combined with any other aspect or aspects unless clearly indicated to the contrary. In particular, any feature indicated as being preferred or advantageous may be combined with any other feature or features indicated as being preferred or advantageous.

Reference throughout this specification to “one embodiment” or “an embodiment” means that a particular feature, structure or characteristic described in connection with the embodiment is included in at least one embodiment of the present invention. Thus, appearances of the phrases “in one embodiment” or “in an embodiment” in various places

throughout this specification are not necessarily all referring to the same embodiment, but may. Furthermore, the particular features, structures or characteristics may be combined in any suitable manner, as would be apparent to a person skilled in the art from this disclosure, in one or more embodiments. Furthermore, while some embodiments described herein include some but not other features included in other embodiments, combinations of features of different embodiments are meant to be within the scope of the invention, and form different embodiments, as would be understood by those in the art. For example, in the appended claims, any of the claimed embodiments can be used in any combination.

In the present description of the invention, reference is made to the accompanying drawings that form a part hereof, and in which are shown by way of illustration only of specific embodiments in which the invention may be practiced. Parenthesized or emboldened reference numerals affixed to respective elements merely exemplify the elements by way of example, with which it is not intended to limit the respective elements. It is to be understood that other embodiments may be utilised and structural or logical changes may be made without departing from the scope of the present invention. The following detailed description, therefore, is not to be taken in a limiting sense, and the scope of the present invention is defined by the appended claims.

The present invention relates to a bioreactor for a vascularized structure. The vascularized structure comprises a vasculated portion and a vascular pedicle. In particular, the bioreactor comprises a first void space configured to receive at least part of the vascular pedicle (and inner part of the VCT if needed). The bioreactor further comprises a second void space configured to receive the at least part of the vasculated portion (other layer compartmentation). The bioreactor further comprises a support element for supporting the vascularized structure and separating the first void space from the second void space, having a body provided with a first side adjoining the first void space and a second side adjoining the second void space, a aperture region comprising one or more through apertures connecting the first side with the second side which aperture region is configured to receive the vascular pedicle therethrough. It may further comprise other inner parts from vasculated portion. The first void space may be contained in a first vessel having a first opening. The second void space may be contained in a second vessel having a second opening, or in a space formed by a flat plate and the support element, in particular an indentation therein. The bioreactor is for *in vitro* perfusion.

The bioreactor allows separation of the vasculated portion from the vascular pedicle allowing them to be maintained in different environments for optimal processing. For instance the vascular pedicle to be immersed in liquid and the vasculated portion exposed to a gaseous environment; allowing for the first time perfusion to be performed under optimal conditions.

The bioreactor has particular utility where the vascularized structure is a body part, such as skin flap, finger, limb and trunks and their subunits, ear, total face, and the like which body part is to be processed for transplantation to a patient, or *in vitro* study model. Typically, processing entails pumping of liquid through an artery or vein of the vascular pedicle, which liquid perfuses into the vasculated portion and whose composition depends upon the requirement (*e.g.* decellularization, recellularization, preservation). According to one aspect, the processing is perfusion. The perfusion may be machine perfusion. By perfusion, it is meant passing liquid into the vasculated portion via the vascular pedicle; typically liquid enters through artery(ies) and drains via vein(s). According to another aspect, the processing is direct injection. Processing may be a combination of perfusion and direct injection.

The bioreactor may be used for decellularization of a vascularized composite tissue, for recellularization of a decellularized vascularized composite tissue scaffold or for cellularization a vascularized synthetic scaffold, or for preservation of native or regenerated vascularized composite tissue.

“Decellularization” refers to a process whereby cells are removed from a vascularized composite tissue, typically by perfusion through the vascular pedicle with one or more suitable decellularization liquids, leaving a tissue scaffold that is an extracellular matrix that provides a mechanical and biochemical support. “Recellularization” refers to a process whereby a decellularized vascularized composite tissue scaffold or a vascularized synthetic scaffold is at least partially repopulated with cells, by perfusion through the vascular pedicle and/or by direction injection and/or by topical application. The cells become seeded in tissue layers. The cell may be differentiated, undifferentiated (*e.g.* stem) cells, genetically engineered cells, synthesised cells or any type of cell.

The inventors have recognised that a separation or compartmentalisation of the vascularized structure, for instance, a separation of the vascular pedicle from the vasculated portion or a separation of an inner part associated with the vascular pedicle

from an outer part (see later below) that the bioreactor provides, improves handling and properties of the vascularized structure. Furthermore, support of the vascularized structure reduces mechanical stresses and damage to the delicate and often fine tissue. It protects the vascular pedicle by housing it in a vessel separate from the vasculated portion. Compared with classic organ transplantation (*e.g.* kidney, liver) where the trailing vasculature is substantial and robust, vascularized structures have typically a thin and fragile pedicle and it requires a substantially different approach. In particular where the vascularized structure includes a skin portion such as in a finger, arm or face, the vasculated portion may be contained within the first vessel under different conditions (*e.g.* gaseous) compared with the vascular pedicle (*e.g.* liquid). It is a departure from classical perfusion technology which typically utilises a single vessel. The inventors have recognised the benefit of maintaining separate environments, in particular, the need to retain the vascular pedicle in a liquid environment that may be different from skin that should not be liquid immersed for an optimum transplant tissue.

The bioreactor refers to a device that provides void spaces for the vascularized structure to provide an optimum environment for carrying out various types of procedures. It may allow a control of the composition of the environment, for instance, composition of a gas or liquid, temperature, humidity, mechanical and/or electrical stimulation. The bioreactor may be used for procedures such as perfusion, machine perfusion, preservation, and injection. The bioreactor may be used to conduct *in vitro* or *in vivo* (*e.g. in situ* regeneration of body parts) procedures. The bioreactor may be configured for use in an incubator, for instance, for control of an external environment. The bioreactor may be provided with a temperature-control jacket. The bioreactor may be provided with a fluid agitation means (*e.g.* a stirring fan or bar) for even distribution of fluid contain in one or more of the void spaces. The dimensional orientation of the bioreactor may be fixed or continuously adjustable.

The vascularized structure refers to any type of structure, including synthetic structures, that comprises a vasculated portion and a vascular pedicle. By vascularized, it is meant that the vasculated portion is provided with one or more of arteries, veins, lymphatic vessels, nerves (*e.g.* motor, sensory) which are associated with tissue types in the vasculated portion.

Examples of vascularized structures include vascularized composite tissue (VCT) (*e.g.* limb or part thereof such as an arm or finger ear, lip, tongue, face, cheek, nose),

vascularized decellularized composite tissue (*e.g.* decellularized limb or part thereof such as an arm or finger ear, lip, tongue, face, cheek, nose), vascularized recellularized composite tissue (*e.g.* recellularized limb or part thereof such as an arm or finger ear, lip, tongue, face, cheek, nose), vascularized synthetic scaffold (*e.g.* 3D printed limb or part thereof such as an arm or finger ear, lip, tongue, face, cheek, nose), and organs for transplant (e.g. liver, kidney, heart for allotransplatation), synthetic organ.

The vascular pedicle typically comprises trailing vasculature *i.e.* an artery and/or vein for connection at one end to an external conduit for the inlet and/or outlet of perfusion fluid and which leads at the other end to the vasculated portion. It may further comprise a lymphatic vessel and/or a nerve (*e.g.* motor, sensory). The vascular pedicle may further comprise bone and other tissue such as fat (adipose) tissue, muscle, and/or tendon.

The vasculated portion is typically the substantial part of the vascularized structure and is may be vascularized composite tissue. It may equally be a decellularized vascularized composite tissue scaffold, a recellularized vascularized composite tissue scaffold, or a vascularized synthetic scaffold. The vasculated portion may comprise an organ.

Vascularized composite tissue refers to tissue having more than one tissue type associated with non-cellular material such as extracellular matrix, which tissue types are typically disposed in layers such as in an arm (containing skin, adipose tissue, tendons, muscle, bone), and ear (containing skin, adipose tissue, cartilage). Other examples of vascularized composite tissue include the face, a finger, a tongue or a lip, and the like.

Decellularized vascularized composite tissue scaffold refers to a structure, typically extracellular matrix, resulting from decellularization of vascularized composite tissue. Recellularized vascularized composite tissue scaffold refers to a structure resulting from recellularision of decellularized vascularized composite tissue. Vascularized synthetic scaffold refers to a scaffold that has been formed by a process other than decellularization, for instance, by 3D printing. The present bioreactor is suitable for use with all types of vascularized structure. The vascularized structure may be from a human or animal (*e.g.* mouse, rat, pig). It may have a synthetic origin.

In some cases vascularized structure may have an inner part and an outer part, the inner part referring to that revealed by a cross section of the vascularized structure and contained within an exterior layer such as skin or epithelium and the outer part being

represented by the exterior layer. The inner part is in connection with the vascular pedicle. It is an aspect that the support element separates the inner part from the outer part; the inner part may be in fluid contact with the first void space, and the outer part may be in fluid contact with the second void space. In some cases, the inner part is contained within the first vessel, and the outer part contained within the second vessel.

The shape of vascularized structure may be essentially flat or "surfacic" wherein the vasculated portion has a height dimension that is smaller than a width dimension or has a low overall height, such as equal to or less than 2 cm. Examples of surfacic vascularized include a skin flap. Alternatively a shape of vascularized structure may be projection-like or "cylindric" (cylinder-like) wherein the vasculated portion has a height dimension that is greater than a width dimension or has a longitudinal height compared, such as greater than 2 cm. Examples of cylindric vascularized include an arm or finger. The surfacic or cylindric vascularized structure may have an influence of the second void space, in particular whether the second void space is contained in a vessel (*e.g.* for limb) or contained within a recess of the structural element (*e.g.* for a skin flap).

A vascularized structure may be typed according to the number of different exterior tissue-type surfaces *i.e.* number of different epithelia. An exterior tissue-type surface is one that can abut with the external atmosphere (*e.g.* skin) or with an interior passage or orifice or cavity (*e.g.* lip, vagina). A monophasic type of vascularized structure has predominantly one type of exterior tissue-type surface; such vascularized structure typically have an exterior tissue-type surface that is skin and includes a limb such as a finger, arm. A biphasic type of vascularized structure has predominantly two types of exterior tissue-type surfaces; for instance a lip has a skin (keratinized epithelia) exterior surface and a non-keratinized stratified squamous epithelium exterior surface that lines the oral cavity. All vascularized structures comprise the vascular pedicle.

The first void space is configured to receive the vascular pedicle. The first void space is contained in a first vessel having a first opening. The first void space or first vessel is configured for holding a fluid, for instance a liquid. The first vessel may be disposed such that a longitudinal axis has an essentially vertical orientation (as shown in **FIG. 4**). The first vessel may be disposed such that a longitudinal axis has an essentially horizontal orientation (as shown in **FIG. 9**). The first vessel may have a cylindrical outer shape. The first opening may have a circular shape. The first vessel preferably has a first vessel base

and a first vessel side wall extending from the first vessel base. The first vessel base may be dismountable.

The first vessel side wall and base define the first opening and first void space. The first vessel side wall may be disposed with one or more ports in fluid connection with the first void space. The ports may be configured for inlet and/or outlet of fluid, tubing, or one or more electrically conducting cables for electrical stimulation of at least part of the vasculated portion, or one or more flexible cords for mechanical stimulation (e.g. stretching). The cord may be made from a single thread or multiple threads woven together. Some of the ports may be arranged at the same or different distances from the first opening. Some of the ports may be arranged at the same or different peripheral (*e.g.* radial) positions around the side wall. The ports provide a self-contained bioreactor by permitting exchanges of fluid that control the environment of the respective void spaces, for instance, a control of temperature, gas levels (*e.g.* CO_2, NO), immersion fluid composition, of waste products and the like. It is as aspect of the invention that the bioreactor is configured for use in an incubator.

The vessel may be provided with a stimulation unit, for simulation of the vasculated portion and/or of the vascular pedicle.The stimulation unit may be provided inside and/or outside the first void space. The stimulation unit may be configured for providing mechanical stimulation; it may comprise one or more transmission elements (*e.g.* a rod, a flexible cord) for transmission of mechanical force such as a tension, compression and/or torque through the support element aperture region and into the vasculated portion. The stimulation unit may in addition or alternatively be configured for providing electrical stimulation; it may comprise one or more electrodes for transferring electrical signals to the vasculated portion for instance directly or via a nerve.

The first vessel, in particular the first vessel side wall may be disposed with a sealable access opening *i.e.* an access window to manual allow access to the first void space. The sealable access opening allows a user to connect manually tubing to the vascular pedicle for instance. It is preferably dimensioned for manual access, for instance, by fingers or hand. The sealable access opening may have any suitable shape, for instance, oval, circular or rectangular. The sealable access opening is sealable against fluid ingress by a sealing cover. The sealing cover is configured for sealing and dismountable attachment to the sealable access opening.

The first vessel may be provided with a first rim around the first opening for sealing attachment of the support element. The first rim may form an essentially planar region that sealingly engages with a co-operating region of the support element. The first rim may be provided with one or more holes or slots for attachment of a clamping device such as a nut and bolt; complementary holes or slots may be provided in the support element which align with those of the first rim.

The first void space is configured to receive the vascular pedicle, as shown for instance, in **FIG. 4**. The first void space may be in fluid connection with an inner part of the vascularized structure. The first void space may be configured to receive at least the vascular pedicle. The first void space may be configured further to receive part of the vasculated portion, for example, in the case of a vagina and uterus as shown in **FIG. 13** wherein, a first vessel contains the vagina and uterus in the first void space, the second void space of the second vessel is in fluid connection via an orifice (vagina) with the inside of the uterus, and the support element sealingly separates the first and second void spaces by clamping around a tissue flap.

The first vessel may be made from any suitable material or materials. Typically, the first vessel is made substantially from a corrosion resistant material such as polycarbonate, glass, stainless steel or titanium. Preferably the vessel is made substantially from a transparent material such as polycarbonate or glass. The sealing cover may be made from the same material or from a different material, for instance, from stainless steel. The first vessel may be provided with a temperature regulating means, such as a temperature control jacket.

In use, the first vessel is typically provided with a liquid for immersion of the vascular pedicle during perfusion. The tubing is disposed though one or more of the ports for perfusion of the vascularized structure. The first vessel dedicated to immersion of the vascular pedicle and inner part during perfusion provides a culture medium saving and a safe pedicle handling, compared with a mono-compartmental device where the whole scaffold/organ is necessarily immersed.

The second void space is configured to be in fluid connection with at least part of the vasculated portion of the vascularized structure. The second void space may be in fluid connection with substantially all of the vasculated portion. The second void space may be in fluid connection with a phase of the vasculated portion. The second void space may be

in fluid connection with the outer part of the vascularized structure. The second void space may be in fluid connection with an orifice of the vasculated portion; it may further be in fluid connection with a cavity accessed by the orifice.

The second void space may be configured to receive at least part of the vasculated portion of the vascularized structure. The second void space may be configured to receive substantially all of the vasculated portion. The second void space may be configured to receive a phase (*e.g.* skin-associated volume of scaffold) of the vasculated portion (see for instance **FIG. 4**). The second void space may be configured to receive an outer part of the vascularized structure. The second void may be configured to receive an orifice of the vasculated portion. As described above in the case of a vagina and uterus as shown in **FIG. 13** wherein, a first vessel contains the vagina and uterus in the first void space, the second void space of the second vessel is in fluid connection via an orifice (vagina) with the inside of the uterus, and the support element sealingly separates the first and second void spaces by clamping around a tissue flap. Where the vascularized structure is "surfacic", the second void space will have a corresponding low height dimension; it may be contained within a recess of the support element. Where the vascularized structure is "cylindric", the second void space will have a corresponding height dimension; it may be contained within the second vessel in communication with the support element.

The second void space may be contained in a second vessel having a second opening. The second void space may be contained contained in a gap between the support element and a covering plate; it is typical where the vascularized structure is essentially planar such as a tissue flap (see for instance **FIG. 15** panels A to D). The second void space or second vessel is configured for holding a fluid, for instance a liquid or gas. The second vessel may be disposed such that a longitudinal axis has an essentially vertical orientation (as shown in FIG. 4), an essentially horizontal orientation (as shown in **FIG. 9**), or in any orientation. The orientation may influence pressure within the vascularized structure. The second vessel may have a cylindrical outer shape. The second opening may have a circular shape. The second vessel preferably has a second vessel base and a second vessel side wall extending from the second vessel base. The second vessel base may be dismountable.

The second vessel side wall and base define the second opening and second void space. The second vessel side wall may be disposed with one or more ports in fluid connection with the second void space. The ports may be configured for inlet and/or outlet of fluid

(*e.g.* gas), tubing, or one or more electrically conducting cables, or one or more flexible cords for mechanical stimulation (e.g. stretching). The cord may be made from a single thread or multiple threads woven together. The ports may be arranged at different distances from the second opening. Some of the ports may be arranged at the same or different peripheral (*e.g.* radial) positions around the side wall.

The second vessel may be provided with a second rim around the second opening for sealing attachment of the support element. The second rim may form an essentially planar region that sealingly engages with a co-operating region of the support element. The second rim may be provided with one or more holes or slots for attachment of a clamping device such as a nut and bolt; complementary holes or slots may be provided in the support element which align with those of the second rim.

As mentioned previously, the vessel may be provided with a stimulation unit, for simulation of the vasculated portion. The stimulation unit may be provided inside and/or outside the second void space. The stimulation unit may be configured for providing mechanical stimulation; it may comprise one or more transmission elements (*e.g.* a rod, a flexible cord) for transmission of mechanical force such as a tension, compression and/or torque to the vasculated portion. The stimulation unit may in addition or alternatively be configured for providing electrical stimulation; it may comprise one or more electrodes for transferring electrical signals to the vasculated portion for instance directly.

The second vessel may be made from any suitable material or materials. Typically, the second vessel is made substantially from a corrosion resistant material such as polycarbonate, glass, stainless steel or titanium. Preferably the second vessel is made substantially from a transparent material such as polycarbonate or glass. The second vessel may be provided with a temperature regulating means, such as a temperature control jacket.

In use, the second void space is typically provided with a fluid for immersion of the vasculated portion during perfusion. The fluid may comprise substantially a gas in some circumstances, for instance, when the vasculated portion has a skin layer in the case of a limb for example. The fluid may comprise substantially a liquid in other circumstances, for instance, when the vasculated portion contains a layer or phase that is normally in liquid contact, for instance, inside with cheek or lip. The size and/or shape of the second vessel

may be adapted according to the vasculated portion, for instance, a longer second vessel might be utilised for a limb such as an arm compared with an ear.

It is an aspect of the invention that the bioreactor comprises one or more further void spaces. Each further void space is contained in a separate further vessel having an opening. In particular, where the vascularized structure is biphasic, the second vessel receives a first exterior tissue type and the further vessel receives the second tissue tissue type. As shown in **FIG. 9**, the bioreactor is disposed with three separate compartmentalised void spaces.

The support element serves to provide compartmentalisation (air and/or watertight) *i.e.* a separation of the void spaces (*e.g.* first void space from second void space), and mechanical support to the vascularized structure. The support element comprises a body provided with a first side adapted for covering the first opening, a second side adapted for covering the second opening, a aperture region comprising one or more through apertures connecting the first side with the second side which aperture region is configured for the passage of at least part of, preferably all of the vascular pedicle therethrough. The first side may be configured for sealingly covering the first opening to prevent the passage of fluid across the support element when the aperture region is sealed-off. The second side may be configured for sealingly covering the second opening to prevent the passage of fluid across the support element when the aperture region is sealed-off. Where fluidly sealing or fluidly separating is mentioned herein, it means sealing or separating to prevent to the passage of fluid

The body of the support element provides a mechanical support for the vasculated portion, for instance, the peripheral edge of the aperture region may support the weight of the vasculated portion when it is disposed on the second side. The body of the support element may further comprise one or more ancillary supporting structures, for instance a hollow cylindrical projection around the aperture region. It may extend from the first side of the support element. It may extend from the second side of the support element, as shown, for instance, in **FIG. 14B**; such ancillary supporting structure may be configured to provide upright support for the arm from within (under the skin of) the arm. Another example of an ancillary support structure is an outer cage formed, for instance, from a hollow cylinder disposed around the aperture region. It may project from the first side of the support element. It may project from the second side, as shown, **FIG. 14A**; such ancillary supporting structure may be configured to provide upright support for the arm

from outside (over the skin of) the arm. Another example of an ancillary support structure is relief structure formed, for instance, from a mesh that covers the aperture region. It may project from the first side of the support element. It may project from the second side of the support element. Such ancillary supporting structure may be configured to provide support and give shape to flaccid vasculated portion such as a face. The relief-type ancillary support structure may custom made. It may be 3D printed. The ancillary supporting structure may be in permanent attachment to the support element body or may be dismountably attached to the support element body.

The body of the support element may be disposed with one or more suture anchors that provide a point for suturing the vascularized structure, preferably the vasculated portion to the support element. A suture anchor may take the form of a hook on a surface of the body or a hole that passes through the body. Suturing the vascularized structure, preferably the vasculated portion may seal the one or more apertures of the aperture region. The seal is preferably fluidic. The aperture region may be sealed-off using the vasculated portion. For instance, when the vascularized structure is an ear, the ear and skin surrounding the ear fit over the aperture region and when clamped thereover effectively seal the aperture region to prevent the passage of fluid across it. The vascularized structure in particular the vasculated portion thus functions as a gasket. The ancillary supporting structures (*e.g.* scaffolds/VCT) may be specifically harvested/designed with an extra cutaneous portion to facilitate a sealing function.

Where there are three or more void spaces, the support element may further comprise a further body containing a further aperture region which further body separates a different pair of void spaces. The further body may be separate or an extension of the body. An example of a bioreactor containing 3 void spaces is shown in **FIG. 9**.

According to one aspect, the support element body is shaped to provide an annular peripheral gap (e.g. **FIG. 5**, 179). The gap may be present on the first side of the support element body. The gap may be created by lowering the position of the aperture region relative to the edge of the support element body; thus the support element body may be further lowered into the first void space compared with the support element body, thus forming an annular peripheral gap. The support element may be configured to position the aperture region within (*e.g.* 1 – 3 cm into) the first void space. A height of the gap may be equal to an axial distance between the first opening and the aperture region. The height of the gap may be 1 – 3 cm. The annular peripheral gap may be in fluid contact with a port

present in the first side wall, allowing exchange of gases between the annular peripheral gap and the exterior environment.

The support element may further comprise a clamp configured to clamp at least part of the vasculated portion around a periphery of the aperture region thereby sealing the one or more apertures of the aperture region. The seal is preferably fluidic. The clamp may comprise a mating body that engages with the support element body around periphery of the aperture. Where the aperture region is circular, the mating body may comprise a ring (annular) shape. The mating body may be provided with one or more holes or slots for receiving a threaded bolt; the support element body may be provided with one or more threaded holes for engagingly receiving the threaded bolt. The mating body may engage with a first side or a second side of the support element body. The mating body may engage with an ancillary supporting structure of the support element body, for instance a hollow cylindrical projection around the aperture region and extending from the second side, as shown, for instance, in **FIG. 14B**.

The support element is dismountable from the bioreactor. It may be interchanged for a support element having a different size and/or shape of aperture region. One aspect of the invention provides a kit comprising bioreactor as defined herein and a plurality of different support elements each having a different size and/or shape of aperture region. The interchangeability allow the same bioreactor to be adapted for use with a large variety of diverse vascularized structures, for instance, a face, ear, finger arm etc. or origins such as small or large animals for a same VCT type.

It is an aspect of the invention to provide a drawing template corresponding to the aperture region size and/or shape. The drawing template is used to draw an outline on the donor patient for excising vascularized structure to be harvested. Where the aperture region comprises a circular aperture, the drawing template may also be circular or annular, and define a circular region for marking the donor skin that is larger than the aperture region. The larger size allows clamping to the support structure around the periphery of the aperture region. One aspect of the invention provides a kit comprising bioreactor as defined herein and a plurality of different support elements each having a different size and/or shape of aperture region, and a plurality of drawing templates each complementary to a support element aperture region for marking a boundary for excision of the vascularized structure to be harvested such that it covers the complementary support element aperture region.

In one configuration, the support element is essentially planar having a first and second side which each sealingly covers the first and second opening respectively, more specially a respective first or second rim. The support element may be provided with one or more holes or slots for attachment of a clamping device such as a nut and bolt; complementary holes or slots may be provided in the first and/or second vessel, in particular in a first and/or second rim respectively which align with those of the support element. The support element comprises an aperture region containing a circular aperture through which the vascular pedicle passes, and an annular clamp for attaching the vasculated portion to the support element such that it seals the circular aperture.

The bioreactor may be provided with one or more additional supporting structures, configured to support the vascularized portion and/or the vascular pedicle. The additional supporting structure is preferably dismountable from the bioreactor. The additional supporting structure may be dismountably attachable to the supporting element, to the first vessel or to the second vessel. According to one aspect the additional supporting structure comprises a rod supported by the first base configured to extend through the first void space, the aperture region and at least part of the first void space; such a rod may be useful for supporting a longitudinal vasculated portion such as a limb (*e.g.* part of an arm or leg).

The present invention further provides a use of a bioreactor as described herein for perfusion of a vascularized structure. The present invention further provides a use of a bioreactor as described herein for decellularization of a vascularized composite tissue. The present invention further provides a use of a bioreactor as described herein for recellularization of a vascularized composite tissue scaffold. The present invention further provides a use of a bioreactor as described herein for preservation of vascularized composite tissue.

The present invention further comprises a method for perfusion of a vascularized structure, comprising the steps:

- providing a bioreactor as described herein,
- attaching the vascularized structure to the support element such that at least part of the vasculated portion is in fluid connection with the second void space and at least part of the vascular pedicle is disposed in the first void space,

- whereby a part of the vascularized structure is clamped over the aperture region to seal it, thereby isolating the first void space from the second void space, and
- perfusing the vascularized structure through the vascular pedicle.

The present invention further comprises a method for perfusion of a vascularized structure, comprising the steps:

- providing a bioreactor as described herein,
- attaching the vascularized structure to the support element such that at least part of the vasculated portion is disposed in the second void space and at least part of the vascular pedicle is disposed in the first void space,
- whereby a part of the vascularized structure is clamped over the aperture region to seal it, thereby isolating the first void space from the second void space, and
- perfusing the vascularized structure through the vascular pedicle.

The bioreactor may be use for perfusion of all types of vascularized structures such as

- Vascularized composite tissue Allografts (*e.g.* limb or part thereof such as an arm, ear, lip, tongue, finger, face, cheek, nose),
- Vascularized decellularized composite tissue (*e.g.* decellularized limb or part thereof such as an arm or finger, ear, lip, tongue, face, cheek, nose),
- Vascularized recellularized composite tissue (*e.g.* limb or part thereof such as an arm or finger, ear, lip, tongue, face, cheek, nose),
- Vascularized synthetic scaffold (*e.g.* 3D printed limb or part thereof such as an arm or finger, ear, lip, tongue, face, cheek, nose),
- Synthetic organs.

The vascularized structure may be of any size of volume, or any layer composition (e.g. skin, adipose tissue, muscle, cartilage, bone, mucosa), or vascularized layer. It may be used to perform decellularization, recellularization, preservation, muscular stimulation (e.g. electrical, mechanical electromechanical).

Description of the Figures

FIG. 1 is a schematic illustration of a cross-section through a first vessel (110) and second vessel (140) of a bioreactor presently described. The first vessel (110) has a first base (116) and first side wall (118) that defines a first void space (112) and a first vessel opening (114). The second vessel (140) has a second base (146) and second side wall (148) that defines a second void space (142) and a second vessel opening (144).

FIG. 2 panels **A** and **B** depict respectively plan and side views of a support element (170) as described herein. The support element (170) has a body (178) that is circular and disposed with a first side (172) that closes over the first opening (114) and a second side (174) that closes over the second opening (144). The body (178) is provided with an aperture region (176) connecting the first side (172) with the second side (174).

FIG. 3 depicts a vascularized structure (200) exemplified as a part of an arm. The substantive part of the arm (hand and lower arm) form the vasculated portion (202) while elements such as arteries (229), veins (228), nerves (226) and lymphatic vessels (220) that supply the vasculated portion (202) in addition to residual muscle (222) and bone (224) form the vascular pedicle. The skin flap (230) that will form an eventual sealing gasket is also depicted.

FIG. 4 illustrates the bioreactor (100) described herein wherein the vasculated portion (202) of the vascularized structure (200) is disposed in the second void space (142) of the second vessel (140) and vascular pedicle (204) is disposed in the first void space (112) of the first vessel (110), separated across (compartmentalised) and supported by the support element (170).

FIG. 5 illustrates cross-sectional view of a support element (170) as described herein further comprising a clamp mating body (180) that is an annular ring co-operating with a part of the body (178) of the support element (170). The support element (170) is shown itself clamped between a first rim (119) of the first vessel (110) and a second rim (149) of the second vessel (140). An annular peripheral gap (179) is formed by lowering the aperture region (176) relative to the peripheral edge of the support element body (178).

FIG. 6 is a photograph of part of a bioreactor showing the second vessel (140) wherein a vasculated portion (202) of vascularized structure (200) that is a hand is disposed in the second void space (112). The hand is supported by the supporting structure (170) and is clamped to a body of the supporting structure (170) using a clamp mating body (180). In this example, the second vessel (140) has a removable base that has been dismounted from the second side wall.

FIG. 7 is a photograph of part of a bioreactor showing the first vessel (110) wherein a vasculated portion (202) of vascularized structure (200) that is a hand is supported by and

clamped to the supporting structure (170), and the vascular pedicle (204) of vascularized structure (200) is disposed in the first vessel (110). The first side wall (118) is provided with sealable access opening (111) for manual access to the first void space in particular to the vascular pedicle (202). The first side wall (118) is further provided with a plurality of ports (113) in fluid connection with the first void space (112). Also depicted is an upper port (113') in fluid connection with the annular peripheral gap (see FIG. 5, 179); a filter (117) is attached to retain sterility.

FIG. 8 is an isometric view of an exemplary bioreactor (100) described herein showing the first vessel (110) having the first side wall (118) provided with sealable access opening (111) for manual access to the first void space covered with a sealing cover (115). The first side wall (118) is further provided with a plurality of ports (113, 113') in fluid connection with the first void space (112). The second vessel (140) has the second side wall (148) and a dismountable base (149). The first side wall (118) is further provided with a plurality of ports (113, 113') in fluid connection with the first void space (112). Between the first (110) and second (140) vessels is the support element (170).

FIG. 9 is a schematic illustration of a cross-section through an exemplary bioreactor (100) as described herein comprising three void spaces (112, 132, 192), each respectively contained in a first (110), second (140) and third (190) vessel. The first void space (112) configured to receive the vascular pedicle, the second void space (142) configured to receive a part of the vasculated portion and the third void space (192) is configured to receive a remainder of the vasculated portion. A supporting element (170) separates the respective void spaces; a first body (174) of the supporting element (170) separates the first (112) and second (142) void spaces and a second body (174') of the supporting element (170) separates the second (142) and third (192) void spaces. A first aperture region (176) provided in the first body (174) is dimension to receive the vascular pedicle. A second aperture region (176') provided in the second body (174') is dimensioned to receive a part of the vasculated portion.

FIG. 10 panels **A to D** depict different sizes of drawing template (large to small), each drawing template being an annular ring.

FIG. 11 panel **A** depicts a vascularized structure (200) that is a skin flap comprising a vasculated portion (202) and a vascular pedicle (204).

FIG. 11 panel **B** depicts the vascularized structure (200) that is the skin flap of panel **A** provided in a bioreactor (100). The vasculated portion (202) is disposed in the second vessel (140) and a vascular pedicle (204) is disposed in the first vessel (110). The respective void spaces of the first (110) and second (140) vessels are sealing separated by the support element (170).

FIG. 12 panel **A** depicts a vascularized structure (200) that is a face comprising a vasculated portion (202) and a vascular pedicle (204).

FIG. 12 panel **B** depicts the vascularized structure (200) that is the face of panel **A** provided in a bioreactor (100). The vasculated portion (202) is disposed in the second vessel (140) and a vascular pedicle (204) is disposed in the first vessel (110). The respective void spaces of the first (110) and second (140) vessels are sealing separated by the support element (170).

FIG. 13 depicts a vascularized structure (200) that is a vagina and uterus comprising a vasculated portion (202, 208 (uterine), 210 (vaginal)) and a vascular pedicle (204) provided in a bioreactor. The majority of the vasculated portion (202) and the vascular pedicle (204) are disposed in the first vessel (110). A part of the vasculated portion (202) is disposed in the second vessel (140). An orifice (206) connects the uterine cavity (212) to the second void space (142) of the second vessel (140).

FIG. 14 panel **A** depicts a vascularized structure (200) that is an arm disposed in a bioreactor (100) as shown in **FIG. 4**, together with an ancillary support structure that is a cylindrical cage (260) for mechanically supporting the exterior of the arm, akin to an exterior scaffold. Panel **B** depicts a further ancillary support structure that is hollow cylindrical projection (262) around the aperture region (176) and extending from the second side. Panel **B** further depicts a mating body (182) of a clamp, for clamping a skin flap to the support element (170) thereby sealing the aperture region (176).

FIG. 15 shows photographs of a vascularized structure (200) that is a skin flap comprising a vasculated portion (202) and a vascular pedicle (204) mounted on a supporting element (170). Panel **A** shows the vasculated portion (202) attached to the second side (174) of the supporting element (170) using sutures. Panel **B** shows the vasculated portion (202) clamped over the aperture using a mating body (180); the skin side of the flap would be exposed to the second void space. Panel **C** shows the vascular pedicle (204) passed

through the aperture region. Panel **D** shows the vasculated portion (202) after removal of the mating body (180).

FIG. 16 shows photographs of a vascularized structure (vasculated portion (202) side) that is a nose and surrounding skin mounted on a support element (170), second side (174). Panel **A** is prior to clamping, in Panel **B**, the clamp mating body (180) has been applied.

FIG. 17 shows photographs of a vascularized structure (vasculated portion (202) side) that is an ear and surrounding skin mounted on a support element (170), second side (174). Panel **A** is prior to clamping, in Panel **B**, the clamp mating body (180) has been applied, and further an ancillary support structure that is a cylindrical cage (262) is depicted.

FIG. 18 shows photographs of two ancillary support structures that are cylindrical cages (260, 262). In Panel **A**, an inner cage (260) is shown, Panel **B**, an outer cage (262) is shown mounted in the bioreactor (100).

FIG. 19 show photographs of harvesting a mouth and nose using a drawing template. In Panel **A**, a drawing template (280) this is an annular ring is applied to the face region of the head (210) so that the hole of the ring covers the nose and mouth. Lines (282) are drawn on the facing using the inner and outer edge of the template as a guide (Panel **B**). The vascularized structure (200) is harvested and placed over the aperture region of the support element (170) (Panel **C**).

*

Claims

1. A bioreactor (100) for a vascularized structure (200) comprising a vasculated portion (202) and a vascular pedicle (204), the bioreactor (100) comprising:

- a first void space (112) configured to receive the vascular pedicle (204) optionally contained in a first vessel (110) having a first opening (114),
- a second void space (142) in fluid contact with at least part of the vasculated portion (202), and
- a support element (170) for supporting the vascularized structure (200) and fluidly separating the first void space (112) from the second void space (142), comprising an aperture region (176) comprising one or more apertures configured to receive at least part of the vascular pedicle (204).

2. The bioreactor (100) according to claim 1 wherein:

- the support element (170) comprises a body provided with a first side (172) adjoining the first void space (112) and a second side (174) adjoining the second void space (142), and wherein the aperture region (176) connects the first side (172) with the second side (174), and
- the second void space (142) is contained in a second vessel (140) having a second opening (144) or contained in a gap between the support element (170) and a covering plate.

3. The bioreactor (100) according to claim 1 or 2, wherein the support element (170) further comprises a clamp or more suture anchors configured to fixedly attach at least part of the vasculated portion (202) around a periphery of the aperture region (176) thereby fluidly sealing the aperture region (176).

4. The bioreactor (100) according to claim 2 or 3, wherein the first (110) vessel and second vessel (140) or covering plate are each dismountably attachable to the support element (170).

5. The bioreactor (100) according to any of claims 1 to 4, wherein the first vessel (110) is further disposed with a sealable access opening (111), for manual access to the vascular pedicle (204).

6. The bioreactor (100) according to any of claims 1 to 5, wherein the first vessel (110) is further disposed with one or more ports (113) in fluid connection with the first void space (112) for inlet and/or outlet of fluid, of one or more electrically conducting cables, or of one or more flexible cords, optionally some ports being arranged at different distances from the first opening (114) or a different peripheral positions around first vessel.

7. The bioreactor (100) according to any of claims 2 to 6, wherein the second vessel (140) is further disposed with one or more ports (113) in fluid connection with the second void space (142) for inlet and/or outlet of fluid, of one or more electrically conducting cables, or of one or more flexible cords, optionally some ports on the second vessel (140) being arranged at different distances from the second opening (114) or a different peripheral positions around second vessel.

8. The bioreactor (100) according to any of claims 1 to 6, wherein the support element (170) is configured to position the aperture region (176) within the first void space (112), and optionally to provide a gap between a wall (118) of the first vessel (110) and the support element (170), optionally the gap having an annular form.

9. The bioreactor (100) according to any of claims 1 to 7, further comprising a third void space (192) separated from the first (112) or second (142) void space by the support element (170), configured to receive at least a part of the vasculated portion (202) not received by the received by the second void space (142).

10. Use of a bioreactor (100) according to any of claims 1 to 9, for perfusion of a vascularized structure (200), for decellularization of a vascularized composite tissue, recellularization of a vascularized composite tissue scaffold or for preservation of vascularized composite tissue.

11. Use according to claim 10, wherein:

- the first void space (112) is configured to contain liquid, and the second void space (142) is configured to contain a gaseous atmosphere or *vice versa*, or
- the first void space (112) and the second void space (142) are each configured to contain a liquid, or
- the first void space (112) and the second void space (142) are each configured to contain a gaseous environment.

12. A method for perfusion of a vascularized structure (200), comprising the steps:

- providing a bioreactor (100) according to any of claims 1 to 9,
- attaching the vascularized structure (200) to the support element (170) such that at least part of the vasculated portion (202) is in fluid connection with the second void space (142) and at least part of the vascular pedicle (204) is disposed in the first void space (112),
- whereby a part of the vascularized structure (200) is sutured and/or clamped over the aperture region (176) to seal it, thereby isolating the first void space (112) from the second void space (142), and
- perfusing the vascularized structure (200) through vasculature of vascular pedicle (204).

13. A kit comprising a bioreactor (100) according to any of claims 1 to 9, wherein there are at least two interchangeable support elements (170), each having a different aperture region (176) size and/or shape.

14. The kit according to claim 13, further comprising at least two different drawing templates, one for each different support element (170) for marking skin of a donor for harvesting such that the size and shape of the skin harvested is suitable for suturing and/or clamping over the corresponding aperture region (176) size and/or shape of the support element (170).

15. The bioreactor (100) according to any of claims 1 to 9, the use according to claim 10 or 11, the method according to claim 12 or the kit according to claim 13 or 14 wherein the vascularized structure (200) is a vascularized composite tissue or a vascularized composite tissue scaffold.

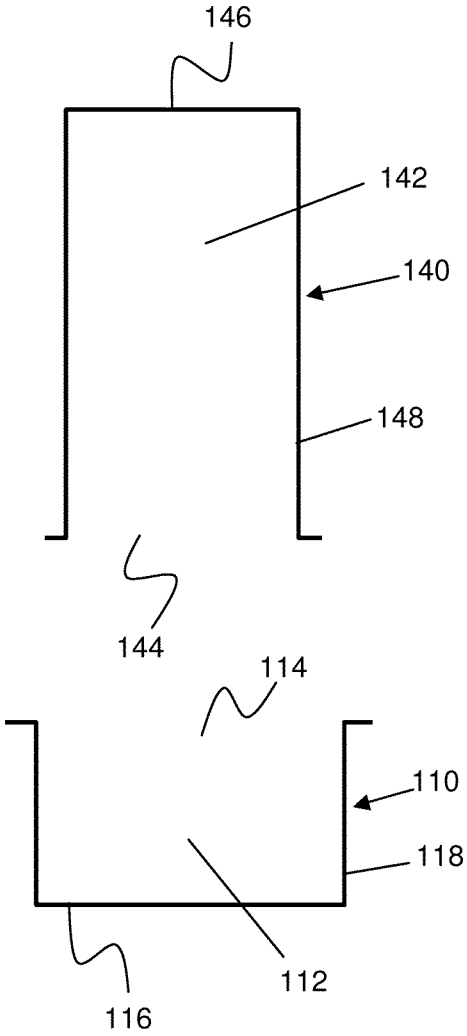

FIG. 1

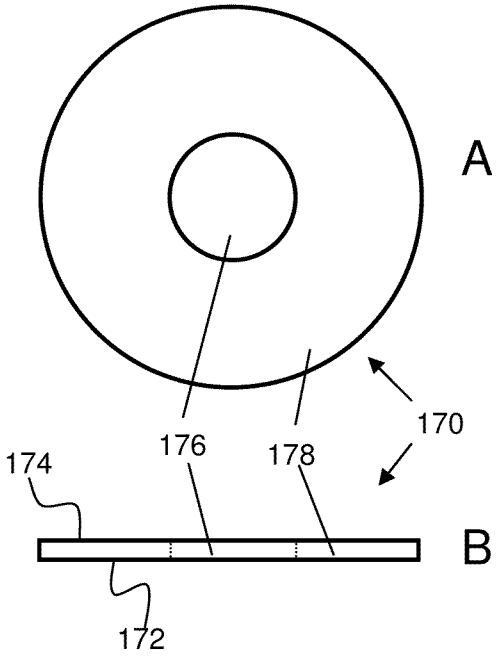

FIG. 2

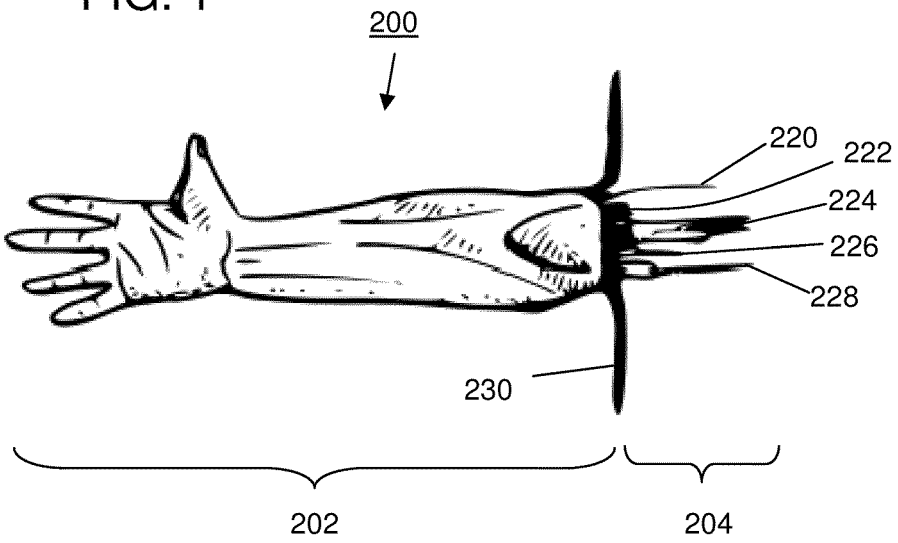

FIG. 3

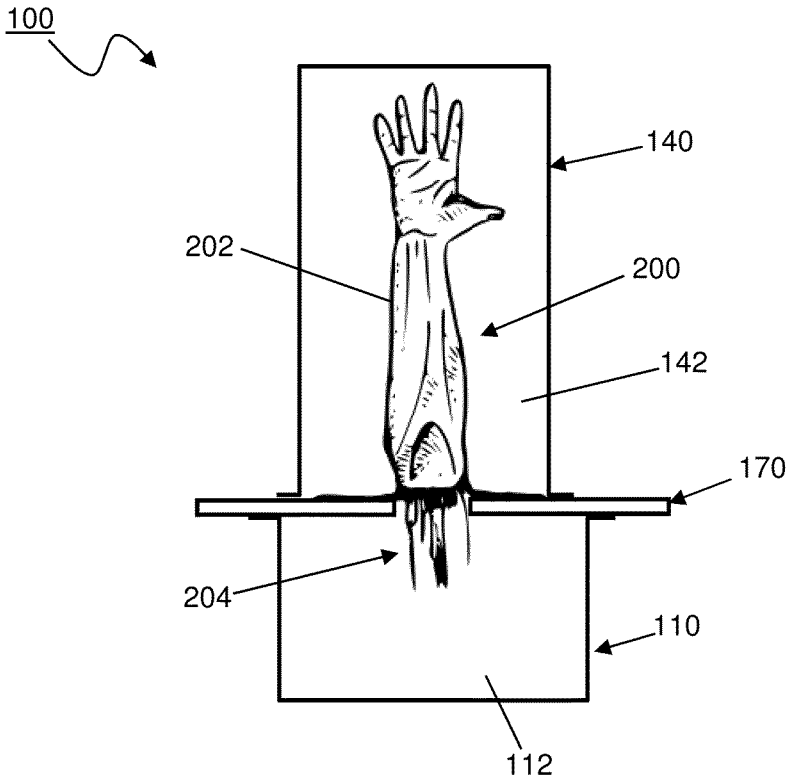
100
140
202
200
142
170
204
110
112

FIG. 4

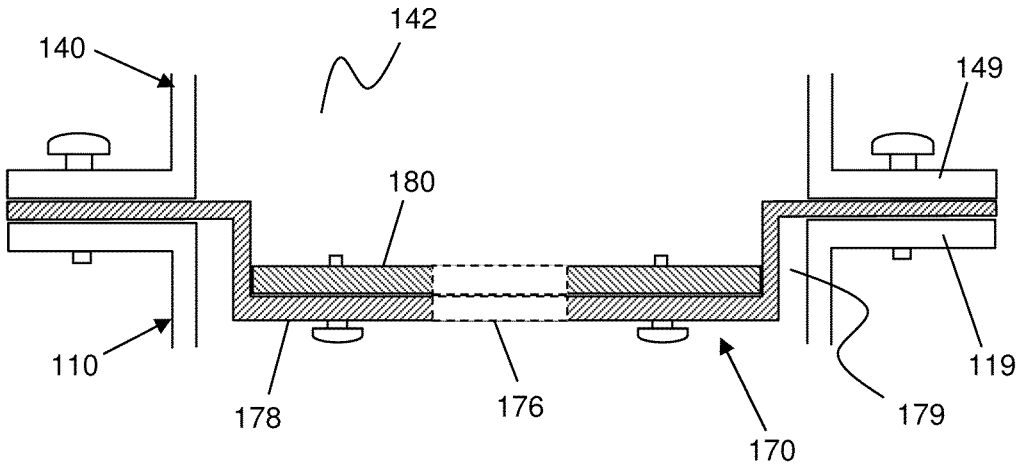
142
140
149
180
110
178
176
170
179
119

FIG. 5

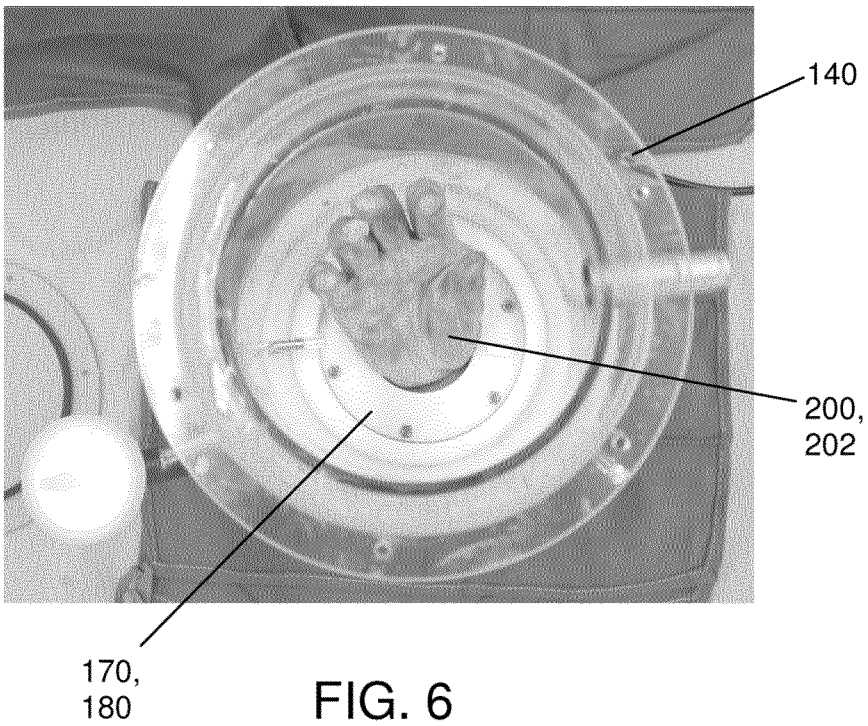
140
200,
202
170,
180

FIG. 6

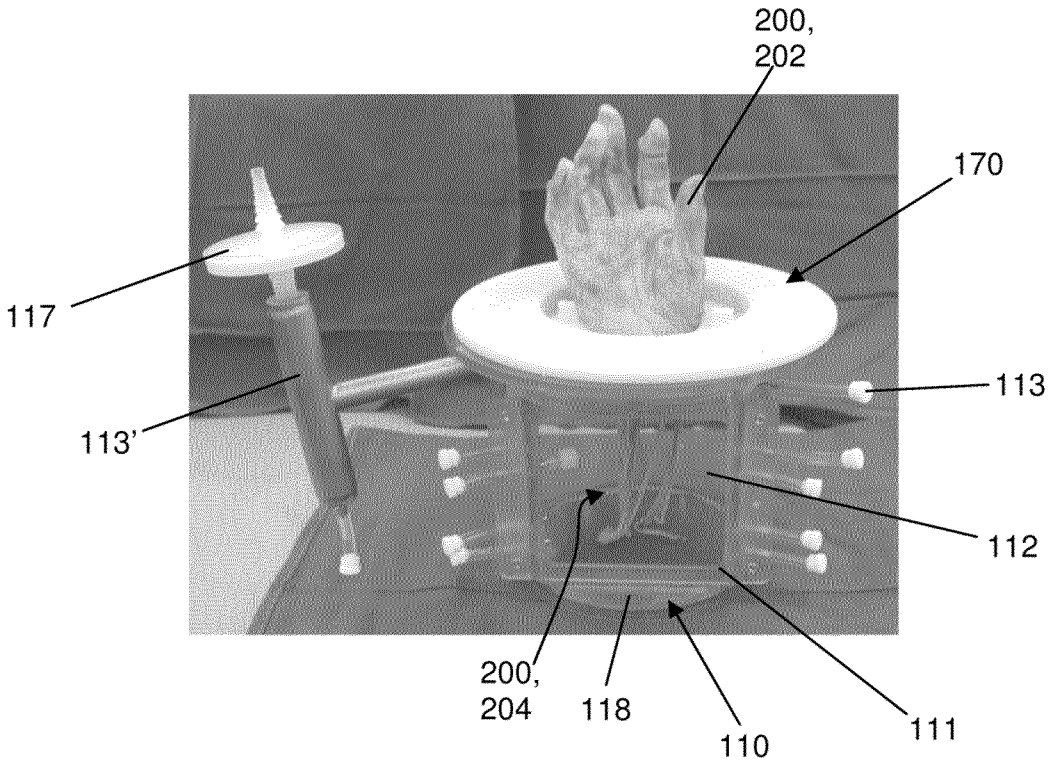
200,
202
170
117
113
113'
112
200,
204
118
110
111

FIG. 7

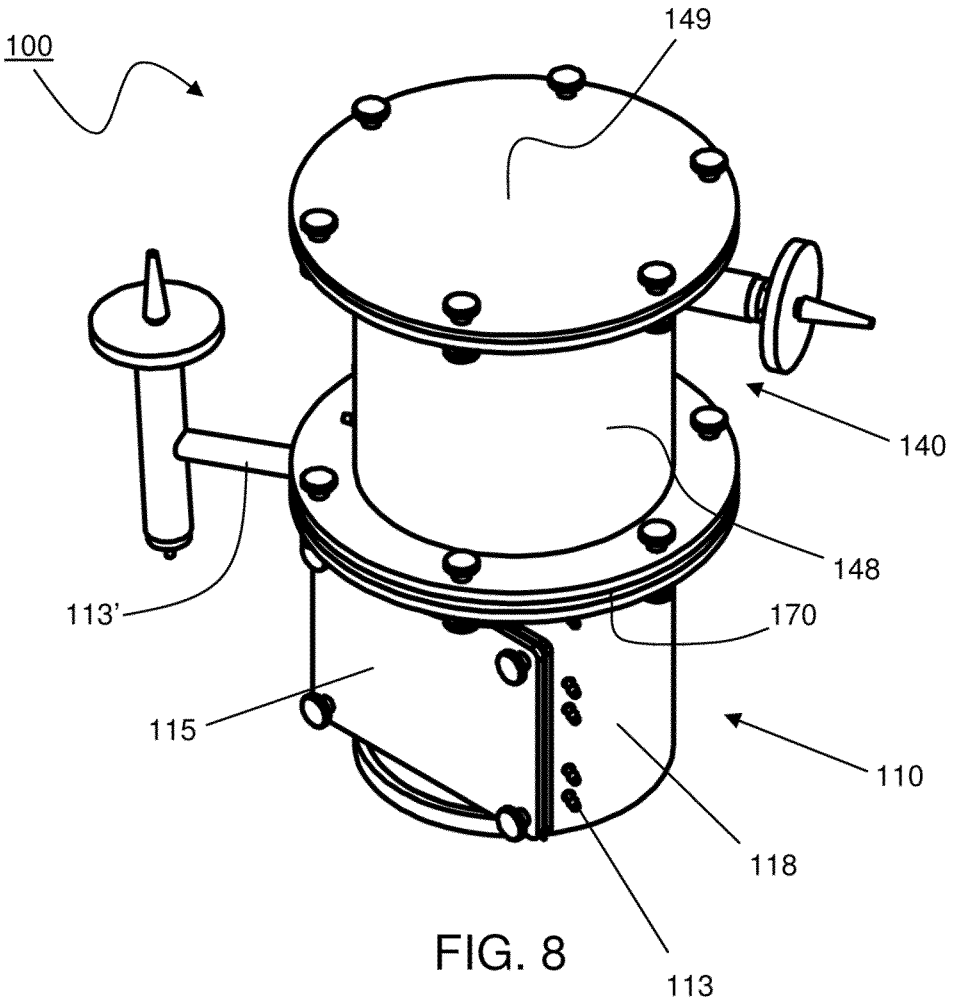
100
149
140
148
113'
170
115
110
118
113

FIG. 8

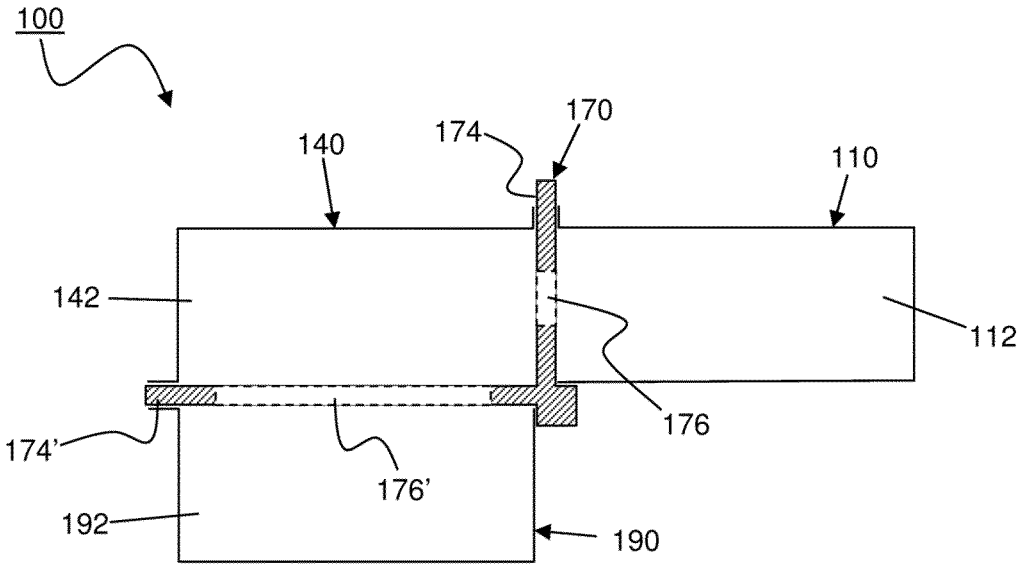
100
140
174
170
110
142
112
176
174'
176'
192
190

FIG. 9

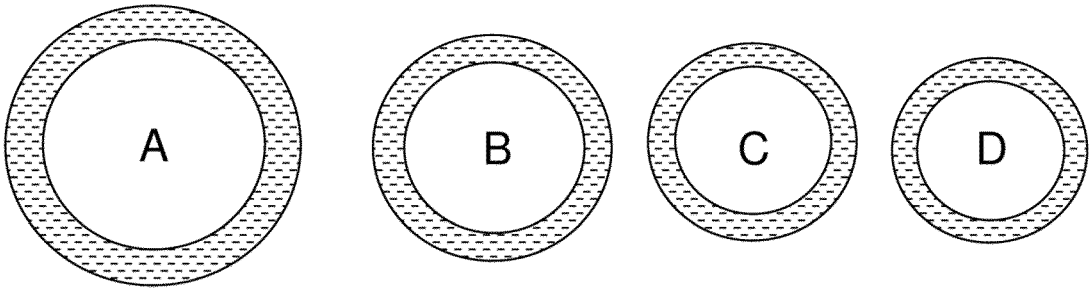

FIG. 10

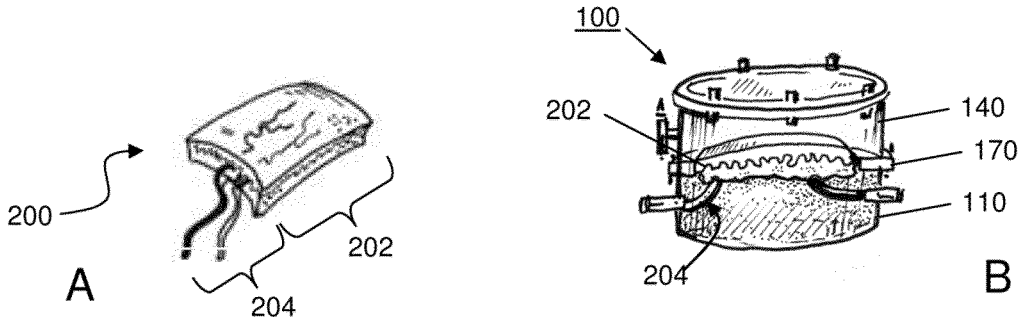

FIG. 11

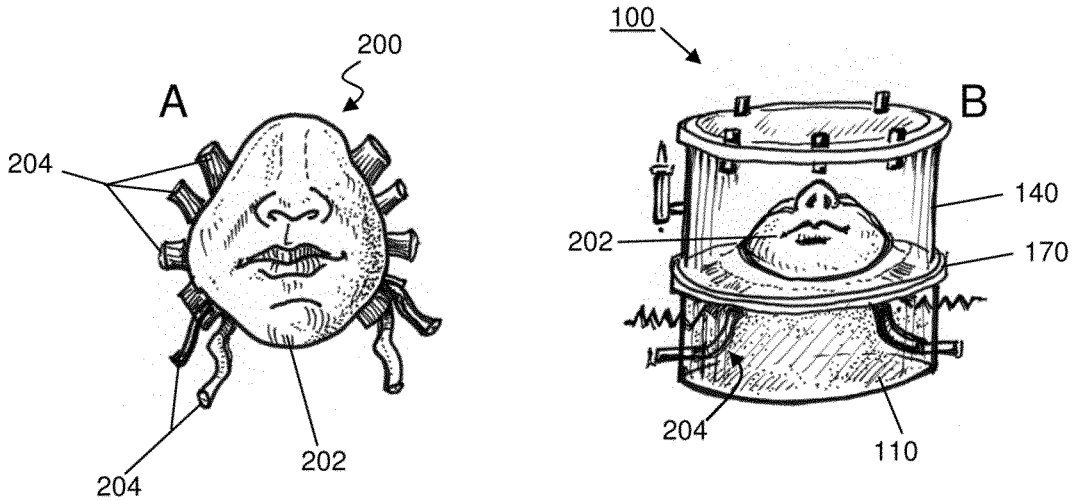

FIG. 12

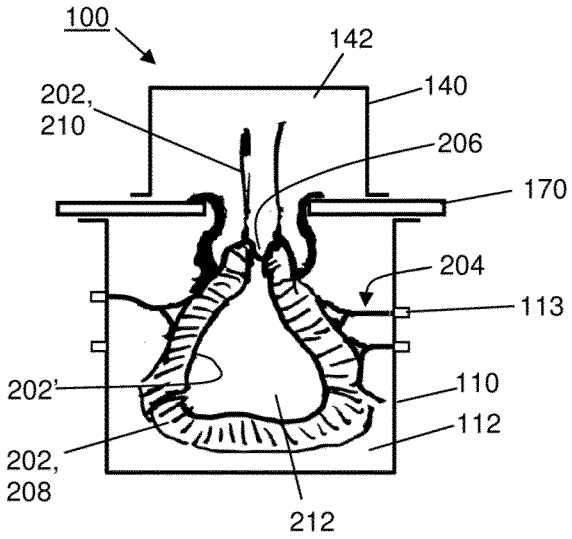
100
142
140
202,
210
206
170
204
113
202'
110
112
202,
208
212

FIG. 13

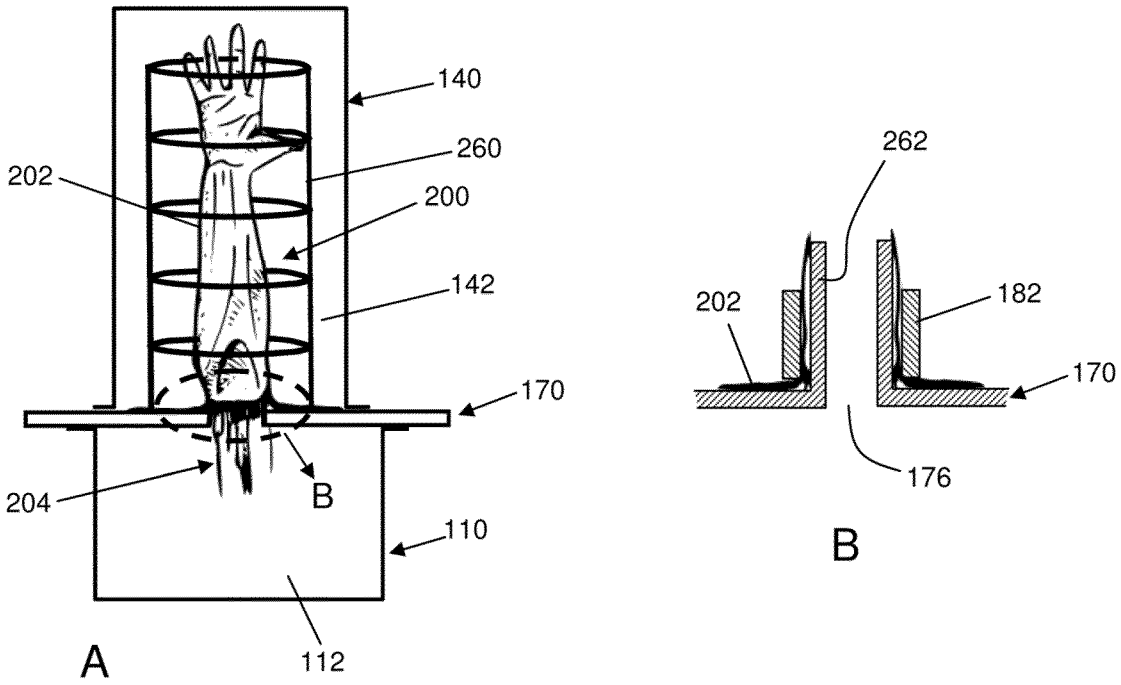
140
260
202
200
142
170
204
B
110
112
A
262
202
182
170
176
B

FIG. 14

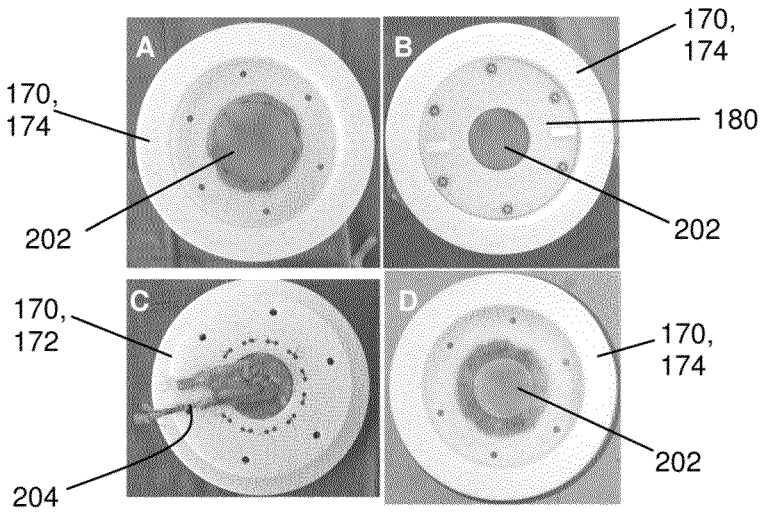

FIG. 15

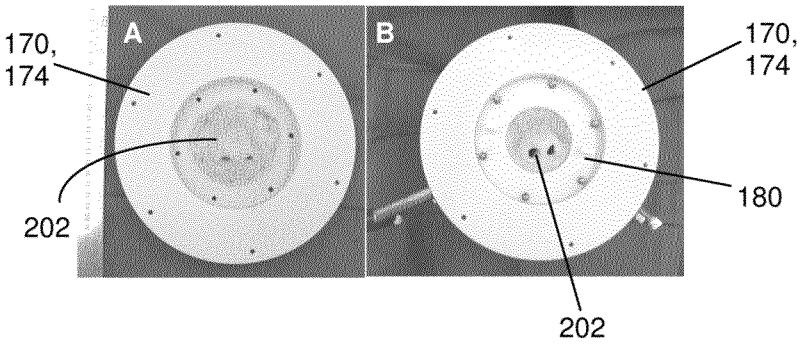

FIG. 16

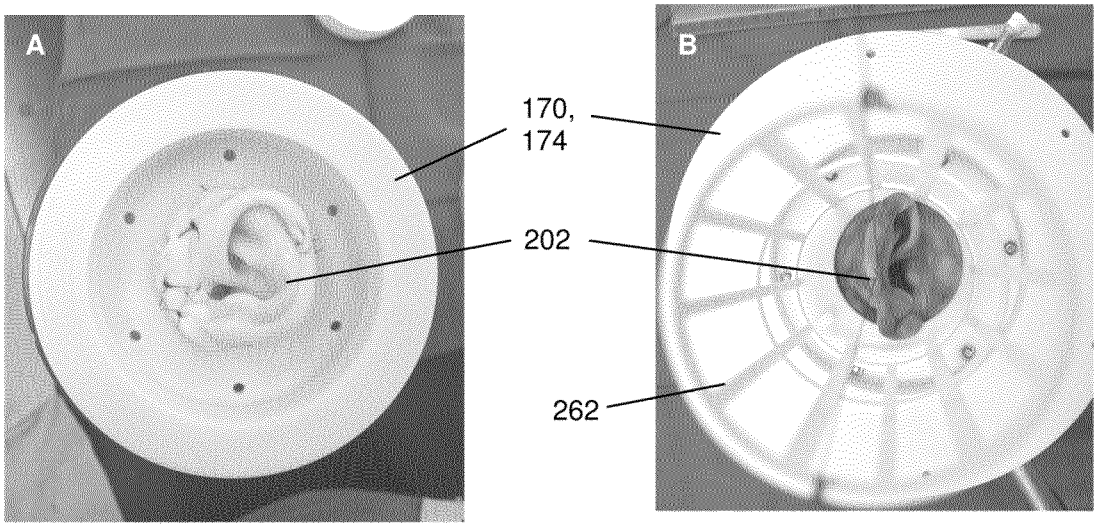

FIG. 17

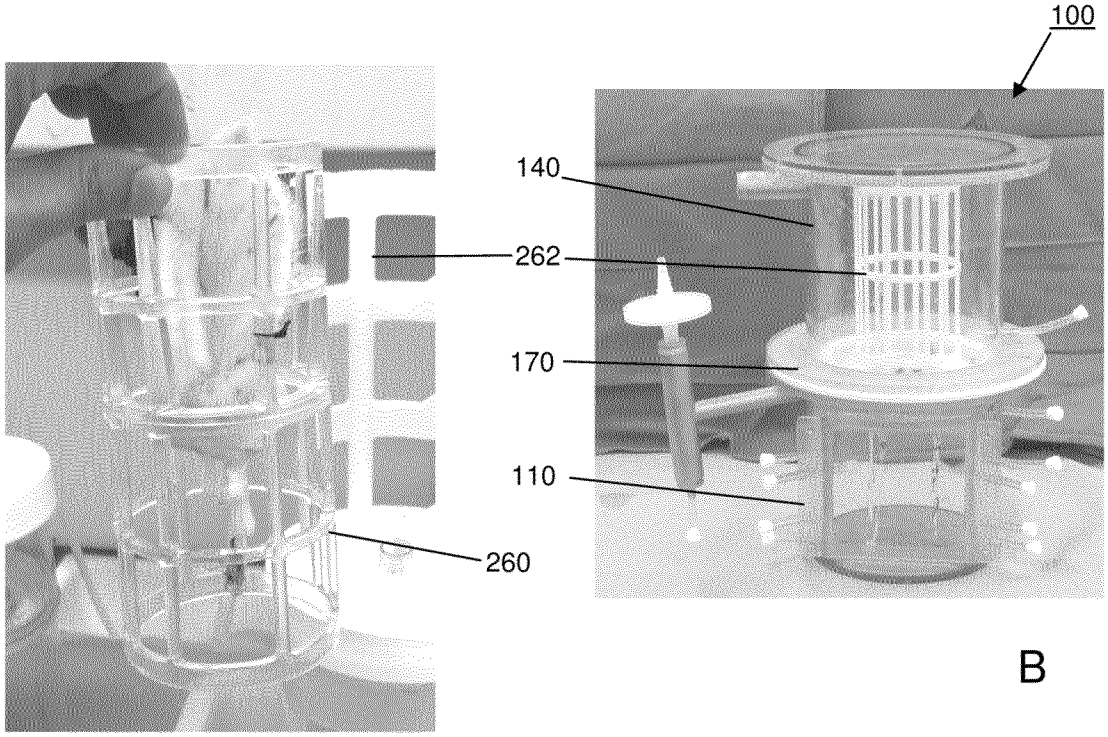

FIG. 18

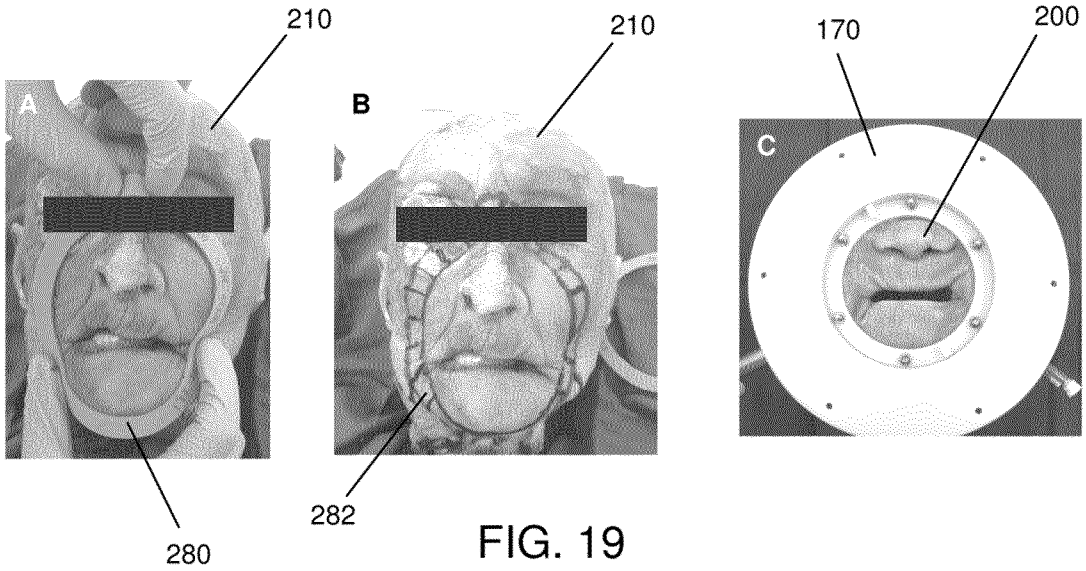

FIG. 19